Quantification of Uncertainty in Coarse-Scale Relative Permeability for Reservoir Production Forecast

Hirofumi Okano

Submitted for the
Degree of Doctor of Philosophy
Institute of Petroleum Engineering
Heriot-Watt University
July 2006

Abstract

Reservoir production forecasts are essentially uncertain due to the lack of data. Specifically, it is impossible to estimate detailed heterogeneity in a reservoir. In order to mitigate the ambiguity of a model, production data is incorporated into a history-matching process. Still, there is insufficient data to constrain the subsurface properties all over the field.

This thesis investigates coarse-scale relative permeabilities which are often adjusted during history-matching, and the theme is the incorporation of sub-grid heterogeneity in multi-phase functions. Coarse-scale models are employed in history-matching, because of computational cost. This work explores the research area between uncertainty and upscaling, and contributes to developing a methodology for quantifying uncertainty in reservoir modelling.

Two issues are addressed in this thesis. Firstly, because the coarse-scale model inevitably misses out sub-grid heterogeneity, physical dispersion is ignored in the simulation. Secondly, the small-scale heterogeneity is not explicitly known and can only be inferred by history-matching. To solve these problems, local features in the coarse-scale relative permeability curves were adjusted in history-matching to capture the effect of physical dispersion and to compensate for the effect of numerical dispersion.

The central idea of this thesis is that the physical priors of the coarse-scale relative permeabilities are estimated from a range of geostatistical parameters using a flow-based upscaling. Furthermore, they are incorporated into the misfit definition of history-matching. This technique is indispensable for avoiding the unrealistic relative permeability curves, especially if a large number of parameters are to be adjusted. The framework is one of the new aspects proposed in this thesis, which leads to physically-meaningful stochastic sampling.

The history-matched relative permeabilities and their uncertainty envelopes were compared with the two-phase upscaling results. A synthetic data set for which the true solution is known was used. The two-phase upscaling was conducted using the truth model to give a reference set of coarse-scale relative permeability curves. After history-matching, uncertainty in production forecasts as well as relative permeabilities was quantified in a Bayesian framework. The results highlight the fact that the parameterisation affects the width of uncertainty envelope.

Dedication

This thesis is dedicated to my parents and my wife.

Acknowledgements

I would like to thank my supervisors, Dr Gillian Pickup and Professor Mike Christie, for their invaluable directions and encouragement. Their enthusiasm toward new and practical research encouraged me in my study at the Heriot-Watt. Without their help I could not have completed this work within the allocated period. Their contribution extended to improvement of my presentation skills as well as thousands of small corrections in my writings. I would like to keep in mind what I have learnt from them during the last three years.

I would also like to thank the other members of the Uncertainty Quantification Group and my colleagues in the Institute of Petroleum Engineering for their support of my work and life in Edinburgh. Thanks to those friends, I have enjoyed my study since I arrived at the Heriot-Watt. I appreciate the kind help from all the staff and students in this department.

The financial support from Japan Oil, Gas and Metals National Corporation (the formerly JNOC) is highly appreciated. I would like to express my gratitude to those who gave me beneficial advice and made a special effort to give me the opportunity to start and pursue the PhD study.

The comments on my work from the sponsors of the Uncertainty Quantification Project (the formerly Uncertainly and Upscaling Project) are also appreciated. The steering group meetings held every six months and the other informal meetings are beneficial for me to communicate with the industry and to identify the practical applications.

I would like to thank the examiners of this thesis, Dr Karl Stephen and Dr Ann Muggeridge, for their helpful comments on my work.

Finally, I thank my parents and wife for their support and understanding which are essential to the accomplishment of this study.

Declaration Statement

(Research Thesis Submission Form is placed here in each of the original copies.)

In accordance with the appropriate regulations I hereby submit my thesis and I declare that:

1. the thesis embodies the results of my own work and has been composed by myself
2. where appropriate, I have made acknowledgement of the work of others and have made reference to work carried out in collaboration with other persons
3. the thesis is the correct version of the thesis for submission.
4. my thesis for the award referred to, deposited in the Heriot-Watt University Library, should be made available for loan or photocopying, subject to such conditions as the Librarian may require
5. I understand that as a student of the University I am required to abide by the Regulations of the University and to conform to its discipline.

Contents

List of Tables

List of Figures

Chapter 1

Introduction

The ultimate aim of reservoir engineering is ‘attainment of a maximum efficiency in the exploitation of oil-bearing reservoirs’, which implies ‘the maximum recovery of oil at a minimum cost’, (Muskat, 1981). For that purpose, the estimation of oil recovery and the planning of efficient developments are indispensable. Moreover, for the estimation of reserves in the economic sense, an article of Journal of Petroleum Technology (JPT, 1996) presents some reserve definitions including proved reserves as follows.

> ‘Proved reserves are those quantities of petroleum which, by analysis of geological and engineering data, can be estimated with reasonable certainty to be commercially recoverable, from a given date forward, from known reservoirs and under current economic conditions, operating methods, and governmental regulations.’

Here, the forecast of subsurface performance with reasonable certainty is an important task for reservoir engineers, since it is directly linked to the recovery prediction, the development planning and the estimation of proved reserves. The task requires understanding the physical principals of fluid flow through the reservoir. In this way, the economics of oil production is related to physical aspects of reservoir engineering. Furthermore, the phrase of ‘with reasonable certainty’ in the above quotation implies that one needs to manage uncertainty which depends

on the geological and engineering data. Whereas deterministic methods use a single estimate, probabilistic methods rely on the statistical analysis of the data and employs a probability distribution to determine the estimate of reserves, (JPT, 1996).

A petroleum reservoir consists of a rock and fluid system where the porous media of rock is saturated with one or more of gas, oil and water. The fluid is trapped or movable in the microscopic pore structures of rock. The ratio of the pore volume to the entire volume is termed as porosity, and it indicates how much of the reservoir rock may contain fluid. Typical sandstone porosities range from 8 to 39 %, and a worldwide average is approximately 18 %, (Smith et al., 1992). It is affected by sorting, cementation, packing, etc. The range of carbonate porosities is usually different from that of sandstone, because the porosities depend on the types of voids in carbonates: intergranular, vugular, fractures, etc. One needs to obtain measurements of porosity in order to estimate the amount of hydrocarbon in reservoir.

Another property which is important for the production forecast is the ability of the rock to pass fluids through the microscopic pore structure, namely permeability. Absolute permeability is defined by Darcy's law which describes single phase flow through porous media. Darcy's law states that the fluid velocity is proportional to the pressure gradient and is inversely proportional to the fluid viscosity, where the constant of proportionality is referred to as absolute permeability. The assumptions behind the relation are homogeneous rock, non-reactive rock, 100% saturated with single phase homogeneous fluid, Newtonian fluid, incompressible flow, laminar flow, steady state, constant temperature, (Smith et al., 1992). For example, the exceptions to the law are gas slippage on the rock grains at very low pressure and the effects of an "inertial" force at very high flow rate, e.g., for gas flow around the wellbore, (Dake, 1978). Absolute permeability has units of area and is traditionally expressed by units of Darcies: $1\,\text{Darcy} = 0.987 \times 10^{-12}\text{m}^2$. Consider a fluid of one centipoise viscosity flowing through a rock sample. When it flows at a velocity of one centimetre per second under a pressure gradient of one atmosphere per centimetre, the rock permeability is one Darcy. In addition to laboratory measurements, well test analysis is conducted to estimate absolute permeability in a reservoir. Permeability in typical reservoir sandstones ranges from 0.1 to 1000 or more millidarcies, and permeability in a tight

carbonate matrix may be less than 0.1 millidarcies, (Tiab and Donaldson, 2002). For carbonate rocks, the correlation between porosity and permeability is often complicated due to the different types of pore such as inter-particle and vug, (Lucia, 1999).

Both porosity and permeability are basic rock properties used to estimate oil production from a reservoir. Also capillary pressure and relative permeability play important roles in describing multi-phase flow in porous media and they depend on the rock type. In the presence of two-phase fluids, the wetting phase fluid tends to spread on the rock surface, and the interface between the different phases form an equilibrium with particular contact angles. Capillary pressure represents the pressure difference between non-wetting and wetting phase fluids. Relative permeability is defined by the extension of single-phase Darcy's law to multi-phase flow, (Muskat, 1981). Both capillary pressure and relative permeability are measured by laboratory experiments called as Special Core Analysis (SCAL).

For fluid properties, the PVT parameters such as formation volume factors and solution gas-oil ratio are measured using reservoir fluid samples to relate surface to reservoir volume, (Dake, 1978). In addition, fluid densities, viscosities and compositions are measured in a PVT analysis. In general, a crude oil contains a number of chemical compounds. Hydrocarbons are comprised of hydrogen and carbon, and may be gaseous, liquid, or solid depending on the composition, temperature and pressure. The subsurface reservoir conditions are high temperature and high pressure compared to the surface conditions, and the reservoir pressure may change during the well operation. So it is necessary to analyse the states of fluids which are defined by pressure, volume and temperature (PVT) and to express the fluid properties as functions of pressure at reservoir temperature.

The ultimate oil recovery from a reservoir can be expressed as the oil volume at stock tank conditions multiplied by the recovery factor which represents the fraction of recoverable oil, (Dake, 1978). The oil volume in the reservoir is calculated by the product of the net bulk volume of reservoir, the porosity and the hydrocarbon saturation. The volume at surface conditions is obtained by dividing the volume at reservoir conditions by the oil formation volume factor.

Here the recovery factor depends on a reservoir drive mechanism. The estimation of recovery factor is not a simple task, because it requires the prediction of the amount of oil remaining in the reservoir at the end of the operation.

The operation of wells results in a decrease in reservoir pressure to overcome the flow resistance for the production, and also the pressure drop leads to the expansion of fluids in the reservoir. When the production is due to the natural energy in the reservoir and its adjacent aquifer, it is referred to as primary recovery. The classification of reservoir energy types can be found in the material balance equation which is one of the fundamental tools of reserve estimates, (Dake, 1978). The material balance equation is a zero dimensional model, because it treats a reservoir as a large tank in which no flow effects are considered, (Smith et al., 1992). In the basic formulation, the volume balance equates the cumulative production to the change in the original oil pore volume. The expansion of fluids results from a pressure drop in a reservoir. It includes the expansion of oil plus originally dissolved gas and the expansion of the gas cap gas. Also there might be some change in the oil pore volume due to the connate water expansion and pore volume reduction. These volume changes correspond to the reservoir fluids production. Each term of the material balance equation represents these drive mechanisms: solution gas drive, gascap drive, natural water drive, compaction drive, etc.

In addition to primary recovery, supplementary recovery represents the oil obtained by increasing the natural energy of the reservoir. Secondary recovery usually aims at maintaining reservoir pressure with some injected fluids such as water and gas, (Lake, 1989). Waterflooding is the most common approach due to its availability and low cost. Tertiary recovery represents the oil recovery after a secondary recovery project, and includes miscible flooding, carbon dioxide flooding, surfactant flooding, etc. In order to estimate the recovery, one needs to consider physical phenomena behind the mechanism. For example, in case of waterflooding two phase flow phenomena need to be modelled. Also miscible flooding requires the modelling of phase behaviour which determines the success of the enhanced oil recovery.

Reservoir simulations are widely used to investigate primary and supplementary recovery processes in a reservoir. Multi-dimensional reservoir simulations have many advantages over a zero-dimensional model of the material balance equation. For example, the material balance equation cannot represent the preferential flow paths of water, due to either natural influx or injection. On the other hand, reservoir simulations have the potential to resolve the spatial heterogeneity in a three dimensional model and to calculate multi-phase flows at certain times in the reservoir development. Here the reservoir is divided into discrete cells between which the flow of the fluids is governed by mass conservation law along with Darcy's law, (Lake, 1989). A mathematical model represents the physical system of reservoir using a set of partial differential equations along with a set of boundary conditions, (Peaceman, 1977). The immiscible phases in a reservoir are oil, water and gas. Mass transfer can occur between the phases: e.g., between the gas and oil phases. Multi-phase flow depends on the force balance in a reservoir, namely the balance between gravity, capillary and viscous forces. For a complex representation of a reservoir, the partial differential equations can be solved only by numerical methods. With an appropriate numerical algorithm and a sufficient computer resources, one can develop a wide range of reservoir models and simulate a variety of situations which may occur in a real reservoir. The input data of commercial reservoir simulators are rock and fluid properties which have been explained briefly in this chapter.

As mentioned above, numerical flow simulations enable complex representation of a reservoir, compared to a classical tool of material balance, and are routinely employed to predict reservoir performance under different depletion and operating scenarios. However, production forecasts for petroleum reservoirs are essentially uncertain for the following reasons. Firstly, the available data in a field are usually sparse. Direct measurements of rock and fluid properties can be obtained at only a small number of sparse well locations. Hence the properties of a large part of a reservoir remain unknown. Secondly, all the data measured either in a laboratory or in a field are usually contaminated by noise. Since there is no guarantee that a reservoir model can be developed appropriately based on the noisy measurements, the resulting production forecasts are uncertain. Thirdly, the measurements of rock sample usually have smaller volume of investigation than a simulation cell. The scale-change between the cell size and the measurement

length produces errors in a simulation model. This also leads to uncertain simulation results.

Due to the reasons listed in the previous paragraph, especially because the available information on rock properties is sparse, a reservoir engineer needs to calibrate the unknown petrophysical parameters based on production data. The petrophysical parameters are measured or estimated, and are incorporated into nonlinear partial differential equations which describe flow through a reservoir and which are usually solved numerically, namely as a reservoir simulation. The unknown parameters are adjusted so that the simulated profile can match the observed data. This process is to solve an inverse problem and is called history-matching in the petroleum industry. The unique solution for the unknown parameters and the corresponding single production forecast cannot be obtained, because of insufficient and noisy production data. In other words, history-matching cannot constrain the subsurface properties all over a field, and so it is necessary to quantify the variability of the future recovery with a 'degree-of-belief'.

The requirement to produce uncertain forecasts has attracted much attention of reservoir engineers in recent years, and a lot of studies on uncertainty quantification have been conducted, (e.g., Barker et al., 2001; Floris et al., 2001; Christie et al., 2002b). When the production data is available for history-matching, Bayesian inference is often adopted for the purpose of the appraisal, (Christie et al., 2002b). In Bayesian inference a 'degree-of-belief' is referred to as a probability (Sivia, 1996), and the probability given production history is calculated from the prior belief and the mismatch between the observed data and the simulated profiles. Here the tasks of reservoir engineers are to conduct history-matching and to quantify the uncertainty in the future recovery with a probability.

The petrophysical parameters which are often adjusted in history-matching are porosity, permeability and relative permeability. Also one sometimes needs to infer geological structures, e.g., channel and fault, and their properties such as sealing of faults and transmissibilities. Among those parameters, this thesis focuses on the adjustment of relative permeability. Relative permeabilities describe multi-phase flow in the porous media of a rock system. In petroleum reservoirs, multi-phase flow occurs, especially when water or gas is injected into reservoir to

enhance oil recovery. The relative permeability is usually represented as a function of fluid saturation. As mentioned earlier, the measurements are sparse and contain some errors. In addition, the rock relative permeabilities measured by core-flooding experiments are different from the upscaled relative permeabilities in a simulation cell. These aspects lead to ambiguity in the relative permeabilities assigned in a simulation cell. So the history-matching tries to mitigate these ambiguous aspects of a simulation model. In practice, coarse-scale models are employed to reduce the computational cost of flow simulation. In this thesis, relative permeabilities in a coarse cell are referred to as coarse-scale relative permeabilities or coarse-scale curves in contrast to rock relative permeabilities.

As Williams et al. (1998) pointed out, a reservoir model history-match requires the detailed interpretation of observed data and simulated results. For example, in the case of large and complex reservoir models, one may need to analyse the flow performance in each layer or in each compartment of the model. It is usually tedious and time-consuming for a reservoir engineer to obtain the sufficient knowledge by trial-and-error. Although manual adjustments may provide much knowledge on the reservoir, some optimisation algorithms are also employed to assist the history-matching. Optimisation algorithms can be classified into two categories: deterministic and stochastic, (Portella and Prais, 1999). In the case of stochastic algorithms, the Genetic Algorithm and the Neighbourhood Approximation Algorithm (Sambridge, 1999a) have gained popularity in the petroleum industry, (Christie et al., 2002b; Stephen et al., 2005). These optimisation schemes enable more efficient history-matching in terms of the search of solutions in the parameter space. However, the drawback is the lack of the physical constraints in the procedure. Obviously, reservoir engineer needs to recall that each property in the model has a physical meaning and should aim at a reasonable adjustment. A reservoir model history-matching usually requires the calibration of multiple parameters. The adjustment of multiple parameters raises a problem. The interrelation between the parameters may lead wrong solutions. For example, when one adjusts absolute permeability and relative permeabilities, bias of absolute permeability affects the adjustment of relative permeabilities, and vice versa. This is because absolute permeability is multiplied by relative permeability in the governing equation of reservoir simulation.

The problem to be solved is:

> How can we separate biases in the adjustments of absolute permeability and relative permeability? In other words, how can we split the misleading mutual effects of absolute permeability and relative permeability in history-matching?

The solution which is presented in this thesis is to place the bound of the adjustment. For example, one wants to determine the limits of absolute permeability and relative permeability. The method to limit the adjustment of relative permeabilities has not been presented so far and is the central idea of this study.

For relative permeability, there are many uncertain aspects in its definitions, measurements and upscaling process. This thesis focuses on the issue of the scale change and seeks physical constraints for history-matching. The key is the use of knowledge of upscaling. The upscaling is the procedure for calculating a set of coarse-scale properties from a fine-scale model so that the coarse-scale model can reproduce the fine-scale solution. Single phase upscaling calculates coarse-scale permeability or transmissibility, (e.g. Christie, 1996; Renard and de Marsily, 1997; Christie and Blunt, 2001), and two phase upscaling calculates coarse-scale relative permeability, (e.g. Barker and Thibeau, 1997; Barker and Dupouy, 1999). Since the detailed fine-scale models consisting of millions of cells were demanded to pursue geological realism, a range of upscaling methods have been developed and assessed. Whereas single phase upscaling is often incorporated into reservoir modelling, two phase upscaling has not gained popularity in terms of practical use. This is probably because two phase upscaling is time-consuming and is not robust. Note that the goal of this thesis is not the improvement of upscaling methods, but the use of the knowledge on the upscaling to guide history-matching. If the possible shapes of coarse-scale relative permeabilities were estimated in some way, one could use the knowledge to alter the curves in history-matching. Little research has been performed on the shape of the coarse-scale curves. To date, research is limited to the one-dimensional problem for homogeneous media (e.g., Hewett et al., 1998), although many works (e.g., Hewett and Behrens, 1991; Muggeridge, 1991) imply that the detailed fine-scale heterogeneity affected the shape of coarse-scale curves. Coarse-scale curves depend on the small-scale variation of absolute permeability which can not be resolved in a coarse-scale cell, that is to say sub-grid heterogeneity. In this

context the theme of the study has been set up. The theme is the incorporation of sub-grid heterogeneity in multi-phase flow functions. In order to solve the problem raised in the previous paragraph, the relation between sub-grid heterogeneity and coarse-scale relative permeability is investigated in this thesis.

The solution to the above problem is:

> To determine the bounds of the adjustment of relative permeabilities using computational experiments which are based on geostatistical information and flow-based upscaling.

In order to demonstrate the solution, this thesis explores the research area covering uncertainty and upscaling in terms of relative permeability. It aims at contributing to a reasonable production forecast under unavoidable uncertainty in reservoir modelling as explained above. It should be emphasised that the proposed method improves not only the adjustment of relative permeability but also that of permeability, because the interrelation between relative permeability and the other parameters appears in practical history-matching procedures. The next section states the problems in more detail, which have been raised in the petroleum industry and are to be solved in this thesis. The background material of the theory and methodology is summarised in Chapters 2 to 5. The numerical experiments conducted to demonstrate the proposed method and the related procedures are described in Chapters 6 to 9. Based on the results, Chapters 10 and 11 give some answers to the questions stated in this chapter.

1.1 Statement of the Problems

For the purpose of reservoir production forecast, in practice, coarse-scale models are employed to reduce the computational cost of flow simulation. Here an inherent problem of coarse-scale models is the inaccuracy of flow simulations due to the following two reasons. Firstly, the coarse-scale model suffers from numerical dispersion. Secondly, it does not resolve sub-grid heterogeneity and ignores the sub-grid physical dispersion. This problem can be summarised as follows:

Problem 1

> Coarse-scale simulations are inaccurate due to numerical dispersion and the neglect of sub-grid physical dispersion.

The usual way to reduce the inaccuracy of coarse-scale models is upscaling which has been a research topic for more than a couple of decades. Two-phase dynamic upscaling calculates coarse-scale relative permeabilities to compensate for numerical dispersion and to take account of sub-grid physical dispersion.

Another problem raised in the procedure of upscaling is the lack of knowledge of detailed small-scale heterogeneity. The detailed distribution of absolute permeabilities is difficult to estimate, and so the complete knowledge on sub-grid heterogeneity cannot be obtained. Hence, although the task is to encapsulate the effect of sub-grid heterogeneity in the coarse-scale relative permeabilities, the sub-grid heterogeneity itself has not been explicitly given. Unless the fine-scale heterogeneity is given, the two-phase upscaling cannot be implemented. Or if there is a range of possible different fine-scale models, it is necessary to upscale them one by one, and the overall process is time-consuming. This is because upscaling operates on one particular fine-scale model. In other words, the upscaling is one-to-one process between a fine-scale model and a coarse-scale model. In summary, the second problem is:

Problem 2

> Small-scale heterogeneity cannot be completely known due to the lack of detailed static information in a reservoir. Unless the fine-scale features are fixed, upscaling alone cannot solve the problems.

Consider the solutions to both problems (Problem 1 and Problem 2). The lack of knowledge makes us resort to the history-matching as discussed above. One way to solve Problem 1 and Problem 2 is to history-match coarse-scale relative permeabilities. This procedure can be said to be upscaling in which a fine-scale model is not fixed.

For the history-matching approach, incomplete dynamic data is common in a real problem and is one of the reasons for non-unique solutions in inverse problems. Production history is

limited to a certain time period, and it is usually contaminated by noise. In addition to Problem 1 and Problem 2, the third problem is:

Problem 3

Insufficient dynamic data as well as the lack of static data results in non-uniqueness of history-matching solutions. Therefore, history-matching solely cannot provide the well-founded production forecast.

As mentioned earlier, this problem requires the quantification of uncertainty. The task is to calculate the probability of a model given production history. So history-matching is followed by the procedure of uncertainty quantification.

For history-matching, another problem is that it is usually impossible to calculate each mismatch between simulated and observed profiles for all the possible relative permeabilities. In particular, the simultaneous adjustment of more than one set of the relative permeability curves or with different parameters makes the evaluations of all the models impossible. There is no guarantee that the true solution is obtained within a limited number of models. This is due to the so called “curse of dimensionality”. That is to say, as an extra dimension is added to parameter space, the computational cost increases rapidly. The same thing can be said for sampling in uncertainty quantification. To make matters worse, the non-uniqueness of history-matching may hide the true solution in the other well-matched models. This means that before reaching the true solution, the other well-matched models can be regarded as the solutions of history-matching, and in this case the forecast uncertainty is quantified based on the other well-matched models. Because the true relative permeabilities are unknown in a real field, it is impossible to validate the history-matching solution. Note that it is neither necessary nor possible to distinguish a true solution from the other well-matched models. However, unless the true solution or a similar solution is included in the history-matched ensemble, the uncertainty appraisal may not respect the true model. The problem raised in this paragraph is summarised as follows:

Problem 4

It is impossible to evaluate all the models, in terms of mismatch between simulated and observed data, throughout the parameter space, and this may make it difficult to find a true

solution in history-matching. Hence the resulting ensemble may consist of well-matched models, but may not include a true solution.

In order to overcome the problem above, a reduction of the parameter space is required. For the adjustment of coarse-scale relative permeabilities, the reduction of the parameter space is related to (1) reducing the range of the relative permeability curves, (2) reducing the number of parameters which express each set of the curves and (3) reducing the total number of the curves.

Problems 1 to 4 form a sequence of problems. By solving these problems, this thesis addresses two issues:

- How should a reservoir engineer adjust coarse-scale relative permeabilities in history-matching?
- How should a reservoir engineer predict uncertain oil production based on the coarse-scale history-matching?

These issues are common for the users of reservoir simulators, because rock relative permeabilities are often altered in coarse-scale history-matching, (e.g., Williams et al., 1998). Furthermore, in order to solve the problems (Problems 1 to 4) and give an insight into the issues above, a number of questions should be answered. The questions are the breakdown of the four problems stated above.

For Problems 1 and 2, coarse-scale relative permeabilities should represent sub-grid physical dispersion accurately. Whereas rock relative permeabilities are often parameterised with power functions and exponential functions, the coarse-scale curves have different shapes from rock curves. From this point, a question evolves:

Question 1 Which parameterisation is most suitable for coarse-scale relative permeabilities?

Even if a rock curve is uniformly distributed throughout a reservoir, the coarse-scale curves may be different in different positions. So another question is raised:

Question 2 How many sets of coarse-scale curves should be adjusted in history-matching?

For Problem 3, it is necessary to quantify the uncertainty appropriately. So Questions 1 and 2 are followed by another question related to uncertainty quantification:

Question 3 Do the parameterisation scheme and the number of the curves affect the results of uncertainty quantification?

Note that Questions 1 to 3 are also involved in Problem 4, since the parameterisation and the number of curves control the number of parameters to be adjusted in history-matching. The reduction of the parameter space, stated in Problem 4, also raises some further questions:

Question 4 How far is the rock curve allowed to change?

Question 5 How can the limits of the adjustment be expressed?

Question 6 How can the limits of the adjustment be incorporated into history-matching?

Questions 1 to 6 listed above cover the extensive research area of uncertainty and upscaling. The exploration of the research area is the main contribution of this thesis.

1.2 Aims and Procedures

The previous section has raised a sequence of problems, and the aims of the thesis are to solve those problems. The aims are:

- To propose a methodology for history-matching of coarse-scale relative permeabilities with which one can perform accurate flow simulations.
- To demonstrate a methodology for uncertainty quantification, which can take account of multiple solutions in history-matching, based on an appropriate parameterisation of coarse-scale relative permeabilities.
- To estimate the physical constraints on the coarse-scale relative permeabilities which can reduce the parameter space for history-matching.

- To express the physical constraints as prior probability distributions which can be incorporated into a Bayesian framework for uncertainty quantification.

This thesis focuses on coarse-scale relative permeabilities. The procedures to assess the proposed framework are:

- To use a synthetic fine-scale model for which the true profiles are known.
- To examine the estimated production profiles at the coarse scale by comparing them with the synthetic observed data and true profiles.
- To examine the estimated coarse-scale relative permeabilities in comparison with the reference upscaled curves which can be calculated using the true model and a dynamic upscaling method.

As far as the author is concerned, the last step listed above has not been previously investigated in this research area to validate the history-matching results. Hence, that particular step of the procedures is one of the new aspects covered in this thesis.

1.3 New Aspects Covered in the Thesis

The new aspects covered in the thesis are:

1. The shape of coarse-scale relative permeabilities in a one dimensional model has been investigated with analytical formulations by Hewett et al. (1998). Although two-phase upscaling in a two dimensional model has been studied, (e.g., Suzuki and Hewett, 2000), the shape of coarse-scale relative permeabilities in a two dimensional model has not been investigated analytically. In this thesis, the shape of coarse-scale relative permeabilities in a two dimensional model was analysed using the numerical experiments for the first time.

2. The above analysis gave an explicit representation of the limits of coarse-scale curves. In this thesis the range of the geostatistical parameters was translated into the limits of the

coarse-scale curves. Because the above analysis is new, the subsequent approach to give the limits of the curves is also a new aspect.

3. Regularisation techniques for inverse problems have been investigated to enforce uniqueness of solution using additional information or assumptions (e.g., Engl et al., 1996) and have been adopted for history-matching of relative permeabilities in the literature (e.g. Yang and Watson, 1991; Kulkarni and Datta-Gupta, 1999). However, the statistical consistency, especially between the likelihood term and the prior term, has not been justified for relative permeabilities there. On the other hand, although some researchers (Reynolds et al., 2004; Eydinov et al., 2005) defined the statistical prior models for relative permeabilities, the process to define the relative permeability priors has not been clearly described. In this thesis, aiming at uncertainty quantification, the prior term for relative permeabilities was derived from computational experiments and was defined so that it can be consistent with the probabilistic theory. The new aspect is that the physical constraints estimated from computational experiments were incorporated into stochastic sampling by a prior probability model.

4. Although relative permeabilities are often altered in history-matching, the resulting shape of the curves is not usually examined. In this thesis, the estimated coarse-scale relative permeabilities were compared thoroughly with the reference upscaled curves which were calculated using the true fine-scale model and a dynamic upscaling method. The examination process was adopted for the first time to assess the results of both history-matching and uncertainty appraisal.

5. Quantification of uncertainty in the coarse-scale relative permeability curves, as represented with exponential functions, has been presented by Christie et al. (2002b), and that in the core-scale relative permeabilities (rock curve) has been investigated by Subbey et al. (2006). In this thesis, quantification of uncertainty in the coarse-scale relative permeability curves represented with B-splines are presented for the first time. The uncertainty quantification in that particular parameterisation for that particular scale has not been previously presented in this research area.

6. B-spline parameterisation for relative permeabilities has been tested in the core-scale history-marching (e.g., Watson et al., 1988; Subbey et al., 2006), and in the field-scale history-matching (Kulkarni and Datta-Gupta, 1999; Eydinov et al., 2005). Those have been presented for the purpose of history-matching. This thesis used the fine-scale model as "truth", and so the history-matched curves can be regarded as upscaled curves which were calculated by the optimisation algorithm. Hence, the use of B-splines to represent upscaled relative permeabilities is new in this work.

7. The effect of the parameterisation schemes on the history-matching result has been presented in the literature (Kerig and Watson, 1986; Watson et al., 1988; Kulkarni and Datta-Gupta, 1999; Eydinov et al., 2005). However, it has not been extended to the uncertainty quantification in a statistical sense. The effect of the parameterisation schemes on the uncertainty appraisal was investigated for the first time in this thesis.

8. The technique for grouping coarse-scale curves has been developed and analysed by Christie (1996) and Dupouy et al. (1998) for the purpose of upscaling. Apart from upscaling, in this study, the effect of the grouping of coarse-scale relative permeabilities for history-matching has been investigated for the first time.

9. The effect of the relation between absolute permeability and relative permeability has been presented in terms of field-scale history-matching in the literature (Kulkarni and Datta-Gupta, 1999; Reynolds et al., 2004; Eydinov et al., 2005), and has also been investigated for core-flooding experiments by Valestrand et al. (2002). However, the analysis has not been extended to the uncertainty quantification for coarse-scale reservoir models. In this study, the effect of the relation between absolute permeability and relative permeability on the uncertainty appraisal has been investigated.

10. According to Thomas (1983), the history-matching of relative permeabilities can be regarded as a search for upscaled curves, whereas two phase upscaling might be merely one of the attempts in history-matching. By nature, history-matching is closely linked to uncertainty appraisal. In addition, relative permeability is the petrophysical parameter which many researchers have been discussing for the definition, measurement and

practical use. This thesis explores the extensive research area overlapped by these four subjects: upscaling, history-matching, uncertainty quantification and the use of relative permeability.

Chapter 2

Literature Survey on Uncertainty Appraisal

The purpose of this chapter is to give a review of literature on uncertainty quantification. The main focus is uncertainty analysis conditioned to production data. This is covered in Sections 2.1 to 2.4.

History-matching and resultant uncertainty appraisal are the central parts of this thesis. The method used is Markov Chain Monte Carlo along with the Neighbourhood Approximation in a Bayesian framework. The theoretical background of this method is described in the next chapter (Chapter 3). Before moving on to the mathematical details, a variety of literature which has been published in this area is reviewed in Sections 2.1 to 2.4. It clarifies the characteristics of the method in contrast to other methods.

In addition, some papers on the perturbation of small-scale petrophysical parameters are reviewed in Section 2.5, because this also relates to the uncertainty in coarse-scale relative permeabilities which is the topic of this thesis.

2.1 Uncertainty Analysis Conditioned to Production Data

In the process of reservoir modelling, we have usually obtained prior information about the spatial distribution of petrophysical properties. The sources are well data such as core samples and well logging, geological input, seismic interpretation and so on. Moreover, we have also been given production data measured on site over some time span: e.g., oil rate, water cut, pressure, gas oil ratio, etc. It is widely acknowledged that the unique solution of unknown properties and the corresponding single production forecast cannot be obtained through reservoir modelling and flow simulation, because of the lack of measurements, the noisy data and the nature of inverse problem. Hence, it is impossible to put forward a single forecast as a result of a reservoir simulation study. Also it is not fair to believe it to be a unique "absolutely true" prediction. Instead, it is necessary to quantify the variability of the future recovery. In other words, the required task is to draw inferences based on both prior information and production history and to represent production forecast with a degree-of-belief. The degree-of-belief is the posterior probability distribution the theory of which is described in detail in the next chapter. This section gives a review of several approaches to quantify the uncertainty for reservoir performance forecast.

Floris et al. (2001) and Barker et al. (2001) summarised a variety of methods to quantify the uncertainty, referring to the results of the EC sponsored comparative project of PUNQ (Production Forecasting with UNcertainty Quantification). The key was to quantify the uncertainty on production forecasts conditioned to both static and dynamic well data. The spatial distributions of the porosity and permeability were parameterised by grid blocks, regions, pilot points or global parameters. In general, posterior sampling is required to quantify the uncertainty. For example, Markov Chain Monte Carlo (MCMC) is a technique to sample from the posterior probability distribution (PPD). This thesis also adopts the MCMC method and its theoretical background is described in Chapter 3. On the other hand, in their papers (Barker et al., 2001; Floris et al., 2001), some alternative techniques were applied to reduce the computational cost which is required by the standard MCMC method. It should be noted that there is no guarantee that these alternative techniques can sample from the full PPD correctly. Here, some of the

methods in the papers (Barker et al., 2001; Floris et al., 2001) are described in the following paragraphs for the purpose of investigating the conventional methods proposed so far.

One of the alternatives to the MCMC method is a local characterisation around a maximum of *a posteriori* (MAP) or around the multiple MAP values. For example, the Scenario Test Method (STM) (Roggero, 1997) was applied to seek for the extreme high and low forecasts around a posterior peak. Roggero (1997) described the general concept of the STM as follows. In order to create a production forecast assumption, a certain scenario is added to production history. Then, a new geological model is obtained so that it may reproduce the scenario, where the simulation result will give a new forecast based on the assumption. In the paper (Roggero, 1997), the STM was applied to find extreme forecasts by solving the two optimisation problems of both an optimistic scenario and a pessimistic scenario. Both optimistic and pessimistic realisations were selected from the history-matched models by minimising and maximising the production forecast criterion. The STM result for the PUNQ study showed quite a large range compared to some other approaches, although a reasonable explanation for the trend has not been given (Barker et al., 2001).

The approach suggested by Oliver et al. (1996) was also applied to the PUNQ case study. Although their method aimed to sample from the PPD, it utilised an optimisation scheme to generate the samples. In the optimisation step, the objective function included the realisations of the model and production data instead of the prior model and the observed data. This meant that a realisation of the model parameters was drawn from the prior probability and a realisation of the production data was drawn using the observed data and the data errors. These realisations were incorporated into the objective function and the optimised model was regarded as a sample from the PPD. This scheme was called Randomised Maximum Likelihood (RML) and has been tested on several models. Liu and Oliver (2003) demonstrated that the results of RML for 1D simple problem were similar to those from the reference MCMC. Omre et al. (1999) also tested the RML method to generate a permeability field in a 2D synthetic model and investigated the spatial distributions. They pointed out that the resulting permeability map of RML was more heterogeneous than that of the standard MCMC. As they mentioned, it is necessary to ensure

that the RML method can sample from the full PPD correctly. As for the result for the PUNQ study (Barker et al., 2001; Floris et al., 2001), a satisfactory comparison with the other methods apart from the STM method has not been conducted, because use of different simulators or the input data transferred between the simulators resulted in the bias of the production forecast.

Moreover, the MCMC result presented in the PUNQ case study (Barker et al., 2001; Floris et al., 2001) was obtained by so called Adaptive Chains instead of a standard MCMC. Whereas the proposed model of a standard MCMC depends only on the last model in the chain, the Adaptive Chain was generated so that the proposed model could depend on all the previous models in the chain. This was believed to improve the computational efficiency to generate the samples. The result of the adaptive MCMC for the PUNQ study showed the narrowest uncertainty range and the accurate estimation of the truth profile. Barker et al. (2001) concluded that the MCMC method was a rigorous sampling approach to quantify the uncertainty, although, strictly speaking, the number of the samples was not enough in this case and approximations were used in the MCMC to reduce the computational cost.

Apart from the PUNQ case study above, there were some other methods demonstrated so far relating to the sampling from PPD conditioned to the production data. For example, Oliver et al. (1997) employed a technique to approximate the likelihood to a linear function of the model parameters and to define the transitions along the MCMC in terms of independent normal deviates with mean value of zero and variance of one. The latter procedure was implemented by calculating a “matrix square root” of the covariance matrix. They demonstrated the methodology in a 2D synthetic horizontal model which had one producer well at the centre and four observation wells away from the producer well. Assuming the single-phase flow of oil, the pressure measurements were obtained from the simulation results of the truth model. The main ideas of their paper were to define the PPD and to sample the models from the PPD with MCMC. Both the variogram of the permeability distribution and the pressure measurements were taken into account to define the PPD. Here the covariance matrix corresponded to either 1) the theoretical variogram for the prior or 2) the sum of the data error covariance matrix and the modelling error covariance matrix for likelihood. An array of log-permeability values equal to the sum of 1) the

mean and 2) the product of "matrix square root" and the independent normal deviates. As for the conditioning to the pressure data, they approximated the likelihood to a linear function of the permeability values by expanding the function in a Taylor series. This approximation allowed them to select transitions of the Markov chain which could be consistent with the pressure data. Here once they calculated the "matrix square root" of the covariance matrix of the prior and likelihood, they could perturb the normal deviates map and generate the realisation of the log permeability map. It should be noted that the linear approximation of likelihood function could only be applied to simple problems as tested in the paper.

Recently, the MCMC method has been adopted along with the Neighbourhood Approximation (Sambridge, 1999a,b) which represents the parameter space using the Voronoi cells. Sambridge (1999b) applied the Neighbourhood Approximation to the sampling from PPD in a Bayesian framework which is referred to as NA-Bayes Algorithm. The applications to reservoir performance forecast have been reported by several papers of Heriot-Watt University, (Christie et al., 2002b,c; Subbey et al., 2002, 2003). Suppose that if some information on the PPD has been obtained during history-matching using a stochastic sampling like Neighbourhood Approximation Algorithm (NA) (Sambridge, 1999a), the next task is to make use of the information to sample from the PPD and predict reservoir performance in a statistical sense. NA-Bayes Algorithm utilised the MCMC method along with the Neighbourhood Approximation to evaluate the posterior expectation without conducting any additional flow simulations. An approximate PPD can be constructed from a fixed ensemble by simply setting the known PPD of each model to be constant inside its Voronoi cell. This approximation avoids calculating the real PPD of the new proposed models at each step of MCMC. In this thesis, the NA-Bayes Algorithm was chosen to evaluate the posterior expectation and P10 and P90 cut-offs. Further details on the algorithm are in Chapter 3. The characteristics of the method can be summarised as follows. First, since it adopts the standard MCMC method, the sampling technique is robust compared to the alternative methods described in this section. Secondly, the Voronoi approximation in parameter space can reduce the computational cost required for the appraisal phase. Finally, the accuracy depends on the input ensemble provided by history-matching, especially the evaluation around the high PPD regions. The stochastic history-matching technique is explained in

the Section 2.2.

2.2 History-matching Methods

History-matching is the procedure to find a model which has the maximum posterior probability, whereas uncertainty quantification requires sketching the full posterior probability distribution. The important thing is that satisfactory history-matching is required to project a reasonable uncertainty envelope on the production forecast. For example, as mentioned in the papers of the PUNQ study (Barker et al., 2001; Floris et al., 2001), the suitable parameterisation scheme which leads to a good history-matching is indispensable for the uncertainty quantification. The reason is that the important features of the PPD cannot be unveiled until a model associated with the maximum PPD has been estimated accurately.

Hence, history-matching plays an important role in quantifying uncertainty. History-matching tackles the inverse problem which is ill-posed and usually has non-unique solutions. It is a quite tedious work for a reservoir engineer to calibrate a reservoir model manually so that it can reproduce history-data correctly. There are some computational algorithms to assist the optimisation procedure of minimising misfit function. Note that the misfit function is also known as the objective function in the context of history-matching. Optimisation algorithms were classified into two categories: deterministic and stochastic, (Portella and Prais, 1999). The details of the two types of the optimisation algorithms have been summarised in several literature (Portella and Prais, 1999; Floris et al., 2001; Christie et al., 2002b; Williams et al., 2004).

The gradient-based method is a deterministic algorithm which has been widely used in the petroleum industry (Lepine et al., 1999; Roggero, 1997). In this type of algorithm, the gradient of the objective function is calculated with respect to the model parameters. This information on the gradient can be used to find a model which has the minimum value of the objective function. Steepest descent, Gauss-Newton and Levenberg-Marquhart are the well-known methods which have been utilised in a gradient-based approach. However, there is no guarantee that it can con-

verge to the global minimum instead of being trapped in a local minimum. This disadvantage was one of the motivations to use another type of algorithm, namely the stochastic approach.

The methods categorised as stochastic algorithms are Simulated Annealing, Genetic Algorithm (GA), Neighbourhood Approximation Algorithm (NA). These methods adopt the stochastic sampling in the global parameter space and were also referred to as random global optimisation methods by Ouenes et al. (1994). They described the details of the simulated annealing method and the application in the petroleum industry. Simulated annealing accepts not only "improving moves" but also "non-improving moves" with a scheduled probability to avoid trapping in a local minimum. This characteristic corresponds to the physical process of annealing of a melted material. In the computational algorithm, it is important to determine the control parameters which are related to an annealing schedule and a perturbation scheme, because they affect the convergence, (Ouenes et al., 1994). The application to history-matching was demonstrated by Portella and Prais (1999). Although Ouenes et al. (1994) mentioned, at that time (1994), that only a few reservoir problems had been history-matched using GA, nowadays there is a variety of publications which report the application of the GA and the modified GA to history-matching problems, (Romero et al., 2000; Floris et al., 2001; Schulze-Rlegert et al., 2002; Schulze-Rlegert and Haase, 2003; Tokuda et al., 2004; Williams et al., 2004; Erbas and Christie, 2006). The GA is a stochastic sampling technique which mimics natural evolution process. The crossover and mutation operations are implemented for generating new models at each iteration. Since these operations determine how the new ensemble differ from the previous ensemble, the relevant control parameters play an important role in converging to the global minimum. The other stochastic sampling algorithm is the NA which was originally developed by Sambridge (1999a) for inverse problem in seismology. At each iteration, the algorithm biases the sampling of model parameters to good-fit regions and uses Voronoi cells to refine the parameter space. The use of Voronoi cells means that the objective function of each model is representative of the region of its neighbourhood. The control parameters related to selecting and refining regions is the key to the algorithm. The amount of exploration and exploitation in the sampling is dependent on the control parameters. The NA was recently introduced to the petroleum industry by Christie et al. (2002a,b) and was followed by several other publications

which report the applications to history-matching problems, (Subbey et al., 2003; Demyanov et al., 2004; Pickup et al., 2004; Subbey et al., 2006). The details of NA are described in Chapter 3, since this thesis also utilised the NA for history-matching.

2.3 Parameterisation Methods

As mentioned previously, the parameterisation of a reservoir model is crucial both in history-matching and uncertainty quantification. The parameterisation is important not only for describing a model accurately but also setting a solvable problem in a practical sense. The number of unknown parameters is strictly limited because of so called the "curse of dimensionality". Even if the MCMC method and an appropriate history-matching algorithm are adopted, the high-dimensional parameter space is often too large to be investigated. Hence, the minimum number of parameters should be chosen carefully to reduce the computational cost. At the same time, satisfactory matching should be accomplished with a sufficient number of parameters. Suppose that the absolute permeability or the porosity field is the property to be calibrated in history-matching. Basically the number of cells in the simulation model would be the number of unknown parameters for either the porosity or the permeability field. The number of parameters can be reduced by lumping layers, homogenising regions, representing the spatial distributions with geostatistical parameters, or using pilot-point methods, (Roggero, 1997; Barker et al., 2001; Floris et al., 2001; Demyanov et al., 2004; Pickup et al., 2004).

As for relative permeabilities, some regions are defined in a simulation model so that the uniform property or function can be assigned in each region. Some typical functions are often adopted to represent a set of relative permeability curves and then the coefficients of the functions can be calibrated during history-matching (e.g., Christie et al., 2002b; Subbey et al., 2003). Many publications in the petroleum industry have reported the developments of typical functions of relative permeabilities for core-flooding experiments, (Corey, 1954; Chierici, 1981; Firoozabadi and Aziz, 1986; Honapour et al., 1986; Siddiqui et al., 1999). However, only a few researchers (e.g., Hewett et al., 1998) have investigated the typical shapes of coarse-scale rela-

tive permeabilities, although the history-matching is usually conducted at the coarse scale. The parameterisation of relative permeabilities is discussed in more detail in the following chapters.

2.4 Likelihood Definition

Because it is basically impossible to evaluate posterior probability in a direct manner, it is calculated through the likelihood function in the Bayesian framework. Hence, the accurate quantification of uncertainty hinges on the appropriate calculation of the likelihood function. This section describes some works related to the definition of the likelihood function. The theory of Bayesian statistics is described in Chapter 3.

Data errors in the production history are usually expressed statistically and is incorporated into likelihood function. For example, Floris et al. (2001) assumed that the time-series data errors would be distributed independently and follow Gaussian distribution. These approximations resulted in a well-known form of logarithmic probability which is the sum of the squares of each discrepancy. Although it leads to the popular method of least-squares, it should be emphasised that the justification of the least-squares form for a logarithmic likelihood relies on the assumptions of the independence and Gaussian distribution of data error.

In addition to data errors, as Lepine et al. (1999) pointed out, model errors should be taken into account to define likelihood function, if the error is not small. The sources of model error are linked to the exactness of solution, the resolution of reservoir model and the accuracy of the fixed parameters. Glimm et al. (2001) described the errors of upscaling and numerical solution. They investigated the difference between the fine-scale solution of a "truth" reservoir model and the coarse-scale solution of another realisation. Model error is also referred to as solution error.

O'Sullivan (2004) and O'Sullivan and Christie (2005) characterised the mean and covariance of solution error for a synthetic reservoir model. In the model, oil viscosity was an unknown parameter to be determined in history-matching. Another unknown, the detailed fine-

scale permeability distribution, was ignored in the history-matching, because a coarse-scale analytical solution was adopted to calculate the production profile. Here the solution error arose from the simplified reservoir model and the approximated solution at the coarse scale, in contrast with the "truth" detailed permeability field and "truth" profile at the fine scale. First, the mean and covariance of the solution error were estimated and were interpolated for a range of viscosity values. Then the solution error model was incorporated into the likelihood function so that the coarse-scale solution could be comparable to the hypothetical observed data without any biases. This process was the key to estimating the unknown parameter, oil viscosity in their model, and predicting the uncertainty of production forecast, (O'Sullivan, 2004; O'Sullivan and Christie, 2005).

In this way, the solution error model can be incorporated into the likelihood function to correct the bias arising from averaged properties, simplified model and computational errors. Because of the limitation of computational resources, the model error is unavoidable unless it is compensated in some way. Moreover, as mentioned in the previous sections, some parameters are assumed to be constant in history-matching to avoid the curse of dimensionality. If the fixed parameters lead to large amount of error due to the approximation, the resulting model error should be involved in likelihood definition. Therefore, it can be said that the choice of calibration parameters and the parameterisation scheme are closely linked to the likelihood definition.

The trade-off between the computational cost and the number of parameters is a big issue in the construction of the likelihood surface. Experimental design is one of the tools to deal with a large parameter space using a limited number of flow simulations, (e.g., White et al., 2001). The applicability to real problems relies on the accuracy of the interpolation of response surface.

2.5 Uncertainty Analysis for Perturbation of Petrophysical Parameters

In contrast to the uncertainty analysis conditioned to production data, this section gives a brief summary about some methods to quantify the uncertainty related to the small-scale heterogeneity and viscous fingering.

Zhang and Tchelepi (1999) examined heterogeneity induced dispersion in immiscible two-phase flow. The proposed method of the moment equation does not require a flow simulation for each realisation. Through transforming to coordinates attached to streamlines, the mean saturation and the variance were evaluated from the time of flight and transverse displacement PDF. For a horizontal two-dimensional case, they assumed that the streamlines change little with time so that the total velocity components were functions of space only. In addition, they considered uniform mean flow, which corresponded to displacement between two large arrays of injection and production wells where a constant mean gradient was maintained. As the variance or the correlation scale of log permeability increased, the dispersive behaviour became more apparent. Zhang et al. (2000) extended this Lagrangian, statistical moment approach to flow in bounded domains and complex flow patterns due to the presence of wells. There were several assumptions and approximations made in their method. (1) The moment method is limited in its applications to relatively small variances in log permeability because of the first-order perturbation approximations. (2) Saturation dependence in the total flow was neglected, because the total flow was at steady state. (3) Gravity and capillary pressure effects were neglected.

For homogeneous media, King and Dunayevsky (1989) examined the fluctuations of saturation planes around their mean position, due to the viscous coupling, which depends on total mobility ratio evaluated across the front. Furthermore, for heterogeneous media, Artus et al. (2004) took into account both of the effect of viscous coupling and the influence of the perturbations of the permeability field with a saturation map. From the Fourier transform of the permeability field in a stratified structure, they extracted the spectrum of the permeability field and derived the spectrum of the saturation front. Then, the shape of the front was predicted with an inverse

Fourier transform. The comparison between the reference flow simulations and their analytical predictions indicated good agreement except for the amplitude at low frequencies. Noetinger et al. (2004) dealt with the isotropic media where permeability was a function of both of two dimensional coordinates. They derived the pressure perturbation due to a permeability fluctuation to relate the statistics of the front line to the stochastic properties of the heterogeneous media. Then, they investigated a balance between the perturbing effects of the heterogeneity and the stabilising effects of the viscous coupling, which lead to a stationary behaviour of the front. For their approaches, gravity and capillary effects were neglected. In addition, porosity was assumed to be constant and relative permeability curves were also assumed to be uniform.

Hastings et al. (2003) presented a separation-of-scale method for small-scale heterogeneity with varying relative permeabilities. For a synthetic model of a fluvial reservoir cross section, a single pressure solution was used to define a set of streamlines. Then, it was fixed to represent the coarse-scale heterogeneity. The streamlines of channel bodies were used for generating the realisations of the small-scale properties within the channel. In the proposed method, each streamline was homogenised using the new 1D upscaling solution to an equivalent homogeneous streamline simulation with constant porosity, permeability, and relative permeabilities. They derived analytically the mean mobility of the realisations along 1D streamline by utilising an existing method for upscaling fractional flow. They hypothesised that the mean production and breakthrough time for all realisations of the small-scale properties could be predicted using the mean mobility in a streamline simulation.

The works described in this section have investigated the flow phenomena related to small-scale heterogeneity. They aim at predicting the effect of small-scale heterogeneity on the oil recovery in a reservoir. In this thesis coarse-scale relative permeabilities in which small-scale heterogeneity should be encapsulated are investigated. The details of coarse-scale relative permeabilities are explained in Section 4.5.

Chapter 3

Probability Theory and Application

This chapter gives a brief summary of Bayesian inference and the Markov Chain Monte Carlo and NA-Bayes algorithms. Bayes theory and the MCMC and NA methods are used in this thesis, and so this chapter provides the background to the material on which the current work is based.

3.1 Bayesian Inference

As described in Section 2.1, a reservoir engineer needs to predict future production of a reservoir, although it is impossible to obtain a unique and "absolutely true" solution. Hence, it is necessary to express a reservoir model and the corresponding future production with a probability. In Bayesian inference, a probability is regarded as a degree-of-belief or plausibility, (Sivia, 1996). Here, the probability should represent how much a reservoir engineer thinks that a model or profile is true based on the relevant information. The information related to the prediction is the observed production data and the prior information on reservoir properties. Here the probability of interest is a probability of a model given production history. In the rest of this thesis, production history is referred to as "history". Bayes' theorem is quite useful when

calculating the probability of a model, given history. This probability is referred to as the posterior probability. The reason why Bayes' theorem is a useful tool is that it relates the posterior probability to the likelihood function which can be calculated, (Sivia, 1996). The likelihood function represents the probability of the history given a model. Because the history has been already given and is fixed in practice, we refer to the likelihood function of a model instead of the probability of data.

Bayes' theorem can be derived easily from the basic probability theory. Suppose that prob(X) represents the probability of 'X', prob(X, Y) denotes the probability of 'X and Y', and prob($X|Y$) denotes the probability of 'X given Y'. The probability of 'Y and X' being true is the same as that of 'X and Y' being true. Hence, firstly, it is obvious that prob(Y, X) = prob(X, Y). Secondly, using the product rule of probability, both sides of the equation can be rewritten:

$$\text{prob}(X|Y) \times \text{prob}(Y) = \text{prob}(Y|X) \times \text{prob}(X). \tag{3.1.1}$$

Finally, Bayes' theorem is derived directly from Equation (3.1.1):

$$\text{prob}(X|Y) = \frac{\text{prob}(Y|X) \times \text{prob}(X)}{\text{prob}(Y)}. \tag{3.1.2}$$

A marginalisation is expressed as the integration of prob(Y, X) with respect to X:

$$\text{prob}(Y) = \int_{-\infty}^{\infty} \text{prob}(Y, X)\, dX \tag{3.1.3}$$

$$= \int_{-\infty}^{\infty} \text{prob}(Y|X) \times \text{prob}(X)\, dX. \tag{3.1.4}$$

By substituting Equation (3.1.4) into Equation (3.1.2), Bayes' theorem of Equation (3.1.2) can be rewritten as another form:

$$\text{prob}(X|Y) = \frac{\text{prob}(Y|X) \times \text{prob}(X)}{\int_{-\infty}^{\infty} \text{prob}(Y|X) \times \text{prob}(X)\, dX}. \tag{3.1.5}$$

Here, prob($X|Y$) represents the posterior probability, prob($Y|X$) is the likelihood function, and prob(X) is the prior probability. The posterior probability can be calculated from the product of the likelihood function and the prior probability. The denominator of the right-hand side is

referred to as the normalisation constant. Further details on Bayesian inference are described in Sivia (1996) and Jaynes and Bretthorst (2003).

In order to make these equations familiar to the petroleum industry, especially for reservoir simulation, Equation (3.1.5) can be rewritten by using a different nomenclature.

$$\text{prob}(\mathbf{m}|\mathbf{o}) = \frac{\text{prob}(\mathbf{o}|\mathbf{m}) \times \text{prob}(\mathbf{m})}{\int \text{prob}(\mathbf{o}|\mathbf{m}) \times \text{prob}(\mathbf{m})\, d\mathbf{m}}. \tag{3.1.6}$$

where $\int d\mathbf{m} = \int\int\cdots\int dm_1 dm_2 \ldots dm_M$ for $\mathbf{m} = (m_1, m_2, \ldots, m_M)^T$. The vector $\mathbf{m}$ represents a set of parameters which describes a reservoir model. For example, if horizontal and vertical permeabilities, kh and kv, are the properties to be calibrated in a reservoir simulation model, the vector $\mathbf{m}$ consists of the two parameters and $\mathbf{m} = (kv, kh)^T$. If four coefficients of certain functions representing relative permeability should be adjusted in history-matching, the vector $\mathbf{m}$ is a four-dimensional vector which consists of the four coefficients. prob($\mathbf{m}$) represents the joint probability for all components in the vector $\mathbf{m}$. Joint probability denotes probabilities of two or more events occurring at the same time. The vector $\mathbf{o}$ represents a set of observed data in the reservoir. For example, imagine that oil rate, water cut, gas oil ratio and well bottom-hole pressure are observed data in history-matching. Then, the vector $\mathbf{o}$ consists of these four production data for all of the measured time steps and all the observed wells. Again, prob($\mathbf{o}$) represents the joint probability for all components in the vector $\mathbf{o}$.

While the term prob($\mathbf{m}$) in Equation (3.1.6) is the prior probability which represents one's state of knowledge about the model before making an observation, the posterior probability prob($\mathbf{m}|\mathbf{o}$) represents one's state of knowledge about model after making an observation. The likelihood function, prob($\mathbf{o}|\mathbf{m}$), is the probability one sees an observation given that the model is correct. This function is used to update the prior probability. The normalisation constant of the denominator in the right-hand side can be omitted in the following way:

$$\text{prob}(\mathbf{m}|\mathbf{o}) \propto \text{prob}(\mathbf{o}|\mathbf{m}) \times \text{prob}(\mathbf{m}). \tag{3.1.7}$$

This is a simple expression of Bayes' theorem which implies how the state of knowledge of

prob(**m**) should be changed after an observation prob(**o**|**m**).

3.2 Markov Chain Monte Carlo

This section provides the explanation of a numerical scheme to evaluate a forecast profile $Q(\mathbf{m})$ given history data **o** in the Bayesian framework. The numerical scheme is referred to as the Markov Chain Monte Carlo (MCMC) method.

3.2.1 Markov Chain Monte Carlo for Bayesian Inference

Suppose that $Q(\mathbf{m})$ is a production forecast of interest and, for instance, represents oil production rate of a reservoir at a certain time t. The measures of the forecast are usually its mean, variance, quantiles, the most likely estimates, etc. The mean and variance are the first moment about the origin and the second moment about the mean, respectively. These moments of $Q(\mathbf{m})$ can be expressed in terms of the conditional expectations of functions $Q(\mathbf{m})$. For example, the mean of $Q(\mathbf{m})$ is defined by:

$$E[Q(\mathbf{m})|\mathbf{o}] = \int Q(\mathbf{m}) \, \text{prob}(\mathbf{m}|\mathbf{o}) \, d\mathbf{m}. \tag{3.2.1}$$

Here, the expression of $E[x]$ denotes the expectation of variable x. On top of that, note that the probability in the right hand side in Equation (3.2.1) should be the posterior probability prob(**m**|**o**), because the observed production data **o** is available. In the same manner, the variance of $Q(\mathbf{m})$ is defined by:

$$E[(Q(\mathbf{m}) - E[Q(\mathbf{m})])^2|\mathbf{o}] = \int (Q(\mathbf{m}) - E[Q(\mathbf{m})])^2 \, \text{prob}(\mathbf{m}|\mathbf{o}) \, d\mathbf{m}. \tag{3.2.2}$$

Not only the mean and variance but also the marginal distribution and other features can be expressed by high dimensional integrals, (Sambridge, 1999b).

Consider the problem calculating the posterior expectation of Equation (3.2.1) as an example of these integrals. Note that the same manipulations can be conducted for the other integrals. Substituting Equation (3.1.6) into Equation (3.2.1), it becomes:

$$E[Q(\mathbf{m})|\mathbf{o}] = \int Q(\mathbf{m}) \frac{\text{prob}(\mathbf{o}|\mathbf{m}) \times \text{prob}(\mathbf{m})}{\int \text{prob}(\mathbf{o}|\mathbf{m}) \times \text{prob}(\mathbf{m})\, d\mathbf{m}} d\mathbf{m}. \tag{3.2.3}$$

Hence, for Bayesian inference, it is required to calculate not only the integral for the expectation but also the integral for the normalisation constant. Calculating these integrations can be the source of computational difficulties, because it requires the integration over possibly high-dimensional parameters. According to Gilks et al. (1996), a Monte Carlo integration using Markov chains can overcome these difficulties, and this is referred to as Markov Chain Monte Carlo (MCMC). In general, Monte Carlo integration provides sample mean to approximate the expectation of interest. Specifically, MCMC draws samples from the required distribution by running a Markov chain and does not need to calculate the normalisation constant as described below.

3.2.2 Monte Carlo Integration

Consider the problem of calculating the integral in Equation (3.2.1). Let $h(\mathbf{m})$ be a probability density function for $\mathbf{m}$. Then Equation (3.2.1) becomes:

$$E[Q(\mathbf{m})|\mathbf{o}] = \int Q(\mathbf{m}) \,\text{prob}(\mathbf{m}|\mathbf{o})\, d\mathbf{m} \tag{3.2.4}$$

$$= \int \frac{Q(\mathbf{m}) \,\text{prob}(\mathbf{m}|\mathbf{o})}{h(\mathbf{m})} h(\mathbf{m})\, d\mathbf{m} \tag{3.2.5}$$

$$= E_h\left[\frac{Q(\mathbf{m}) \,\text{prob}(\mathbf{m}|\mathbf{o})}{h(\mathbf{m})}\right], \tag{3.2.6}$$

where E_h denotes expectation with respect to h. Here, when the mean of $\frac{Q(\mathbf{m}) \,\text{prob}(\mathbf{m}|\mathbf{o})}{h(\mathbf{m})}$ is denoted as μ, it is expressed as:

$$E_h\left[\frac{Q(\mathbf{m}) \,\text{prob}(\mathbf{m}|\mathbf{o})}{h(\mathbf{m})}\right] = \mu. \tag{3.2.7}$$

In the same way, the variance, σ^2, is expressed as

$$E_h\left[\left(\frac{Q(\mathbf{m})\,\mathrm{prob}(\mathbf{m}|\mathbf{o})}{h(\mathbf{m})}-\mu\right)^2\right]=\sigma^2. \tag{3.2.8}$$

If a sample $\{\mathbf{m^{(1)}},\mathbf{m^{(2)}},\ldots,\mathbf{m^{(n)}}\}$ from $h(\mathbf{m})$ is available, the sample mean, denoted by $\hat{\mu}$, becomes:

$$\hat{\mu}=\frac{1}{n}\sum_{k=1}^{n}\frac{Q(\mathbf{m^{(k)}})\,\mathrm{prob}(\mathbf{m^{(k)}}|\mathbf{o})}{h(\mathbf{m^{(k)}})}. \tag{3.2.9}$$

When a large sample from $h(\mathbf{m})$ is available, the population mean μ is estimated by a sample mean $\hat{\mu}$:

$$E_h\left[\frac{Q(\mathbf{m})\,\mathrm{prob}(\mathbf{m}|\mathbf{o})}{h(\mathbf{m})}\right]\approx\frac{1}{n}\sum_{k=1}^{n}\frac{Q(\mathbf{m^{(k)}})\,\mathrm{prob}(\mathbf{m^{(k)}}|\mathbf{o})}{h(\mathbf{m^{(k)}})}. \tag{3.2.10}$$

This is the numerical method referred to as Monte Carlo integration. The variance of the sample mean is given by

$$E_h[(\hat{\mu}-E_h[\hat{\mu}])^2]=\frac{E_h\left[\left(\sum_{k=1}^{n}\frac{Q(\mathbf{m^{(k)}})\,\mathrm{prob}(\mathbf{m^{(k)}}|\mathbf{o})}{h(\mathbf{m^{(k)}})}-E_h\left[\sum_{k=1}^{n}\frac{Q(\mathbf{m^{(k)}})\,\mathrm{prob}(\mathbf{m^{(k)}}|\mathbf{o})}{h(\mathbf{m^{(k)}})}\right]\right)^2\right]}{n^2} \tag{3.2.11}$$

$$=\frac{\sum_{k=1}^{n}E_h\left[\left(\frac{Q(\mathbf{m^{(k)}})\,\mathrm{prob}(\mathbf{m^{(k)}}|\mathbf{o})}{h(\mathbf{m^{(k)}})}-\mu\right)^2\right]}{n^2} \tag{3.2.12}$$

$$=\frac{\sigma^2}{n}. \tag{3.2.13}$$

Here, note that the samples are independent. Equation (3.2.13) means that the standard deviation of the mean of n samples is equal to the population standard deviation σ divided by $\sqrt{n}$. Therefore, the accuracy of the approximation in Equation (3.2.10) depends on $\frac{\sigma}{\sqrt{n}}$, , (Sambridge, 1999b). In other words, the accuracy of Monte Carlo integration does not depend on the dimensionality but the number of samples and the population variance. In summary, Monte Carlo integration can evaluate the integral in Equation (3.2.1):

$$E[Q(\mathbf{m})|\mathbf{o}]=E_h\left[\frac{Q(\mathbf{m})\,\mathrm{prob}(\mathbf{m}|\mathbf{o})}{h(\mathbf{m})}\right] \tag{3.2.14}$$

$$\approx\frac{1}{n}\sum_{k=1}^{n}\frac{Q(\mathbf{m^{(k)}})\,\mathrm{prob}(\mathbf{m^{(k)}}|\mathbf{o})}{h(\mathbf{m^{(k)}})}, \tag{3.2.15}$$

where the generating density $h(\mathbf{m})$ is usually called the importance density and the sampling from $h(\mathbf{m})$ is called importance sampling, (Gamerman, 1997).

As mentioned above, not only increasing the number of samples but also minimising the population variance σ^2 leads to minimising the estimation error of Equation (3.2.14). According to some literature on MCMC (e.g., Gilks et al., 1996; Gamerman, 1997; Sambridge, 1999b), the population variance σ^2 depends on the choice of $h(\mathbf{m})$. Moreover, the optimal choice in terms of minimising the population variance σ^2 is to take $h(\mathbf{m}) \propto$ constant $\times$ prob$(\mathbf{m}|\mathbf{o})$. Letting $h(\mathbf{m}) \approx$ prob$(\mathbf{m}|\mathbf{o})$, Equation (3.2.15) becomes:

$$E[Q(\mathbf{m})|\mathbf{o}] \approx \frac{1}{n}\sum_{k=1}^{n} Q(\mathbf{m}^{(\mathbf{k})}). \tag{3.2.16}$$

Here, one way of sampling $\{\mathbf{m}^{(\mathbf{k})},\ k = 1, 2, \ldots, n\}$ from the posterior probability prob$(\mathbf{m}|\mathbf{o})$ is to generate a Markov Chain having prob$(\mathbf{m}|\mathbf{o})$ as its stationary distribution. A Markov Chain is a stochastic "time" process where given the present state, past and future states are independent apart from its adjacent states. The next state depends only on the current state of the chain. The independent samples in a Markov Chain can be used to estimate the expectation for Monte Carlo integration. This is the numerical scheme referred to as Markov Chain Monte Carlo. In practice, after a sufficient number of "burn-in" iterations, all of the remaining samples are regarded as independent samples and are used to calculate the expectation of Equation (3.2.16), (Gilks et al., 1996). In this way, the burn-in samples are usually discarded for this calculation in order to avoid the effect of the initial condition.

3.2.3 Markov Chain and Gibbs Sampler

In general, a Markov Chain is a discrete stochastic process $\{m^{(0)}, m^{(1)}, \ldots\}$ with the property that the distribution of $m^{(t+1)}$, given all previous values of the process $\{m^{(0)}, m^{(1)}, \ldots, m^{(t)}\}$, only depends upon $m^{(t)}$. It can be written as:

$$\text{prob}[\, m^{(t+1)} \in A \mid m^{(0)}, m^{(1)}, \ldots, m^{(t)} \,] = \text{prob}[\, m^{(t+1)} \in A \mid m^{(t)} \,] \ \text{ for all set } A \subset S, \tag{3.2.17}$$

where S is the state space. The transition probabilities P_{ij} are defined by:

$$P_{ij} = \text{prob}[\, m^{(t+1)} = j \mid m^{(t)} = i \,]. \tag{3.2.18}$$

where $P_{ij} \geqslant 0$, $\sum_{j \in S} P_{ij} = 1$. The transition probabilities do not depend on t.

As mentioned above, the task is to use MCMC for the purpose of Bayesian inference: e.g., calculating the posterior expectation. Then, the requirement for this purpose is the asymptotic behaviour of the chain to a stationary distribution as the number of iterations increases, (Gamerman, 1997). In this subsection, for simplicity, a stationary distribution is denoted by $\pi(m)$ for one-dimensional parameter m, or $\pi(\mathbf{m})$ for multi-dimensional parameter vector $\mathbf{m}$, whereas it is taken to be the posterior probability prob($\mathbf{m}|\mathbf{o}$) for the Bayesian inference. Here, for calculating the posterior expectation by MCMC, the key requirement is that $\pi(m)$ should be the stationary distribution of the chain. Then, for ensuring this requirement, the chain has to satisfy three properties, (Gilks et al., 1996). These conditions are that the chain needs to be *irreducible*, *aperiodic* and *positive recurrent*. The condition for *positive recurrence* is the existence of a stationary probability distribution for m, that is there exists $\pi(m)$ such that

$$\sum_{i \in S} \pi(i) P_{ij} = \pi(j) \quad \text{for all } j \in S. \tag{3.2.19}$$

The further mathematical descriptions and proofs on the convergence to stationary distribution were provided in the literature (e.g., Gilks et al., 1996; Gamerman, 1997) and are not repeated here. A sufficient condition for the distribution of $m^{(t)}$ to converge to a stationary distribution is the *detailed balance equation*. This condition is written as:

$$\pi(i) P_{ij} = \pi(j) P_{ji} \quad \text{for all } i, j \in S. \tag{3.2.20}$$

Therefore, if a numerical scheme to generate a chain satisfies the condition of Equation (3.2.20), the chain can be utilised to calculate posterior expectation of Equation (3.2.16).

According to Gilks et al. (1996), there are some algorithms to generate a Markov Chain satisfying Equation (3.2.20). Metropolis-Hastings algorithm is the most simple method among

them. Then, the Gibbs sampler is one of the special forms of Metropolis-Hastings algorithm and can be implemented easily in practical problems. In Metropolis-Hastings, at each t, supposing the current state $m^{(t)} = X$, the next state $m^{(t+1)}$ is chosen by first sampling a candidate point Y from a proposal distribution $q(Y \mid X)$. The candidate point Y is then accepted with probability $\alpha(X \to Y)$ where

$$\alpha(X \to Y) = \min\left(1, \frac{\pi(Y)q(X \mid Y)}{\pi(X)q(Y \mid X)}\right). \tag{3.2.21}$$

If the candidate point is accepted, the next state becomes $m^{(t+1)} = Y$. If the candidate is rejected, the chain does not move, $m^{(t+1)} = m^{(t)} = X$. Here, the transition probability is the product of the two functions and is written as:

$$P_{XY} = q(Y \mid X)\,\alpha(X \to Y) \tag{3.2.22}$$

It can be easily shown that Equations (3.2.21) and (3.2.22) reduce to Equation (3.2.20). It can also be shown that the theory mentioned above for a discrete variable m is held for a continuous random variable m, where the summations are replaced by the integrals.

As stated above, the Gibbs sampler is the special case of Metropolis-Hastings algorithm. In the case of an M-dimensional parameter vector $\mathbf{m}$, it is often more convenient and computationally efficient to update the components of a vector, $\mathbf{m} = (m_1, m_2, \ldots, m_M)^T$, one by one rather than updating the whole of the components as a group, (Gilks et al., 1996). Let $\mathbf{m}_{-i} = (m_1, m_2, \ldots, m_{i-1}, m_{i+1}, \ldots, m_M)^T$ so that $\mathbf{m}_{-i}$ comprises all of the components of $\mathbf{m}$ except m_i. Note that an iteration of this algorithm comprises M updating steps. At each step in the Gibbs sampler, one component of the vector $\mathbf{m}$ is perturbed along its parameter axis. Then, one iteration is completed when all dimensions have been cycled through once, and a complete new vector has been generated, (Sambridge, 1999b). Letting $m_i^{(t)}$ denote the state of m_i at the end of iteration t, imagine that its current state is defined so that $m_i^{(t)} = X$. In the Gibbs sampler, for step i of iteration $t+1$, $m_i^{(t)}$ is updated as follows. The candidate Y for $m_i^{(t+1)}$ is generated from a proposed distribution $q_i(Y \mid X, \mathbf{m}_{-i}^{(t)})$. Here, $\mathbf{m}_{-i}^{(t)}$ denotes the value of $\mathbf{m}_{-i}$ after completing step $i-1$ of the iteration $t+1$:

$$\mathbf{m}_{-i}^{(t)} = (m_1^{(t+1)}, m_2^{(t+1)}, \ldots, m_{i-1}^{(t+1)}, m_{i+1}^{(t)}, \ldots, m_M^{(t)})^T, \tag{3.2.23}$$

where components $1, 2, \ldots, i-1$ have already been updated. For the Gibbs sampler, the proposed distribution $q_i(Y \mid X, \mathbf{m}_{-i}^{(t)})$ for updating the ith component of $\mathbf{m}^{(t)}$ is defined by:

$$q_i(Y \mid X, \mathbf{m}_{-i}^{(t)}) = \pi(Y \mid \mathbf{m}_{-i}^{(t)}) \tag{3.2.24}$$

$$= \frac{\pi\left(\mathbf{m} = (m_1^{(t+1)}, m_2^{(t+1)}, \ldots, m_{i-1}^{(t+1)}, Y, m_{i+1}^{(t)}, \ldots, m_M^{(t)})^T\right)}{\int \pi\left(\mathbf{m} = (m_1^{(t+1)}, m_2^{(t+1)}, \ldots, m_{i-1}^{(t+1)}, Y, m_{i+1}^{(t)}, \ldots, m_M^{(t)})^T\right) dY} \tag{3.2.25}$$

where Y is a continuous random variable. $\pi(Y \mid \mathbf{m}_{-i}^{(t)})$ represents the conditional probability of $m_i = Y$ under the fixed remaining components, $\mathbf{m}_{-i}^{(t)}$. Then, as in the Metropolis-Hastings algorithm, suppose that the candidate would be accepted with the probability $\alpha_i((\mathbf{m}_{-i}, X) \to Y)$ in the following scheme:

$$\alpha_i((\mathbf{m}_{-i}^{(t)}, X) \to Y) = \min\left(1, \frac{\pi(Y \mid \mathbf{m}_{-i}^{(t)})\, q_i(X \mid Y, \mathbf{m}_{-i}^{(t)})}{\pi(X \mid \mathbf{m}_{-i}^{(t)})\, q_i(Y \mid X, \mathbf{m}_{-i}^{(t)})}\right). \tag{3.2.26}$$

Note that $q_i(. \mid .)$ and $\alpha_i(.)$ update only the ith component $m_i{}^{(t)}$ and the other components $\mathbf{m}_{-i}^{(t)}$ are fixed. Actually, Equation (3.2.24) reduces to an acceptance probability $\alpha_i(.)$ of 1 in Equation (3.2.26). This means that if a candidate is drawn from $\pi(m_i \mid \mathbf{m}_{-i}^{(t)})$ at each ith step in each iteration, it is always accepted by the criterion of Equation (3.2.26). Then, it can be easily shown that the Gibbs sampler satisfies the detailed balance equation, because $\alpha_i(.) = 1$ and $q_i(Y \mid X, \mathbf{m}_{-i}^{(t)}) = \pi(Y \mid \mathbf{m}_{-i}^{(t)})$. Because $\pi(\mathbf{m})$ is uniquely determined by the set of its 1-D conditional probabilities, the Gibbs sampler can generate samples from the target distribution $\pi(\mathbf{m})$, (Gilks et al., 1996). According to the Equation (3.2.25), the transition probability for the ith component, $m_i^{(t+1)}$, does not depend on the current state of the ith component, $m_i^{(t)}$, but is conditioned to the current state of all the other components, $\mathbf{m}_{-i}^{(t)}$. In this way, each updating step produces a move in the direction of a coordinate axis. Here, the only task to be considered in the Gibbs Sampler is to draw random deviates from the ith axis 1-D conditional distribution $\pi(m_i \mid \mathbf{m}_{-i}^{(t)})$. One way of doing this is the rejection method, (Press et al., 1992; Sambridge, 1999b). In contrast to the other simple methods for generating a random deviate, the benefit of

the rejection method is that it does not need to calculate the cumulative distribution for 1-D conditional PDF, $\pi(m_i \mid \mathbf{m}_{-i}^{(t)})$. When the Gibbs sampler with the rejection method is adopted to generate the ensemble from the posterior probability in Equation (3.1.7), one of its benefits is that it does not need to calculate the normalisation constant. This is because the rejection method requires only the ratio of 1-D conditional PDFs of posterior probabilities. Actually the same benefit can be said for Metropolis-Hastings algorithm of Equation (3.2.21). In Bayesian inference of Equation (3.1.7), the known term is $\text{prob}(\mathbf{o}|\mathbf{m})\,\text{prob}(\mathbf{m})$. But it is not easy to evaluate the normalisation constant $\int \text{prob}(\mathbf{o}|\mathbf{m})\,\text{prob}(\mathbf{m})\,d\mathbf{m}$ because of the high-dimensional integrals. Therefore, the benefit of MCMC mentioned above is important for the Bayesian inference.

This paragraph gives an explanation on the rejection method which can be adopted in the Gibbs sampler to sample from 1-D conditional PDF. It can draw deviates from the 1-D PDF by choosing a random point in two dimensions in the following way. In general, the rejection method requires a comparison function $f(x)$ which has finite area and lies everywhere above the target PDF $\text{prob}(x)$, (Press et al., 1992). Instead of evaluating directly the area of the target PDF itself, this scheme first draws a random deviate x_0 from a comparison function $f(x)$ and then draws a second uniform deviate between 0 to 1 to be compared with the ratio of $\frac{\text{prob}(x_0)}{f(x_0)}$. If the second deviate is less than $\frac{\text{prob}(x_0)}{f(x_0)}$, x_0 is accepted as a random deviate from the target PDF $\text{prob}(x)$. Otherwise, it is rejected and the same process is repeated from drawing the first deviate x_k until x_k is accepted so that the second deviate is less than $\frac{\text{prob}(x_l)}{f(x_l)}$. Note that the ratio of the number of accepted deviates to the total number merely depends on the ratio of the area of the target PDF to the comparison function, not on the details of the shape of either function. So, if the comparison function is chosen so that its indefinite integral is known analytically and is also analytically invertible to give x as a function of "area under the comparison function to the left of x", a random deviate can be generated from the target PDF with the guide of the comparison function, (Press et al., 1992).

To summarise, the Gibbs sampler with the rejection method can generate a Markov Chain for calculating the posterior expectation in the Bayesian framework, which is expressed as the integration of Equation (3.2.1). It can be also applied to the other integrals such as the variance

and 1D marginal distribution in the same manner. As for reservoir performance forecast, the method requires a number of flow simulations to evaluate a ratio of 1-D conditional PPD at each step. Sambridge (1999b) adopted the neighbourhood approximations in conjunction with the Gibbs sampler. The approach aims to approximate the parameter space and reduce the computational cost. This algorithm is referred to as NA-Bayes Algorithm and is explained below.

3.3 Neighbourhood Approximation (NA) Algorithm and NA-Bayes Algorithm

In this section, before moving on to the NA-Bayes Algorithm, the NA algorithm is explained as one of the stochastic history-matching methods, because the resulting ensemble constructs the approximate PPD over the parameter space and is closely linked to the NA-Bayes Algorithm. After that, the NA-Bayes Algorithm, which samples from the approximate PPD, is described. The objectives of a sequence of the numerical schemes are to sample from the approximate PPD and contribute to Bayesian inference through MCMC.

The Neighbourhood Approximation (NA) algorithm is a stochastic sampling algorithm, which was originally developed to solve an inverse problem in seismology, (Sambridge, 1999a). The algorithm biases the sampling at each iteration based on the information which has been obtained from previous iterations. The sampling of model parameters is biased to regions of parameter space where a good fit is likely. The algorithm aims to overcome a concern of stochastic sampling that is poor convergence. The central idea of the algorithm is to bias the sampling to high PPD regions of the parameter space using Voronoi cells. Here, the high PPD region is regarded as low misfit or good history-matching region. At each iteration, the algorithm generates n_s models and calculates their misfit values. Then, the neighbourhood regions are defined by the Voronoi cells which can be calculated by the coordinates of the models in parameter space. Thus it can be said that the misfit of each model is representative of the region of its neighbourhood. After placing the approximate misfit values throughout the parameter space, it explores

and refines the regions as follows. All the models are ranked to determine the best n_r Voronoi cells. Note that the models include all the previously generated models. Then, n_s new models are generated in these n_r Voronoi cells. This means that n_s/n_r models are newly sampled in each cell so that the n_s/n_r models may scatter uniformly inside a cell. To summarise, at each iteration, new samples are concentrated in the neighbourhoods surrounding the high PPD models. There are two tuning parameters which control the performance of the algorithm. The two parameters are n_s and n_r. These parameters control the amount of exploration and exploitation of the stochastic sampling.

Sambridge (1999b) also applied this Neighbourhood Approximation to the sampling from the posterior probability distribution (PPD) in a Bayesian framework. Suppose that the information on the PPD has been obtained during the history-matching with the NA algorithm. Here, the next task is to evaluate the posterior expectation using MCMC without conducting any further flow simulations. The key is that the known PPD of each model is set to be constant inside its Voronoi cell. In other words, an approximate PPD can be constructed from a fixed ensemble. This approximation allows us to avoid calculating the real PPD of the new proposed models at each step of the Gibbs sampler. Sambridge (1999b) used the rejection method in the Gibbs sampler to draw random deviates from 1-D conditional PDF of the posterior PDF prob(**m**|**o**). Suppose that n' models have been obtained as the result of the history-matching phase and the model parameter vector **m** has M components. So the M-dimensional model space has been split into n' Voronoi cells in each of which the posterior PDF is constant. The 1-D conditional PDF for each axis is simply a set of step functions with abrupt changes at the points where axis passes into a new Voronoi cell. Letting $P_{NA}(x_i \mid x_{-i})$ denote the 1-D conditional PDF for the i-axis and defining its range as (l_i, u_i), the task is to draw a random deviate from $P_{NA}(x_i \mid x_{-i})$ with the rejection method. In order to conduct the rejection method, Sambridge chose the comparison function as a uniform function so that it could be equal to the maximum of the 1-D conditional PDF, $P_{NA}(x_i^{max} \mid x_{-i})$ in the range of (l_i, u_i). By this choice, the first random deviate x_i^p from the comparison function reduces to the uniform random deviate between the endpoints of i-axis in the interval (l_i, u_i). This proposed step is accepted if a second random deviate, r, generated on the unit interval (0,1), satisfies:

$$r \leqslant \frac{P_{NA}(x_i^p \mid x_{-i})}{P_{NA}(x_i^{max} \mid x_{-i})}, \tag{3.3.1}$$

where the value of the comparison function at the proposed x_i^p is $P_{NA}(x_i^{max} \mid x_{-i})$ regardless of the point x_i^p, because it is uniform in the range of (l_i, u_i). If the proposed step is rejected then the whole procedure is repeated until an accepted step is produced. The only information which we obtain in the history-matching phase is prob($\mathbf{o}|\mathbf{m}$) prob($\mathbf{m}$). Note that it does not include the normalisation constant. Here, because the Gibbs sampler with the rejection method requires only the ratio of the 1-D conditional PPDs, it is not necessary to evaluate the normalisation constant. Then, imagine that the likelihood has been assigned with a Gaussian distribution, as described in Section 3.4. When the PPD varies exponentially with respect to the misfit, e.g., −log(PPD), the ratio of the PPD values can become infinitesimally small and tends to cause numerical underflow problems, (Sambridge, 1999b). By taking logarithms of sides of the condition (3.3.1), the task is to merely evaluate the difference between logarithms of the PPD and such problems do not arise. If the misfit is defined as (−log(PPD)), the input ensemble is provided as the form of (−log(prob($\mathbf{o}|\mathbf{m}$) prob($\mathbf{m}$))).

In summary, MCMC with Neighbourhood Approximation can evaluate the posterior expectation in a Bayesian framework without conducting any additional flow simulations and calculating the normalisation constant. In the NA-Bayes Algorithm, the Gibbs sampler is adopted which is one of the popular methods for MCMC. Also the rejection method is utilised to implement the Gibbs sampler. Note that, in this framework, the accuracy of the Monte Carlo integration depends on the approximation of Voronoi space as well as the sample size and population variance in Equation (3.2.13). Therefore, the accuracy relies on how well the input ensemble samples the regions of high data fit. Recently this method has been adopted to evaluate the posterior expectation and P10 and P90 cut-offs for the purpose of forecasting reservoir performance, (Christie et al., 2002b,c; Subbey et al., 2002, 2003).

3.4 Assigning Probability

The task of Bayesian inference is to evaluate the posterior PDF. For this purpose, it is necessary to assign the prior PDF and the likelihood function in Equation (3.1.7). Once both of them are assigned, the MCMC can provide samples from PPD to evaluate its characteristic: e.g., the posterior expectation by Equation (3.2.16). Also, as mentioned above, in the framework of the NA Algorithm and the NA-Bayes algorithm, it is usually important to investigate the best estimate of model $\mathbf{m}^{\mathbf{opt}}$ resulting in the highest PPD, because the framework needs to construct the approximate PPD as precisely as possible especially around the highest posterior probability. This section gives some examples on assigning the prior probability distribution and likelihood function. First, the prior distribution is assigned to a uniform distribution. Secondly, the likelihood function is assigned to a Gaussian distribution.

The prior PDF should reflect all the relevant information about the parameters **m** before the analysis of observed data **o**. A largely "ignorant" situation might result in a flat or very broad PDF, (Sivia, 1996):

$$\text{prob}(\mathbf{m}) = \text{constant}, \tag{3.4.1}$$

for, effectively, all values of **m**. This uniform prior reduces to the constant which can be omitted in Equation (3.1.7) as a normalisation constant has been omitted from (3.1.6). Then the posterior PDF can be rewritten to be directly proportional to the likelihood function:

$$\text{prob}(\mathbf{m}|\mathbf{o}) \propto \text{prob}(\mathbf{o}|\mathbf{m}). \tag{3.4.2}$$

Statistics textbooks (e.g., Sivia, 1996; Taylor, 1997; Bevington and Robinson, 2003) explain that the Gaussian distribution is an approximation to the binomial distribution and the Poisson distribution for special limiting cases. Sivia (1996) also conducted a formal derivation of the Gaussian distribution with maximum entropy approach. These derivations are not repeated here. The 1-dimensional Gaussian distribution with respect to a variable x is defined as follows:

$$\text{prob}(x) = \frac{1}{\sigma\sqrt{2\pi}} \exp\left(-\frac{(x-\mu)^2}{2\sigma^2}\right), \tag{3.4.3}$$

where μ and σ are mean and standard deviation of the distribution. Also the N-dimensional multivariate Gaussian distribution is defined as follows:

$$\text{prob}(\mathbf{x}) = \frac{1}{2\pi^{N/2}|\mathbf{C}|^{1/2}} \exp\left[-\frac{1}{2}(\mathbf{x}-\boldsymbol{\mu})^T \mathbf{C}^{-1}(\mathbf{x}-\boldsymbol{\mu})\right], \tag{3.4.4}$$

where $\boldsymbol{\mu}$ and $\mathbf{C}$ are mean vector and covariance matrix, respectively. This general form can be derived from the independent multivariate Gaussian distribution using variable transformation and matrix manipulations, (Bancroft and Han, 1981).

The Gaussian distribution is often used to model the noise associated with experimental data. It assumes that 1) a measurement would be subject to many small sources of random error, and 2) systematic error in the measurement is negligible, (Sivia, 1996; Taylor, 1997). Suppose that the observations consist of time series data and each measurement is labelled as the kth datum. When μ and σ denote the true value of the parameter and a measure of the measurement error respectively, the probability of the kth datum having value x_k is given by the Gaussian distribution:

$$\text{prob}(x_k) = \frac{1}{\sigma\sqrt{2\pi}} \exp\left(-\frac{(x_k-\mu)^2}{2\sigma^2}\right). \tag{3.4.5}$$

The use of the Gaussian distribution for measurement errors is justified by the central limit theorem, (Sivia, 1996; Cowan, 1998). According to the theorem, the sum of n independent continuous random variables $\{z_i\}$ with means μ_{zi} and variances ${\sigma_{zi}}^2$ becomes a Gaussian random variable with mean $\mu = \sum_{i=1}^{n} \mu_{zi}$ and variance $\sigma^2 = \sum_{i=1}^{n} {\sigma_{zi}}^2$ in the limit that n approaches infinity. Therefore, when a measurement x_k can be decomposed into the hypothetical independent random variables $\{z_i\}$, the theorem simply relates the measurement to a random sample from the Gaussian distribution. It holds even if each PDF of the $\{z_i\}$ does not follow Gaussian distribution. An exception is the Cauchy distribution, since the variance is not defined due to its very wide wings, (Sivia, 1996).

If the noise of the observed data is assumed to be a set of deviates from the Gaussian distribution, the probability of the hypothetical occurrence of observed data **o** given the model **m** can be written as

$$\text{prob}(\mathbf{o}|\mathbf{m}) = \frac{1}{2\pi^{N/2}|\mathbf{C}|^{1/2}} \exp\left[-\frac{1}{2}(\mathbf{o}-\mathbf{s})^T\mathbf{C}^{-1}(\mathbf{o}-\mathbf{s})\right], \tag{3.4.6}$$

Here, **s** represents the ideal (noiseless) data and consists of N time series data. Each of the components of **s** is a function of the model parameters **m**. In this thesis, **s** is calculated from **m** using a reservoir simulator and the relation between **s** and **m** is nonlinear. In Equation (3.4.6), each component of the vector **o** is compared with the corresponding component of **s**; $\mathbf{s} = (s_1, s_2, \ldots, s_N)^T$ and $\mathbf{o} = (o_1, o_2, \ldots, o_N)^T$. In addition, the matrix **C** is the expected covariance matrix of the measured data, because it is assumed that the mean vector of the measured data is equal to the ideal data vector **s**. The diagonal term of **C** represents the variance at each measured time step and the off-diagonal term represents the covariance between the different time steps.

Then, if it is assumed that the time series data are independent, the off-diagonal terms of **C** are all zero and the likelihood function of Equation (3.4.6) becomes

$$\text{prob}(\mathbf{o}|\mathbf{m}) = \prod_{k=1}^{N}\left(\frac{1}{\sigma_k\sqrt{2\pi}}\exp\left[-\frac{(o_k-s_k)^2}{2\sigma_k^2}\right]\right) \tag{3.4.7}$$

$$= \left\{\prod_{k=1}^{N}\left(\frac{1}{\sigma_k\sqrt{2\pi}}\right)\right\}\exp\left[-\frac{1}{2}\sum_{k=1}^{N}\left(\frac{o_k-s_k}{\sigma_k}\right)^2\right], \tag{3.4.8}$$

where σ_k is the variance of kth component of **o**. Equation (3.4.8) leads to the following expression of the likelihood function:

$$\text{prob}(\mathbf{o}|\mathbf{m}) \propto \exp\left(-\frac{\chi^2}{2}\right), \tag{3.4.9}$$

where χ^2 is the sum of the squares of the normalised residuals:

$$\chi^2 = \sum_{k=1}^{N}\left(\frac{o_k-s_k}{\sigma_k}\right)^2. \tag{3.4.10}$$

With the uniform prior assumption of Equation (3.4.1) and Equation (3.4.2), the logarithm L of the posterior PDF is simply given by

$$L = \log_e [\text{prob}(\mathbf{m}|\mathbf{o})] = \text{constant} - \frac{\chi^2}{2}. \tag{3.4.11}$$

Here, because the logarithm of a PDF is a monotonic function of the PDF, seeking the maximum of the PDF is equivalent to searching for the maximum of its logarithm. Therefore, in Equation (3.4.11), the maximum of the posterior will occur when χ^2 is smallest and the corresponding optimal solution $\mathbf{m}^{\mathbf{opt}}$ is usually called the least-squares estimate, (Sivia, 1996).

As shown so far, the least-squares estimate is merely a simplified form of Bayes' theorem when certain approximations are suitable. The justification of its use relies on the assignment of a uniform prior of Equation (3.4.1). In addition, it hinges on the assignment of the likelihood which assumes Gaussian approximations of each measured data and the independence of the time-series data. The least-squares form can be used as misfit function in the NA algorithm and the NA-Bayes algorithm, when the same assumptions are suitable. It should be noted that without a uniform prior and independent Gaussian likelihood, it is not appropriate to characterise the PPD with least-squares form of Equations (3.4.10) and (3.4.11).

Chapter 4

Reservoir Simulation and Re-Scaling Issues

This chapter starts by explaining the continuum approach of porous media and presents an overview of reservoir simulation. Then, it clarifies numerical dispersion and discusses re-scaling issues. In addition, physical dispersion is explained, which is related to upscaling procedure and contrasts with numerical dispersion. The re-scaling methods are described by referring to upscaling and downscaling literature.

4.1 Continuum Approach of Porous Media

Bear (1972) explained the continuum approach to porous media. This is adopted to replace the actual porous media with a hypothetical continuum. Physical parameters can be assigned to the hypothetical continuum by regarding the parameters as continuous functions of spatial coordinates of the point and of time. In addition, the porous media can be replaced by a number of overlapping continua. In this case, each of these continua represents one phase; e.g, solid phase, water phase, oil phase, etc. The physical parameters of these continua, e.g., porosity, permeability, relative permeability, are assigned to every point in space. Here, the space is referred to as the macroscopic space, (Bear and Bachmat, 1990). Consider each point in the macroscopic

space to which the parameters are assigned. At each point, average values of the properties can be taken over elementary volumes which are centred at the point. The averaged values depend on the size of the elementary volume. Therefore, it is necessary to consider a range of averaging volumes within which the properties are assumed to be constant. An averaging volume in the range is referred to as Representative Elementary Volume (REV), (Bear, 1972; Bear and Bachmat, 1990).

Although there are some discussions about the concept of REV (Lake and Srinivasan, 2004), the continuum approach is indispensable from a practical point of view. As Bear and Bachmat (1990) pointed out, it has the following advantages: 1) the configurations of the boundaries at the pore scale do not need to be specified. 2) differentiable quantities can be defined for each parameter. 3) the macroscopic quantities are measurable. Hence, using the parameters of the hypothetical continua, which has been averaged over an REV, multi-phase flow phenomena through porous media can be described by partial differential equation (Bear, 1972). In the governing equations of commercial reservoir simulators, the control volume fixed in space is used along with the Euler's approach instead of the Lagrangian approach. The control volume must satisfy the criterion of the REV, (Aziz and Settari, 1979). Note that since the Navier-Stokes equations require specifying the boundary conditions in each pore, it is impossible to apply it to the complex geometry of porous media. The alternative is to use Darcy's law, as described in Section 4.2.

4.2 Basics of Reservoir Simulation

Reservoir simulation is routinely employed in the petroleum industry and the basic theory is summarised in some literature, (e.g., Peaceman, 1977; Aziz and Settari, 1979; Ewing, 1983). In its governing equations, Darcy's law is incorporated into the mass conservation equation in order to describe flow through porous media.

The partial differential equations (PDEs) which describe oil-water two phase flow in the

reservoir, assuming that free gas neither exists nor evolves in the reservoir condition, are expressed as follows:

$$\vec{\nabla} \cdot \left(\lambda_o \vec{\nabla} P_o \right) = \frac{\partial}{\partial t} \left(\frac{\phi S_o}{B_o} \right) + q_o, \tag{4.2.1}$$

$$\vec{\nabla} \cdot \left(\lambda_w \vec{\nabla} P_w \right) = \frac{\partial}{\partial t} \left(\frac{\phi S_w}{B_w} \right) + q_w, \tag{4.2.2}$$

$$\text{where } \lambda_l = \frac{k k_{rl}}{\mu_l B_l}, \quad \text{for } l = o, w. \tag{4.2.3}$$

Here, the effect of gravity is ignored in Equations (4.2.1) and (4.2.2). In the two dimensional horizontal domain, the left hand side of Equation (4.2.1) is rewritten as:

$$\vec{\nabla} \cdot \left(\lambda_o \vec{\nabla} P_o \right) = \frac{\partial}{\partial x} \left[\lambda_{ox} \frac{\partial P_o}{\partial x} \right] + \frac{\partial}{\partial y} \left[\lambda_{oy} \frac{\partial P_o}{\partial y} \right]. \tag{4.2.4}$$

λ_{lx} and λ_{ly} correspond to the evaluations of Equation (4.2.3) along the x and y axes, respectively. Although permeability k is assumed to be a scalar in Equation (4.2.3), it can be replaced by a tensor including diagonal and off-diagonal terms. The l-th phase relative permeability k_{rl} is usually a function of saturation and can be different in the different directions (it is also actually a full tensor). S_o and S_w represent saturations for oil and water, respectively. ϕ is porosity of rock. P_l is the l-th phase pressure and μ_l denotes viscosity of the l-th phase. B_o and B_w are formation volume factors of oil and water. q_l is a sink / source which represents an amount of production or injection of the l-th phase fluid. In this thesis, an oil-water two-phase system is considered and the details of multi-phase flow phenomenon are explained in the following chapters.

The additional constraints for Equations (4.2.1) and (4.2.2) are given as follows:

$$S_o + S_w = 1, \tag{4.2.5}$$

$$P_{cow} = P_o - P_w. \tag{4.2.6}$$

Note that if capillary pressure P_{cow} is ignored and is assumed to be zero, $P_o = P_w$. According to the constraints of Equations (4.2.5) and (4.2.6), the unknown parameters of the PDEs are

saturation of one phase, S_o or S_w, and pressure of one phase, P_o or P_w. The coupling of the PDEs is numerically solved by adopting a discretisation scheme: Finite Difference Method, Finite Element Method, Control Volume Finite Element Method, etc.

Here, the finite difference approximations are adopted to discretise the PDEs. In other words, a "differential" equation is replaced by a "difference" equation using the approximations. Consider that P_i denotes pressure at position i in the x axis and the distance between P_i and P_{i+1} is small amount of Δx. P_{i+1} can be expressed using Taylor series:

$$P_{i+1} = P_i + \Delta x \left.\frac{\partial P}{\partial x}\right|_i + \frac{\Delta x^2}{2!}\left.\frac{\partial^2 P}{\partial x^2}\right|_i + \frac{\Delta x^3}{3!}\left.\frac{\partial^3 P}{\partial x^3}\right|_i + \cdots . \tag{4.2.7}$$

Hence, the first order differential term can be written as:

$$\left.\frac{\partial P}{\partial x}\right|_i = \frac{P_{i+1} - P_i}{\Delta x} - \frac{\Delta x}{2!}\left.\frac{\partial^2 P}{\partial x^2}\right|_i - \frac{\Delta x^2}{3!}\left.\frac{\partial^3 P}{\partial x^3}\right|_i - \cdots . \tag{4.2.8}$$

The above equation is replaced by a difference equation with the first order error:

$$\left.\frac{\partial P}{\partial x}\right|_i = \frac{P_{i+1} - P_i}{\Delta x} + O(\Delta x). \tag{4.2.9}$$

The scheme of Equation (4.2.9) is referred to as the forward difference. As for the discretisation in time, the implicit method corresponds to the backward difference, which is expressed as:

$$\left(\frac{\partial P}{\partial t}\right)^{n+1} = \frac{P^{n+1} - P^n}{\Delta t} + O(\Delta t), \tag{4.2.10}$$

where n denotes time in the t axis. Using Equations (4.2.9) and (4.2.10), the PDEs of Equations (4.2.1) and (4.2.2) can be discretised with the fully implicit method.

Now consider the discretisation of Equation (4.2.4). Relative permeabilities included in Equation (4.2.3) should be evaluated between the adjacent cells along the x or y axis. Aziz and Settari (1979) pointed out that the upstream weighting of the saturation function, instead of the midpoint weighting, converged to the correct solution. Here, the upstream weighting means that relative permeabilities between the adjacent cells are the functions of the saturation of the upstream cell from which the fluid flows.

4.3 Numerical Dispersion

The numerical error in reservoir simulation includes round-off error and truncation error. The truncation error is caused by replacing a differential equation by a difference equation, (Peaceman, 1977). This replacement is equivalent to using a truncated Taylor's series, as explained in Section 4.2. Peaceman (1977) examined numerical solutions of a non-linear convection equation in one dimensional space. Because of the truncation error, even if there is no round-off error, the solution of the difference equation differs from the solution of the corresponding differential equation. The difference can be described by adding a hypothetical diffusive term to the convection equation. Then it is often referred to as numerical diffusion, (Lantz, 1971), or numerical dispersion, (Peaceman, 1977).

Thomas (1995) described the terminology and the concepts of dispersion and dissipation for partial differential equations. When a Fourier mode is substituted into the differential equation, the relation between frequency of the wave and the wave number is obtained. In other words, the frequency of the wave must be expressed as a certain function of the wave number so that it can satisfy the PDE. Note that wave number is equal to 2π divided by wave length. The relation is referred to as the dispersion relation. Moreover, when the dispersion relation is substituted into the Fourier mode, the solution of the PDE is obtained. Hence, when looking at the solution, the propagation of the wave and decay of the amplitude are linked to the dispersion relation. In general, when the Fourier modes do not amplify with time and at least one mode decays, the PDE is called dissipative. On the other hand, when the Fourier modes which have different wave lengths propagate at different speeds, the PDE is called dispersive. As mentioned above, the classification depends on the dispersion relation.

Thomas (1995) also described dispersion and dissipation for difference equations. O'Sullivan (2004) explained this for a saturation equation of the Buckley-Leverett problem. When a Fourier mode was substituted into the difference equations, the dispersion relation of the difference equation was compared with that of the differential equation. In the saturation equation, the dispersion relation of the differential equation shows that the frequency of the wave is proportional

to the wave number. This is a linear relation and the frequency is a real number. On the other hand, in the dispersion relation of the difference equation, the frequency can be expressed as a complex number which consists of both real part and imaginary part. The imaginary part in the dispersion relation leads to the time dependent amplitude in the solution. This can introduce the decay of the amplitude in time, which is recognised as dissipation. In addition, the real part cannot always coincide with the dispersion relation of the differential equation and can have a non-linear relation with the wave number. Then, the speed at which the mode in the solution propagates depends on the wave number. Hence, in the solution of the difference equation, the speeds associated with the different modes can be different, which results in dispersion. In summary, when comparing the difference equation with the corresponding differential equation, the disagreement between the two dispersion relations indicates how the truncation error behaves in time and space.

In a waterflood simulation, as Kyte and Berry (1975) proposed, the relative permeabilities can be altered to compensate for numerical dispersion and control the spread of the front. The dynamic two-phase upscaling method is described in more detail in Section 4.5. As Christie and Bond (1985) pointed out, the approach can be regarded as a simple implementation of Harten's Artificial Compression Method (Harten, 1977). Harten (1977) described the mathematical background of the Artificial Compression Method. The main idea of the method is to modify standard finite difference schemes in order to prevent the smearing of contact discontinuities and improve the resolution of shocks. In other words, a term of a finite difference equation is modified so that a shock for a differential equation can be also a shock for the modified finite difference equation.

4.4 Physical Dispersion

Bear (1972) explained hydrodynamic dispersion in a porous media as follows. When flow containing a tracer takes place through a porous media, the tracer gradually spreads out to occupy a larger portion of the flow domain than the region which the average flow alone may occupy.

The individual tracer moves through the pores, and the physical and chemical phenomena take place within the pores. The macroscopic outcome is hydrodynamic dispersion. It is also called as physical dispersion.

The dispersion involves both convection and molecular diffusion, (Bear, 1972; Bear and Bachmat, 1990). The mechanical dispersion occurs as convection in heterogeneous media both at microscopic and macroscopic scales. In a microscopic system, the velocity distribution within each pore results in variations in local velocity along the tortuous flow paths and between adjacent flow paths. The heterogeneous permeability field also causes the mechanical dispersion. On the other hand, molecular diffusion can take place in the absence of convective motion. However, the separation between mechanical dispersion and molecular diffusion is artificial, because both processes cannot be separated in the actual phenomenon of hydrodynamic dispersion, (Bear, 1972).

When using a coarse-scale reservoir model, physical dispersion due to sub-grid heterogeneity is omitted in flow simulation. In waterflooding, physical dispersion may smear the front. Hence, if the effect of sub-grid heterogeneity is not incorporated in a reservoir model, the flow simulation cannot represent physical dispersion and fails to calculate the correct front. The issue is related to upscaling methods described in Section 4.5.

4.5 Upscaling Methods

This section gives a brief summary of the methods to upscale a fine-scale model to coarse-scale model. The method of single phase upscaling has been investigated for a couple of decades, and there are some good summaries for a number of the methods, (e.g. Christie, 1996; Renard and de Marsily, 1997; Christie and Blunt, 2001). The simplest methods are harmonic / arithmetic-mean techniques. The extensions are the combinations of these means; e.g., taking geometric mean or deriving a correlation, (Li et al., 1999; Nomura, 2002). Apart from these averaging methods, pressure solver methods are often adopted to calculate upscaled absolute permeabili-

ties or transmissibilities. Local or global boundary conditions are specified for fine-scale flow simulations, (Pickup et al., 1992; Wen et al., 2005; Zhang, 2005). The same approach, namely single phase flow simulations, can be also utilised to calculate the coarse-scale well connection factors and the transmissibilities between well cells and the adjacent cells, (Ding, 1995; Durlofsky et al., 2000; Muggeridge et al., 2002). The renormalisation method (King, 1989) is an alternative approach for linear flow which is faster, but less accurate. It breaks a large fine-scale model down into a hierarchy of coarser models and repeats an analytical upscaling procedure at each stage in the hierarchy. The applications and the limitations of these single phase upscaling methods are well discussed in some literature (e.g. Christie, 1996; Renard and de Marsily, 1997; Christie and Blunt, 2001) and it is not repeated here.

Two-phase upscaling methods are summarised in some literature, (e.g. Barker and Thibeau, 1997; Barker and Dupouy, 1999). Although there have been a lot of methods developed, the accuracy and applicability are still doubtful. Static and dynamic approaches are often adopted in a field case study. A static approach assumes capillary, viscous or gravity equilibrium, (e.g. Pickup et al., 2000; Suzuki et al., 2004; Pickup et al., 2005). Hence, it relies on the balance of viscous, capillary and gravity forces in a reservoir, (Stephen et al., 2001). On the other hand, the dynamic approach utilises dynamic fine-scale simulation results, (e.g. Kyte and Berry, 1975; Stone, 1991; Coll et al., 2001; Schlumberger, 2004b). It can compensate for numerical dispersion, as described in Section 4.3. For example, Coll et al. (2001) found that the Pore Volume Weighted (PVW) method gave the best results for upscaling in the models which they tested. This is a dynamic upscaling method, which proceeds as follows: a two-phase, fine-scale flow simulation is performed; the total flow of oil and water between coarse grid cells is calculated; the average pressure is computed using pore-volume weighting; and the phase permeabilities are computed using Darcy's law, (e.g., Schlumberger, 2004b). It should be recalled that the upscaled relative permeabilities depend on the upscaled absolute permeabilities, because the former is calculated from the latter and the phase permeabilities. In other words, the outcome of the two phase upscaling is affected by the choice of the single phase upscaling method. Also note that the procedure to average each property is the most controversial, and there are some alternatives and the discussions in the research of the two-phase upscaling, (Stone, 1991; Christie

et al., 1995; Barker and Thibeau, 1997; Barker and Dupouy, 1999; Darman et al., 2002). These discussions are not repeated here, since it is not the objective of this thesis.

The upscaled relative permeabilities require grouping into a limited number of tabular functions for coarse-scale simulation, (Christie, 1996; Dupouy et al., 1998), since two-phase upscaling may result in different upscaled relative permeabilities for every coarse-grid cell in each direction. One way of grouping relative permeabilities is to group on the basis of several key physical parameters, (Christie, 1996). For example, the Buckley-Leverett shock height, the slope of the fractional-flow curve at that point and the minimum on the total mobility curve give a set of three parameters to characterise the two-phase flow phenomena. These can be adopted to group relative permeabilities curves on their closeness. Dupouy et al. (1998) proposed the grouping scheme using the cluster analysis. The parameters of the cluster analysis may be the three parameters proposed by Christie (1996), the values of k_{rw} and k_{ro} at certain saturation points, or some other parameters related to relative permeabilities. Furthermore, Christie and Clifford (1998) demonstrated a different method which used the breakthrough curve and the cluster analysis. Although it was demonstrated for grouping of α-factors of compositional upscaling, the main idea can be applied to two-phase flow problem. In their case, the tracer breakthrough curve was obtained by calculating the arrival time at the outlet face of each coarse-scale cell. By classifying the breakthrough curves with an iterative cluster analysis, similar cells are selected so that the same relative permeabilities can be assigned to each group of cells.

Hewett et al. (1998) investigated coarse-scale relative permeabilities analytically. The relative permeabilities for a differential equation of the Buckley-Leverett problem were corrected in an analytical method to take account of the coarse-grid effect in the corresponding difference equation. As for the corrections, the key factor is the ratio of the distances from the injection boundary to the inlet and outlet faces of a cell. Hewett et al. (1998) found that the correction depends only on the ratio of the two distances. According to the analytical investigation based on the method of characteristics, (e.g., Haberman, 1987, 1998), they pointed out the following features using a one-dimensional displacement problem. The saturation buildup in a cell begins when the front enters the upstream face of the cell and continues until the front reaches the

downstream face of the cell. Before the fractional flow changes from zero to the value at the front, the saturation builds up to the average saturation behind the front. In other words, during this period, the saturation builds up without changing the value of the fractional flow. The saturation buildup in the first cell is more than that in the subsequent cells. It diminishes as the cell number from the injection boundary increases. The average mobility of the cell also changes, before the fractional flow changes from zero to the value flow at the front. The mobility begins to change, when the front enters the region between the centres of the two adjacent cells. As in the saturation buildup, this mobility change continues, until the fractional flow changes to the value at the front.

Apart from the above upscaling methods, the calibration or regression to the fine-scale solution is sometimes utilised to obtain the coarse-scale properties, (e.g., Johnson et al., 1982; Tan, 1995). It is similar to a history-matching procedure rather than just an upscaling method. Johnson et al. (1982) used the regression approach to calculate the upscaled relative permeabilities. In the SPE 10th comparative solution project (Christie and Blunt, 2001), a few entries adopted the history-matching to the fine-scale solution and presented the regression-based relative permeabilities, whereas no entries used two-phase dynamic upscaling methods like the Kyte and Berry method or the PVW method.

4.6 Downscaling Methods

Downscaling methods are used to refine the model and assign the properties in the fine-scale cells, after the coarser-scale properties are obtained in a certain manner, such as history-matching or seismic-derived models.

Behrens et al. (1998) introduced Sequential Simulation with Block Kriging to integrate seismic data and well-log data. Whereas seismic data represents interval-average properties, well-log data represents point properties more closely. That is to say, the method took account of not only quasi-point data of the well-log but also the arithmetic average in the vertical column

which was estimated from seismic data. Here, they used "point-to-point covariance", "point-to-block covariance" and "block-block covariance" to obtain the estimate and kriging variance at a point. "Point-to-point" means between locations, "point-to-block" means between point and the vertical column containing the point, and "block-block" means the column containing the point with itself.

Tran et al. (2001) used Sequential Gaussian Simulation (SGS) with either block kriging or Bayesian updating to downscale the history-matched model. The coarse-scale logarithmic permeability distributions in the history-matched models were downscaled to fine-scale models. The average of fine-scale properties within a coarse cell was preserved as the history-matched value at the coarse scale. SGS with block kriging accounted for the coarse-block average constant and the point-to-block covariance between the value at cell and the block value. On the other hand, in the approach of SGS with Bayesian updating, a value at the current cell could be simulated by random sampling of the local posterior probability distribution. The local posterior probability distribution was a product of the conditional probability from SGS and the likelihood function from the coarse cell constraint. Markov-type assumptions and the additional kriging equation allowed the likelihood to be expressed as the Gaussian conditional distribution.

Yoon et al. (2001) presented a multi-scale history-matching method. The method involved conditioning the history-matched coarse-scale model to well data at the fine scale. This was downscaling to incorporate small-scale variations into the models while preserving the large-scale structure and continuity. They examined two different approaches: Residual Sequential Simulation and Sequential Simulation with block kriging. Residual Sequential Simulation assumed that the variability of reservoir properties could be split into two parts: a deterministic large-scale trend and a stochastic component reflecting the small-scale variability. The large-scale trend was derived from the history-matching. The small-scale variability was obtained by a stochastic simulation using the residuals of history-matching error at each well location. This stochastic component was added to the large-scale trend. On the other hand, Sequential Simulation with block kriging was performed on a logarithmic transform domain, when the block-scale parameter values had been derived from the multi-scale inversion on a coarse cell.

Lee et al. (2002) generated fine-scale random fields based on both sparse fine-scale data and coarse-scale data. Their proposed method was a Bayesian approach to spatial modelling based on Markov Random Fields (MRF). The method consisted of two major parts (i) construction of a posterior distribution for multi-scale data integration using a hierarchical model and (ii) implementing MCMC to explore the posterior distribution. In a 2D example, they assigned a parameter for the prior distribution so that the fine scale realisations could preserve exactly the coarse scale block values. Compared to SGS with Block Kriging, the proposed method could obtain similar performance with less restrictive assumptions. The kriging-based methods are usually restricted to multi-Gaussian and stationary random fields. This means that those methods require data transformation and variogram construction. On the other hand, MRF can be extended to account for non-stationarity at various scales and non-linear interactions between different scales.

Panda et al. (2001) proposed a scale-consistent methodology using the wavelet transform. The kriging-based downscaling method produces stationary fields. However, a realistic image often possesses properties that vary with location. Their proposed method had two steps. In the first step, coarse-scale and fine-scale data were transformed using wavelets, where the wavelet coefficients were analysed. The wavelet coefficient which were generated at a finer scale could preserve the characteristics of the coarser cell. Such a treatment of multi-scale data was largely possible and mathematically valid, because the wavelet coefficients were local derivatives of the data. In the second step, the correlation which had been established in the first step was used to generate wavelet coefficients at inter-well locations on a desired grid mesh. The generated coefficients and the coarse-scale data were then back-transformed using reverse-wavelet transform into the physical space.

The scales to which downscaling takes place in the above literature are summarised as follows. Behrens et al. (1998) generated a model which has the resolution of well-log data by taking account of coarse-scale seismic data. Tran et al. (2001) and Lee et al. (2002) demonstrated the methods to downscale a coarse-scale model to a fine-scale model: e.g., the size of

the coarse cell is $50 \times 50 \times 20$ ft and that of the fine cell is $10 \times 10 \times 5$ ft. Yoon et al. (2001) refined a coarse-scale model gradually to reach sufficient match to the production history.

Chapter 5

Multi-Phase Flow Functions for Porous Media

Aziz and Settari (1979) pointed out that when physical phenomena are modelled in reservoir simulation, assumptions are necessary from a practical point of view. For instance, although the concept of relative permeabilities has limitations, at the moment there is no alternative but to input the relative permeabilities into commercial reservoir simulators. This chapter starts by clarifying the basic concept behind the relative permeabilities. It also describes the evaluation of relative permeabilities using core-flood experiments, the representation as a certain function of fluid saturation and the history-matching of relative permeabilities.

Apart from the above points, gravity and capillary forces sometimes play an important role in multi-phase flow in a reservoir, (e.g., Ringrose et al., 1993; Namba and Hiraoka, 1995; Huang et al., 1996; Coll et al., 2001; Stephen et al., 2001; Pickup et al., 2005). However, this thesis focuses on two-dimensional horizontal models. Hence, gravity is not incorporated in the simulation. Moreover, the pressure gradient between the adjacent coarse cells is often larger than the gradient of capillary pressure. With these assumptions, the effects are ignored in the numerical experiments described in the following chapters. Note that capillary pressure effects may

be taken into account in the relative permeabilities by performing small-scale simulations and upscaling.

The task of this thesis is to history-match the coarse-scale relative permeabilities and quantify the uncertainty due to sub-grid heterogeneity. The focus is on the effect of 1) heterogeneity-induced dispersion and 2) numerical dispersion, which should be captured in the coarse-scale relative permeabilities. Then the numerical experiments in the following chapters assumes that the small permeability fluctuations within the fine-scale cells are negligible. This means that the main concern is the heterogeneity-induced "fingers" as channelling effects rather than unstable viscous fingering. Detailed discussions on viscous fingering, stability analysis and accurate numerical schemes to represent it are presented in a number of references (Hagoort, 1974; Christie and Bond, 1985, 1986; Sorbie et al., 1995).

5.1 Theory and Assumptions

In reservoir simulation, two-phase flow is described by using macroscopic equations. This representation for the two-phase flow phenomenon is a generalisation of Darcy's law of single-phase flow in porous media. The absolute permeability k is defined by Darcy's law:

$$Q = \frac{kA}{\mu}\frac{\Delta P}{L}, \tag{5.1.1}$$

where Q is the volumetric flow rate, A is the normal cross sectional area, L is the length in the macroscopic flow direction, ΔP is hydrostatic pressure drop and μ is the viscosity of the fluid. Darcy's law is assumed to be correct under some assumptions: viscous, Newtonian fluids, absence of physical or chemical changes due to the fluids, no slip and isotropic media, (Dullien, 1992). As analogy with the Darcy's law, the macroscopic equations for two-phase flow are expressed as follows:

$$Q_i = \frac{k_i A}{\mu_i}\frac{\Delta P_i}{L}, \quad \text{for } i = 1, 2, \tag{5.1.2}$$

where Q_i is the volumetric flow rate, ΔP_i is the pressure drop and μ_i is the viscosity of the fluid i. As in Equation (5.1.1), A is the normal cross sectional area, L is the length in the macroscopic flow direction. k_i is referred to as the “phase permeability”of the porous media to fluid i. Equation (5.1.2) is rewritten by introducing "relative permeability" $k_{ri} = k_i/k$:

$$Q_i = \frac{k_{ri} k A}{\mu_i} \frac{\Delta P_i}{L}, \quad \text{for } i = 1, 2. \tag{5.1.3}$$

According to the summary by Rose (1999), it is Richards (1931) who introduced the concept of relative permeability as an extension of Darcy’s law and chose implicitly the saturation dependent relative permeability. Richards (1931) investigated water-air two-phase systems in soil. Darcy’s law was applied to the two-phase flow system using the following reasoning. If the air spaces occupying the porous media could be replaced with solid in some ways, the condition of the flow would be unchanged and the proportionality between the flow and the water-moving force would be still hold. Richards (1931) also discussed the difference between flow through a porous media which is fully saturated with water and flow through one that is unsaturated. Under the latter condition of a two-phase system, the pressure of water was determined by capillary forces, and then the conductivity of water depended on water saturation. For a few rock samples, he presented the experimental relation between water saturation and capillary potential and that between capillary conductivity and capillary potential. Capillary potential is equivalent to capillary pressure in the case of unit and constant water density. Capillary conductivity is the flow of water across unit area in unit time for unit potential gradient. These relations for each sample correspond to the capillary pressure functions for water saturation and relative permeability. Then these can be converted into the saturation functions for capillary pressure and relative permeability which it has been customary to use for two-phase flow function.

As for another source of “relative permeability”, the extension of Darcy’s law was introduced by Muskat and Meres (1936); Wyckoff and Botset (1936); Muskat et al. (1937). They conducted core flooding experiments for oil-gas mixture systems and plotted the specific permeabilities, so called “relative permeability”, versus liquid saturation. In addition, they proposed

the following ideas on which they based the introduction of the “relative permeability”, (Muskat and Meres, 1936; Wyckoff and Botset, 1936; Muskat et al., 1937; Muskat, 1981). Darcy’s law states that the fluid velocity is proportional to the pressure gradient and inversely proportional to the fluid viscosity and the constant of proportionality is referred to as permeability. Although it is natural to suppose that the flow of a two-phase fluid will also be expressed by the law of proportionality, the coefficient of proportionality for each phase may not be a constant, independent of the nature of the fluid mixture. Moreover, since the local liquid saturations will change from point to point, and with time, in the system, the porous media itself must be considered as changing from point to point, and with time. Therefore, in terms of two-phase flow, the porous media can no longer be defined by a single invariable permeability. Then it is necessary to assign to the medium a local structure defined by the local saturation which determines the local permeabilities for both phases of the mixture. In other words, the local permeabilities for the individual phases are variable, even if the absolute permeability is uniform, and their variation as a function of the phase saturations needs to be determined with the pressure and velocity distributions in the system. Muskat et al. (1937) introduced the ratio of “phase permeability” to absolute permeability, referred to as “relative permeability” afterward, and deduced the relations between the ratio and the saturation from two-phase flooding experiments which were conducted using four different core samples and a few different viscosities and surface tensions of fluids. From then on, it has been customary to define relative permeability as the ratio of phase permeability to absolute permeability and it is assumed to be a function of saturation, (Muskat et al., 1937; Honapour et al., 1986; Willhite, 1986; Dullien, 1992).

The effect of contact angle, viscosity ratio, interfacial tension, total flow rate and pore structure on relative permeabilities are discussed in various papers, (Muskat et al., 1937; Honapour et al., 1986; Dullien, 1992). Even now, it is controversial to assume that Darcy’s law can be extended to the multiphase flow in an analogous way and that relative permeability may depend solely on saturation, (Ayub and Bentsen, 1999; Rose, 1999). However, it should be noted that as long as a commercial reservoir simulator is utilised, it requires the approximation that the so-called saturation-dependent relative permeability should encapsulate the complex nature of the multiphase flow through porous media.

5.2 Measurement and Evaluation

Relative permeability curves for a core sample can be obtained from steady-state or unsteady-state core flooding experiments, (Honapour et al., 1986; Dullien, 1992). The unsteady-state method is usually preferred to the steady-state method because of the time required. The JBN method (Johnson et al., 1959) is used to calculate relative permeabilities from unsteady-state displacements. The details of this method are described in the next paragraph. Alternatively, relative permeabilities may be derived by history-matching at the core scale, so that the simulation result from a numerical model of the core flooding matches the observed data. Although the new approaches have been presented and the new apparatus has been developed, it is still customary to conduct unsteady-state displacements and adopt the JBN methods in order to obtain relative permeability, because it is feasible from a practical point of view.

The JBN method (Johnson et al., 1959) is based on Buckley-Leverett theory (Buckley and Leverett, 1942) and Welge integration (Welge, 1952). Buckley and Leverett (1942) determined that the rate of advance of a plane that has a certain saturation was proportional to the change in the fractional flow caused by a small change in the saturation of the displacing fluid, assuming unidirectional flow through a small element of sand within a continuous sand body. Then, neglecting the effects of gravity and capillary pressure, they derived the equation relating position along the path of flow, saturation and time. Furthermore, they described the discontinuity in the saturation distribution, referred to as a “shock”, to sort out the physical problem of triple-valued saturations at a distance. In general, the foregoing theory can be stated using the method of characteristics, (e.g., Haberman, 1987, 1998). Welge (1952) extended the Buckley-Leverett theory to derive the equation relating the saturation at the outlet of the sand and the average saturation. He substituted the derivative of the fractional flow for the distance in the integration for averaging the saturation. He also presented the calculation result of the ratio of relative permeabilities vs. saturation which were evaluated at the outlet. Johnson et al. (1959) further extended the Welge formulation to calculate individual relative permeabilities. They derived the equation

which relates the ratio of pressure gradient to average velocity, the ratio of pressure gradient to average velocity at the start of injection, the derivative of fractional flow of displaced phase at the outlet face and the relative permeability of displaced phase at the outlet face. That relation was the ordinary differential equation in which "the derivative of fractional flow of displaced phase at the outlet face" was the only independent variable. Since that variable could be replaced with the reciprocal of cumulative injection in pore volumes, the relative permeability of displaced phase at the outlet was calculated from the available data of the core-flooding experiments. They also calculated the relative permeability of displacing phase and the saturation at the outlet. Finally, they presented the set of relative permeability curves evaluated at the outlet face.

What should be noted here concerning the JBN method is that the relative permeabilities are evaluated at the effluent end of the core. In order to evaluate the relative permeabilities at the effluent end, the method uses the fractional flows measured at outlet face and also calculates the saturation at the effluent end from the average saturation in the core. So, as pointed out by Crotti and Cobenas (2001), rock relative permeability curves obtained by the JBN method are the functions of point saturations and not as those of average saturations.

It is not appropriate to use relative permeability curves obtained from core flooding experiments directly in coarse-scale simulation models. Ideally they should be upscaled to account for geological heterogeneity, fluid forces and numerical gridding effects. The method to evaluate the coarse-scale relative permeability is two-phase upscaling. The detail is not repeated here, since it has been summarised in Section 4.5.

5.3 Models for Relative Permeabilities

A range of mathematical models of relative permeabilities are summarised in the literature, (e.g., Honapour et al., 1986; Dullien, 1992; Siddiqui et al., 1999). According to Siddiqui et al. (1999), there are more than 30 models which have been developed and investigated for rep-

resenting the two-phase relative permeabilities. The models form a certain function of fluid saturation and are often used in history-matching especially for core flooding experiments. The details of the history-matching are explained in Section 5.4. This section describes the some models such as the so called Corey and Chierici functions, (Corey, 1954; Chierici, 1981).

Corey (1954) represented relative permeabilities as a set of the power functions of fluid saturation. Corey (1954) simplified the relative permeability equations which had been proposed by Burdine (1953). The equations are based on the Carman-Kozeny equation for single phase flow in porous media, which can be derived using capillaric models and a Hagen-Poiseuille type equation. According to the Carman-Kozeny equation, absolute permeability can be expressed by a function of porosity, hydraulic radius and tortuosity. Here, the main idea is to extend the permeability equation to the two-phase flow system and express it in a simple formulation.

In a single-phase system the tortuosity is defined by the ratio of the effective length of flow path to the the length of the entire domain. When it is extended to two-phase systems, the tortuosity of one phase is the ratio of the effective length of the flow path of the phase to the the length of the entire domain. Burdine (1953) proposed that the multi-phase tortuosity factor can be approximated by a simple function of fluid saturation, although the complexity of multi-phase porous system makes the precise estimation impossible.

In the Carman-Kozeny equation the hydraulic radius is used as a measure of pore throats, because it can be a measure of the size even in the case of irregularly shaped pore system, (Dullien, 1992). According to Purcell (1949), because the radius is related to capillary pressure, the permeability equation can be expressed in terms of capillary pressure instead of the hydraulic radius. Moreover, Corey (1954) assumed that the capillary pressure is approximated as a simple function of saturation so that relative permeability of each phase can be expressed by a power function of fluid saturation. The value of the exponent in the power function varies for different porous media, (Dullien, 1992). The number of the parameters is two for a set of two-phase relative permeabilities, which means one parameter for one phase, apart from the end points.

Chierici (1981) proposed the use of exponential functions to represent two phase relative permeabilities. The number of parameters in a set of the relative permeability equations is larger than that of the Corey equations. In the Chierici equations, these are four in total apart from the end point parameters, namely two parameters for one phase. Those values apart from the end point parameters must be determined empirically. Chierici (1981) showed that the functions enable the experimentally determined relative permeability curves to be reproduced with good accuracy especially in the neighbourhood of the initial and end points of the curves.

Whereas there are several models used for representing core-scale relative permeabilities, the investigation into the shape of coarse-scale relative permeability curves has never been presented intensively. To date, it is limited to the one-dimensional problem for homogeneous media (e.g., Hewett et al., 1998) which has been summarised in Section 4.5.

5.4 History-matching of Relative Permeabilities

The Corey and Chierici functions are often utilised in history-matching relative permeabilities for Special Core Analysis (SCAL), (e.g. Sigmund and McCaffery, 1979; Firoozabadi and Aziz, 1986; Tokuda et al., 2004), well test analysis, (e.g. Namba and Horne, 1989) and field-scale reservoir simulation, (e.g. Subbey et al., 2002, 2003; Reynolds et al., 2004).

Firoozabadi and Aziz (1986) presented the results of history-matching relative permeabilities at the core scale. They simulated the two-phase drainage-type centrifuge experiments and calculated both wetting and non-wetting phase permeabilities in a two-phase system. They used the recovery data from the core for history-matching. Since it was a drainage process, the recovery of the wetting phase was matched. The two phase relative permeabilities were estimated by adjusting the parameters of either the Corey or Chierici function. They pointed out that both the Corey and Chierici representations failed to match the recovery performance at late states of drainage, where the Chierici function gave a little better match than the Corey function. The Chierici representation gave higher wetting phase relative permeabilities than the

Corey one. Although both representations could match the recovery performance apart from the late stages, the resulting two sets of relative permeabilities were different. This indicates that the shape of history-matched relative permeabilities depends on the choice of the function.

More flexible approaches can be used to represent a variety of relative permeability curves in history-matching, (e.g., Kerig and Watson, 1986; Tan, 1995; Sun and Mohanty, 2003; Eydinov et al., 2005). Tan (1995) directly varied the tabulated values of the saturation functions. Although this method could vary all the tabulated values, these might be too many parameters in practice. For the analysis of core-flooding experiments, Kerig and Watson (1986, 1987) investigated the use of cubic splines and concluded that it enabled more accurate estimates of relative permeabilities than using exponential functions. Their method using cubic splines needs to maintain the continuity of the function and the first and second derivatives at each spline knot where the spline segments are joined. To do this, it requires the user to derive the independent parameters from all the coefficients in the piecewise polynomial representation.

Watson et al. (1988) extended the method to utilise B-spline representations. Whereas their previous method (Kerig and Watson, 1987) needs to derive the independent coefficients in the polynomial expressions, B-splines do not require this procedure, because B-spline basis functions satisfy the continuity requirements. The definition of a B-spline is based on the the concept of divided difference, (Dierckx, 1993). The mathematical details can be found in the literature (Schumaker, 1981; de Boor, 2001) and are not repeated here. Watson et al. (1988) also investigated the effects of the order of the spline, the number of the knots and their locations, which are to be selected in the representation. They pointed out that the order of the spline is not critical, and that parabolic or cubic splines are usually smooth enough. On the other hand, it was suggested that the location of the knots can influence the estimates, and the selection of the appropriate number of knots should be considered carefully. Following their work, Richmond and Watson (1990) presented a systematic procedure for selecting knot locations. At the initial stage the coefficients were estimated without any interior knots. Then, when a knot was added to the centre of the saturation interval, the coefficients were estimated again. This procedure was repeated until the error was converged to a low value. The new knot was added to the

saturation interval for which the greatest improvement was obtained.

Yang and Watson (1991) incorporated the prior information into history-matching, although the way to derive the prior curves was not clear there. They tested the method using a hypothetical 2D reservoir model for 5-spot pattern water flooding. Apart from the difference between the simulated production data and the observed data, an additional term was added to the objective function. The additional term evaluated the difference between the estimated relative permeability curves and the prior curves, and then penalised the deviation of the generated curves from the prior curves. It aimed to constrain the estimated curves to the prior curves in the high water saturation region where the production data did not provide the relevant information for history-matching. In general, the procedure is called regularisation. They investigated the effect of a weighting parameter for the additional term, which could be selected to improve the efficiency of optimisation process. However, from the statistical point of view as explained in Chapter 3, the additional term should reflect the definition of the prior distribution which updates the likelihood function. In that sense, the formulation including weighting parameter should be derived from the definition of the prior distribution.

Kulkarni and Datta-Gupta (1999) also presented the regularisation approach with the additional terms in the objective function, using a method which is similar to the above method of Yang and Watson (1991). Kulkarni and Datta-Gupta (1999) history-matched relative permeabilities using B-splines in a hypothetical reservoir model of 9-spot pattern water flooding. The 2-dimensional projection of the objective function with respect to two of the B-spline coefficients were shown in order to investigate the multi-dimensional objective function. It indicated that the regularisation reduced the non-uniqueness of inverse problem. Again, especially when it is aimed to investigate the uncertainty, the definition of each regularisation term including the weighting parameters should reflect the definitions of prior distribution. However, in their paper the procedure to determine the terms was explained only from the penalising purpose, presumably because it aimed at only the history-matching rather than the uncertainty quantification in a statistical sense.

Eydinov et al. (2005) adopted B-spline parameterisations for relative permeabilities in a three-phase problem by extending their previous work (Reynolds et al., 2004) which used the Corey-type functions. Also they presented the regularisation approach using the statistical prior model for relative permeabilities. For example, Reynolds et al. (2004) defined the mean and variance of each of model parameters which represent relative permeabilities. However, especially from the upscaling point of view, the procedure to derive the prior models for relative permeabilities was not clearly described there.

Christie et al. (2002b) applied the uncertainly quantification method to a field-scale reservoir model using an exponential representation of coarse-scale relative permeabilities. The hypothetical truth profile was generated from the results of a finer-scale simulation. Subbey et al. (2006) history-matched relative permeabilities for core-flooding experiments using B-splines. It was confirmed that the maximum likelihood model was accurate in reproducing the observed data. Then they sampled from the posterior distribution by running a long chain of MCMC and performed a Bayes update of the probabilities. The details of the method have been explained in Chapter 3. The uncertainty envelopes of the production profiles and the relative permeabilities were presented in their paper. Extending their work (Christie et al., 2002b; Subbey et al., 2006), this thesis uses the B-spline representation as well as power / exponential functions for the coarse-scale relative permeabilities. It focuses on the quantification of uncertainty in coarse-scale relative permeabilities.

Chapter 6

Uncertainty in Relative Permeabilities for 1D Models

6.1 General Remarks

Reservoir production forecasts are essentially uncertain due to the lack of data. Specifically, it is impossible to know the detailed heterogeneity in a reservoir. In order to mitigate the ambiguity of a model, production data is incorporated into a history-matching process. However, there is insufficient data to constrain the subsurface properties all over the field. Furthermore, coarse-scale models which do not have high resolution are often employed during history matching, because of computational cost. In this thesis coarse-scale properties are investigated with respect to history-matching and uncertainty quantification. The flow simulator used in this thesis is ECLIPSE 100 (Schlumberger, 2004a).

Two issues are addressed in this thesis. Firstly, because the coarse-scale model inevitably misses out sub-grid heterogeneity, physical dispersion is usually ignored in the simulation. Secondly, the small-scale heterogeneity is not explicitly known and can only be inferred by

history-matching. To solve these problems, local features in the coarse-scale relative permeability curves are adjusted in history-matching to capture the effect of physical dispersion and to compensate for the effect of numerical dispersion.

The approach proposed in this thesis aims at encapsulating sub-grid heterogeneity in multiphase flow functions directly at the coarse-scale, and predicting uncertainty. Rock relative permeability curves are often altered to reproduce production data during the process of history-matching, although guidelines for changing the shape of the curves have not been clearly established. In this chapter, B-spline functions are employed to parameterise relative permeabilities and try to clarify their influence on the uncertainty estimation. B-spline parameterisation is flexible allowing the capture of local features in the relative permeability curves, as described in Section 5.4.

The history-matched relative permeabilities and their uncertainty envelopes are examined in comparison with the two-phase upscaling results. A synthetic data set for which the true solution is known is used for the purpose of the comparison. The two-phase upscaling is conducted using the truth model to give a reference set of coarse-scale relative permeability curves. Also the truth production profiles are compared with the uncertainty envelopes which are quantified in Bayesian framework. The framework used is the Neighbourhood Approximation (NA) Algorithm and NA-Bayes Algorithm, which has been explained in Section 3.3.

6.2 Model and Problem Description

In this chapter, history-matching is conducted on a one dimensional coarse-scale model. There are two reasons for choosing a 1D coarse-scale model. Firstly, it is important to analyse the result using a simple model and to seek insight which could contribute to the later studies in more complicated two dimensional models. Actually, a two dimensional model is chosen in Chapter 9. Before moving on to the two dimensional model, this chapter describes the numerical experiments using the simple model. Secondly, the small-scale heterogeneity nested in large-scale heterogeneity has been investigated in terms of uncertainty quantification in a reservoir model,

(e.g., Hastings et al., 2003), as summarised in Section 2.5. In that sense, a one dimensional coarse-scale model used in this chapter can be regarded as a part of a channel configuration or a stream-line. Here, the small-scale heterogeneity inside the channel corresponds to sub-grid heterogeneity in the coarse-scale model and is to be captured using the proposed approach. So the result can contribute to the analysis in small-scale heterogeneity inside the fixed large-scale heterogeneity.

Note that whereas the coarse-scale model is one dimensional, the truth fine-scale model is two dimensional. The details are explained in the below. Also this section provides the description of the problem.

6.2.1 Fine-Scale Model, Coarse-Scale Model and Observed Data

A water flooding scenario in an oil reservoir is assumed for the numerical experiments. A 2D truth model is generated, which is shown in Figures 6.1 (permeability distribution) and 6.2 (histogram). This is also referred to as the fine-scale model, in contrast to the coarse-scale model used for history matching (Figure 6.3). There are 55×275×1 cells in this fine-scale model, each of size 5m×5m×20m. Porosity is 0.2 and is uniform throughout the model. The permeability was generated by Sequential Gaussian Simulation (SGS) (Deutsch and Journel, 1998, p. 144) and was conditioned to data for 2 vertical wells (200mD), the locations of which are described in the next paragraph. The correlation length is 135m in the Y-direction (North) and 67.5m in the X-direction (East). The Gaussian random numbers were transformed to logarithmic permeabilities, ln(k), by multiplying them by the standard deviation and adding the mean. In this case, the mean and standard deviation of ln(k) were assumed to be 5.3 and 0.5 respectively. The relative permeability for the truth model was assigned by adopting Corey-type rock curves (Corey, 1954) with an exponent of 2, i.e.,

$$K_{ro}(S_w) = \left(\frac{1 - S_w - S_{or}}{1 - S_{wc} - S_{or}}\right)^2, \tag{6.2.1}$$

$$K_{rw}(S_w) = \left(\frac{S_w - S_{wc}}{1 - S_{wc} - S_{or}}\right)^2, \tag{6.2.2}$$

$$S_{wc} = S_{or} = 0.2, \tag{6.2.3}$$

where $K_{ro}(S_w)$ and $K_{rw}(S_w)$ denote oil and water relative permeabilities, S_w is water saturation, S_{wc} is connate water saturation and S_{or} is residual oil saturation. Oil viscosity is approximately 1.0 [cp] and water viscosity is 0.3 [cp]. The other parameters for the fluid properties are the same as those in the second data set of the 10th SPE Comparative Solution Project (Christie and Blunt, 2001). Note that the units used in the paper (Christie and Blunt, 2001) were converted from field units to metric units (Schlumberger, 2004a) in this case. The PVT table is provided in Table 6.1.

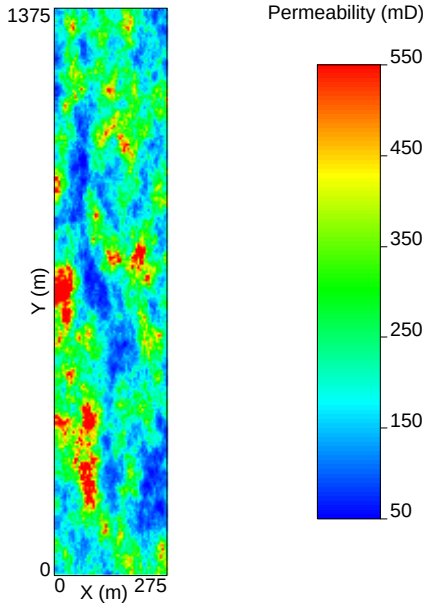

Figure 6.1: Permeability distribution of the "truth" fine-scale model. The "truth" permeability field was generated by Sequential Gaussian Simulation. Note that history-matching was conducted using the 1D coarse-scale models (Figure 6.3).

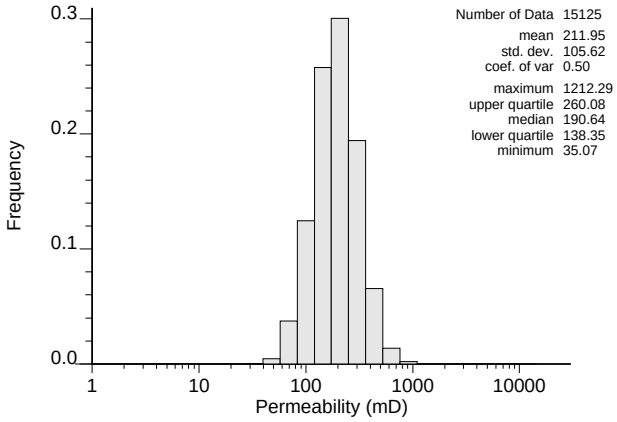

Figure 6.2: Permeability histogram of the "truth" fine-scale model (Figure 6.1). Note that the *x*-axis is logarithmic.

Table 6.1: PVT Table for the flow simulations in Chapter 6

Pressure [Bars]	Oil Formation Volume Factor [rm^3/sm^3]	Viscosity [cp]
20.684271	1.05	0.950
55.158056	1.02	0.997
551.58056	1.01	1.000

The coarse-scale model (Figure 6.3) was employed for multiple flow simulations for history-matching. The coarse cell size is 275m×275m×20m and the number of cells is 1×5×1. The producer and water injector wells were placed at the centres of the edge coarse cells, and the well positions in the coarse-scale model are exactly the same as those in the fine-scale (truth) model. The boundary conditions were the same in both scale models: the producer well was controlled by a bottom hole pressure (BHP) of 400 [bar], the injector well was controlled by a rate of 330.0 [m^3/day] (reservoir conditions) and BHP limit of 689.48 [bar], and the sides of the model were sealed.

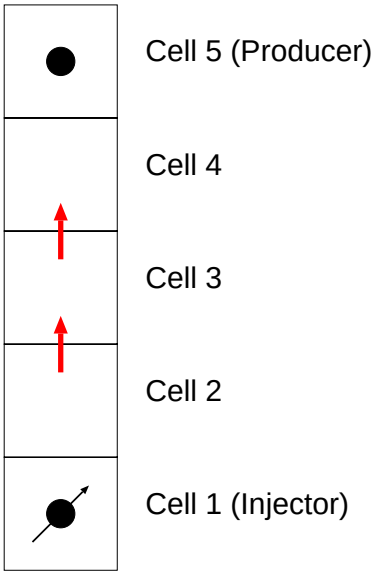

Figure 6.3: 1D coarse-scale model for history-matching. The two arrows in the inter-well cells represent flows for which the relative permeabilities are adjusted during history-matching.

Here, the main task is to estimate relative permeabilities at the coarse scale through history-matching rather than varying parameters at the fine scale. The correlation length of the truth model is less than half of a coarse-scale cell (275m). In other words, each coarse-scale cell contains sub-grid heterogeneity for which the range is smaller than a cell. In most models, a range of coarse-scale relative permeability curves is required to take account of fine-scale effects. Also, the relative permeability usually depends on distance from the wells in coarse-scale models, (Hewett et al., 1998). In this study, however, the second and third cells from the injector cell have been chosen as the target cells for history matching, and they are referred to as Cell 2 and Cell 3, respectively (Figure 6.3). For simplification, although the truth model is unknown in real situations, the truth model was used to fix all parameters other than relative permeabilities of Cells 2 and 3. Note that the small-scale heterogeneity was absent in the coarse-scale model.

As mentioned already, the calibration parameters are the relative permeabilities in the inter-well region of the model, i.e. the relative permeabilities for cells 2 and 3 (Figure 6.3). The near-well regions were treated as a special case, and the upscaled permeability and relative permeability were calculated for these regions. In a real reservoir, there is more data available in the near-well regions, so this is a reasonable procedure. Additionally, the near-well region has to be treated with care, because it is radial flow rather than linear flow. The method adopted here is described in Ding (1995), Durlofsky et al. (2000) and Muggeridge et al. (2002), and calculates the coarse-scale well connection factor in cells 1 (injector) and 5 (producer), and the transmissibilities between cells 1 and 2, and 4 and 5. Then this method was extended to two-phase flow, to calculate the upscaled relative permeabilities for the well connections and the interfaces between the wells and adjacent cells (Appendix). At the two inter-well cells (2 and 3), the absolute transmissibilities were calculated using the averaging method adopted in the PVW method of the Eclipse Pseudo Package (Schlumberger, 2004b, p. 87).

The model was history-matched by adjusting a single set of relative permeability curves for those two cells. For comparison, two sets of the upscaled relative permeabilities were also calculated for the two cells using the PVW method (ECLIPSE PSEUDO package (Schlumberger, 2004b, p. 87)). Figures 6.4 and 6.5 show the production performance of the fine-scale model,

the coarse-scale model with rock curves and the coarse-scale model with the upscaled relative permeabilities. The oil rate and injector bottom hole pressure (BHP) of the coarse-scale model with the upscaled relative permeabilities coincide with those of the fine-scale model, whereas the coarse-scale model with rock curve fails to reproduce the fine-scale profiles in some intervals. In the section below, the two sets of the upscaled relative permeabilities were replaced with the one set of optimised relative permeability curves, and the results were compared.

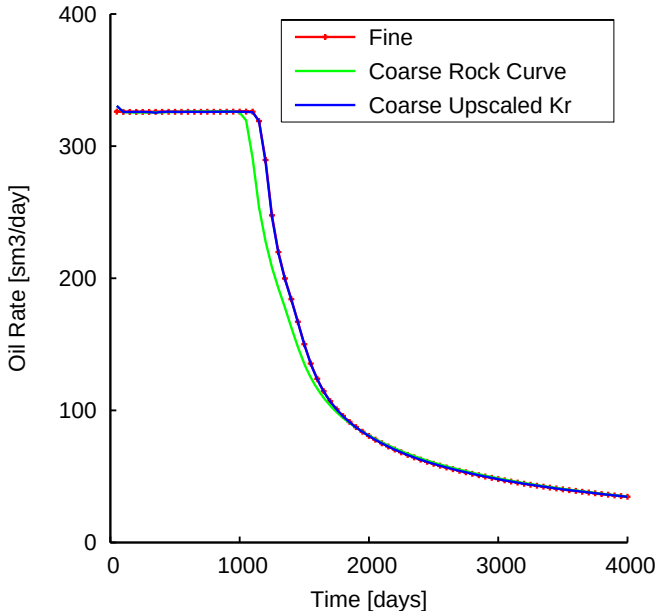

Figure 6.4: Oil production rate. The production profiles of the fine-scale model, the coarse-scale model with rock curves and the coarse-scale model with the upscaled relative permeabilities are compared. Note that the curves of the fine-scale model and the coarse-scale model with upscaled relative permeabilities are superimposed.

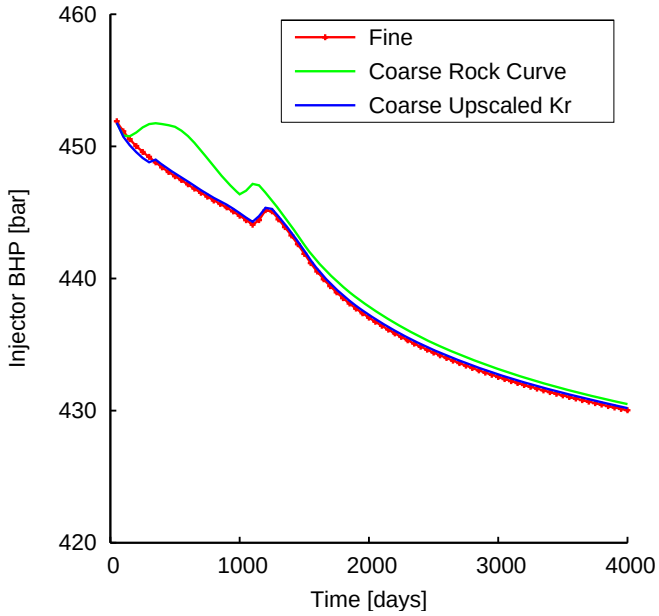

Figure 6.5: Injector bottom hole pressure (BHP). The production profiles of the fine-scale model, the coarse-scale model with rock curves and the coarse-scale model with the upscaled relative permeabilities are compared.

The oil rate and injector BHP were used as history data. To create a more realistic case, uncorrelated random noise was added to the fine-scale data in the following way. A set of random numbers *rnd* was drawn from a normal distribution, $rnd \sim N(0,1)$, and Observed Oil Rate and Observed Injector BHP were defined:

$$(\text{Observed Oil Rate}) = (\text{Fine model Oil Rate}) + \sigma_q \, rnd, \tag{6.2.4}$$

$$(\text{Observed Inj. BHP}) = (\text{Fine model Inj. BHP}) + \sigma_p \, rnd, \tag{6.2.5}$$

where σ_q and σ_p are the standard deviations of the data errors for the oil rate and injector BHP respectively. Here, it is assumed that $\sigma_q = 15.0\,[\mathrm{m}^3/\mathrm{day}]$ and $\sigma_p = 1.0\,[\mathrm{bar}]$. The fine-scale data was denoted as the truth in the sections below. Then the data upto 1350 days was used as history data. The task is to history-match the coarse-scale model to the observed data, by adjusting the relative permeability curves. Finally, the production performance is predicted to 4000 days, and the uncertainty in the forecast is quantified.

6.2.2 Misfit Definition

In the numerical experiments, it is assumed that the data errors are independent and identically distributed (i.i.d.). The likelihood function is defined in the following Gaussian expression.

$$\text{prob}(\mathbf{o}|\mathbf{m}) \quad \propto \quad \prod_{k=1}^{N} \exp\left(-\frac{(q_k - q'_k)^2}{2\sigma_q^2} - \frac{(p_k - p'_k)^2}{2\sigma_p^2}\right). \tag{6.2.6}$$

Here q' and p' represent the simulated oil rate and BHP respectively, and q and p represent the observed oil rate and BHP respectively. The subscript $k = 1, 2, \ldots, N$ represents the time step. N is the total number of the time series data. As above, σ_q and σ_p are the standard deviations of the data errors. Accordingly, the measure of misfit, M, as an objective function can be given in the least squares sense by the following equation.

$$M = \sum_{k=1}^{N} \left(\frac{(q_k - q'_k)^2}{2\sigma_q^2} + \frac{(p_k - p'_k)^2}{2\sigma_p^2}\right). \tag{6.2.7}$$

6.3 Parameterisation for Relative Permeabilities

As described in Chapter 5, relative permeability is defined as the ratio of phase permeability to absolute permeability and is assumed to be a function of saturation, (e.g., Honapour et al., 1986; Willhite, 1986). It is not appropriate to use relative permeability curves obtained from core flooding experiments directly in coarse-scale simulation models. Ideally they should be upscaled to account for geological heterogeneity, fluid forces and numerical gridding effects. However, two-phase upscaling is time consuming and is not robust, (Barker and Thibeau, 1997; Barker and Dupouy, 1999). An alternative approach is to obtain relative permeabilities directly at the coarse scale by history-matching, and this is the approach taken here.

6.3.1 B-spline Function for Relative Permeabilities at the Coarse Scale

B-splines are piecewise polynomials which form useful local basis elements for spline spaces, (Schumaker, 1981). The shapes of the basis elements are determined by a knot-vector, which is a partition of the interval on which the function is to be defined. The advantage is that any continuous function can be approximated by polynomial splines with sufficient number of knots. Introduction of knots in an interval gives flexibility in defining the function over that interval. As described in Sections 5.3 and 5.4, whereas the power law (Corey, 1954) and exponential function (Chierici, 1981) have only a small number of parameters to control the shape of the whole relative permeability curve, B-spline functions can have more parameters each of which control a limited part of the curve, (e.g., Subbey et al., 2006). This characteristic of B-spline function leads to the local flexibility for adjusting curves during the history-matching. In this chapter, the relative permeability is parameterised with the fourth order (cubic) B-spline function in the following way.

$$K_{ri}(S_w) = \sum_{j=1}^{n} c_j^i N_j^4(S_w) \quad \text{for } i = o, w, \tag{6.3.1}$$

where $K_{ri}(S_w)$ is the relative permeability for the i-th phase, $N_j^4(S_w)$ is the j-th normalised cubic B-spline basis function (Schumaker, 1981), c_j^i is the j-th B-spline coefficient for the i-th phase

and n is the B-spline dimension, (Schumaker, 1981; Subbey et al., 2006).

It is important to select appropriate parameters for the spline function (number of dimensions and knot spacing) to produce a realistic shape for the relative permeabilities, (Watson et al., 1988; Richmond and Watson, 1990). Preliminary tests for approximately linear water flooding cases, that is to say nearly line-drive, were performed on 2D stochastic models, which were upscaled using dynamic upscaling (the PVW method (Schlumberger, 2004b, p. 87)). These tests showed that when a model was upscaled, the upscaled relative permeabilities were shifted to the right compared with the rock curve to compensate for numerical dispersion, (Kyte and Berry, 1975). If there is a long correlation in the principal flow direction, however the upscaled relative permeabilities are shifted to the left to represent early breakthrough. According to these results, 6 B-spline basis functions (6-dimension) were adopted with non-uniformly spaced knots at water saturations of 0.20, 0.35, 0.50 and 0.80. This allows the representation of complex upscaled relative permeabilities, especially in the saturation range between 0.2 and 0.5. The B-spline basis functions are shown in Figure 6.6.

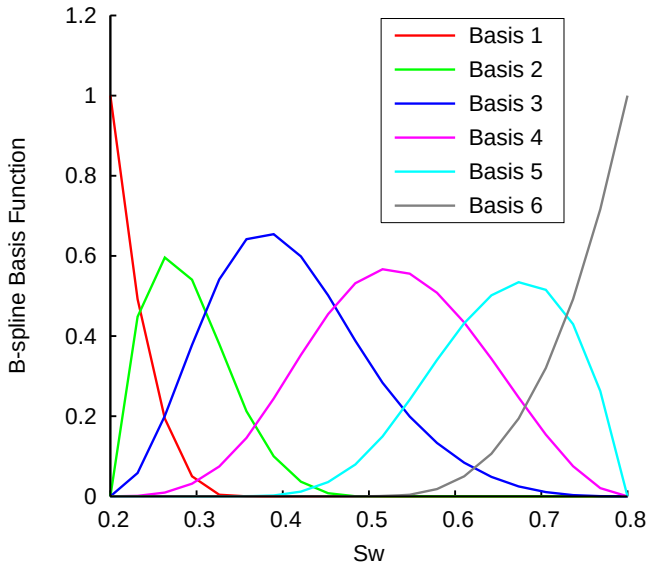

Figure 6.6: Normalised cubic B-spline basis functions. The dimension of the B-splines is 6. Non-uniformly spaced knots were used. The values of water saturation at the knots are 0.20, 0.35, 0.50 and 0.80.

6.3.2 Prior Distribution and NA-Algorithm Parameters

The prior information was based on both the rock curves and the scale-change effect in order to narrow down the parameter space of B-spline coefficients. This tends to reduce the computational cost for history-matching, i.e. the number of flow simulations required to converge to the best fit regions in the parameter space. The minimum and maximum values for each B-spline coefficient were fixed as shown in Table 6.2. The range of relative permeabilities corresponding to the minimum and maximum coefficients are shown in Figure 6.7.

Table 6.2: Min. and Max. values for the B-spline coefficients

Basis No., j	c_j^o min.	c_j^o max.	c_j^w min.	c_j^w max.
1	1.0	1.0	0.0	0.0
2	0.3	1.0	0.0	0.4
3	0.0	1.0	0.0	0.7
4	0.0	1.0	0.0	1.0
5	0.0	0.7	0.0	1.0
6	0.0	0.0	1.0	1.0

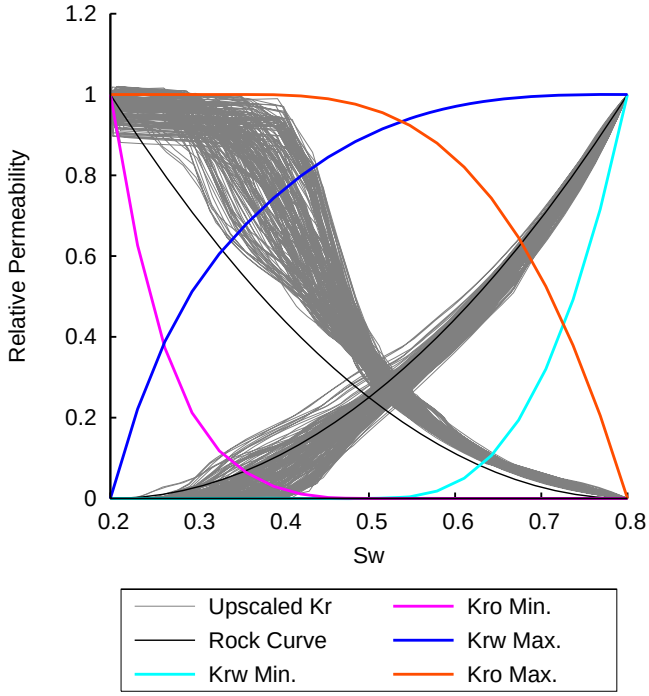

Figure 6.7: Range of K_{rw} and K_{ro}. The ranges of the curves were determined from the allowed ranges of the B-spline coefficients.

In real situations it is impossible to calculate the upscaled relative permeabilities for thousands of fine-scale models. So here instead of abstracting the detailed features, the possible parameter ranges of the upscaled relative permeabilities were roughly speculated from a variety of models which have different correlation lengths. Figure 6.7 shows the upscaled relative permeabilities, calculated for a range of correlation lengths: $0 \leq \lambda_X \leq 67.5\,\mathrm{m}$, and $0 \leq \lambda_Y \leq 1350\,\mathrm{m}$. The total number of models generated by SGSIM is 96, 16 cases times 6 realisations for each case, including the truth model. The standard deviation and mean assumed in the transformation to logarithmic permeabilities are the same as those for the truth model explained above. Figure 6.7 also includes a homogeneous model in which the only effect is the compensation of numerical dispersion. Figure 6.7 indicates that the minimum and maximum values of B-spline coefficients were selected in advance so that it could narrow down the parameter space and cover a wide variety of the upscaled relative permeabilities encapsulating the possible fine-scale features.

As shown in Table 6.2, the history-matching of a set of relative permeabilities for cells 2 and 3 are conducted by adjusting 8 parameters, 4 for each phase, within the specified ranges. In the section below, parameters 1 to 4 denote c_2^o to c_5^o for the oil phase. In the same manner, parameters 5 to 8 denote c_2^w to c_5^w for the water phase. Since the NA-algorithm samples parameters within the prior ranges, it can be said that the resultant ensemble is automatically truncated by the edges of a uniform prior distribution. Then, the next task is to sample the resulting ensemble using MCMC with Neighbourhood Approximation. This step of MCMC is referred to as sampling from posterior probability distribution (PPD). Here, because of the Neighbourhood Approximation, the product of the likelihood and prior distribution, $\mathrm{prob}(\mathbf{o}|\mathbf{m}) \times \mathrm{prob}(\mathbf{m})$, of the second ensemble has already been evaluated in the first step.

The characteristic of NA-sampling, in terms of exploration and exploitation, is largely controlled by the two tuning parameters n_s and n_r, (Sambridge, 1999a). The values of n_s and n_r used here were 96 and 48 respectively for the purpose of the exploratory sampling within the limitations of computational cost. The sample size of the initial iteration was the same as n_s, and the number of iterations was 76 in this case. The convergence was confirmed by increasing

the number of iterations and the other tuning parameters. For example, even if both n_s and n_r were doubled, the resultant relative permeabilities were similar to the original case.

6.4 Results of History-matching and Uncertainty Quantification

History-matching multiple models requires several hundreds to thousands of realisations. This section presents results obtained from the numerical experiments which used the NA-algorithm to generate 7296 models by sampling a 8-dimensional parameter space. To quantify the uncertainty in the predictions, a long chain of MCMC was run on the misfit surface to collect 100000 models in total, and then a Bayes update of the probabilities was performed. The frequency of visits to each Voronoi cell were monitored during the random walk. It allowed the calculation of the relative probability of each model in the ensemble. Since the MCMC algorithm samples from the PPD through the product of the likelihood and the prior distribution, the calculated probability is representative of the posterior probability of each model. The probability of each model determined not only the expectation, but also P10 and P90 cut-offs for each of the estimated relative permeabilities and production profiles (e.g., Christie et al., 2002b).

The observed data was used up to 1350 days, corresponding to 38.9% of water cut, for history-matching, and then the uncertainty was quantified up to 4000 days. The results are shown in Figures 6.8 to 6.17. Figures 6.8, 6.9 and 6.10 confirm the convergence of NA-sampling to regions of good fit. In Figure 6.9, the misfit of the model which has the reference upscaled relative permeabilities in Cells 2 and 3 is shown for comparison. The misfit of the history-matched model became lower than that of the upscaled model, since the well-matched models were sampled in the history-matching. Figure 6.10 plots the misfit divided by the number of the observed data and multiplied by 2, where the number of the history data is 54 which means 27 for each of the oil production rate and injector BHP. This manipulation provided a convergence criteria 1.0 in the y-axis of Figure 6.10, since the square of the error divided by the number of

the data should be equal to the variance for an ideally matched model. According to Figure 6.10, the generated models reached the sufficient match indicated by 1.0 in the *y*-axis. Figure 6.11 indicates that the optimised relative permeability curves are similar to the upscaled relative permeabilities. The history-matched curves are slightly different from the rock curve and capture the trend of the upscaled relative permeabilities. Also, the diagram shows that the two upscaled relative permeabilities were successfully grouped into one set of curves through history-matching. Figures 6.12 and 6.13 illustrate the history-matching results for the oil rate and the injector BHP. Note that only the observed data indicated by the squared symbols were used in history-matching. As shown in the figure, the history-matched profiles are surrounded by the observed data. Also, in this case the simulated oil rate and injector BHP seem to almost overlap with the truth profile.

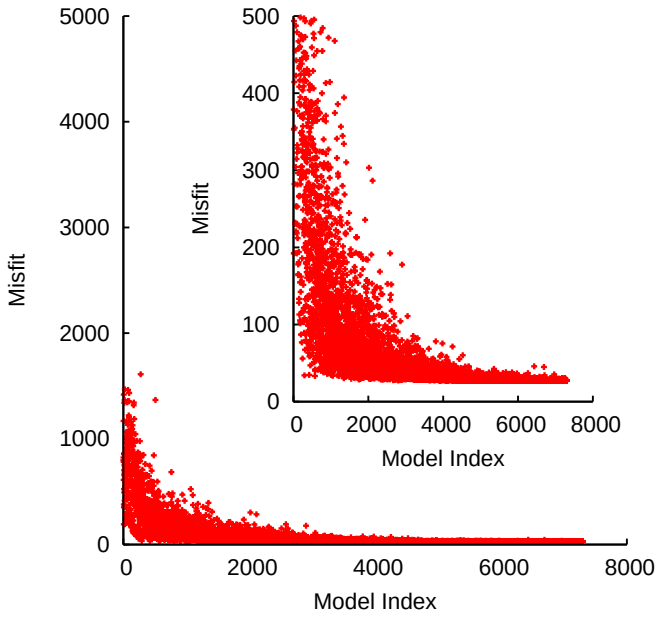

Figure 6.8: Misfit values during history-matching. History-matching of the relative permeabilities was conducted at the coarse scale using the B-splines. Note that the *y*-axis in the inserted figure has the magnified scale (the magnified version of the larger figure).

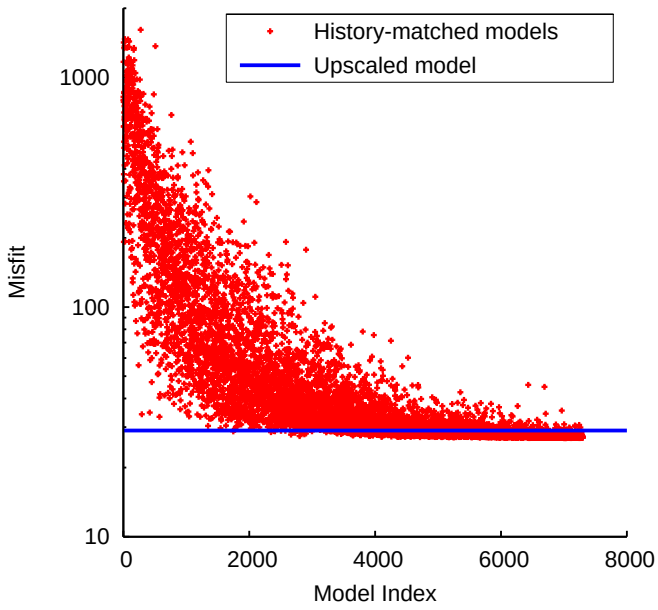

Figure 6.9: Misfit values during history-matching. Note that the *y*-axis is logarithmic. The misfit value of the upscaled model (Figures 6.4 and 6.5) is 29.0129 which is shown by the blue line for comparison.

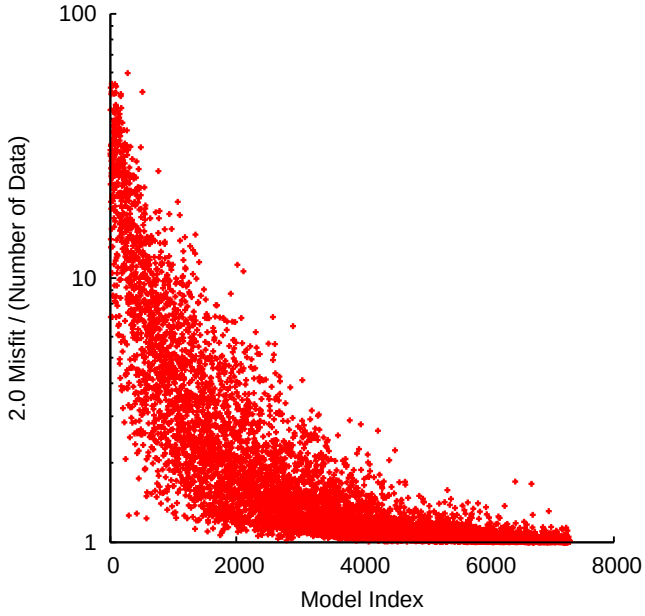

Figure 6.10: Misfit values divided by Number of Data. The y-axis is $2.0 \times$ Misfit/(Number of Data). The number of observed data was 54 which means 27 for each of oil production rate and injector BHP.

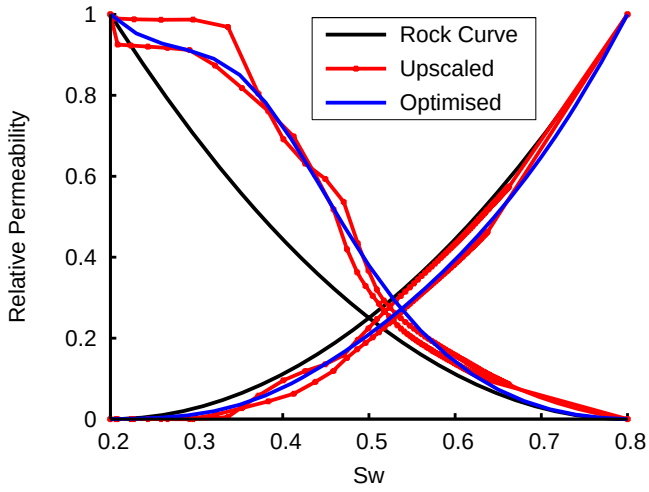

Figure 6.11: Optimised relative permeabilities. The optimised curves were obtained by minimising the misfit values in history-matching.

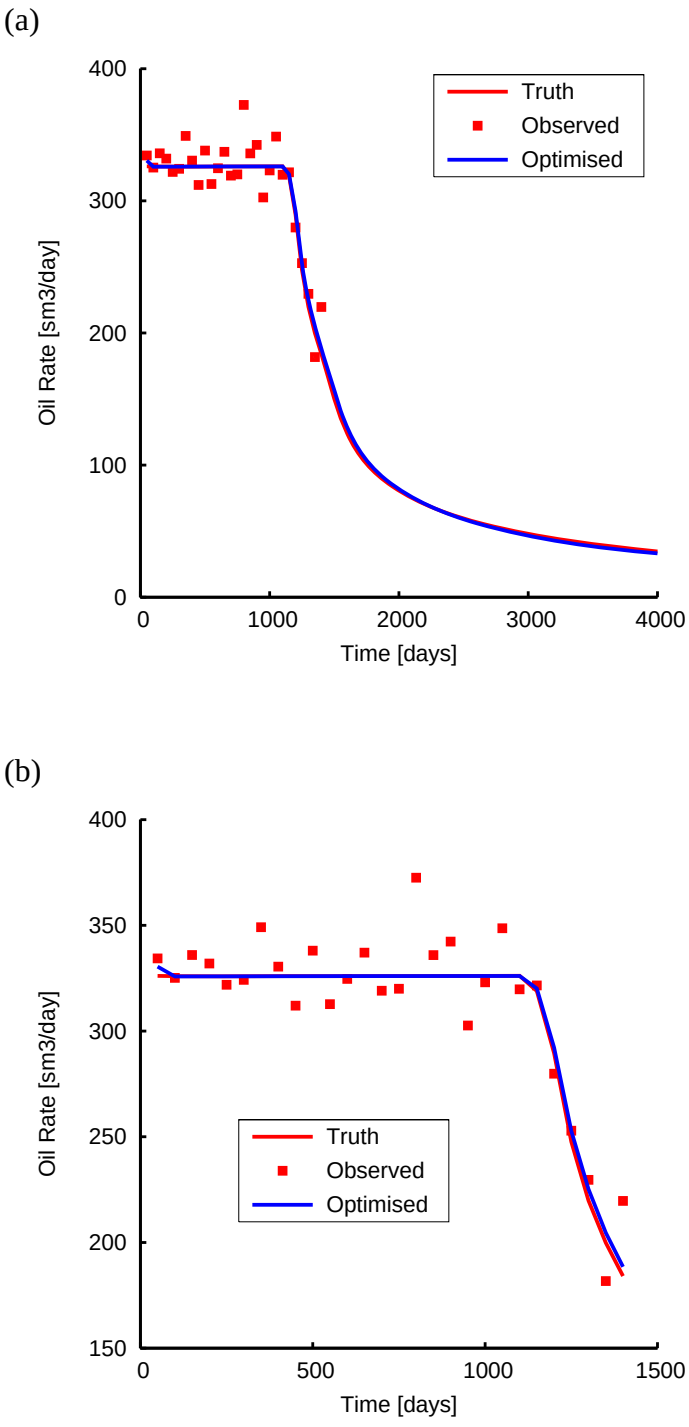

Figure 6.12: Oil production rate calculated using the optimised relative permeabilities. (a) The whole period is shown. (b) Only the history period is shown.

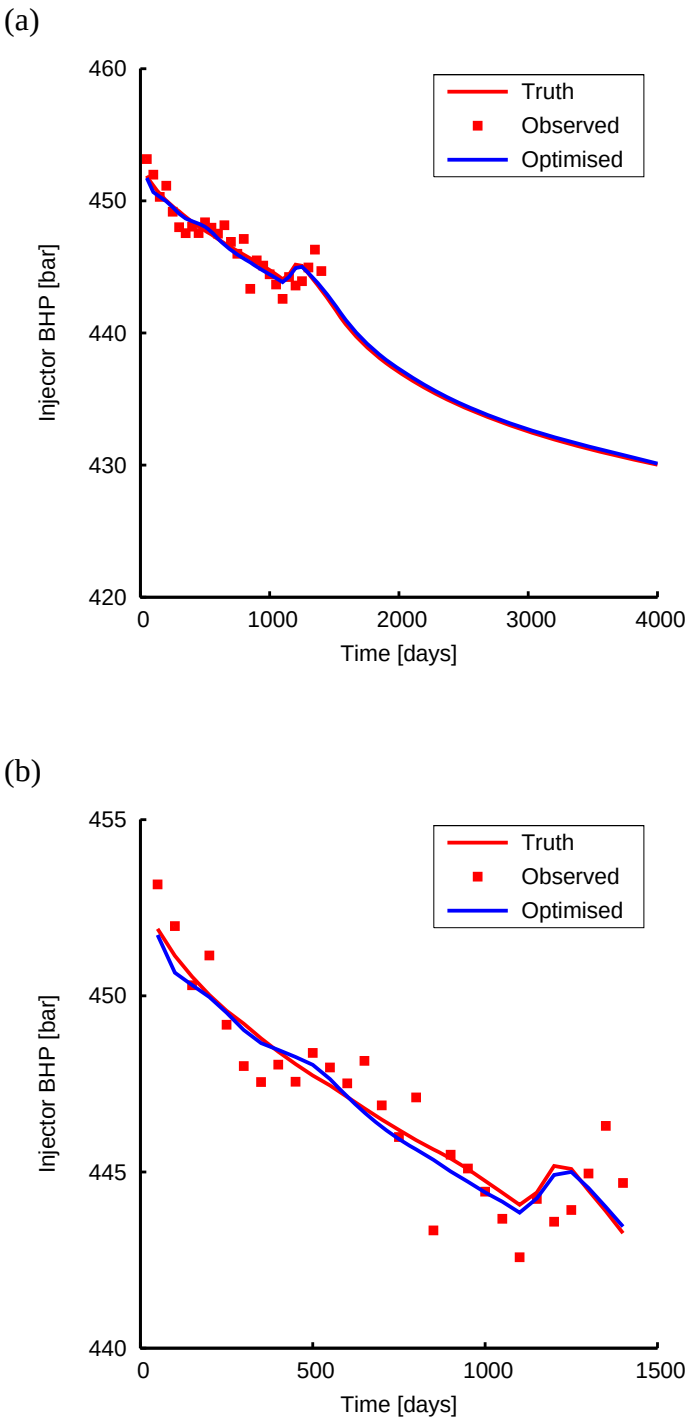

Figure 6.13: Injector bottom hole pressure calculated using the optimised relative permeabilities. (a) The whole period is shown. (b) Only the history period is shown.

Figure 6.14 plots the 1-dimensional marginal posterior probability distribution for each of the parameters. As shown in Figure 6.14, the marginal distributions of some parameters, e.g. Parameter 1, Parameter 4 and Parameter 8, have wide shapes rather than the narrow skewed shapes seen in the other parameters. The wide PPD means that the parameters may not be fixed through history-matching because of the lack of adequate information or noisy observed data. Also, the features of the wide PPD caused a wide uncertainty envelope in the relative permeability curves (Figure 6.15) and in the production profiles during the prediction period (Figures 6.16 and 6.17). The spread in oil rate, between the P10 and P90 values, is relatively small. However, in a real reservoir, this could represent a significant difference in cumulative oil, and shows the importance of taking uncertainty into account when planning the development of a field. Figures 6.16 and 6.17 show that the P10-90 envelopes spread in the forecast period. Figure 6.15 indicates that the P10-90 envelopes spread especially in the high water saturation region and there is also substantial spread in the oil relative permeability in the low water saturating region. These results of uncertainty quantification are discussed further in the next section.

Figure 6.18 plots water saturation vs. time which was calculated using the history-matched curves. It indicates that water saturation in Cells in 2 and 3 did not reach 0.60 in the history-period, and it caused the uncertainty as discussed in the next section and chapter.

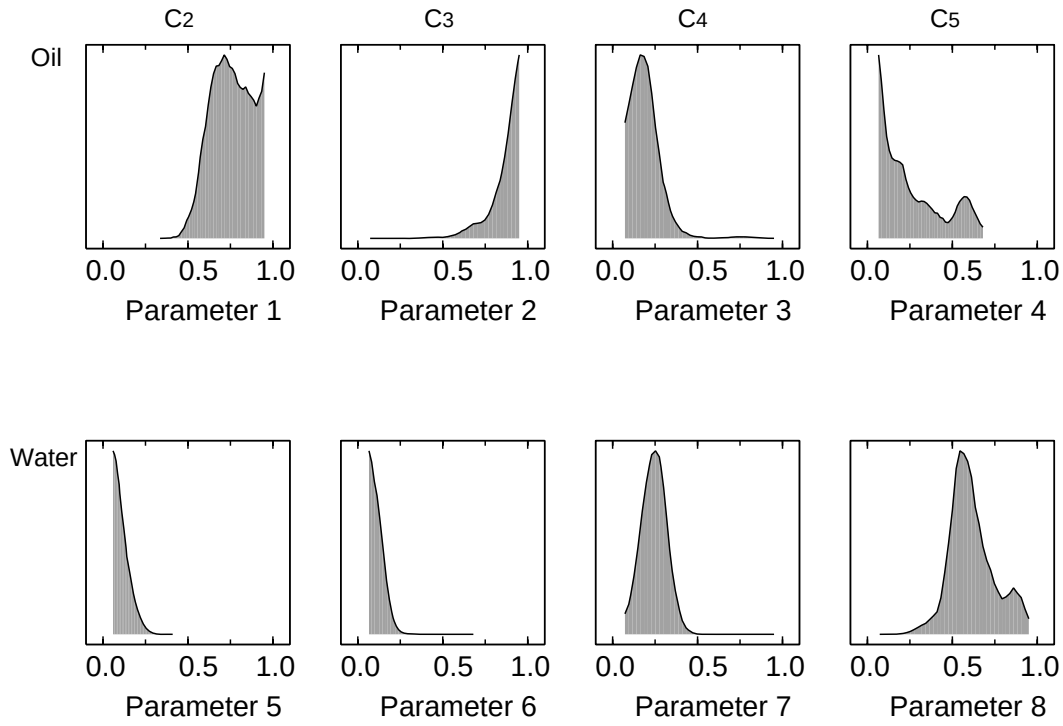

Figure 6.14: 1D marginal distribution for 100000 samples in the Markov chains. Note that each curve is scaled to its maximum height not the same area. The vertical axis ranges from 0 to each maximum with a linear scale. Each maximum height is provided in Table 6.3.

Table 6.3: Max. of each curve in Figure 6.14

	c_2	c_3	c_4	c_5
Oil	0.05	0.20	0.11	0.09
Water	0.10	0.18	0.12	0.09

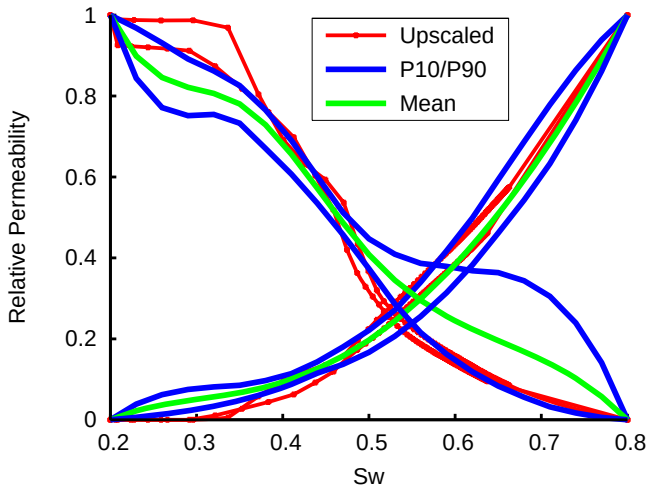

Figure 6.15: Uncertainty in relative permeabilities. The P10 and P90 cut-offs and mean were calculated.

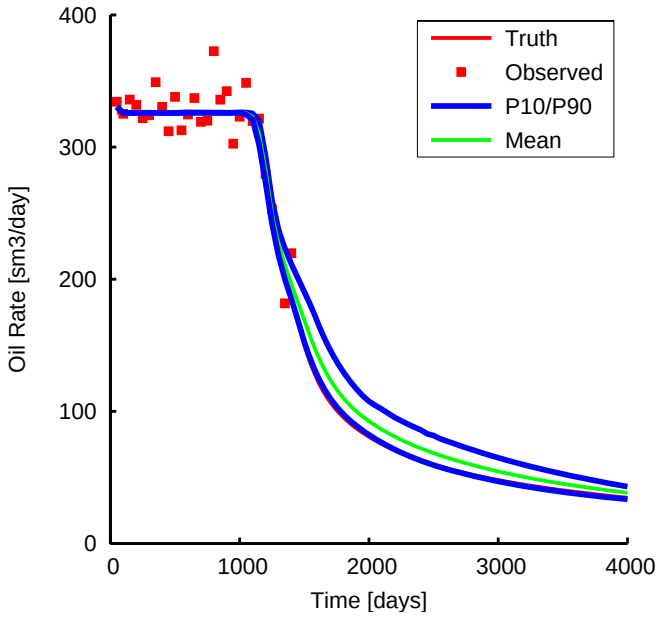

Figure 6.16: Uncertainty in oil production rate. The P10 and P90 cut-offs and mean were calculated.

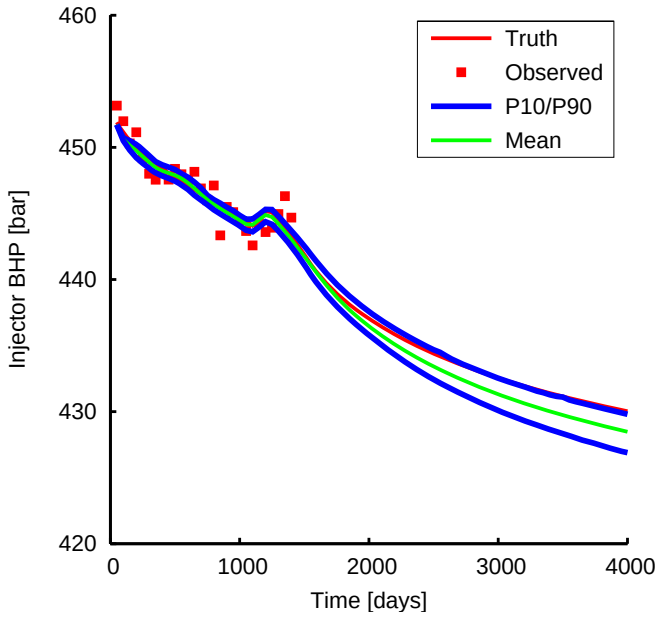

Figure 6.17: Uncertainty in injector bottom hole pressure. The P10 and P90 cut-offs and mean were calculated.

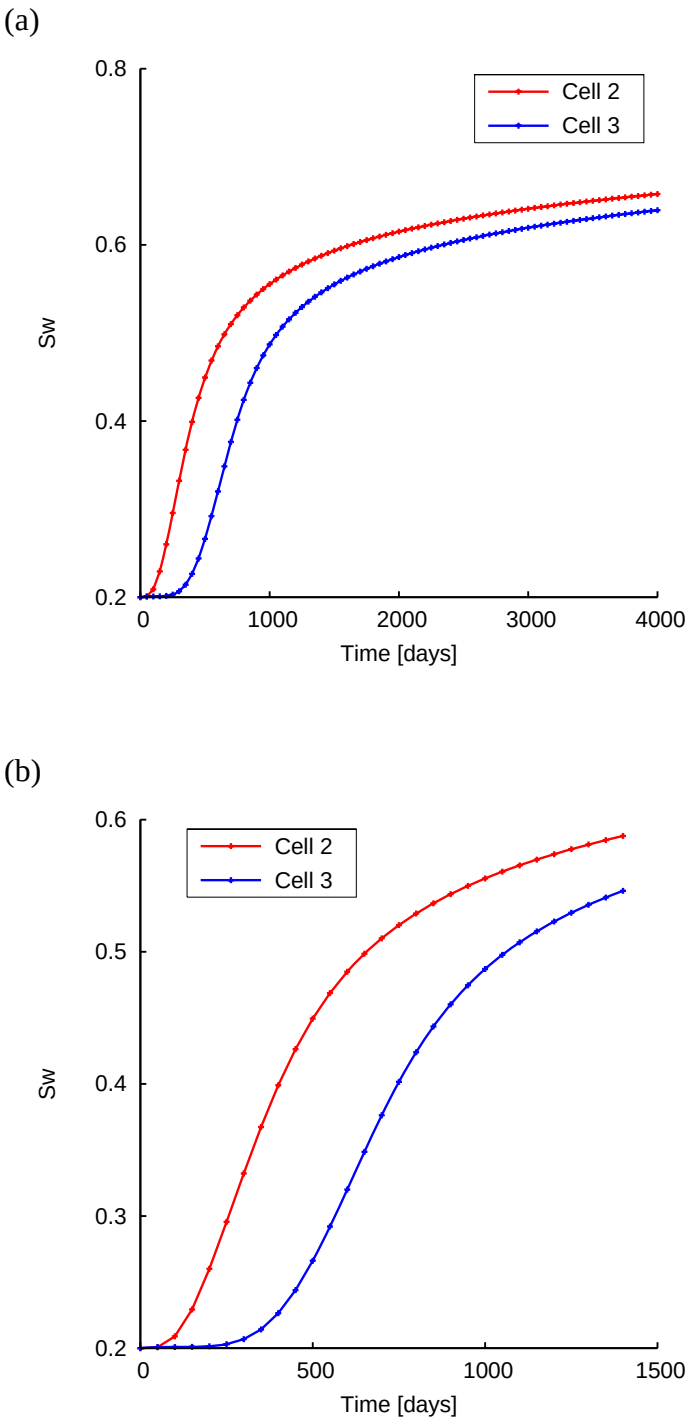

Figure 6.18: Water saturation in Cells 2 and 3 calculated using the optimised relative permeabilities. (a) The whole period is shown. (b) Only the history period is shown.

6.5 Sensitivity of History Data

This section presents additional results concerning the sensitivity of history data. It aims to analyse the results of the previous section further from different points of view. Another three numerical experiments are set up to see the effect of the observed data in terms of the standard deviation of noise and the period covered by history data.

Base Case In the previous section, the observed data was used up to 1350 days, corresponding to 38.9% of water cut, for history-matching, and then the uncertainty was quantified up to 4000 days. The standard deviations assumed in the oil production rate and the injector bottom hole pressure were $\sigma_q = 15.0\,[\mathrm{m}^3/\mathrm{day}]$ and $\sigma_p = 1.0\,[\mathrm{bar}]$, respectively. The case is referred to as the base case in this section. In the following cases, only the observed data and the corresponding misfit definition are changed, and the rest of the settings remain the same as the base case.

Case 1 The first case in this section was set up so that the noise in the observed data could be negligible: the standard deviations were one hundred times smaller than those of the base case. The history period was 4000 days, corresponding to 89.4% of water cut, and it was the same as the total period for which the uncertainty was quantified. The history-matching results are shown in Figures 6.19, 6.20 and 6.21. The simulated profiles are exactly overlapped with the truth profiles. Figure 6.19 supports the idea that the B-spline representation has a potential to capture the trend of the irregular shapes of the upscaled curves. Here, the important thing is that the results of uncertainty quantification are different from those of the base case. Figure 6.22 plots the 1-dimensional marginal distribution for each of the parameters, and corresponds to Figure 6.14 in the base case. The comparison of these figures reveals that all the parameters in Figure 6.22 have very narrow ranges, and only a single point on each axis has a high probability. Actually, the NA-Bayes program returned a single model index as a collected sample. This means that all the 100000 models collected had the same set of parameters, and it can be a single solution of the inverse problem. Hence, the figures corresponding to Figures 6.15, 6.16

and 6.17 are omitted, because they do not have any width in the envelope and are the same as the optimised curves and profiles in Figures 6.19, 6.20 and 6.21. This leads to a conclusion that Figures 6.15, 6.16 and 6.17 of the base case have the wide envelope because of a combination of the limited production history (up to 1350days) and a substantial amount of noise.

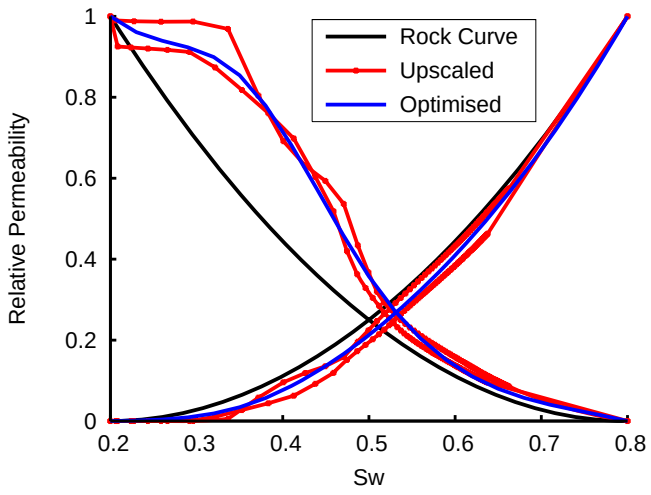

Figure 6.19: Optimised relative permeabilities (Case1). The history data used was up to 4000 days without noise.

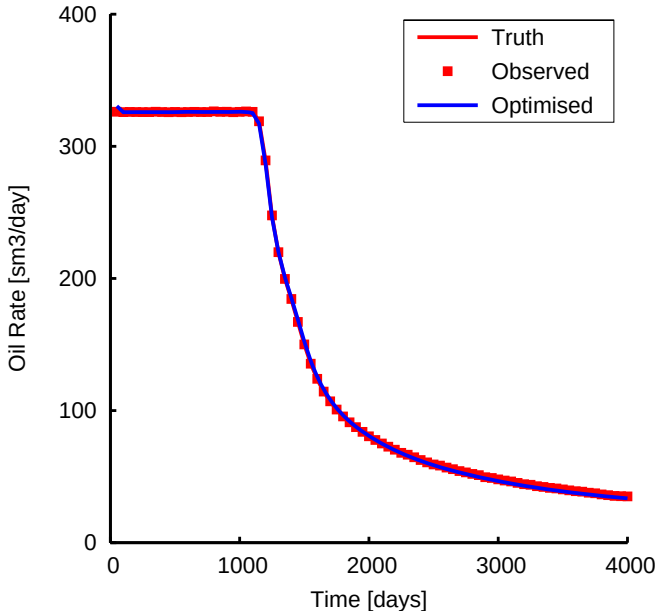

Figure 6.20: Oil production rate calculated using the optimised relative permeabilities (Case1). The history data used was up to 4000 days without noise.

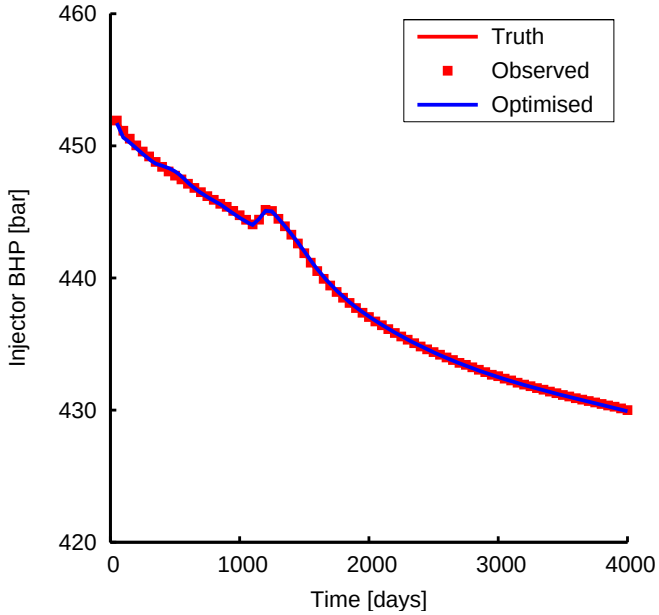

Figure 6.21: Injector bottom hole pressure calculated using the optimised relative permeabilities (Case1). The history data used was up to 4000 days without noise.

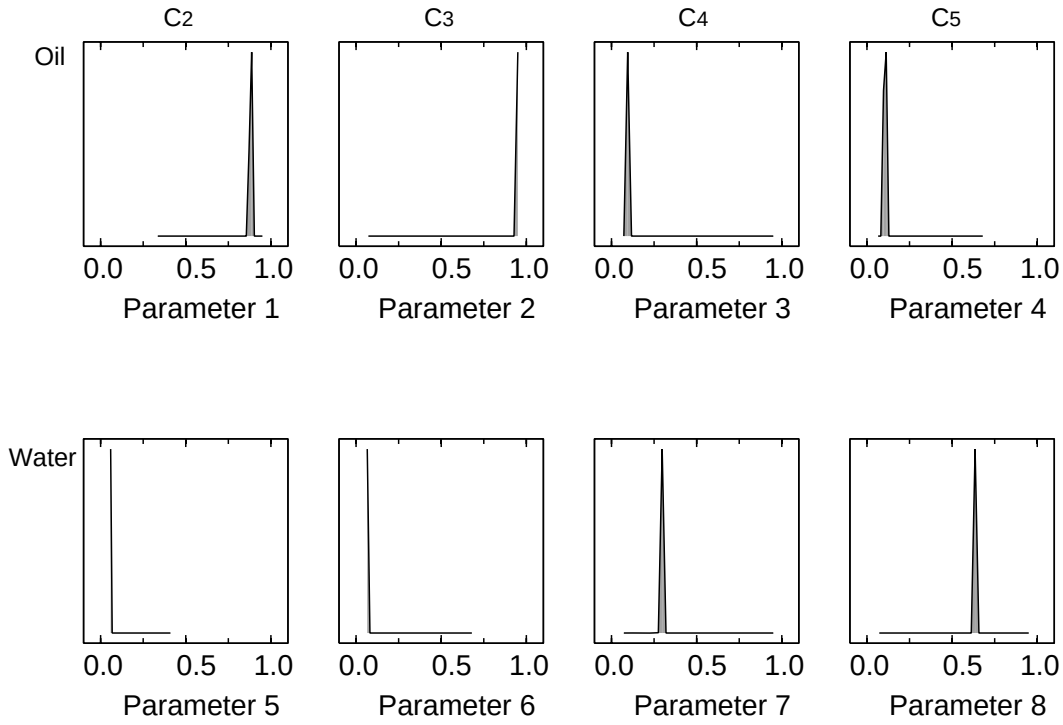

Figure 6.22: 1D marginal distribution for 100000 samples in the Markov chains (Case1). The history data used was up to 4000 days without noise. Note that each curve is scaled to its maximum height not the same area. The vertical axis ranges from 0 to each maximum with a linear scale. Each maximum height is provided in Table 6.4.

Table 6.4: Max. of each curve in Figure 6.22

	c_2	c_3	c_4	c_5
Oil	0.69	1.00	1.00	0.56
Water	1.00	1.00	1.00	1.00

Case 2 The second case was set up so that the noise in the observed data could be nearly zero as in the first case, and the history period was 1350days as in the base case. The history-matching results are shown in Figures 6.23, 6.24 and 6.25. Figure 6.23 shows that the relative permeabilities are close to the upscaled relative permeabilities in the low and middle water saturation region, and are slightly different from the upscaled curves in the high water saturation region. Figures 6.24 and 6.25 show that there is a small deviation between each of the optimised profiles and the corresponding truth one in the forecast period. This means that even if the noise in the observed data is negligible, the estimated parameters can be biased because of the limited period of history data. Figure 6.26 plots the 1-dimensional marginal distribution for each of the parameters, which corresponds to Figure 6.14 of the base case and Figure 6.22 of the first case in this section. All the parameters apart from parameter 1 in Figure 6.26 have a narrow peak as in Case 1. The NA-Bayes program returned only four model indexes in the collected 100000 sample. The uncertainty envelopes are very narrow as shown in Figures 6.27, 6.28 and 6.29. Parameter 1 in Figure 6.26 has two peaks in the distribution, which corresponds to a little opened envelope of oil relative permeabilities in Figure 6.27 between 0.2 and 0.35 in the water saturation axis. This is presumably because that the particular part of the relative permeabilities cannot have only the single solution but may have a few possible solutions in the inverse problem. Moreover, each distribution of parameters 4 and 8 in Figure 6.26 has a peak at the different position from the corresponding peak in Figure 6.22 of the Case 1. Since the Case 1 had the correct solution which matched the truth profile, the difference resulted in the bias in the estimated relative permeabilities of the second case. Hence, although the B-spline representation can capture the irregular shapes of the upscaled curves, there is no guarantee that the parameters corresponding to an insensitive saturation region, such as parameters 4 and 8 in this case, can be estimated correctly.

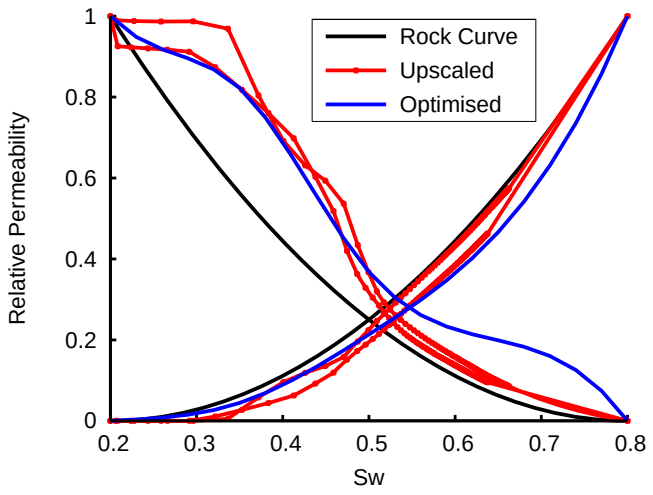

Figure 6.23: Optimised relative permeabilities (Case2). The history data used was up to 1350 days without noise.

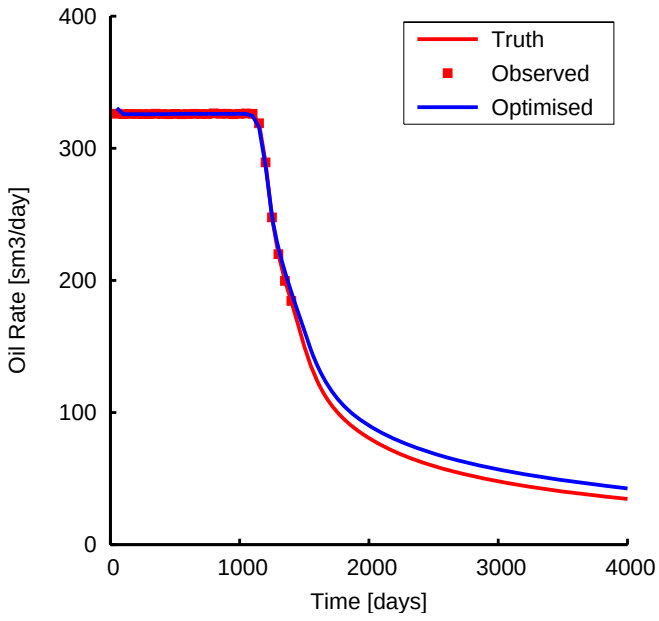

Figure 6.24: Oil production rate calculated using the optimised relative permeabilities (Case2). The history data used was up to 1350 days without noise.

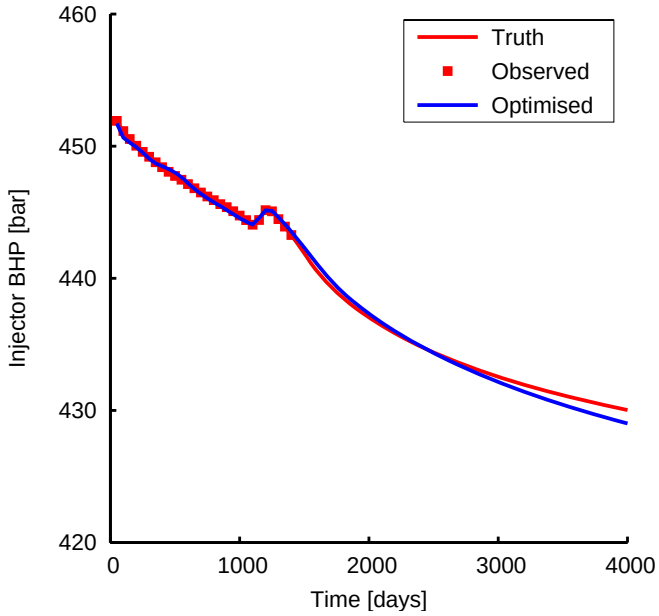

Figure 6.25: Injector bottom hole pressure calculated using the optimised relative permeabilities (Case2). The history data used was up to 1350 days without noise.

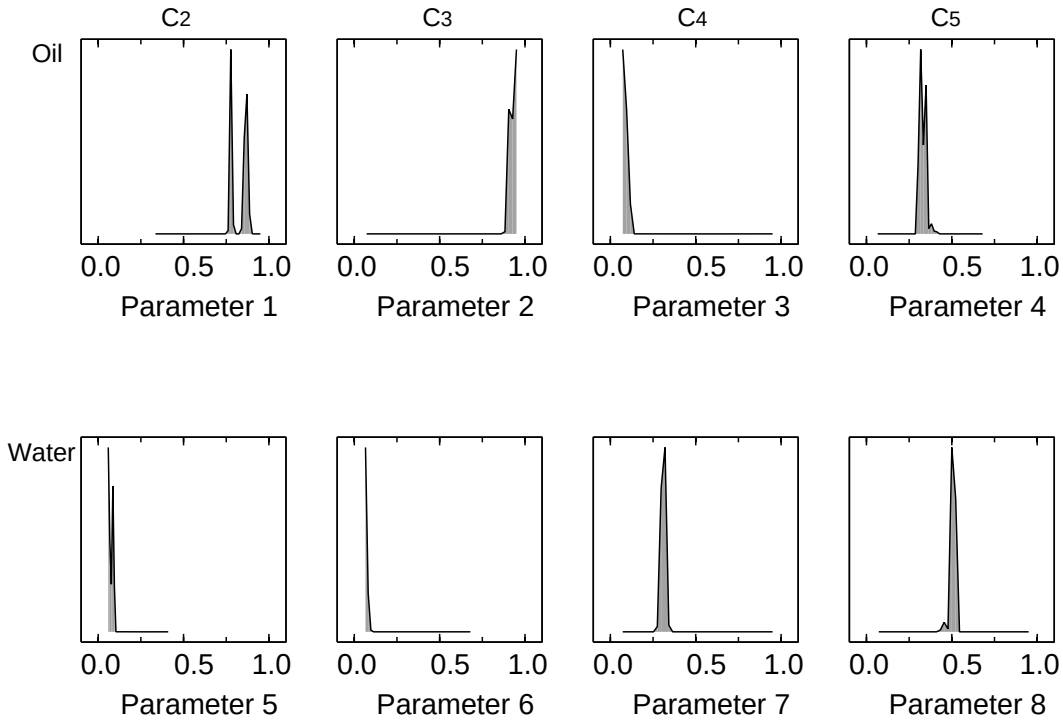

Figure 6.26: 1D marginal distribution for 100000 samples in the Markov chains (Case2). The history data used was up to 1350 days without noise. Note that each curve is scaled to its maximum height not the same area. The vertical axis ranges from 0 to each maximum with a linear scale. Each maximum height is provided in Table 6.5.

Table 6.5: Max. of each curve in Figure 6.26

	c_2	c_3	c_4	c_5
Oil	0.31	0.43	0.54	0.36
Water	0.35	0.82	0.54	0.56

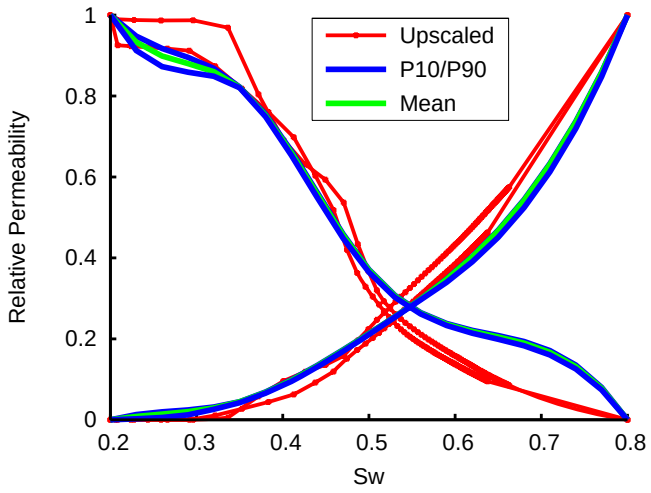

Figure 6.27: Uncertainty in relative permeabilities (Case2). The history data used was up to 1350 days without noise.

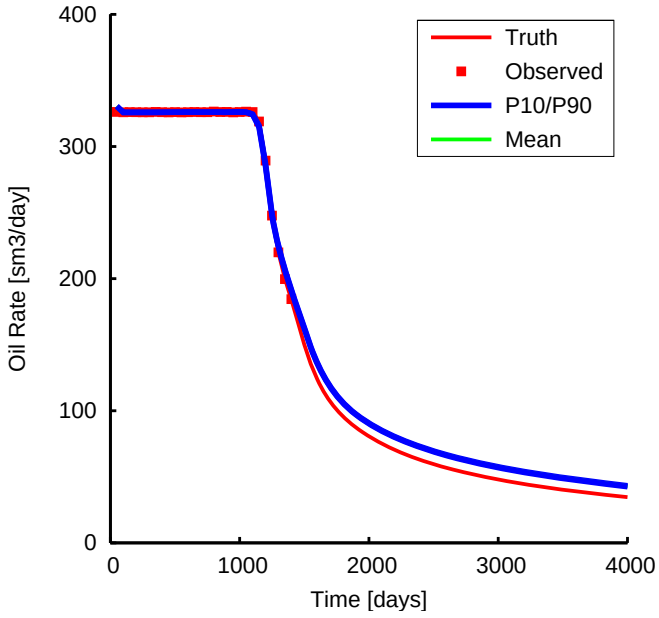

Figure 6.28: Uncertainty in oil production rate (Case2). The history data used was up to 1350 days without noise.

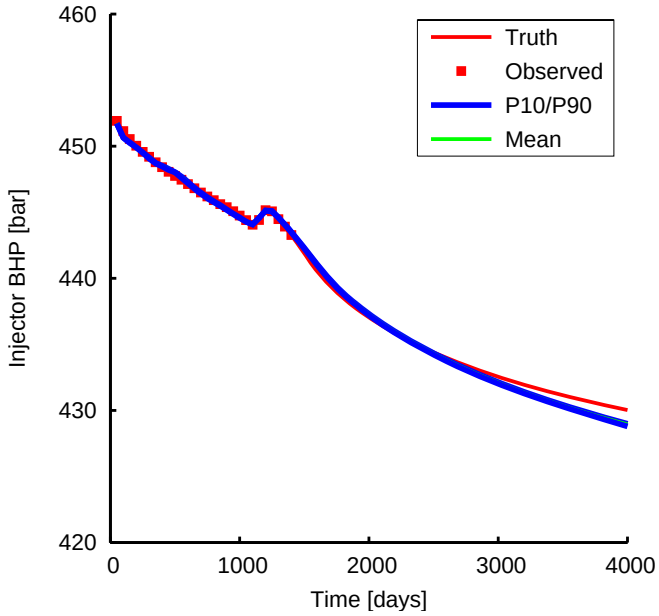

Figure 6.29: Uncertainty in injector bottom hole pressure (Case2). The history data used was up to 1350 days without noise.

Case 3 Finally, in the third case the standard deviations of data noise were assumed to be the same as those of the base case, but the history period was extended to 4000days as in the first case. The history-matching results are shown in Figures 6.30, 6.31 and 6.32. Those are almost the same as the corresponding results of Case 1, so the estimated relative permeabilities were not biased. Figure 6.33 plots the 1-dimensional marginal distribution for each of the parameters. Comparing this with Case 1 of Figure 6.22, the position of each peak of all the parameters coincides with that of the first case, while the width of each distribution is larger than that of the first case. The difference on the widths is the result of the substantial amount of noise in the observed data. On the other hand, comparing Case 3 with the base case of Figure 6.14, the width of each distribution is smaller than that of the base case. In particular, parameters 4 and 8 of the base case in Figure 6.14 have much wider distributions than those of the third case in Figure 6.33. This is the consequence of lack of information about this saturation region due to the limited history period. These comparisons confirmed that both level of noise in the observed data and the limited history period affect the posterior probability distribution. The uncertainty envelopes of Case 3 are shown in Figures 6.34, 6.35 and 6.36. Figure 6.34 indicates that the envelopes are very narrow on the whole, but the oil relative permeability for water saturation 0.2 and 0.4 has a wider envelope. The width is larger than the corresponding envelope of Case 2 in Figure 6.27. As explained in the previous paragraph, this is related to the variability of the parameter 1 in Figure 6.33. Figure 6.36 shows a slightly opened envelope around 500 days in the injector bottom hole pressure, which is wider than any other part of the envelope. The time span is in the history period and is before the water breakthrough. Probably the oil relative permeability in the low water saturation region may be sensitive to the noise in the injector BHP during that particular time period. If water relative permeability is zero at early times, the oil relative permeability alone contributes to the total mobility. In addition, due to the viscosity ratio, the total mobility is more sensitive to the oil relative permeability than to the water relative permeability. Since the total mobility affects the pressure performance, the uncertainty envelope of the early stage BHP caused by the noise affects the variability of Parameter 1 through the oil relative permeability and implicitly the total mobility. For the base case discussed in the previous section, the relations discussed above may explain the wide range of the marginal distribution of parameter 1 in Figure 6.14 and the wide envelope of the oil relative permeability

in the low water saturation region in Figure 6.15.

The above description for the posterior uncertainty in Parameter 1 should be confirmed by looking at the interrelation between the parameters, i.e. the relationship between the water and oil relative permeabilities (e.g., Parameters 1 and 5) and the relationship between the B-spline coefficients which have common saturation ranges (e.g., Parameters 1, 2 and 3). The interrelation between the parameters is also linked to the production history through the misfit of the model. Hence, the relationship between the parameters needs to be investigated in conjunction with the relationship between a set of parameters and the production history. In other words, there are many relationships to be considered. For history-matching, a set of parameters should keep the misfit value small. That is to say, a set of parameters should be adjusted to give the similar production profiles to the observed data. The effect of the parameters on the oil production rate is different from that on the injector BHP. Also the effect of the parameters on the production history at a certain time step is different from that at the other time steps. The investigation of all the interrelations described above may reveal the reason for the large width of the marginal distribution of Parameter 1. It seems that the reason is related to the saturation range to which Parameter 1 is sensitive. In addition to the explanation in the previous paragraph, it might be worthwhile discussing another reason. For example, the saturation in the cell changes quicker in the S_w range between 0.2 and 0.35 than in the rest of the S_w range (Figure 6.18), where the S_w range between 0.2 and 0.35 corresponds to the range of the B-spline basis function of Parameter 1 (Figure 6.6). However the relationship between the time taken to go through the saturation range and the width of the marginal distribution is not clear. In order to support the reason, the relationship between Parameter 1 and the production profiles needs to be investigated.

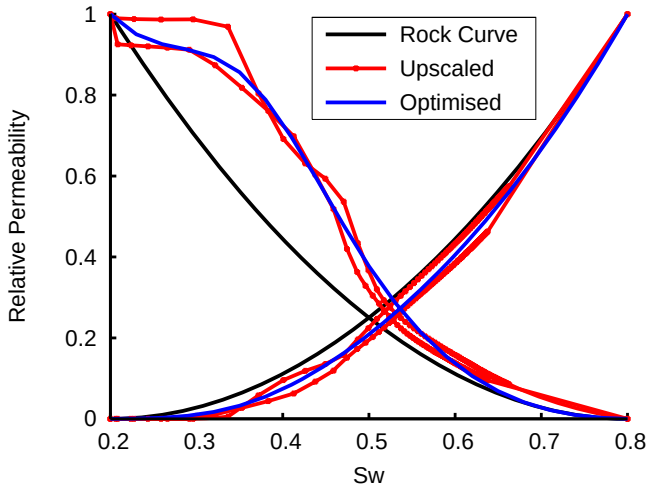

Figure 6.30: Optimised relative permeabilities (Case3). The history data used was up to 4000 days with noise.

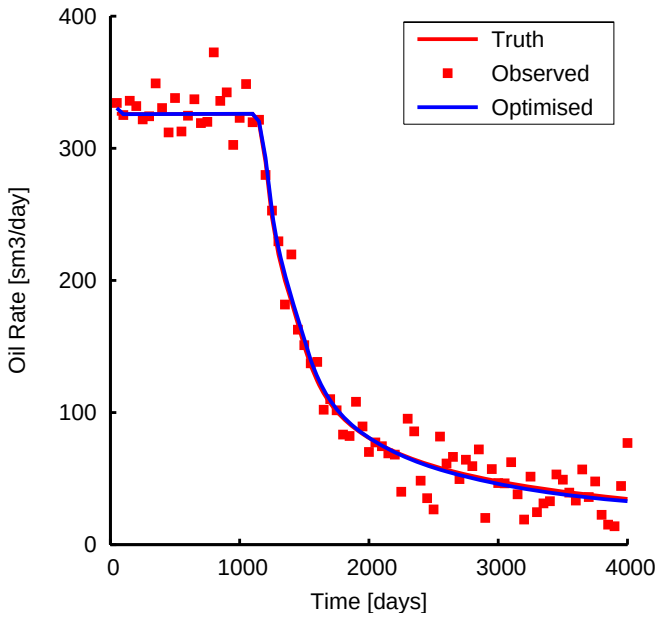

Figure 6.31: Oil production rate calculated using the optimised relative permeabilities (Case3). The history data used was up to 4000 days with noise.

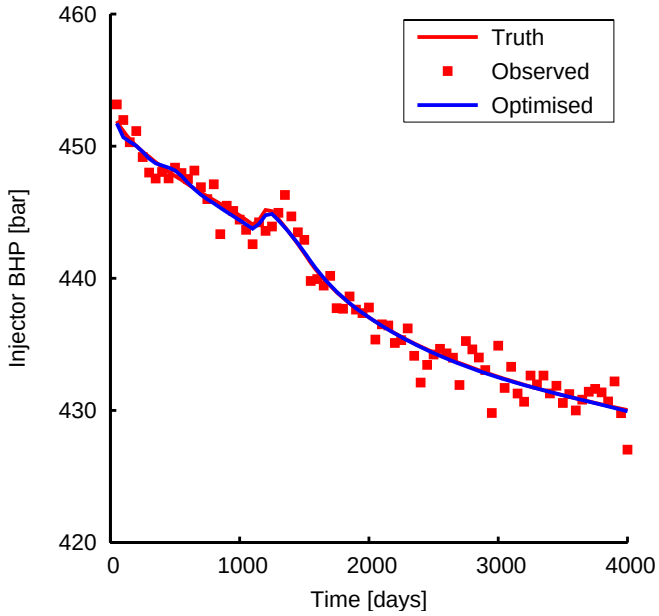

Figure 6.32: Injector bottom hole pressure calculated using the optimised relative permeabilities (Case3). The history data used was up to 4000 days with noise.

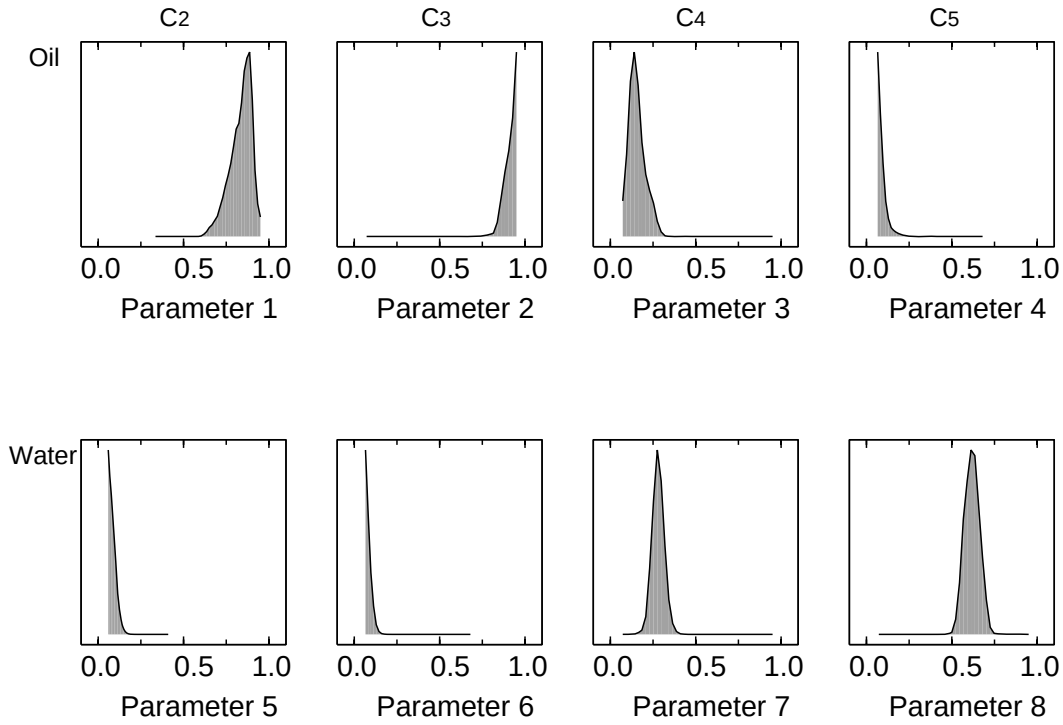

Figure 6.33: 1D marginal distribution for 100000 samples in the Markov chains (Case3). The history data used was up to 4000 days with noise. Note that each curve is scaled to its maximum height not the same area. The vertical axis ranges from 0 to each maximum with a linear scale. Each maximum height is provided in Table 6.6.

Table 6.6: Max. of each curve in Figure 6.33

	c_2	c_3	c_4	c_5
Oil	0.12	0.36	0.21	0.40
Water	0.21	0.45	0.26	0.19

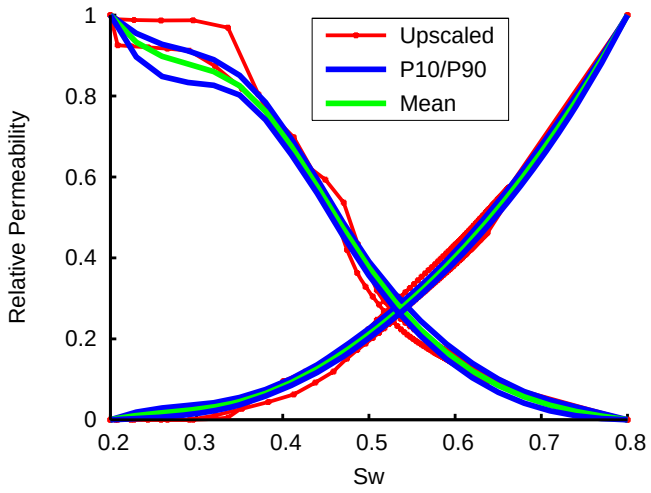

Figure 6.34: Uncertainty in relative permeabilities (Case3). The history data used was up to 4000 days with noise.

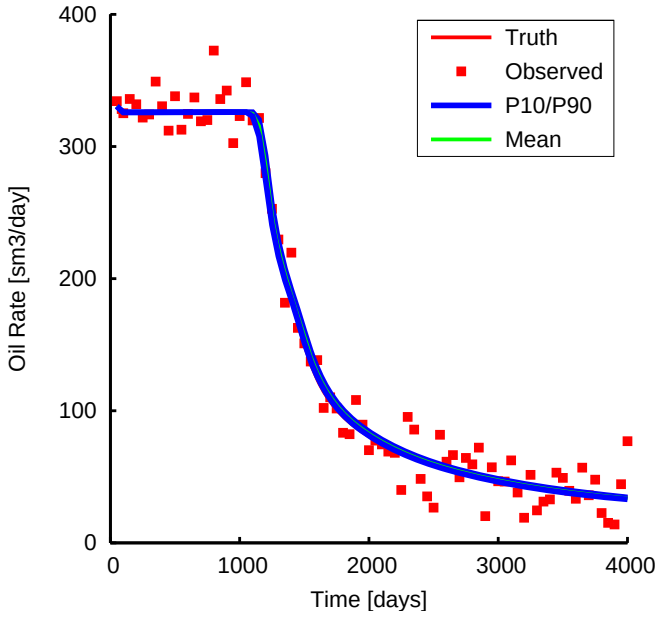

Figure 6.35: Uncertainty in oil production rate (Case3). The history data used was up to 4000 days with noise.

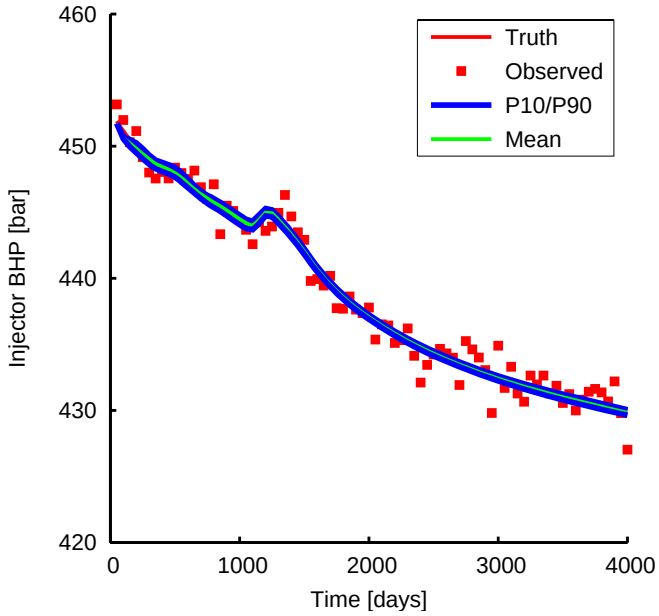

Figure 6.36: Uncertainty in injector bottom hole pressure (Case3). The history data used was up to 4000 days with noise.

6.6 Discussion and Conclusions

Recently a new concept of "Top-down reservoir modelling" has been discussed (Williams et al., 2004). The approach is to start at the coarse scale, keep the model simple and add the detailed features later to evaluate the uncertainty, for instance using downscaling methods (Tran et al., 2001; Yoon et al., 2001; Lee et al., 2002). In the context of "Top-down reservoir modelling", the procedure proposed in this thesis can contribute to history-matching and uncertainty prediction at the coarse scale without refining the model. For example, suppose that you are given a roughly history-matched model, and the large-scale heterogeneity, such as channel delineation and fault compartmentalisation, has already been fixed. The next task is to take into account the small-scale heterogeneity which the main features of the simple model may miss. Here, it is an inevitable bar to appropriate modelling that we do not know the true fine-scale permeability distribution. In such situations, the procedure demonstrated in this chapter shows how it may be possible to encapsulate small-scale flow phenomena in relative permeabilities of the coarse-scale cells, using the flexible B-spline parameterisation and the NA-sampler. The effect of the parameterisation is further discussed in Chapter 7. Also the approach is applied to the 2D course-scale model in Chapter 9.

In summary, this chapter has demonstrated a methodology for adjusting relative permeabilities to generate history-matched models at a coarse scale, and quantifying uncertainty in reservoir performance forecast using the Neighbourhood Approximation algorithm and Markov Chain Monte Carlo. In order to conduct the numerical experiments, a synthetic data set for which the true solution is known was used. The optimised relative permeabilities and their uncertainty envelope were examined by comparing them with the upscaled relative permeabilities that were generated from the truth model. The optimised relative permeabilities and their uncertainty envelope were found to resemble the upscaled relative permeabilities. This evidence indicated that the estimated relative permeability curves would encapsulate the fine-scale flow phenomenon through the local features of the B-spline functions. The key is to evaluate the relative permeabilities so that they can represent both the sub-grid heterogeneity and the numerical coarse-scale effect.

From a practical point of view, it is the essential task of reservoir simulation to speculate on the future performance from only a limited number of production data. Therefore, you need to understand how the relative permeabilities affect the overall production performance, whatever procedure is used to adjust the curves during history-matching. From this requirement, the results in this chapter clarified the possible influence of relative permeabilities on the envelope of uncertainty in production.

The tasks implemented in this chapter are summarised as follows.

- The Bayesian framework along with a stochastic sampling was applied to the inverse problem, namely the history-matching of coarse-scale relative permeabilities.
- The uncertainty in the estimation was explained by the relation among the observed production data, B-spline coefficients, relative permeabilities and the calculated production profiles.
- The history-matched relative permeabilities and their uncertainty envelopes were explained by comparing them with the reference upscaled relative permeabilities.

The conclusions drawn from the results are:

- The noise in the history data and the limited amount of data resulted in substantial amount of uncertainty in the relative permeabilities and production forecast.
- B-spline parameterisation has the potential to represent the irregular shapes of coarse-scale relative permeabilities.

Chapter 7

Influence of Parameterisation Schemes

7.1 General Remarks

The previous chapter applied the Bayesian framework and stochastic sampling to the history-matching of coarse-scale relative permeabilities. Also it described the use of B-splines to represent the relative permeability curves. With B-splines there are a lot of parameters to be adjusted, which is time consuming, and the number of parameters could be prohibitive, if this method is extended to different types of relative permeabilities. This chapter examines four different parameterisation schemes which are simpler than the B-splines used in the previous chapter. The other settings in the numerical experiment are the same as those in the base case explained in Section 6.2. The results of the flexible B-spline function in the previous chapter are compared with those of a power or exponential function, namely the Corey or Chierici functions, respectively. The aims of this chapter are to assess the success of history-matching relative permeabilities and to investigate the effect of the parameterisation on the width of uncertainty envelope.

7.2 Parameterisation for Relative Permeabilities

Relative permeability is assumed to be a function of saturation, and the coarse-scale flow functions are not the same as the rock curves obtained from core flooding experiments. The coarse-scale relative permeabilities may have irregular shapes: e.g., steep slope, non-monotonic curve, etc., as in Hewett et al. (1998). Hence, the success of history-matching relative permeabilities may depend on the flexibility of the saturation function.

In the previous chapter a certain type of B-spline function was adopted. As explained in Section 6.3, the representation consisted of 6 basis functions which were determined by non-uniformly spaced knots at water saturations of 0.20, 0.35, 0.50 and 0.80. Although this scheme aimed at flexibility, the number of parameters was minimised to some extent: four for one curve. This is important in order to reduce the computational cost and to avoid the curse of the dimensionality. In this chapter, the number of parameters is reduced further. The functions chosen are power and exponential functions. As described in Section 5.3, the number of the parameters in the power function (Corey, 1954) is one for one curve apart from the end points, and that in the exponential function (Chierici, 1981) is two for one curve. If the water saturation at which water becomes mobile is involved in the calibration parameters, the number of parameters for one curve is increased to two in the Corey function and three in the Chierici function. These four types of the parameterisation, each of which has a smaller number of parameters than the function used in the previous chapter, are described in the below.

7.2.1 Corey Function

The Corey function has an exponent for one curve to be adjusted in history-matching:

$$K_{ro}(S_w) = \left(\frac{1 - S_w - S_{or}}{1 - S_{wc} - S_{or}}\right)^a, \tag{7.2.1}$$

$$K_{rw}(S_w) = \left(\frac{S_w - S_{wc}}{1 - S_{wc} - S_{or}}\right)^b, \tag{7.2.2}$$

where $K_{ro}(S_w)$ and $K_{rw}(S_w)$ denote oil and water relative permeabilities, S_w is water saturation, S_{wc} is connate water saturation and S_{or} is residual oil saturation. These two end-point satura-

tions were fixed as in Chapter 6: $S_{wc} = S_{or} = 0.2$. Note that a and b are the exponents of the oil and water relative permeabilities and are denoted as Parameter 1 and Parameter 2 in the following numerical experiments. The two parameters were adjusted in the history-matching, and then the uncertainty in the estimation was quantified, as in Section 6.4. The prior range had been defined so that each parameter had uniform distribution between 0.0 and 10.0, which could cover a wide range of relative permeability curves. The history-matching results are shown in Figures 7.1, 7.2, 7.3 and 7.4. Figure 7.1 indicates that the misfit could not be reduced to the level of the upscaled model. Figure 7.2 demonstrates an important point. Even if the rock relative permeabilities in the truth fine-scale model were expressed by the same type of function, namely the Corey type function in this case, the optimised relative permeability did not converge to the reference upscaled curves. In particular, the oil relative permeability has a different shape from the reference upscaled curve. As for Figures 7.3 and 7.4, whereas the oil production rate was matched to the observed data to some extent, the injector BHP could not be matched appropriately. This was caused by the deviation in the oil relative permeability in Figure 7.2. Figure 7.5 plots the 1-dimensional marginal distribution for each of the parameters. The uncertainty envelopes are shown in Figures 7.6, 7.7 and 7.8. The width of each marginal distributions is very small, and so each of the estimated envelopes is narrow. Hence, this type of parameterisation failed to match the observed data because of the lack of flexibility, and there is little uncertainty in the estimations.

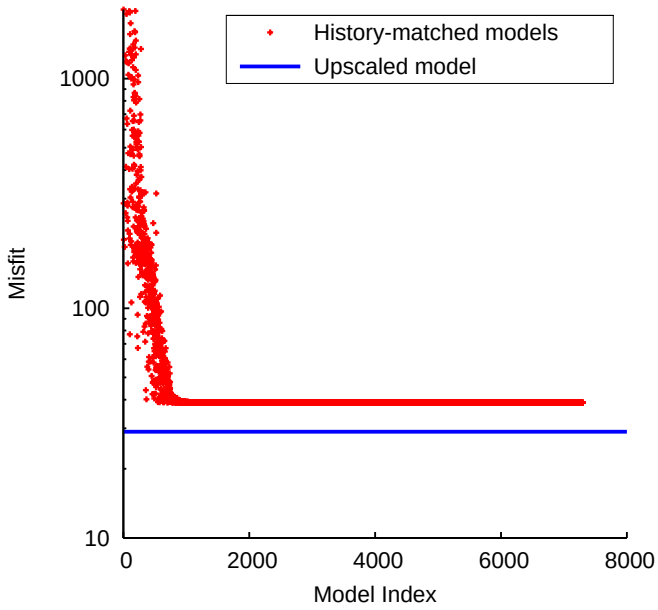

Figure 7.1: Misfit values during history-matching (Corey). Note that the *y*-axis is logarithmic. The misfit value of the upscaled model (Figures 6.4 and 6.5) is 29.0129 which is shown by the blue line for comparison.

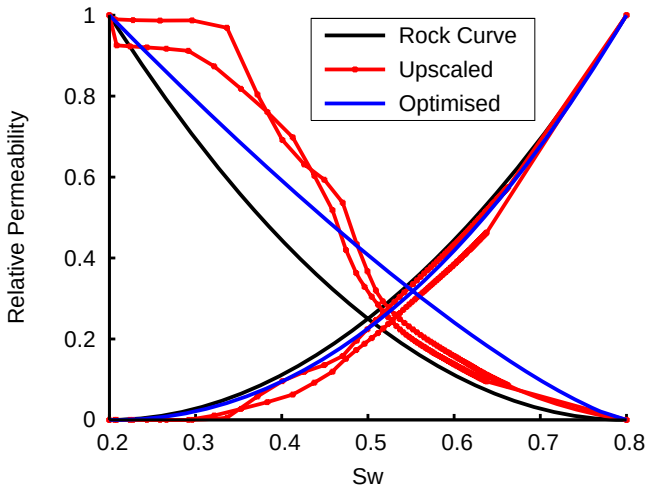

Figure 7.2: Optimised relative permeabilities (Corey). Two parameters were adjusted for one set of the curves.

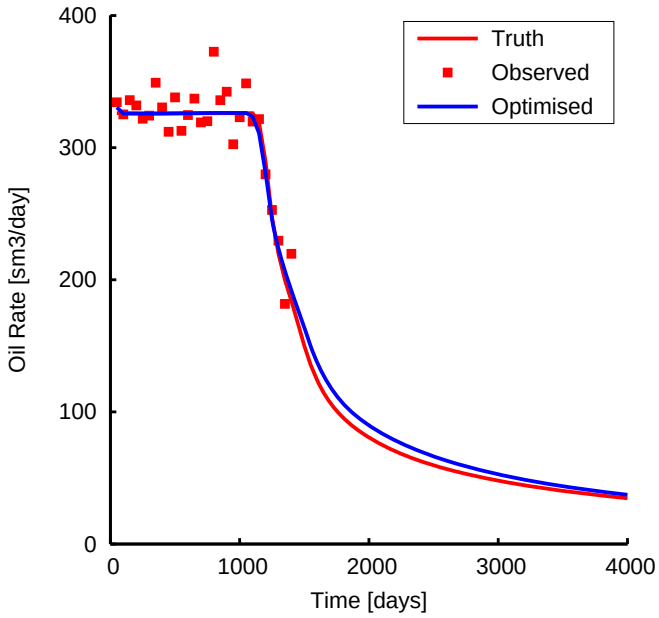

Figure 7.3: Oil production rate calculated using the optimised relative permeabilities (Corey). Two parameters were adjusted for one set of the curves.

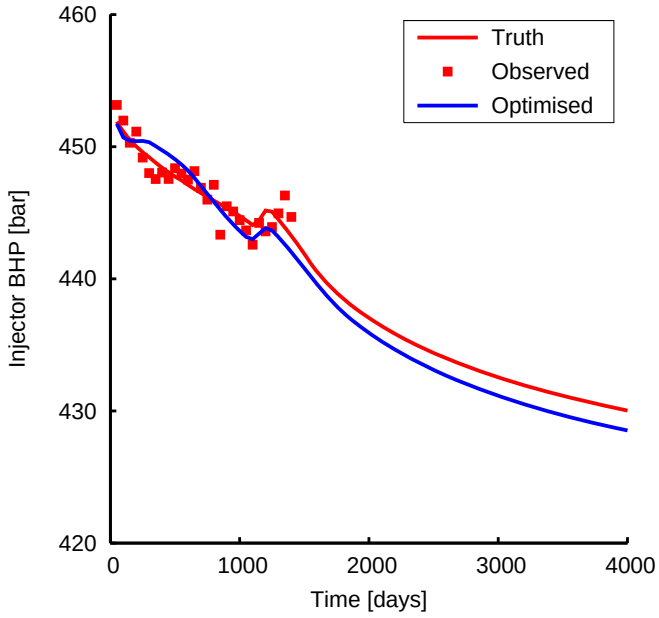

Figure 7.4: Injector bottom hole pressure calculated using the optimised relative permeabilities (Corey). Two parameters were adjusted for one set of the curves.

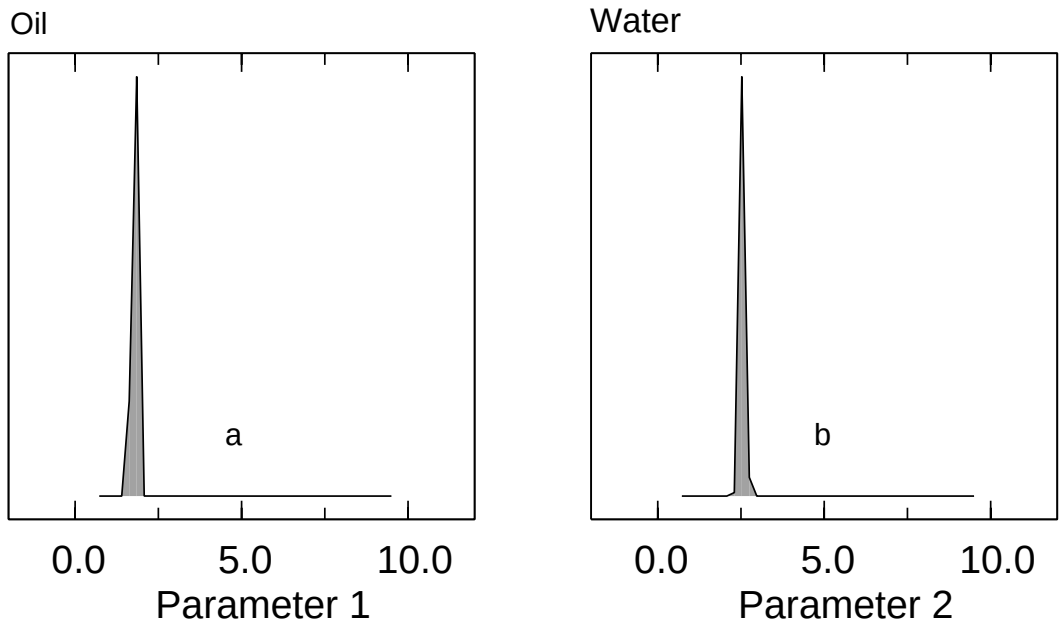

Figure 7.5: 1D marginal distribution for 100000 samples in the Markov chains (Corey). Note that each curve is scaled to its maximum height not the same area. The vertical axis ranges from 0 to each maximum with a linear scale. Each maximum height is provided in Table 7.1. $K_{ro}(S_w) = \left(\frac{1 - S_w - S_{or}}{1 - S_{wc} - S_{or}}\right)^a$, $K_{rw}(S_w) = \left(\frac{S_w - S_{wc}}{1 - S_{wc} - S_{or}}\right)^b$.

Table 7.1: Max. of each curve in Figure 7.5

Oil (a)	Water (b)
0.82	0.95

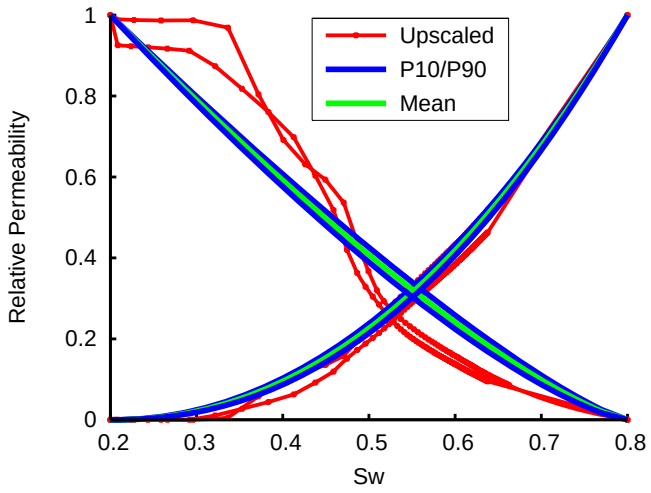

Figure 7.6: Uncertainty in relative permeabilities (Corey). Two parameters were adjusted for one set of the curves in history-matching.

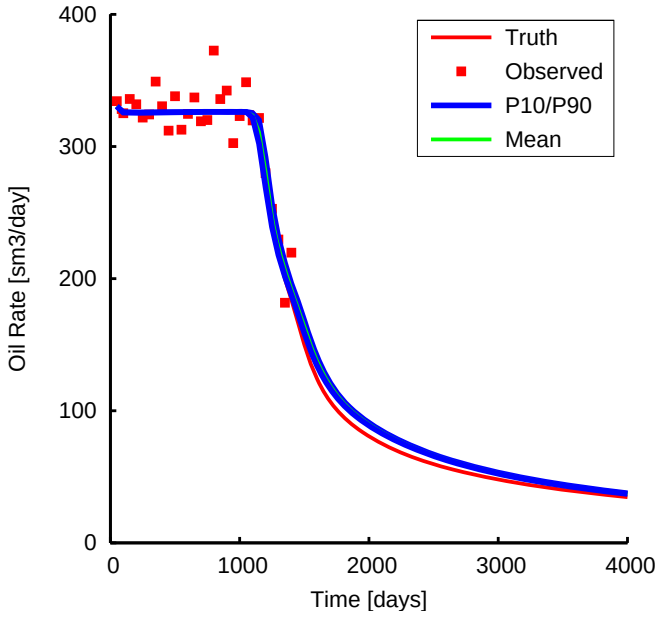

Figure 7.7: Uncertainty in oil production rate (Corey). Two parameters were adjusted for one set of the curves in history-matching.

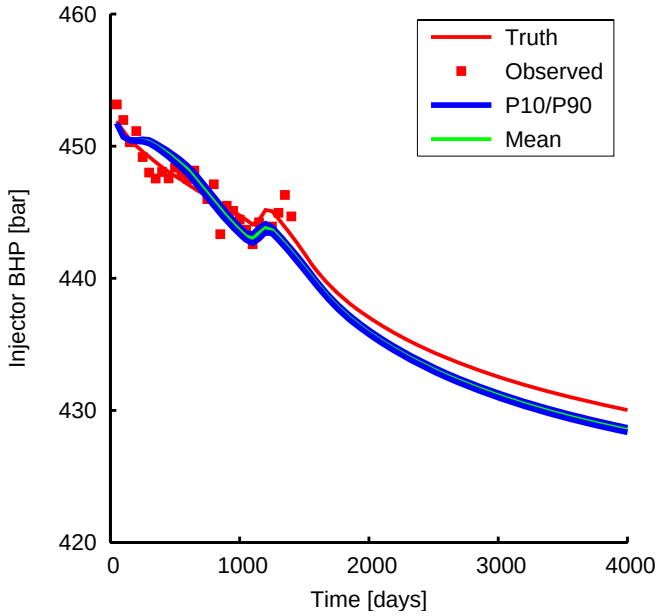

Figure 7.8: Uncertainty in injector bottom hole pressure (Corey). Two parameters were adjusted for one set of the curves in history-matching.

7.2.2 Chierici Function

The Chierici function has two parameters for one curve to be adjusted in history-matching:

$$K_{ro}(S_w) = \exp\left[-a\left(\frac{S_w - S_{wc}}{1 - S_w - S_{or}}\right)^b\right], \tag{7.2.3}$$

$$K_{rw}(S_w) = \exp\left[-c\left(\frac{S_w - S_{wc}}{1 - S_w - S_{or}}\right)^{-d}\right], \tag{7.2.4}$$

where $K_{ro}(S_w)$ and $K_{rw}(S_w)$ denote oil and water relative permeabilities, S_w is water saturation, S_{wc} is connate water saturation and S_{or} is residual oil saturation. These two end-point saturations were fixed as in Chapter 6: $S_{wc} = S_{or} = 0.2$. Note that a and b are the parameters for the oil relative permeability, and c and d are the parameters for the water relative permeability. In the following numerical experiments, a and b are denoted as Parameter 1 and Parameter 2, and c and d are denoted as Parameter 3 and Parameter 4. All four parameters were adjusted in the history-matching, and then the uncertainty in the estimation was quantified, as in Section 6.4. The prior range had been defined so that each parameter had uniform distribution between 0.0 and 10.0, which could cover a range of relative permeability curves. The history-matching results are shown in Figures 7.9, 7.10, 7.11 and 7.12. As in the previous subsection using Corey function, the misfit could not be reduced to the level of the upscaled model (Figure 7.9). Figure 7.10 shows that the optimised relative permeabilities both for oil and water phases are far from the reference upscaled curves. Although the Chierici function has more parameters than the Corey function, the deviations are much larger than that in Figure 7.2. Probably this is because the coarse-scale relative permeabilities may have inherited some features of the Corey-type rock curve in this case, and then the features cannot be expressed by the Chierici function. As with the Corey parameterisation, the oil production rate (Figure 7.11) was matched to the observed data to some extent, but the injector BHP (Figure 7.12) could not be matched appropriately. Again this was due to the deviation in the optimised relative permeability in Figure 7.10. Figure 7.13 plots the 1-dimensional marginal distribution for each of the parameters. The width of the marginal distribution for each of Parameters 1 and 2 (oil phase) is very small , and that for each of Parameters 3 and 4 (water phase) is relatively wider toward the maximum. The uncertainty envelopes are shown in Figures 7.14, 7.15 and 7.16. Whereas the uncertainty envelopes of the relative permeabilities and the oil production rate are small, the envelope of the injector BHP is

large. The relatively large width may be related to the poor match to the observed BHP in the history period.

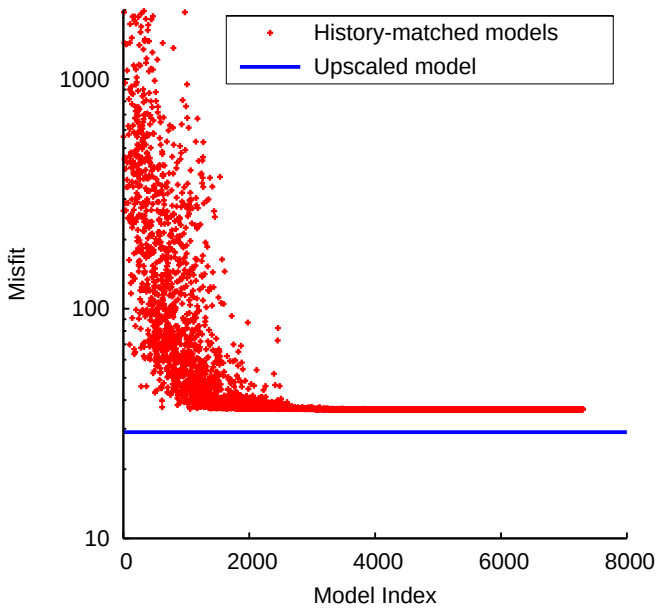

Figure 7.9: Misfit values during history-matching (Chierici). Note that the *y*-axis is logarithmic. The misfit value of the upscaled model (Figures 6.4 and 6.5) is 29.0129 which is shown by the blue line for comparison.

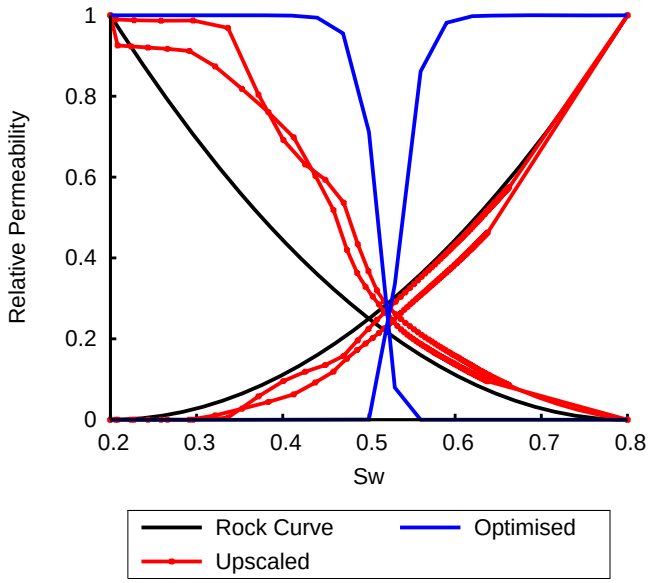

Figure 7.10: Optimised relative permeabilities (Chierici). Four parameters were adjusted for one set of the curves.

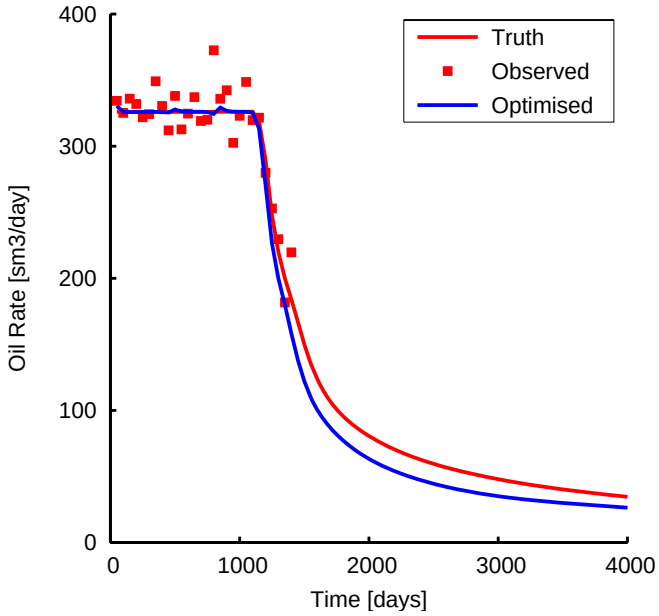

Figure 7.11: Oil production rate calculated using the optimised relative permeabilities (Chierici). Four parameters were adjusted for one set of the curves.

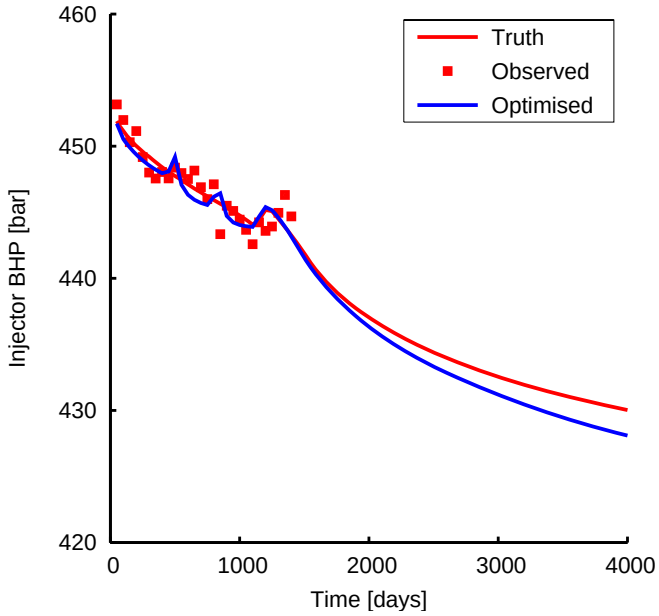

Figure 7.12: Injector bottom hole pressure calculated using the optimised relative permeabilities (Chierici). Four parameters were adjusted for one set of the curves.

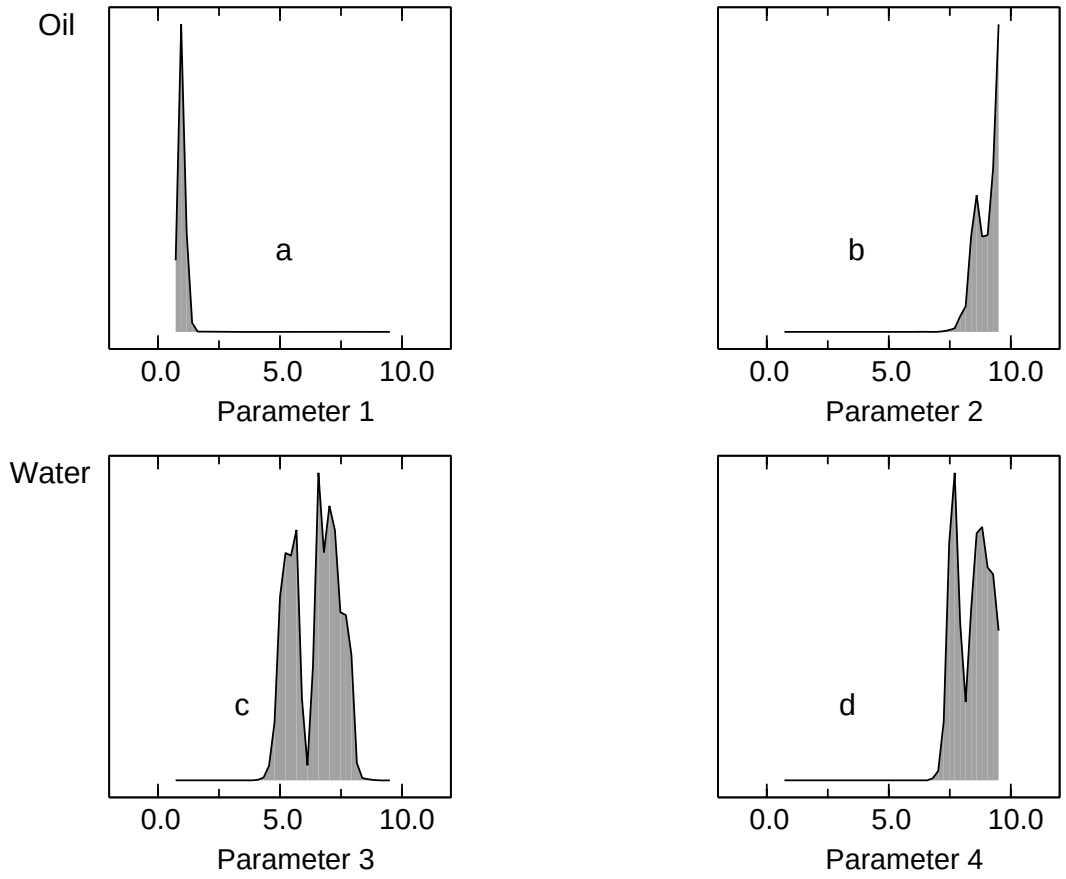

Figure 7.13: 1D marginal distribution for 100000 samples in the Markov chains (Chierici). Note that each curve is scaled to its maximum height not the same area. The vertical axis ranges from 0 to each maximum with a linear scale. Each maximum height is provided in Table 7.2. $K_{ro}(S_w) = \exp\left[-a\left(\frac{S_w - S_{wc}}{1 - S_w - S_{or}}\right)^b\right]$, $K_{rw}(S_w) = \exp\left[-c\left(\frac{S_w - S_{wc}}{1 - S_w - S_{or}}\right)^{-d}\right]$.

Table 7.2: Max. of each curve in Figure 7.13

	a or c	b or d
Oil	0.63	0.33
Water	0.11	0.15

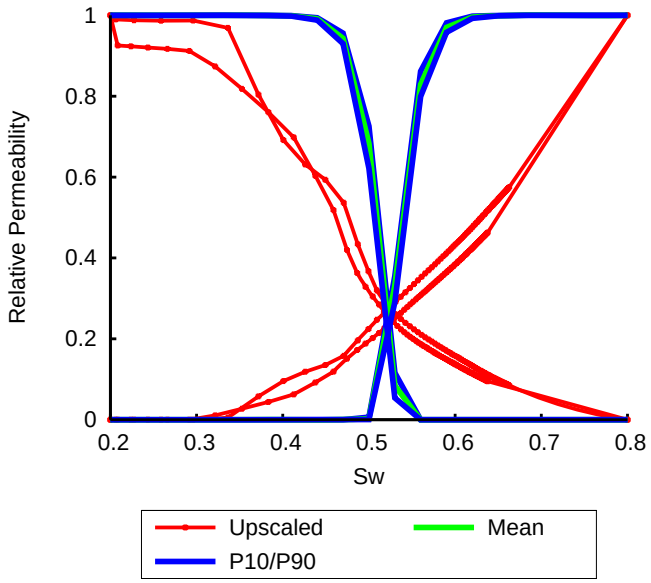

Figure 7.14: Uncertainty in relative permeabilities (Chierici). Four parameters were adjusted for one set of the curves in history-matching.

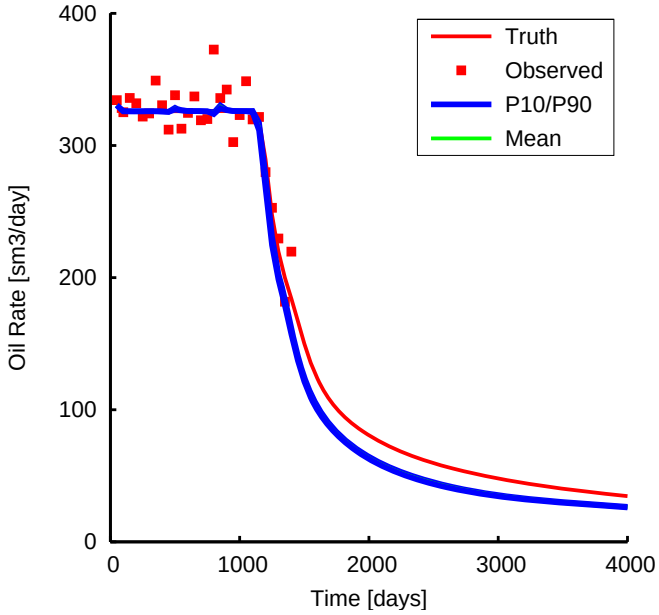

Figure 7.15: Uncertainty in oil production rate (Chierici). Four parameters were adjusted for one set of the curves in history-matching.

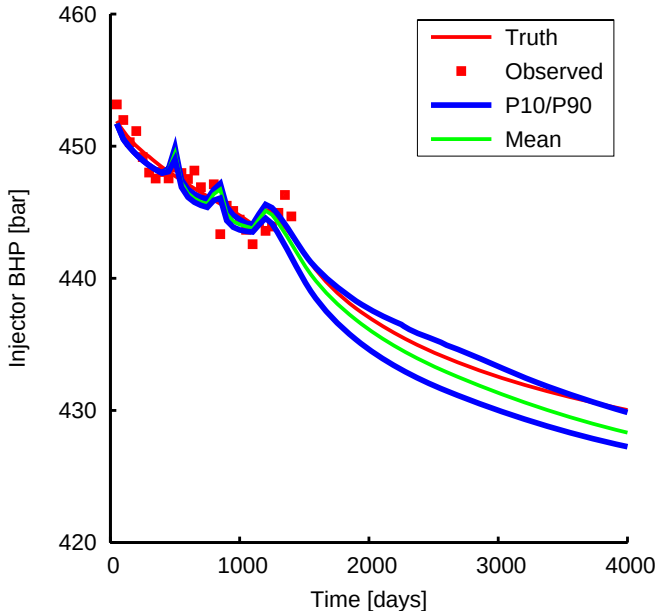

Figure 7.16: Uncertainty in injector bottom hole pressure (Chierici). Four parameters were adjusted for one set of the curves in history-matching.

7.2.3 Corey Function with End-Point Shifting

In order to add more flexibility to the Corey function used above, the equation was modified so that the end point saturation can be shifted:

$$K_{ro}(S_w) = \left(\frac{1 - S_w - S_{or}}{1 - (S_{wc} + a) - S_{or}}\right)^b, \tag{7.2.5}$$

$$K_{rw}(S_w) = \left(\frac{S_w - (S_{wc} + c)}{1 - (S_{wc} + c) - S_{or}}\right)^d, \tag{7.2.6}$$

where $K_{ro}(S_w)$ and $K_{rw}(S_w)$ denote oil and water relative permeabilities, S_w is water saturation, S_{wc} is connate water saturation and S_{or} is residual oil saturation: $S_{wc} = S_{or} = 0.2$ as in Chapter 6. Note that the parameter a is the shift to the end point for the oil relative permeability, and the parameter c is the shift to the end point for the water relative permeability. The parameters b and d are the exponents for the oil and water relative permeabilities, respectively. In the following numerical experiments, a and b for the oil phase are denoted as Parameter 1 and Parameter 2, and c and d for the water phase are denoted as Parameter 3 and Parameter 4. The prior range was defined so that each parameter had a uniform distribution. Parameters 1 and 3 for shifting S_{wc} range between 0.0 and 0.5, and Parameters 2 and 4 for the Corey exponents range between 0.0 and 10.0, which could cover a range of relative permeability curves. The four parameters in total were adjusted in the history-matching, and then the uncertainty in the estimation was quantified, as in the same as Section 6.4. The history-matching results are shown in Figures 7.17, 7.18, 7.19 and 7.20. The misfit was reduced to the level of the upscaled model (Figure 7.17). Figure 7.18 shows that the optimised relative permeabilities are closer to the reference upscaled curve, compared to Figure 7.2. In particular, the deviation in the oil relative permeability is much smaller than in the two parameter case. As a result, the oil production rate and the injector BHP could be matched to the observed data. Hence the introduction of the shift factors, especially Parameter 1 in this problem, improved the history-matching accuracy. Figure 7.21 plots the 1-dimensional marginal distribution for each of the parameters. The uncertainty envelopes are shown in Figures 7.23, 7.24 and 7.25. The width of each marginal distributions is small, and so each of the estimated envelopes is narrow. Among them, Parameter 1 has a slightly wide distribution, which is the shift to the oil relative permeability. So the uncertainty envelope in the oil relative permeability is wider than that of the water relative permeability. When they

are compared to Figures 6.15, 6.16 and 6.17 which are the results using B-splines, all the envelopes are much narrower. This is because the combination of the parameters which gave a good fit were fewer in this four parameter scheme than in the eight parameter scheme using the B-splines. Figure 7.22 plots the 2-dimensional marginal posterior probability distribution for the oil relative permeability (Parameter 1 and Parameter 2) and that for the water relative permeability (Parameter 3 and Parameter 4), when the Corey function with the end-point shifts is employed. The small areas in both the 2D marginal distributions indicate that the combination of the parameters of well-matched models is limited. Compared with the Chierici function, the Corey function with the end-point shifts could fit to the coarse-scale relative permeability more efficiently, although the number of parameters in this case is the same as the Chierici function used above. This means that the coarse-scale relative permeability may have retained the trend of the Corey-type rock curve but been shifted along the water saturation axis. Because this representation leads to the flat line in the oil relative permeability behind the shifted end point, and it cannot express local bumps or dents on the curve. So there are some limitations to the flexibility compared to the B-spline representation in the previous chapter.

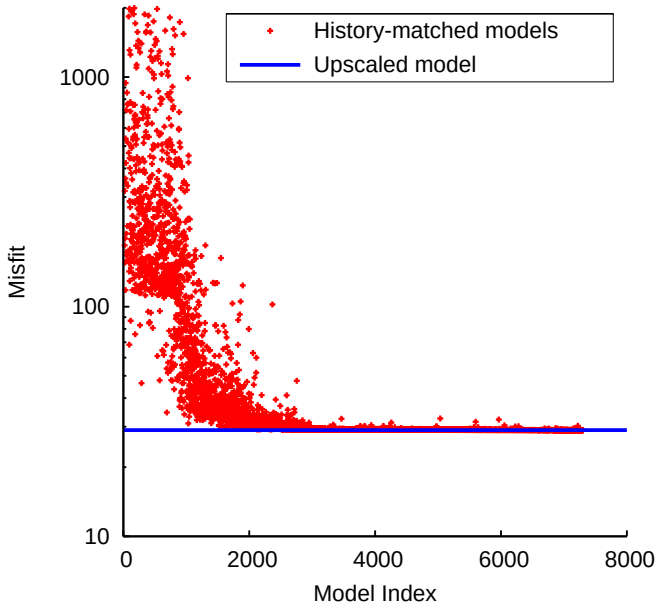

Figure 7.17: Misfit values during history-matching (Corey plus Shift). Note that the *y*-axis is logarithmic. The misfit value of the upscaled model (Figures 6.4 and 6.5) is 29.0129 which is shown by the blue line for comparison.

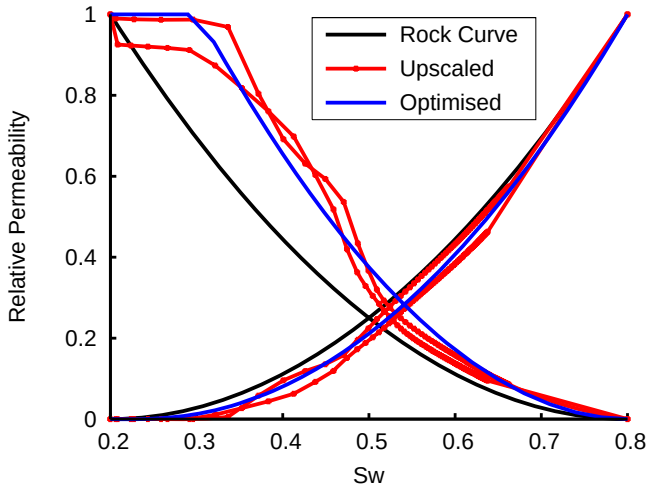

Figure 7.18: Optimised relative permeabilities (Corey plus Shift). Four parameters were adjusted for one set of the curves.

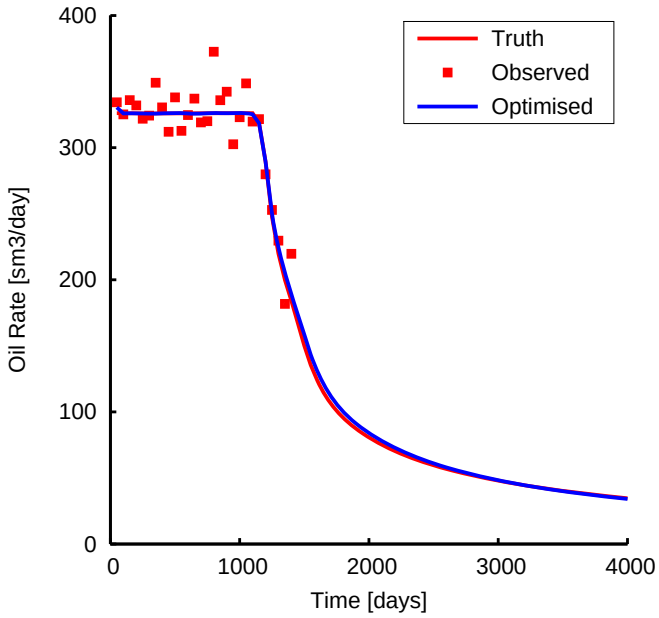

Figure 7.19: Oil production rate calculated using the optimised relative permeabilities (Corey plus Shift). Four parameters were adjusted for one set of the curves.

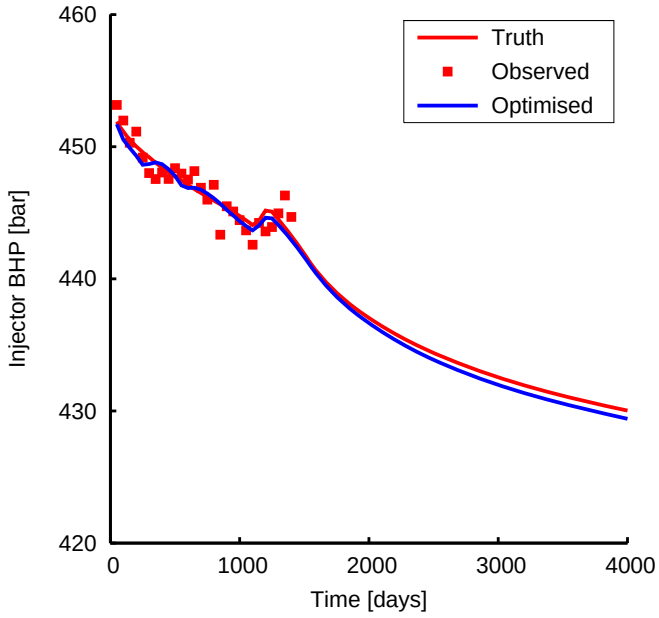

Figure 7.20: Injector bottom hole pressure calculated using the optimised relative permeabilities (Corey plus Shift). Four parameters were adjusted for one set of the curves.

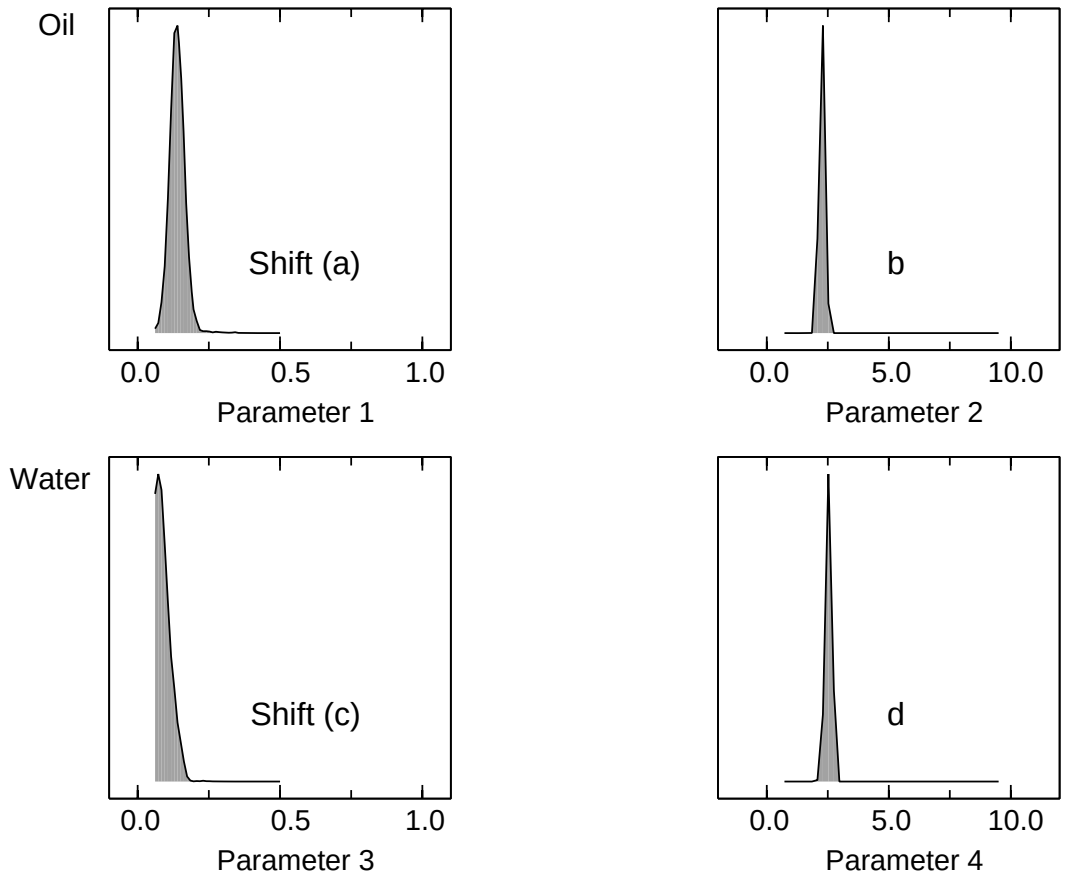

Figure 7.21: 1D marginal distribution for 100000 samples in the Markov chains (Corey plus Shift). Note that each curve is scaled to its maximum height not the same area. The vertical axis ranges from 0 to each maximum with a linear scale. Each maximum height is provided in Table 7.3. $K_{ro}(S_w) = \left(\frac{1 - S_w - S_{or}}{1 - (S_{wc} + a) - S_{or}}\right)^b$, $K_{rw}(S_w) = \left(\frac{S_w - (S_{wc} + c)}{1 - (S_{wc} + c) - S_{or}}\right)^d$.

Table 7.3: Max. of each curve in Figure 7.21

	Shift (a or c)	b or d
Oil	0.18	0.71
Water	0.19	0.66

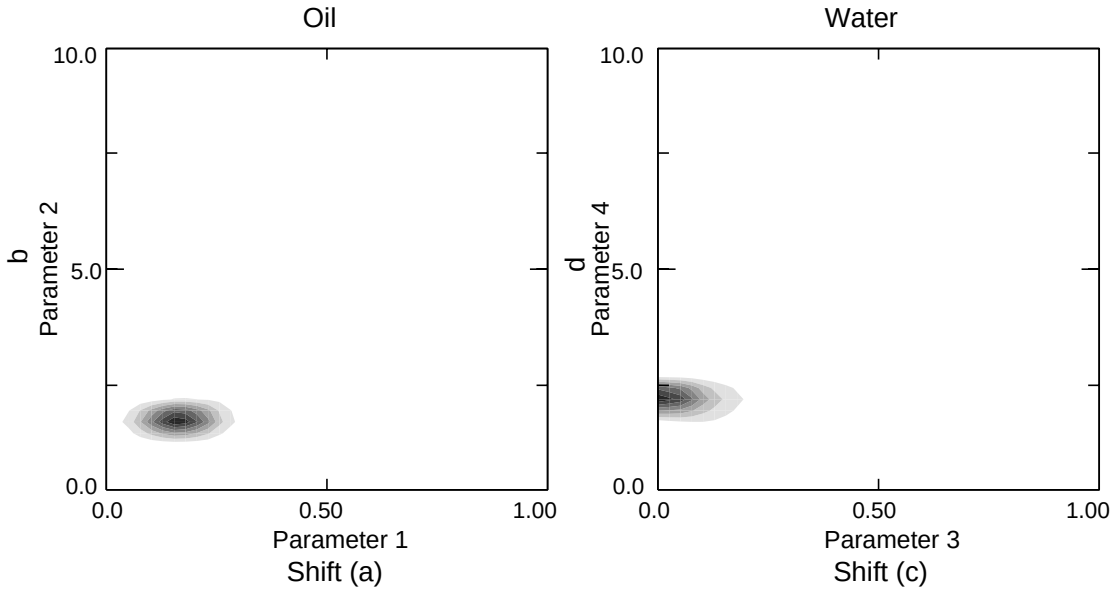

Figure 7.22: 2D marginal distribution for 100000 samples in the Markov chains (Corey plus Shift). Note that the grey scale contour ranges linearly from 0 (white) to 0.33 (black).

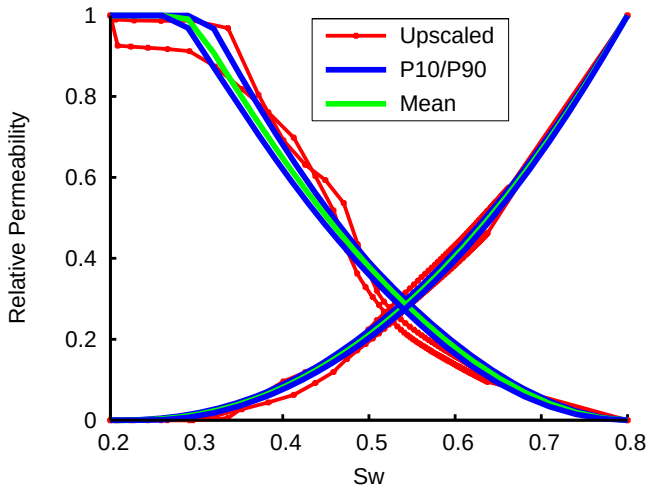

Figure 7.23: Uncertainty in relative permeabilities (Corey plus Shift). Four parameters were adjusted for one set of the curves in history-matching.

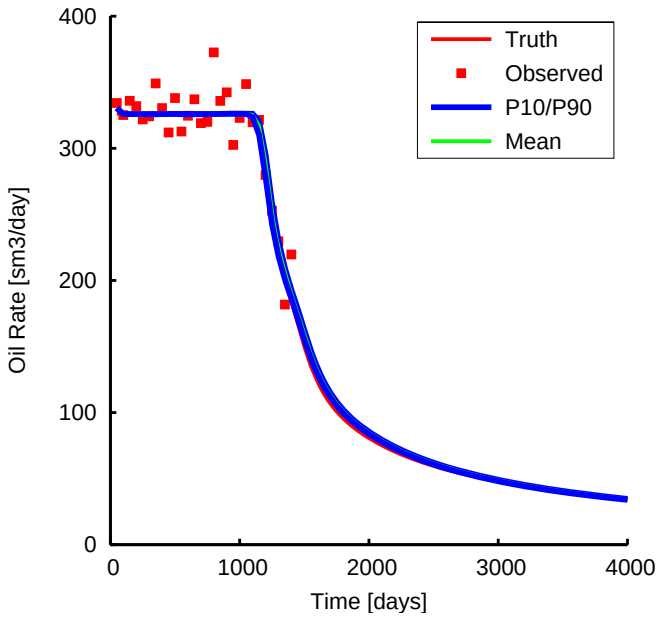

Figure 7.24: Uncertainty in oil production rate (Corey plus Shift). Four parameters were adjusted for one set of the curves in history-matching.

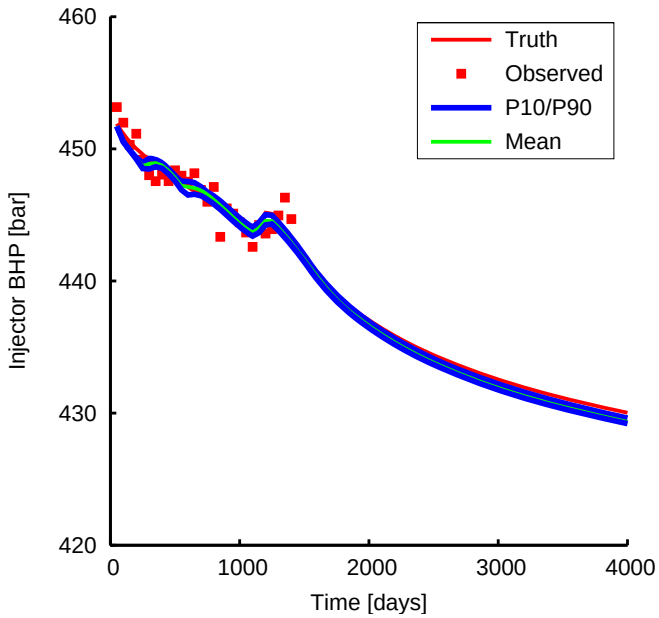

Figure 7.25: Uncertainty in injector bottom hole pressure (Corey plus Shift). Four parameters were adjusted for one set of the curves in history-matching.

7.2.4 Chierici Function with End-Point Shifting

In order to add more flexibility to the Chierici function used above, the equation was modified so that the connate water saturation could be shifted:

$$K_{ro}(S_w) = \exp\left[-b\left(\frac{S_w - (S_{wc} + a)}{1 - S_w - S_{or}}\right)^c\right], \tag{7.2.7}$$

$$K_{rw}(S_w) = \exp\left[-e\left(\frac{S_w - (S_{wc} + d)}{1 - S_w - S_{or}}\right)^{-f}\right], \tag{7.2.8}$$

where $K_{ro}(S_w)$ and $K_{rw}(S_w)$ denote oil and water relative permeabilities, S_w is water saturation, S_{wc} is connate water saturation and S_{or} is residual oil saturation: $S_{wc} = S_{or} = 0.2$ as in Chapter 6. Note that the parameter a is the shift to the end point for the oil relative permeability, and the parameter d is the shift to the end point for the water relative permeability. The parameters b and c are the other two parameters for the oil relative permeability, and the parameters e and f are the other two parameters for the water relative permeability. In the following numerical experiments, a, b and c for the oil phase are denoted as Parameter 1, Parameter 2 and Parameter 3, and then c, d and e for the water phase are denoted as Parameter 4, Parameter 5 and Parameter 6. The prior range was defined so that each parameter had a uniform distribution. Parameters 1 and 4 for shifting the end points range between 0.0 and 0.5, and the other parameters range between 0.0 and 10.0, which could cover a range of relative permeability curves. All six parameters were adjusted in the history-matching, and then the uncertainty in the estimation was quantified, as in the same as Section 6.4. Figures 7.26, 7.27, 7.28 and 7.29 show the history-matching results. Although it took a large number of iterations of the NA-sampler, the misfit was reduced to the level of the upscaled model (Figure 7.26). Compared to Figure 7.10 of the four-parameter representation using the fixed end points, the optimised relative permeabilities (Figure 7.27) are not far from the reference upscaled curve. As a consequence, the estimated oil rate and BHP were closer to the observed data. Figure 7.30 plots the 1-dimensional marginal distribution for each of the parameters. Although the width of each marginal distributions is not large on the whole, Parameter 1 and Parameter 4 (the shifts) have a slightly wider distribution. This led to the wide envelope of the relative permeability in Figure 7.31. The uncertainty envelopes of the production profiles are shown in Figures 7.32 and 7.33. Interestingly, in this case the oil production forecast tended to be underestimated in contrast to the truth profile, and the

forecast envelope of the injector BHP spread toward the high side. Each bias of the envelopes was in the opposite side of the B-spline results which were shown in Figures 6.16 and 6.17. This difference in both trends may have stemmed from the characteristic of the function used. Note that the above observation depended on the noise in the production data: e.g., realisations in random noise.

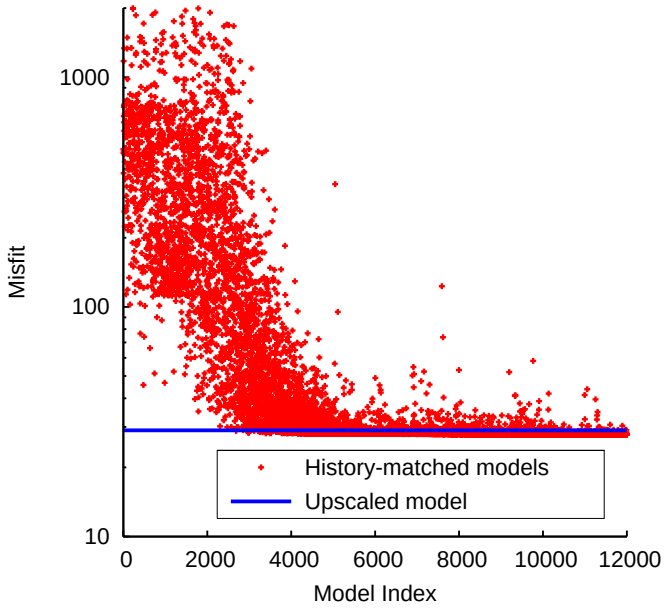

Figure 7.26: Misfit values during history-matching (Chierici plus Shift): Note that the *y*-axis is logarithmic. The misfit value of the upscaled model (Figures 6.4 and 6.5) is 29.0129 which is shown by the blue line for comparison.

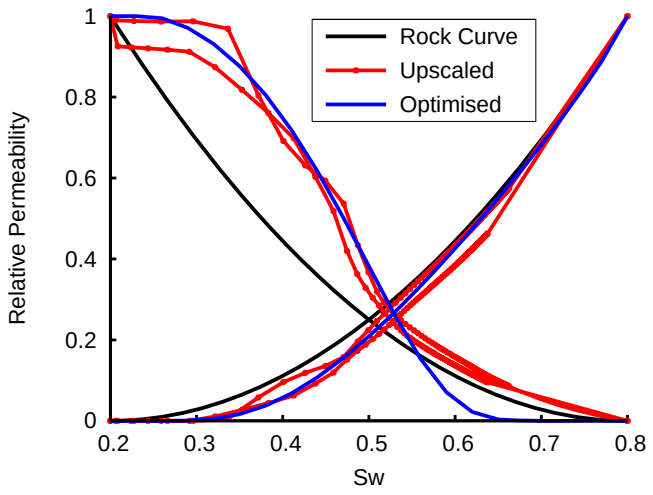

Figure 7.27: Optimised relative permeabilities (Chierici plus Shift). Six parameters were adjusted for one set of the curves.

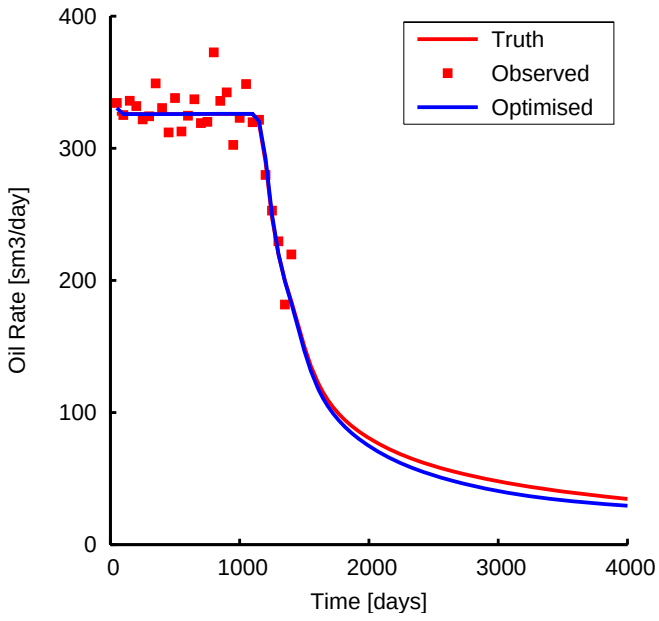

Figure 7.28: Oil production rate calculated using the optimised relative permeabilities (Chierici plus Shift). Six parameters were adjusted for one set of the curves.

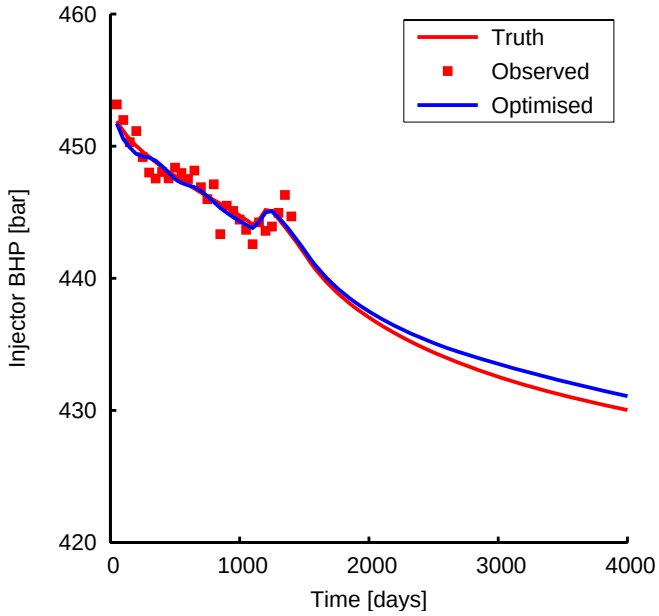

Figure 7.29: Injector bottom hole pressure calculated using the optimised relative permeabilities (Chierici plus Shift). Six parameters were adjusted for one set of the curves.

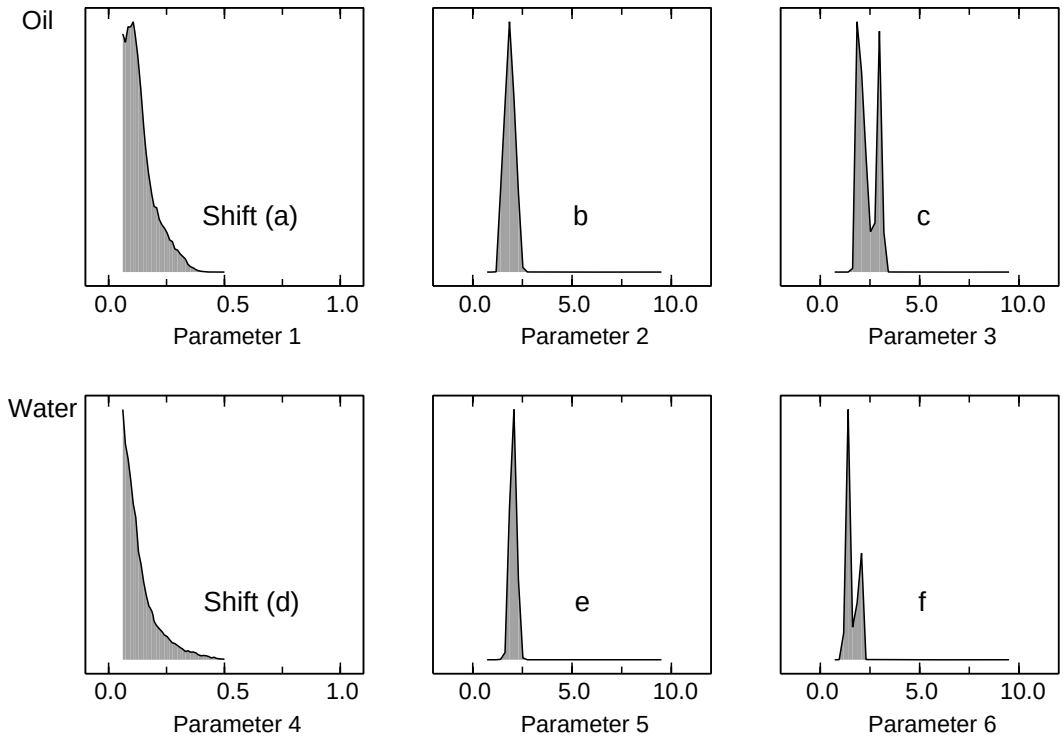

Figure 7.30: 1D marginal distribution for 100000 samples in the Markov chains (Chierici plus Shift). Note that each curve is scaled to its maximum height not the same area. The vertical axis ranges from 0 to each maximum with a linear scale. Each maximum height is provided in Table 7.4. $K_{ro}(S_w) = \exp\left[-b\left(\frac{S_w - (S_{wc} + a)}{1 - S_w - S_{or}}\right)^c\right]$, $K_{rw}(S_w) = \exp\left[-e\left(\frac{S_w - (S_{wc} + d)}{1 - S_w - S_{or}}\right)^{-f}\right]$.

Table 7.4: Max. of each curve in Figure 7.30

	Shift (a or d)	b or e	c or f
Oil	0.09	0.33	0.27
Water	0.13	0.51	0.53

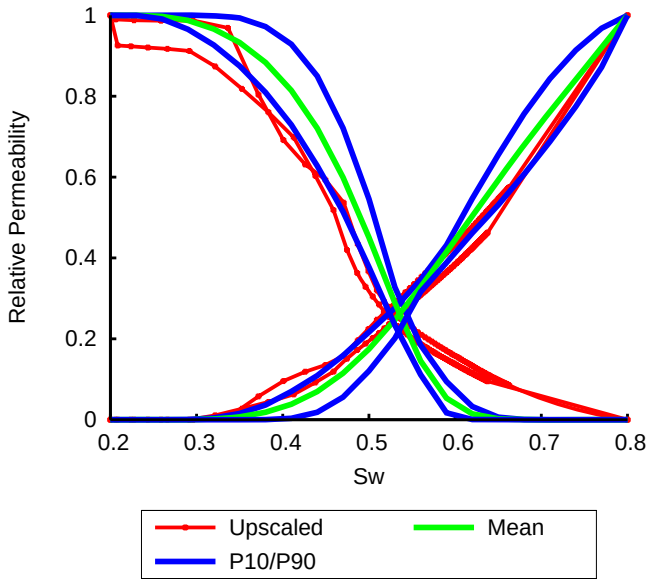

Figure 7.31: Uncertainty in relative permeabilities (Chierici plus Shift). Six parameters were adjusted for one set of the curves in history-matching.

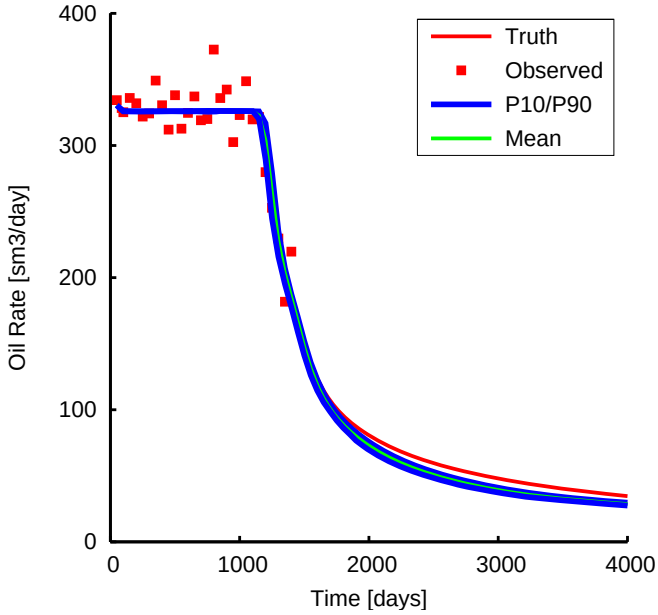

Figure 7.32: Uncertainty in oil production rate (Chierici plus Shift). Six parameters were adjusted for one set of the curves in history-matching.

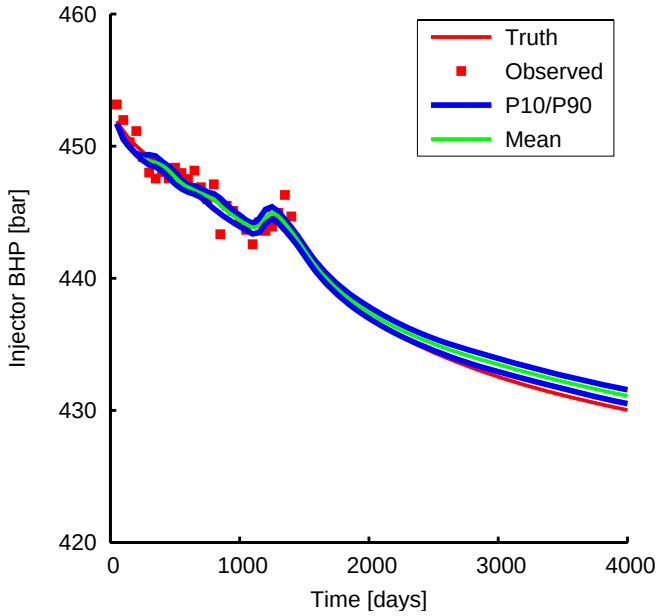

Figure 7.33: Uncertainty in injector bottom hole pressure (Chierici plus Shift). Six parameters were adjusted for one set of the curves in history-matching.

The Chierici function with end-point shifting appears to take more iterations of the NA sampler in history-matching to converge to the optimised curves than the other parameterisations schemes including the B-splines. The results shown here were obtained by 150 iterations, whereas the cases of the other parameterisations were confirmed to converge within no more than 75 iterations as in Section 6.4. Probably there are two reasons why it took longer to converge. Firstly, the Chierici function alone could not fit the reference curves as shown in Figure 7.10. Secondly, it included the end-point adjustment to reduce the deviation between the reference curves and the resultant curves. Both reasons tended to make history-matching more time-consuming than the other parameterisation schemes.

7.2.5 Comparisons with B-spline Parameterisation

Among the four cases described above, the Corey and Chierici functions with the end-point shifting can compete with the B-spline parameterisation. Without the end-point adjustment, they failed to match the observed data and deviated from the reference upscaled curves. When introducing the end-point adjustment, both Corey and Chierici could match the observed data. But the forecast uncertainty showed different trends in the Corey, Chierici and B-spline functions. Note that the B-splines did not include the end-point adjustment. As shown in Figure 6.6, the B-spline representation consists of 6 basis functions, and Basis 2 and Basis 5 have the local supports. Specifically, Basis 2 affects the relative permeability value between 0.2 and 0.5 on the S_w axis, and Basis 5 does so between 0.35 and 0.8. Because of the limited saturation range in the water flooding scenario (Figure 6.18), Basis 5 for the mid-high water saturation region tended to be less sensitive to the observed data than the other Basis functions. The evidence is the wide marginal distribution for Parameters 4 and 8 in Figure 6.14. On the contrary, all the parameters in the Corey and Chierici functions with end points affected the whole saturation region between 0.2 and 0.8 along the S_w axis. These functions can be called global parameterisation in contrast to local parameterisation of B-splines. When the relative permeabilities were history-matched with the global parameterisations, the variability of the curves in the less sensitive saturation region, namely high water saturation, was constrained through the other parts

of the relative permeability curves which were more sensitive to the observed data. The global parameterisations rely on the particular formulations which control the whole part of the curve. These characteristics resulted in the different uncertainty envelopes in the different parameterisations.

7.3 Discussion and Conclusions

The conclusions drawn from these results are:

- The Corey and Chierici parameterisations needed to adjust the end-point saturation to properly represent the coarse-scale relative permeabilities.
- Although the various functions can match the observed production data, the forecast uncertainty may differ in the parametrisation schemes.
- Compared to the Corey and Chierici functions, the B-spline parameterisation tended to lead to larger envelopes of the relative permeability in the high water saturation region which was less sensitive to the history data in the water-flooding scenario.

These conclusions suggest that the function should be chosen to fit to the coarse-scale relative permeabilities. In these numerical experiments, the rock curve was given and was uniformly distributed throughout the truth model. However, in a real situation, one cannot obtain ideally "correct" rock curves, nor assume a single set of curves throughout the model. Hence, in advance of estimating the coarse-scale relative permeabilities, there might be some uncertainty in the rock curve. This means that if the assumed rock curve is not correct, the appropriate form of coarse-scale function is difficult to estimate in advance of history-matching. Presumably the B-spline coarse-scale curve is a good choice, because it avoids assuming any particular function for the rock curve.

In terms of the convergence for history-matching, 1) the Corey function with the shifts, 2) the Chierici function with the shifts and 3) the B-splines successfully reduced the misfit to the

level of the upscaled model as shown in Figures 7.17, 7.26 and 6.9, respectively. According to these Figures, the number of iterations taken to reach the convergence appears to be small in 1) the Corey function with the shifts and appears to be large in 2) the Chierici function with the shifts and 3) the B-splines. It seems that 2) the Chierici function with the shifts required the largest number of iterations in this case.

Although the Corey function with the end-point adjustment could fit the coarse-scale curve to some extent, in general it leads to a flat line behind the shifted end point, and cannot express a rapid change of slope, local bumps and dents. The necessity to use more flexible form depends on the possible shape of the coarse-scale relative permeabilities. The next chapter investigates the coarse-scale curves in 2D models to estimate the shape prior to history-matching.

Chapter 8

Estimation of Constraints for Prior Relative Permeabilities at the Coarse Scale

8.1 General Remarks

The aim of this chapter is to provide prior constraints to relative permeabilities for history-matching and uncertainty appraisal (Figure 8.1). The motivation behind this is to seek for efficient stochastic sampling in history-matching and uncertainty appraisal, which is discussed in Chapter 9.

In this chapter, the physical characteristics of the coarse-scale relative permeability curves are investigated in two-dimensional horizontal models for simulating quarter five-spot pattern water-flooding. As far as the author knows, the shape of the coarse-scale relative permeabilities has never been analysed in two or three dimensional problems. The main task is to investigate the heterogeneity-induced dispersion effects through computational experiments. The numerical experiments were conducted using a range of fine-scale models and an upscaling method. It has been assumed that the permeability fluctuations within the fine-scale cells were negligible. So the focus is on the effect of the heterogeneity-induced “fingers” instead of viscous fingering

resulting from small-scale heterogeneity.

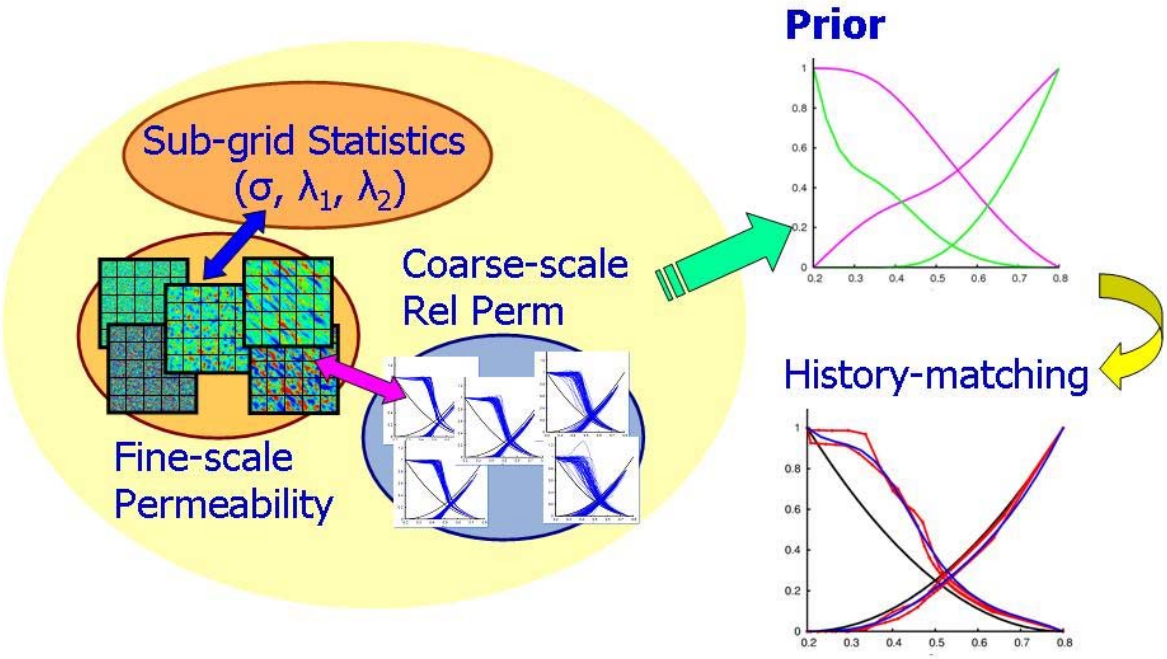

Figure 8.1: Schematic diagram of the proposed method. The first step is to extract the prior information on coarse-scale relative permeabilities. The second step is to constrain the parameter ranges for the calibration in history-matching.

Note that the effects of fingering, channelling and dispersion have been studied for miscible displacement for many years and there are several definitions of the various flow regimes along with viscosity ratio and heterogeneity, (e.g., Waggoner et al., 1992; Sorbie et al., 1994; Li and Lake, 1995; Lenormand, 1996). For example, according to Lenormand (1996), macrodispersion takes place at a unit viscosity ratio and short correlation length, viscous instability at a high viscosity ratio and short correlation length, channelling at a unit viscosity ratio and long correlation length. Also Lenormand (1996) describes the front spreading with time as follows. In convective spreading such as viscous instability and channelling, the mixing zone grows linearly with time. In dispersive spreading, the mixing zone grows linearly with the square root of time. The relation between the system effective aspect ratio and the various flow regimes has been investigated in Sorbie et al. (1994) and Li and Lake (1995)

8.2 Procedure and Method

Relative permeabilities at the coarse scale depend on the multi-phase flow phenomena determined by the "rock curve", viscosity, heterogeneity and flow pattern. Note that this chapter only considers the viscous force for simplicity and ignores capillary and gravity forces. Firstly, the effect of flow path in each coarse cell is investigated using a homogeneous model. Secondly, the physical dispersion induced by the sub-grid heterogeneity is analysed by using a number of possible geostatistical fine-scale models. The standard deviation and correlation length of logarithmic permeability were varied so that we could analyse the relationship between the sub-grid heterogeneity and relative permeabilities. Based on the the results from these simulations, the coarse-scale relative permeability curves were grouped into a number of distinct shapes. Also the minimum and maximum limits were estimated. The prior information on the curves can give us some insights into physically meaningful calibration of the multi-phase flow function in history-matching (Figure 8.1).

The method in this chapter is to use upscaling to determine priors for input into history matching. Note that, the main aim is in the context of "Top-down reservoir modelling" (Williams

et al., 2004), which starts with a simple coarse model rather than a detailed fine-scale model, and "upscaling" is used only to assess the nature of the relative permeabilities at the coarse scale. The Pore Volume Weighted (PVW) method was selected for the numerical experiments, because this was found by Coll et al. (2001) to give the best results for upscaling in the stochastic models which they tested. This is a dynamic upscaling method and proceeds as follows: a two-phase, fine-scale flow simulation is performed; the total flow of oil and water between coarse grid cells is calculated; the average pressure in each coarse cell is computed using pore-volume weighting; and the phase permeabilities are computed using Darcy's law (Schlumberger, 2004b). Relative permeabilities are calculated by dividing by the effective absolute permeability. In the version used in Chapters 8 and 9, single-phase transmissibilities determined from a global single-phase simulation were incorporated into the calculation, (Zhang, 2005). The PVW coarse-scale curves were calculated using global two-phase flow simulations, and the program used was an in-house software package of Heriot-Watt University, not a commercial one. The procedure apart from the calculation of transmissibility is the same as a commercial software (Schlumberger, 2004b).

8.3 Description of Model

A number of computational experiments were set up to test how well relative permeability priors could be constrained by geostatistical information. It was assumed that the information on fine-scale heterogeneity was given by a range of geostatistical parameters. Using those geostatistical parameters, a range of fine-scale models were generated. The coarse-scale model does not have the resolution to represent the small-scale features. Hence, the coarse-scale relative permeabilities are required to encapsulate the effect of sub-grid heterogeneity.

In order to investigate the relationship between the sub-grid statistics and coarse-scale relative permeabilities, 2D synthetic models were set up, and a water flooding scenario was simulated in an oil reservoir. The size of the model was 1km square. There are 125×125×1 cells in this fine-scale, and each of size was 8m×8m×20m. The upscaled relative permeabilities for a coarse-scale model were calculated by two-phase dynamic upscaling as described in the pre-

vious section. The size of each coarse cell was 200m×200m×20m and the number of cells was 5×5×1. The fine-scale and coarse-scale models are illustrated by Figures 8.2 and 8.3 respectively. The details of the model are summarised in the Table 8.1. The comparisons of the cell size and the number of cells between the fine-scale and coarse-scale models are shown in Table 8.2.

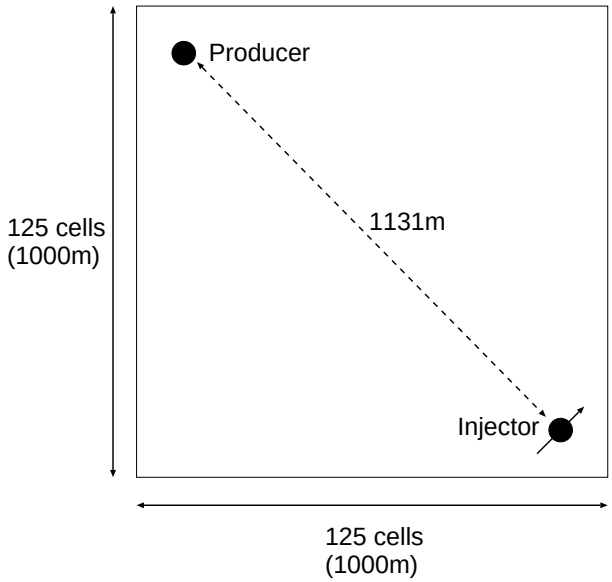

Figure 8.2: 2D fine-scale model. The number of cells in the fine-scale model is 125×125.

Table 8.1: Quarter five-spot pattern model

Model Size	1000m × 1000m
Injector Well	Centre of SE-corner cell of Coarse-scale Model
Producer Well	Centre of NW-corner cell of Coarse-scale Model
Distance between Wells	1131m
Flow Direction	SE to NW

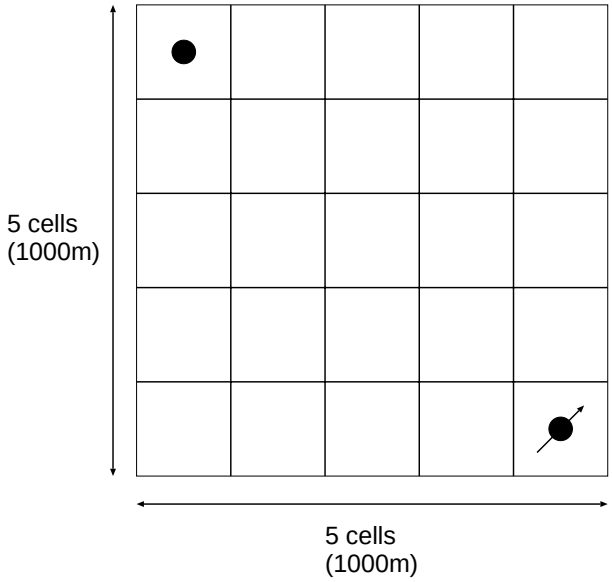

Figure 8.3: 2D coarse-scale model. The number of cells in the coarse-scale model is 5×5.

Table 8.2: Fine-scale model and coarse-scale model

	Fine-scale Model	Coarse-scale Model
Cell Size	8m $\times$ 8m	200m $\times$ 200m
Number of Cells	125 $\times$ 125	5 $\times$ 5

The producer and water injector wells were placed at the centres of the corner coarse cells, and the well positions in the coarse-scale model were exactly the same as those in the fine-scale model. The boundary conditions were assumed to be the same in both scale models: the producer well was controlled by a bottom hole pressure (BHP) of 400 [bar], the injector well was controlled by a rate of 330.0 [m^3/day] (reservoir conditions) and BHP limit of 689.48 [bar], and the sides of the model were sealed.

A homogeneous model in which permeability and porosity are 200 mD and 0.2 respectively was used in Section 8.4. Then, in Section 8.5, the permeability distribution was varied using Sequential Gaussian Simulation (SGSIM) (Deutsch and Journel, 1998) to investigate the effects of the sub-grid heterogeneity.

In the models above, relative permeabilities for the fine-scale model, referred to as the "rock curves", were assigned by adopting Corey-type rock curves (Corey, 1954) with an exponent of 2 and the fixed end-points as in Section 6.2. Although the end-points can be varied using the end-point scaling (Schlumberger, 2004a), they were fixed throughout the model in this case assuming a single facies reservoir with a rock curve. The parameters used in the fine-scale model are given in Table 8.3. Note that, it is assumed that the reservoir properties are uniform within each fine-scale cell and the resolution is adequate for assigning the core-scale "rock curve". Water viscosity is 0.3 cp and oil viscosity is 1.0 cp. The other parameters of the fluid properties are the same as those in the second data set of the 10th SPE Comparative Solution Project Christie and Blunt (2001). Note that the units used in the paper (Christie and Blunt, 2001) were converted from field units to metric units (Schlumberger, 2004a) in this case.

The difference between the model description of this chapter and that of Chapter 6 is in the model and cell size, the well locations, the time step and the permeability field. Also in Chapter 6 oil viscosity was dependent on pressure (Table 6.1). In this chapter oil viscosity is a constant independent of pressure so that it is consistent with the assumption of the upscaling software used below, although the difference is very small. Apart from these properties, the input data for the flow simulation in this chapter is the same as in Chapter 6.

Table 8.3: Parameters of the fine-scale and coarse-scale models

Permeability	200 mD or Generated by SGSIM
Porosity	0.20
Rock Curve	Corey function as in Section 6.2
Oil viscosity [cp]	1.0
Water viscosity [cp]	0.3

8.4 Coarse-Scale Relative Permeabilities

Coarse-scale relative permeabilities were calculated using two-phase dynamic upscaling. The two-phase upscaling scheme adopted here is Pore Volume Weighted (PVW) methods using transmissibilities which were calculated under global boundary conditions (i.e. the well controls specified in Section 8.3, and sealed boundaries) and global boundary conditions for the two-phase simulations. There are 40 sets of curves in the pattern: 2 directions times 20 pairs of the adjacent cells. It is difficult to analyse all the curves one by one. Moreover, in realistic cases with larger models, it is impossible to input all the curves in a flow simulator because of the limited memory. In this chapter, the 40 sets of the curves were grouped into the four categories using the homogeneous model. The four groups of relative permeabilities are shown in Figure 8.4. These groups can be classified by the regions and flow directions as illustrated in Figures 8.5 to 8.8. The analysis of Hewett et al. (1998) for one dimensional flooding was applied to the foregoing problem of quarter five-spot pattern. The focus is on the average water saturation which has built up before the shock front reaches the side of a coarse cell. The flow regime was clarified by investigating the saturation distributions at several time steps. To make the explanation below simpler, only the cells which are located to the south of the NW-SE diagonal are described. The flows between the other cells located to the north of NW-SE diagonal are the same because of symmetry in the homogeneous model.

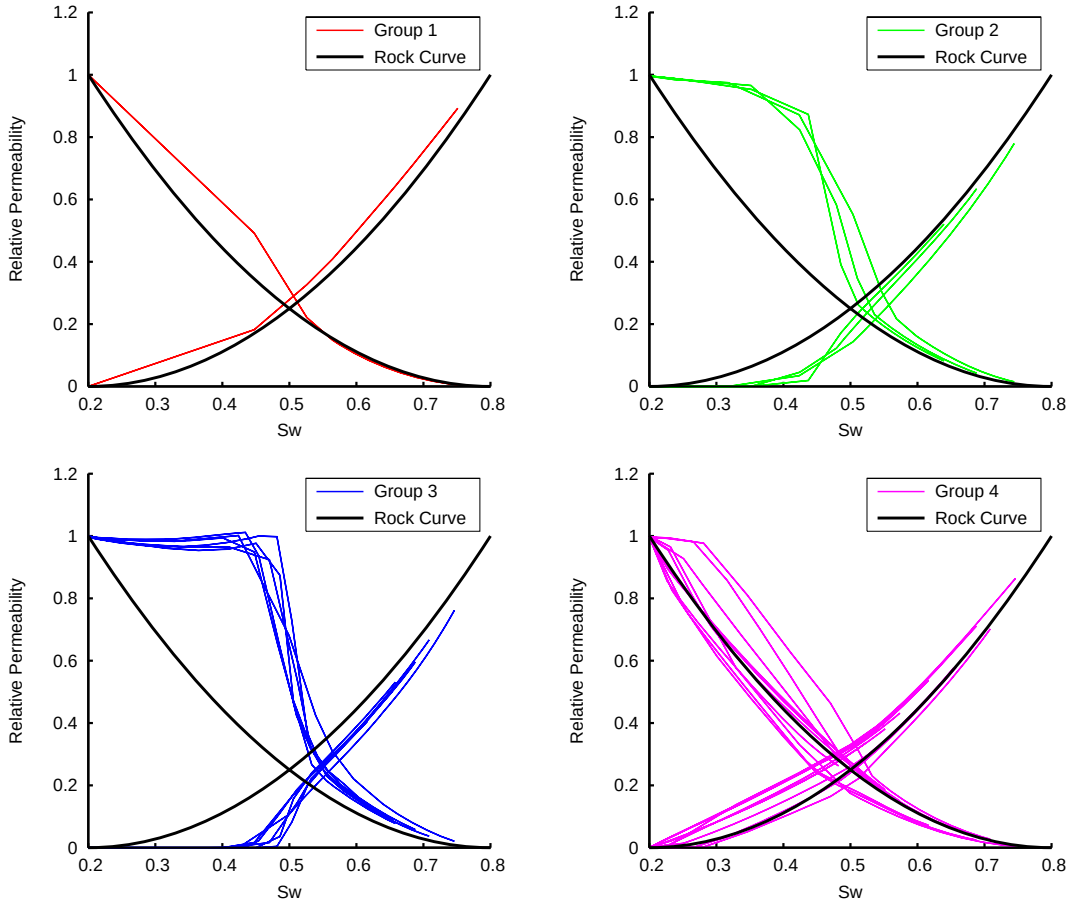

Figure 8.4: Upscaled relative permeabilities in the homogeneous model (Oil viscosity = 1 [cp]). Top left is Group 1, top right is Group 2, bottom left is Group 3 and bottom right is Group 4.

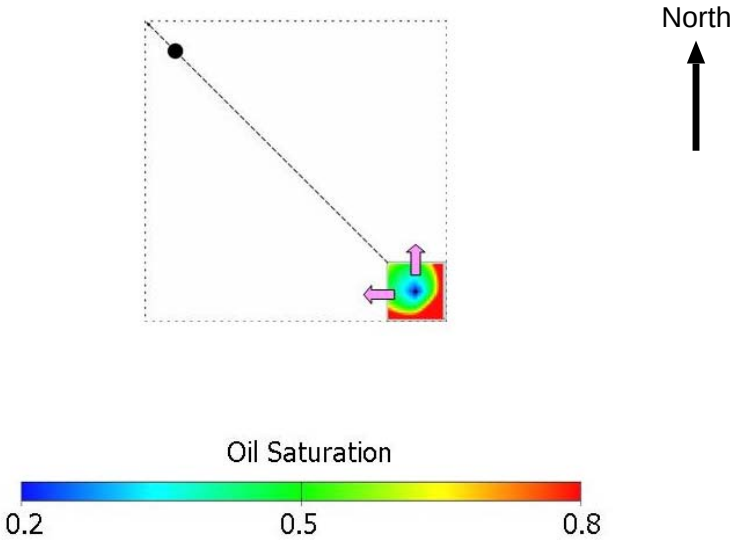

Figure 8.5: Group 1 in the Pattern. Saturation distribution in the cell of Group 1 is shown in the diagram.

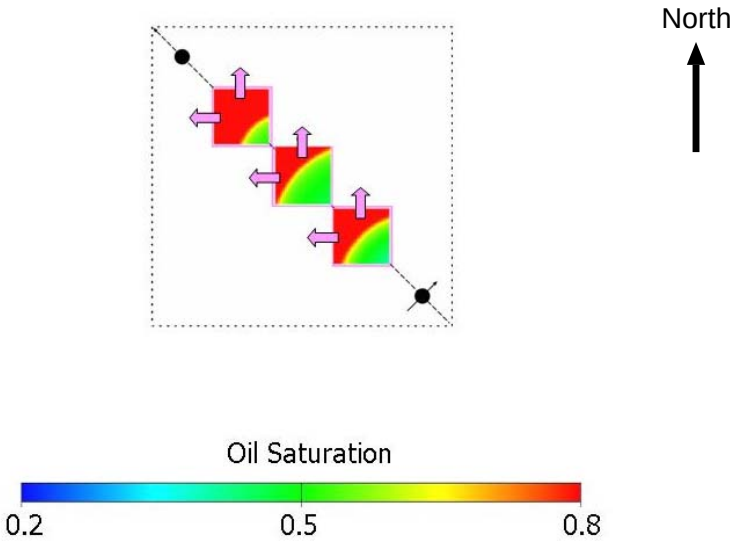

Figure 8.6: Group 2 in the Pattern. Saturation distribution in the cells of Group 2 is shown in the diagram.

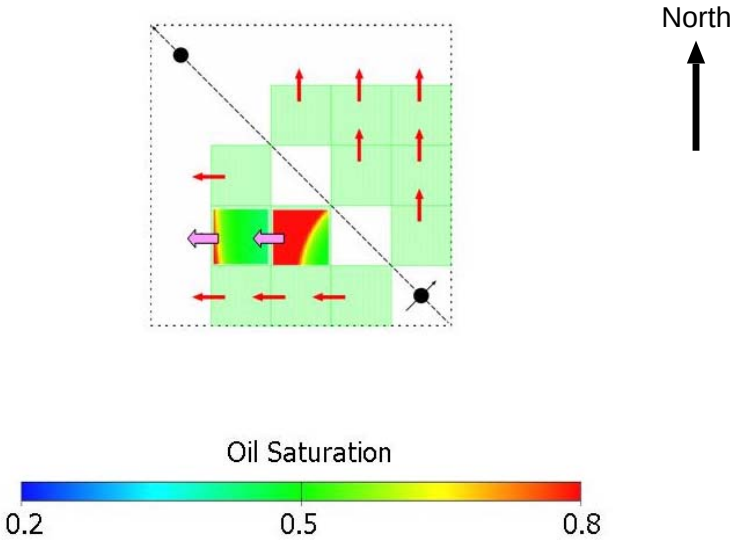

Figure 8.7: Group 3 in the Pattern. Typical saturation distribution in the cells of Group 3 is shown in the diagram.

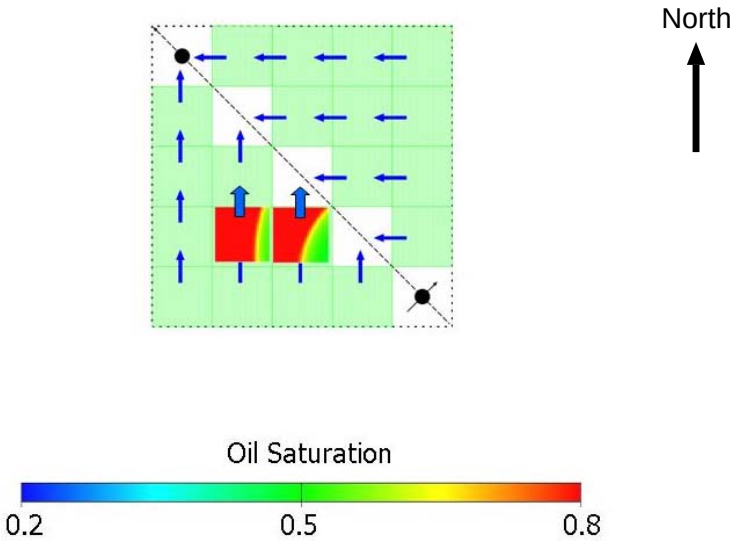

Figure 8.8: Group 4 in the Pattern. Typical saturation distribution in the cells of Group 4 is shown in the diagram.

8.4.1 Description of Each Group

Group 1 The injector is located in the centre of the coarse cell, so the saturation builds up from the centre outwards. In our foregoing model, the two boundaries in the east and south are sealed, since the model was extracted along those boundaries from one pattern of five spot, and those were set as no-flow boundaries. Therefore, the saturation changes preferentially spread toward the other two sides of the cell which are the west and north edges. The relative permeability curves for the flow to these two edges are labelled as Group 1 (Figure 8.5), because the saturation build-up scheme is different from that in the other cells in the model.

Group 2 Apart from the injector and producer cells, the relative permeabilities for the cells along the NW-SE diagonal are labelled as Group 2 (Figure 8.6). According to the investigation of the saturation distribution, the advancing front expands forming the arc of a circle from the SE corner of each cell to the entire cell. This group is distinguished from Group 3 below, since the arc of advancing front is axially symmetric along the NW-SE diagonal.

Group 3 In the other regions, the "outward flow" which proceeds away from the NW-SE diagonal gives relative permeabilities which are labelled as Group 3 (Figure 8.7). Although the relative permeabilities of Group 3 are shifted to the right in the same way as those for Group 2, the advancing front of Group 3 forms an elliptic arc rather than the arc of a circle. The front of Group 3 seems nearly linear and parallel to the east side. As a result, compared to Group 2 above, Group 3 has larger average water saturation, when water reaches the west side of the coarse cell.

Group 4 In the same cells as the Group 3, the relative permeabilities from "inward flow" which proceeds toward the NW-SE diagonal is labelled as Group 4 (Figure 8.8). Whereas Group 3 has the large average water saturation at the breakthrough to the west side, Group 4 has much smaller average water saturation, when the front reaches the cell boundary on the

north side. As mentioned in the description of Group 3, the advancing front is nearly linear, moving westwards. The front reaches the north side just after it enters from the east side of the cell. In other words, the shock front in Group 4 enters from the one side of the cell and exits immediately to the adjacent perpendicular side. That is why the average water saturation is so small that it may leave the large amount of oil in the coarse cell at the breakthrough.

8.4.2 Sensitivity of Viscosity

Although the viscosities are fixed as the values in Table 8.3 for the rest of the thesis, this subsection shows the sensitivity of the viscosity on the relative permeability curves for completeness. The main findings on this issue have been already presented in other literature which studied the 1D problem (Hewett et al., 1998). So instead of repeating the details, the current objective is to check the ongoing grouping strategy for different viscosities.

First, the oil viscosity was changed from 1.0 cp to 3.0 cp. The upscaled relative permeabilities are shown in Figure 8.9. Secondly, the oil viscosity was changed from 1.0 cp to 10.0 cp. The upscaled relative permeabilities are shown in Figure 8.10. The non-monotonic shapes in the curves of Groups 2 and 3 clearly appeared in Figures 8.9 and 8.10, which can be explained due to the effect of the total mobility at the coarse scale (Hewett et al., 1998). It turned out that the non-monotonic shapes in the curves of Groups 2 and 3 in Figure 8.4 are almost invisible, but they become significant as the oil viscosity increases.

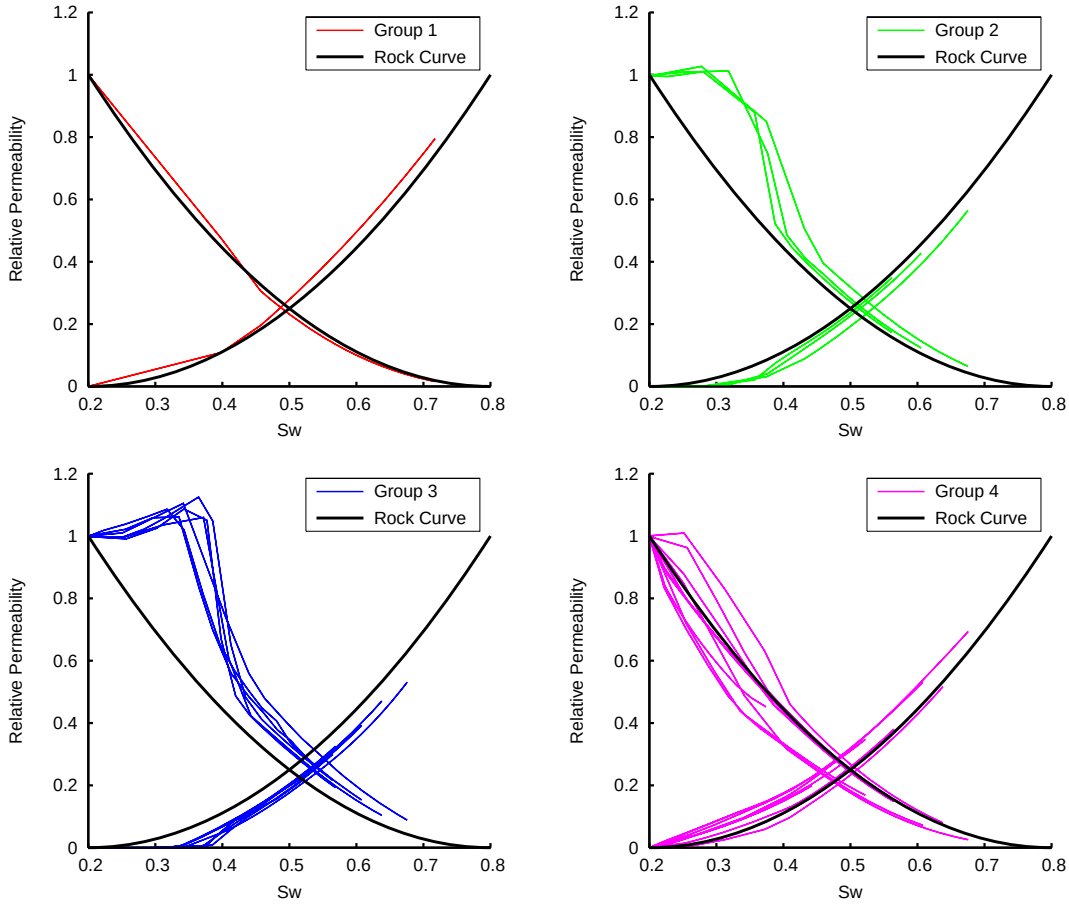

Figure 8.9: Upscaled relative permeabilities in the homogeneous model (Oil viscosity = 3 [cp]). Top left is Group 1, top right is Group 2, bottom left is Group 3 and bottom right is Group 4.

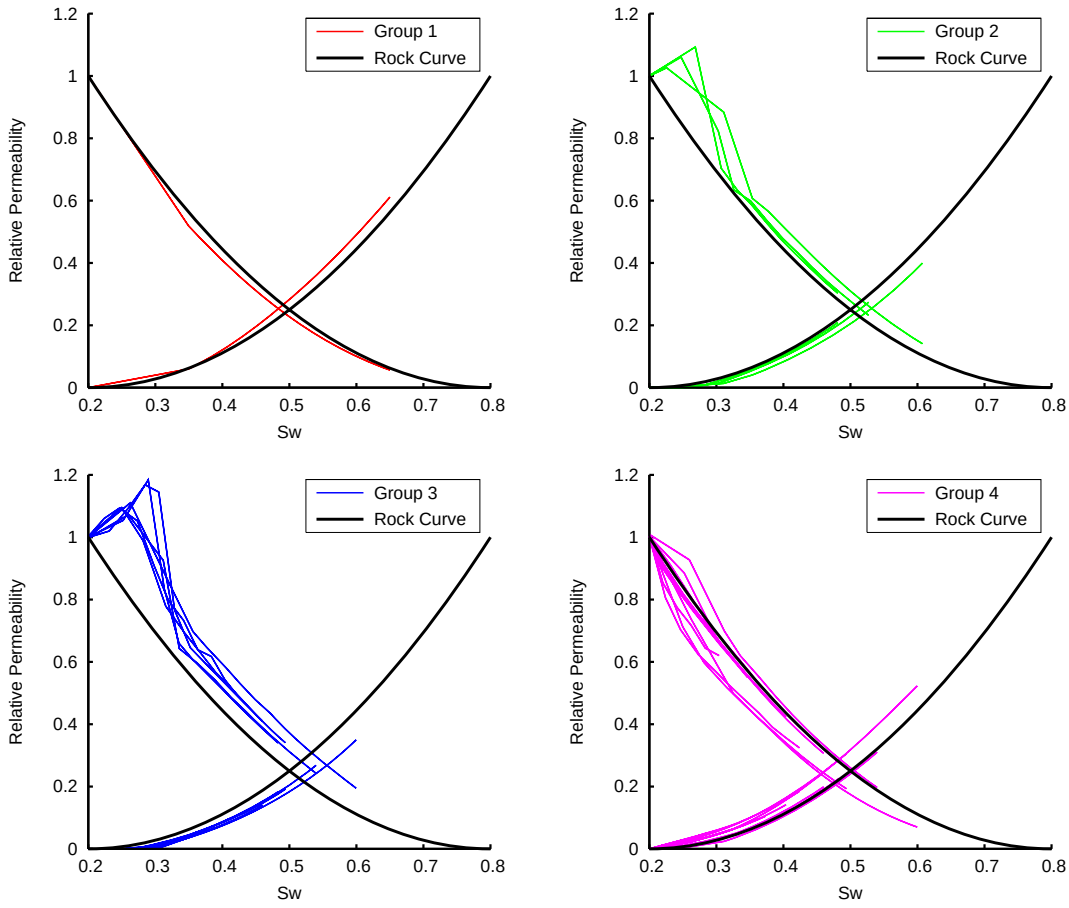

Figure 8.10: Upscaled relative permeabilities in the homogeneous model (Oil viscosity = 10 [cp]). Top left is Group 1, top right is Group 2, bottom left is Group 3 and bottom right is Group 4.

Here, although each curve is different for the different viscosity values, the categories defined above can hold in these two cases. For instance, the inward flow and outward flow have definitely different trends on the curves.

8.4.3 Summary

The coarse-scale relative permeabilities for a homogeneous model may be categorised into 4 groups, determined by the flow direction and water saturation at breakthrough. This classification has been used in Section 8.5, where the effect of sub-grid heterogeneity on the shapes of relative permeabilities is investigated. Note that the viscosity values are fixed as shown in Table 8.3.

8.5 Effect of Sub-Grid Heterogeneity

The heterogeneous permeability distribution was generated by Sequential Gaussian Simulation (SGS) (Deutsch and Journel, 1998) and was conditioned to data for 2 vertical wells (200 mD). The Gaussian random numbers were transformed to logarithmic permeabilities, ln(k), by multiplying them by the standard deviation and adding the mean. In this case, the mean of ln(k) was assumed to be 5.3 which corresponds to 200 mD. The correlation length in the NW-SE direction (λ_1), the NE-SW direction (λ_2) and the standard deviation (σ) of logarithmic permeability were varied to investigate the sensitivity of the sub-grid heterogeneity to the upscaled relative permeabilities. The following ranges are used: $0.0 \leq \sigma \leq 1.0$, $0 \leq \lambda_1 \leq 200\,\text{m}$ and $0 \leq \lambda_2 \leq 100\,\text{m}$. The upscaled relative permeabilities for a range of standard deviations (σ) and correlation lengths (λ_1, λ_2) were calculated. The case with a standard deviation of 0.0 corresponds to a homogeneous model for which the results have been shown in Section 8.4.

In this section, firstly the effect of the standard deviation (σ) and the correlation length in the NW-SE direction (λ_1) on the upscaled relative permeabilities is demonstrated. The effect of the correlation length in the NE-SW direction, λ_2, was not so significant as that for λ_1 in this case,

because the main flow direction was the NW-SE direction in the model and was perpendicular to the NE-SW direction. So the results for λ_2 are omitted in this section. Secondly, the coarse-scale relative permeabilities are analysed using saturation distributions in a semi-quantitative way. Finally, the limits of the coarse-scale relative permeabilities are estimated.

8.5.1 Sensitivity of Standard Deviation

Three values of σ were chosen to investigate the effect of the standard deviation. There were 0.0, 0.5 and 1.0 (Table 8.4). The correlation length in NW-SE direction and that of NE-SW directions were fixed at 100.0 m and 50.0 m respectively so that the model was an anisotropic correlated-Gaussian field. Note that C_V in Table 8.4 is the coefficient of variation which is defined as the standard deviation divided by the mean. In this case C_V of permeability was calculated from the variance of the logarithmic permeability: $C_V^2 = \exp(\sigma^2_{\ln(k)}) - 1$, (Jensen et al., 2000). A classification of heterogeneity associated with C_V of permeability is provided by Jensen et al. (2000): e.g., homogeneous ($C_V \leq 0.5$), heterogeneous ($0.5 < C_V \leq 1$) and very heterogeneous ($C_V > 1$). The classification is also provided in Table 8.4.

Table 8.4: Sensitivity analysis of standard deviation

	σ	C_V	λ_1 (m)	λ_2 (m)
Case 1	0.0 (Homogeneous)	0.0	100.0	50.0
Case 2	0.50 (Heterogeneous)	0.53	100.0	50.0
Case 3	1.00 (Very Heterogeneous)	1.31	100.0	50.0

The permeability distributions of one of the realisations for Cases 2 and 3 are shown in Figures 8.11 and 8.12. The corresponding saturation distributions at 3000 days (from the start of injection) are shown in Figures 8.14 and 8.15 and that for the homogeneous model is also shown in Figure 8.13. As the standard deviation increases, the contrast between high permeability and low permeability becomes larger, and large fingers form in the saturation distribution. Figures 8.16 and 8.17 represent the upscaled relative permeabilities for Cases 2 and 3, respectively. Those curves for Case 1 are shown in Figure 8.4 in the previous chapter. As the standard

deviation increases, the bunch of the relative permeability curves spreads out and the curves are shifted to the left.

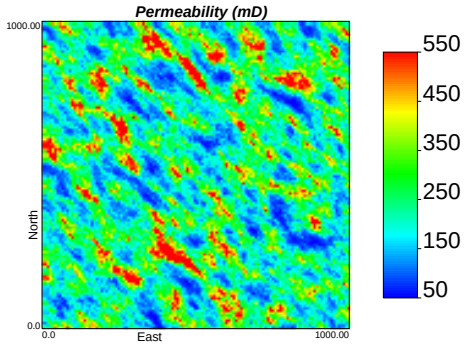

Figure 8.11: Permeability distribution (Case 2, $\sigma = 0.5$). The permeability field is heterogeneous.

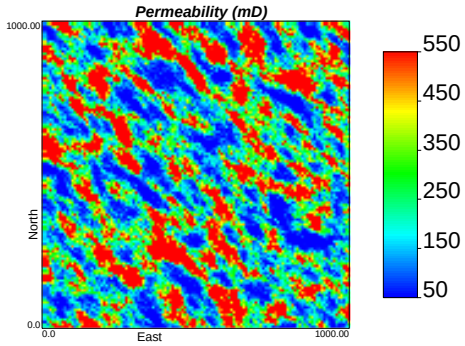

Figure 8.12: Permeability distribution (Case 3, $\sigma = 1.0$). The permeability field is very heterogeneous.

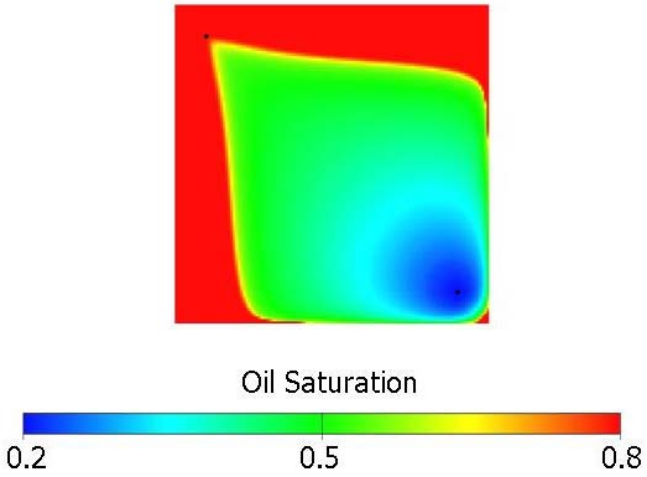

Figure 8.13: Saturation distribution at 3000 days (Case 1, $\sigma = 0.0$). The permeability field is homogeneous.

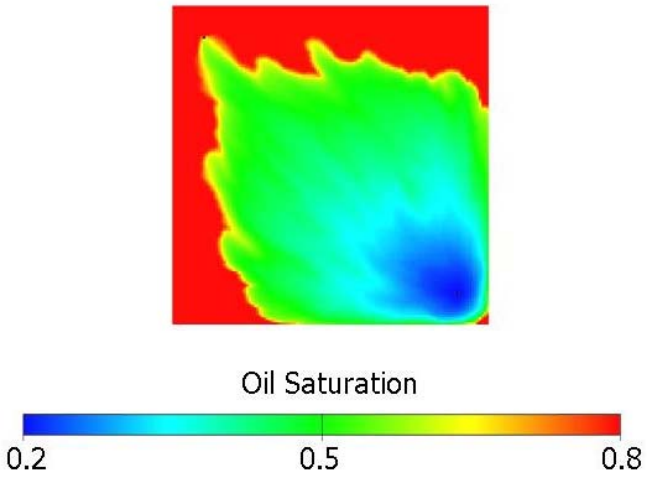

Figure 8.14: Saturation distribution at 3000 days (Case 2, $\sigma = 0.5$). The permeability field is heterogeneous.

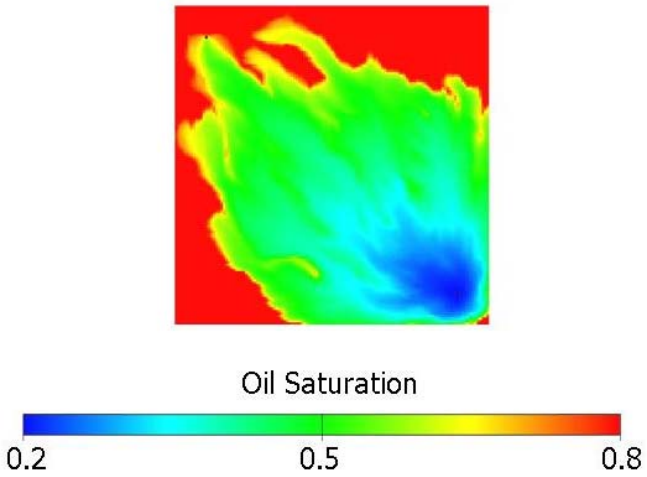

Figure 8.15: Saturation distribution at 3000 days (Case 3, $\sigma = 1.0$). The permeability field is very heterogeneous.

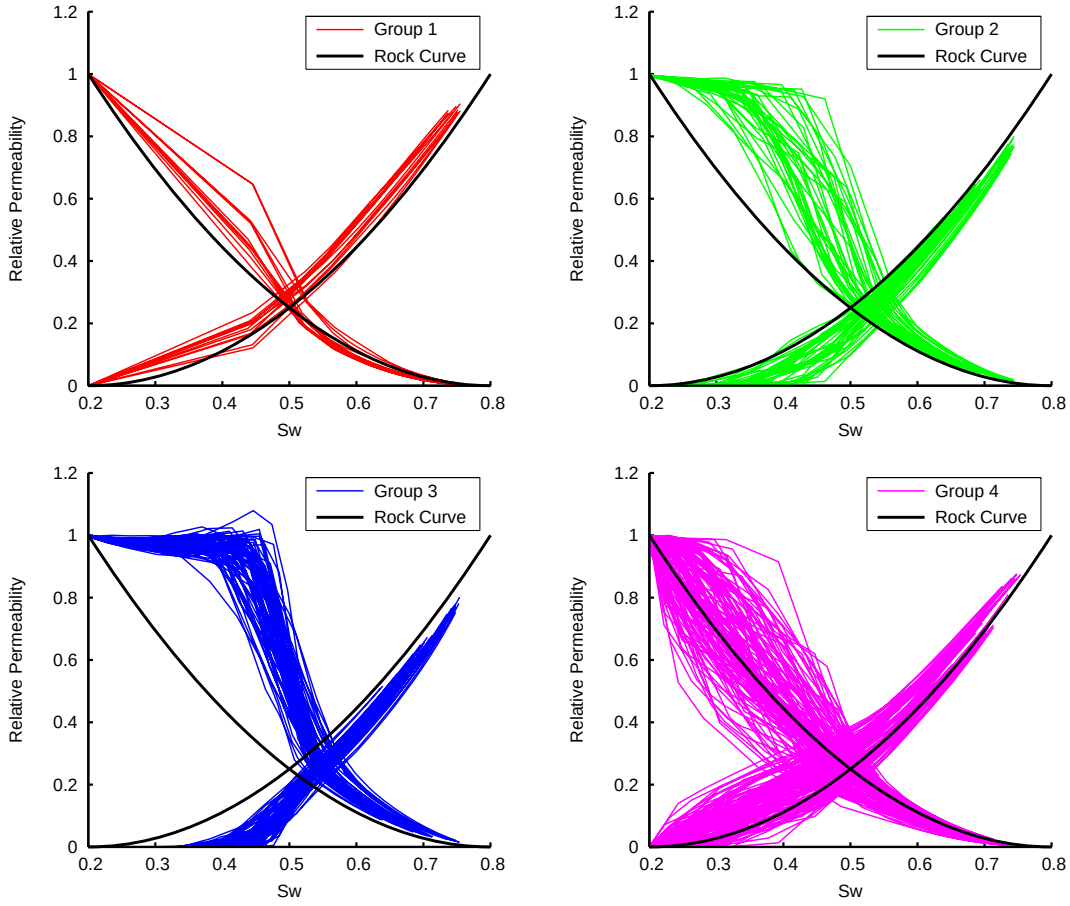

Figure 8.16: Upscaled relative permeabilities in the heterogeneous models (Case 2). Top left is Group 1, top right is Group 2, bottom left is Group 3 and bottom right is Group 4.

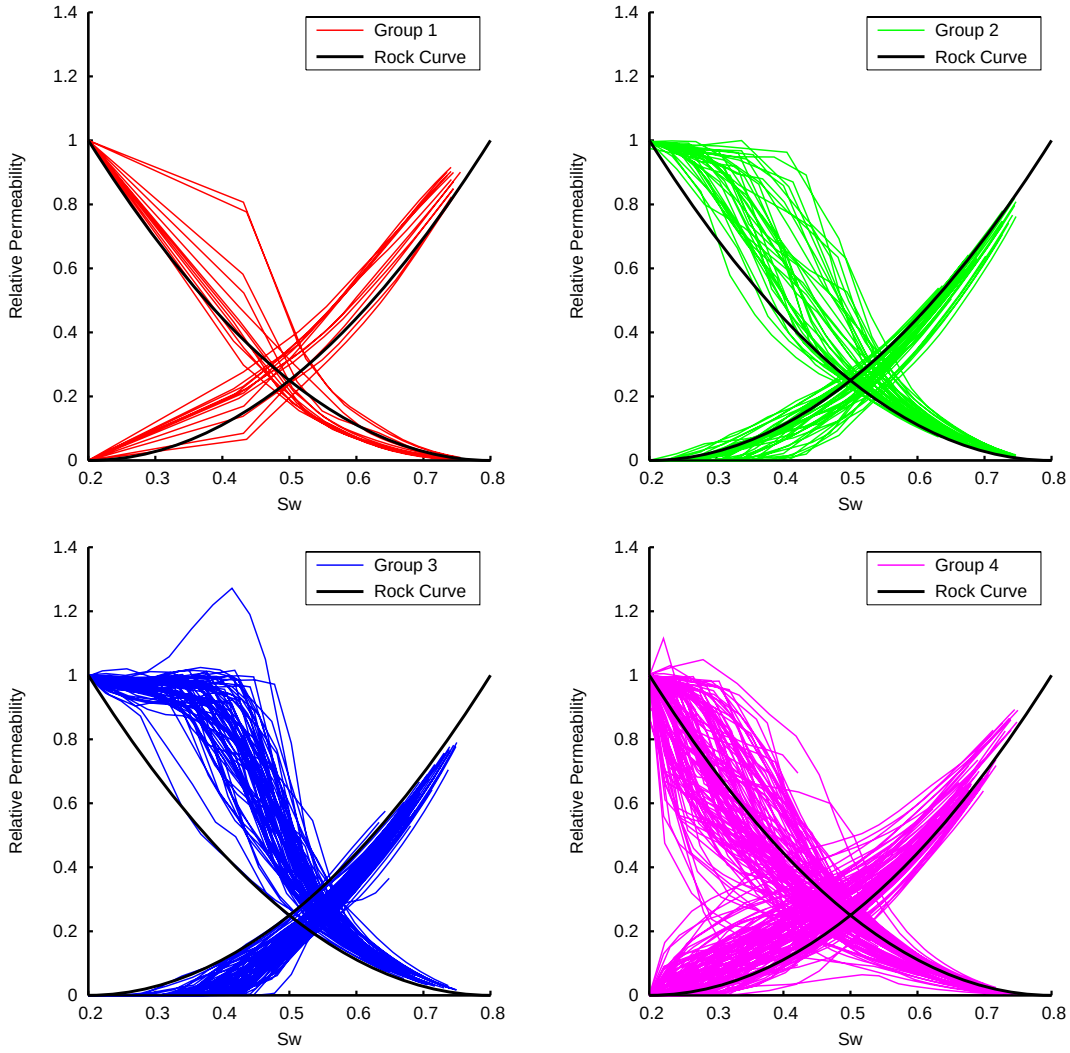

Figure 8.17: Upscaled relative permeabilities in the very heterogeneous models (Case 3). Top left is Group 1, top right is Group 2, bottom left is Group 3 and bottom right is Group 4.

8.5.2 Sensitivity of Correlation Length

In order to investigate the effect of the correlation length, three values of λ_1 were set as shown in Table 8.5. The standard deviation was fixed at 0.50. The correlation length in NE-SW direction was fixed at 50.0 m.

Table 8.5: Sensitivity analysis of correlation length in NW-SE direction

	σ	λ_1 (m)	λ_2 (m)
Case 4	0.50	50.0	50.0
Case 5	0.50	100.0	50.0
Case 6	0.50	200.0	50.0

The permeability distributions of one of the realisations for Cases 4 and 6 are shown in Figures 8.18 and 8.19. The corresponding saturation distributions at 3000 days (from the start of injection) are shown in Figures 8.20 and 8.21. Those figures for Case 5 are the same as Figures 8.11 and 8.14. As λ_1 increases, the structures extend and the fingers stand out along the structures. Figures 8.22 and 8.23 represent the upscaled relative permeabilities for Cases 4 and 6, respectively. Those curves for Case 5 are shown in Figure 8.16. When λ_1 is large, some relative permeabilities are shifted to left as shown in Figures 8.22 and 8.23.

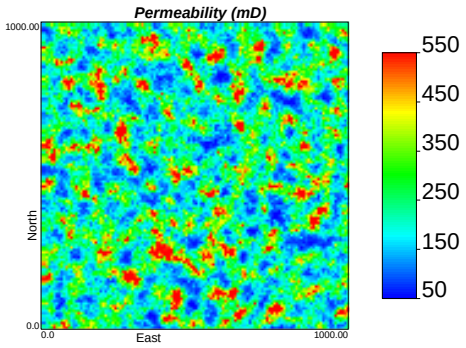

Figure 8.18: Permeability distribution (Case 4, $\lambda_1 = 50$). The permeability field has a short correlation length.

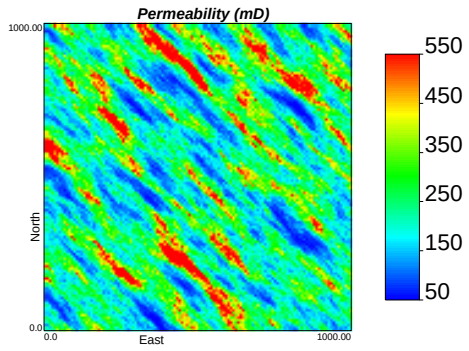

Figure 8.19: Permeability distribution (Case 6, $\lambda_1 = 200$). The permeability field has a long correlation length.

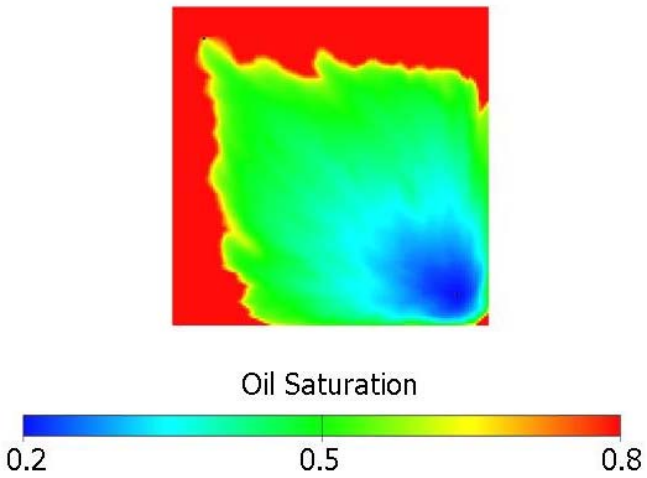

Figure 8.20: Saturation distribution at 3000 days (Case 4, $\lambda_1 = 50$). The permeability field has a short correlation length.

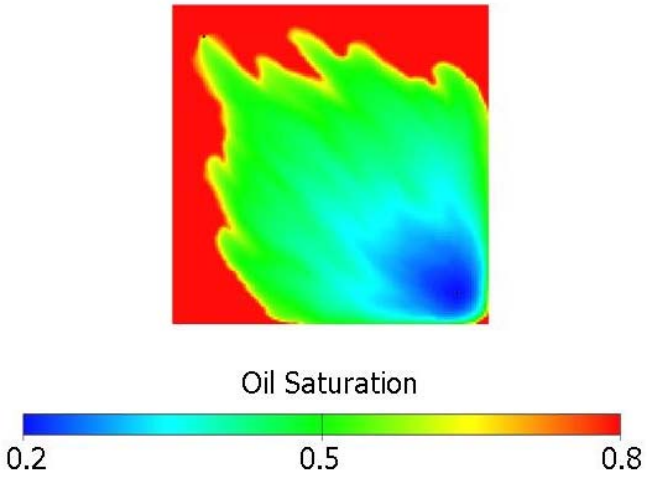

Figure 8.21: Saturation distribution at 3000 days (Case 6, $\lambda_1 = 200$). The permeability field has a long correlation length.

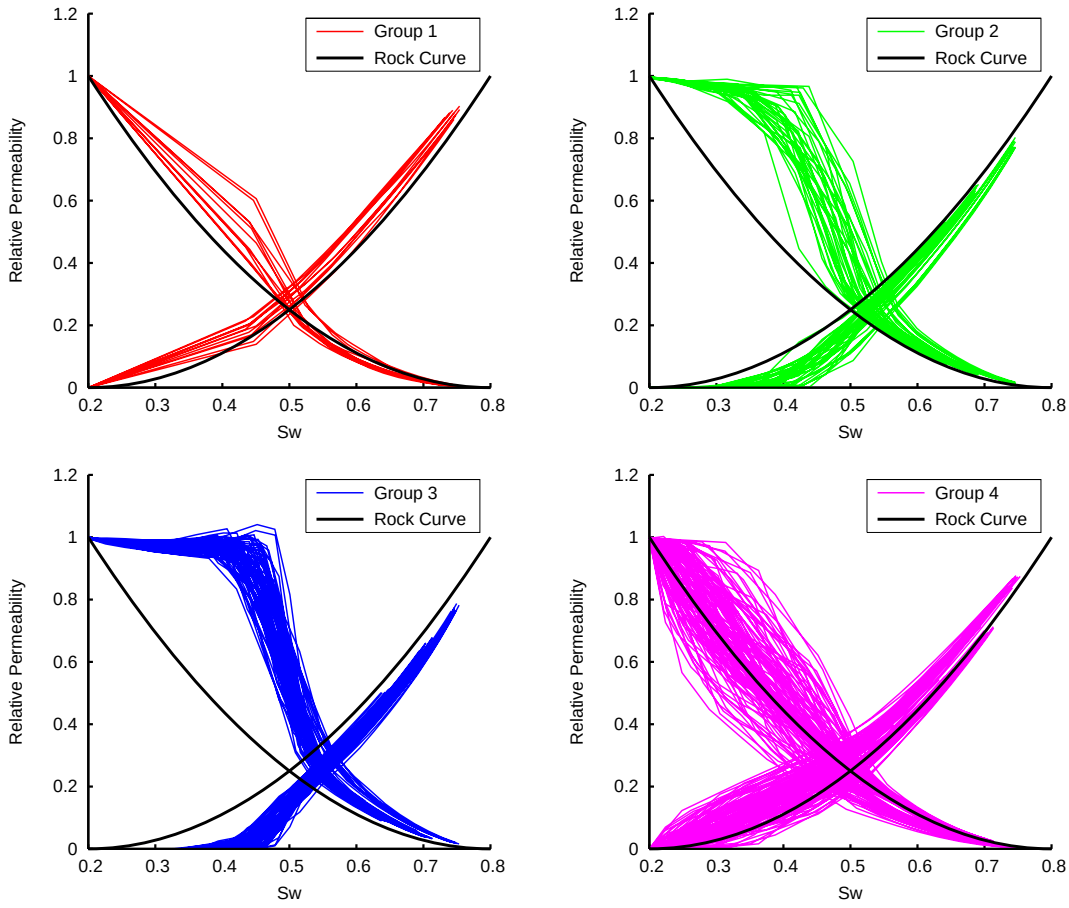

Figure 8.22: Upscaled relative permeabilities (Case 4). The permeability field has a short correlation length. Top left is Group 1, top right is Group 2, bottom left is Group 3 and bottom right is Group 4.

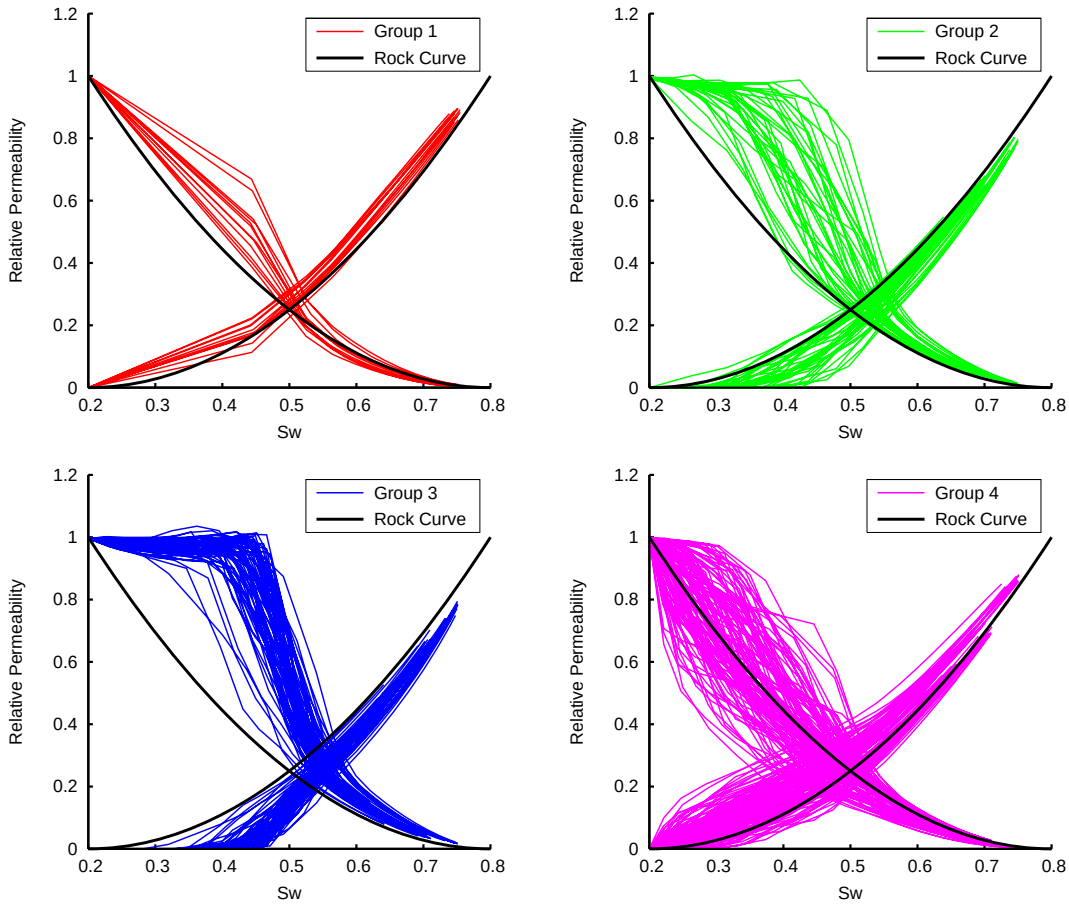

Figure 8.23: Upscaled relative permeabilities (Case 6). The permeability field has a long correlation length. Top left is Group 1, top right is Group 2, bottom left is Group 3 and bottom right is Group 4.

8.5.3 Analysis of Coarse-Scale Relative Permeabilities

According to the observations above, the shape of relative permeabilities depends on the fingers induced by heterogeneity. For example, the "build-up" saturation at the breakthrough of the cell is affected by those fingers. At the time of breakthrough, the average water saturation in the heterogeneous model tends to be smaller than that in the homogeneous model.

In cells of Group 3, the shock front advances linearly from the one side to the opposite side. When the heterogeneity-induced fingers stand out from the front, this leads to a smaller average water saturation at breakthrough and shifts the curve to the left along the water saturation axis. It can be said that the standard deviation and the correlation lengths control the number and length of fingers. In this case, the larger the standard deviation and the correlation length, the more clearly the fingers stand out from the front. That is why the heterogeneous models shift the upscaled relative permeabilities to the left along the water saturation axis.

This paragraph analyses the coarse-scale relative permeability curve more quantitatively. The aim is to predict the shape of the relative permeability curves from the sub-grid statistics. Note that the precise estimation using an upscaling method is demonstrated in the other Subsections 8.5.1, 8.5.2 and 8.5.4. The upscaling method used there conducts a fine-scale flow simulation and calculates coarse-scale properties from the fine-scale solution. In this paragraph, the fine-scale saturation distribution is assumed to be estimated from the sub-grid statistics and then the approximate shape of the coarse-scale relative permeabilities is calculated. Although the precise saturation distribution has been already calculated in the above subsections, it is to be estimated in a different way here to show that the coarse-scale relative permeabilities are predictable from the sub-grid statistics. Figure 8.24 represents the water saturation profile from a 1D analytical solution. In this case, the irreducible water saturation (S_{wi}) is 0.2 and the shock saturation (S_{wf}) is 0.49. The profile can also be demonstrated using 2D numerical simulations. The focus is on one cell circled in Figure 8.25 and the flow to the west edge of the cell. Figures 8.26 and 8.27 show the saturation distributions in the homogeneous and heterogeneous models ($\sigma = 1.0, \lambda_1 = 100, \lambda_2 = 50$), respectively. These are the saturation distributions at

breakthrough in a cell when water just reached the west edge. In the case of the homogeneous model, the shock front has passed through most of the cell. For example, the flooded area can be estimated at about 95% of the cell and the other 5% is at the irreducible water saturation. Assuming the same shock front for each finger as that of the 1D profile in Figure 8.24, the average water saturation can be estimated at 0.48 (Note that, in these calculations, the increase of saturation behind the front was ignored). This corresponds to the water saturation at which the water relative permeability (K_{rw}) starts rising in the upscaled relative permeability curves, (Figure 8.4, bottom left). In the case of the heterogeneous model, the area behind the front is smaller than that in the homogeneous model because of the channelling effect along the structure. This area could be estimated at about 60% of the cell and then the average water saturation can be estimated as 0.37. This indicates that the water saturation value at which K_{rw} starts rising decreased below 0.4 (Figure 8.17). The value plays an important role in describing the relative permeability curves. This semi-quantitative analysis can be conducted in the other cells in the pattern. For example, given a set of geostatistical parameters, one might estimate the shape of fingers induced by the heterogeneity and the area behind the shock front saturation. Then the average saturation at breakthrough in a cell could be predicted from the information on the sub-grid heterogeneity.

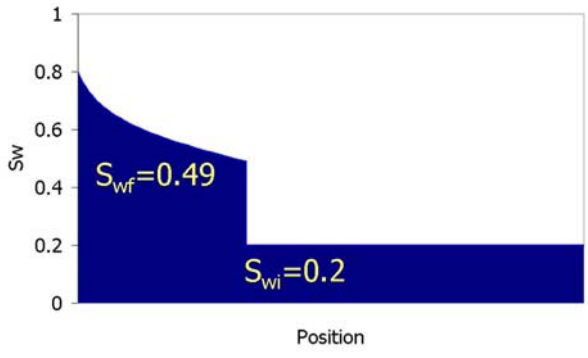

Figure 8.24: 1D analytical solution of saturation profile. The Buckley-Levrett analysis was employed.

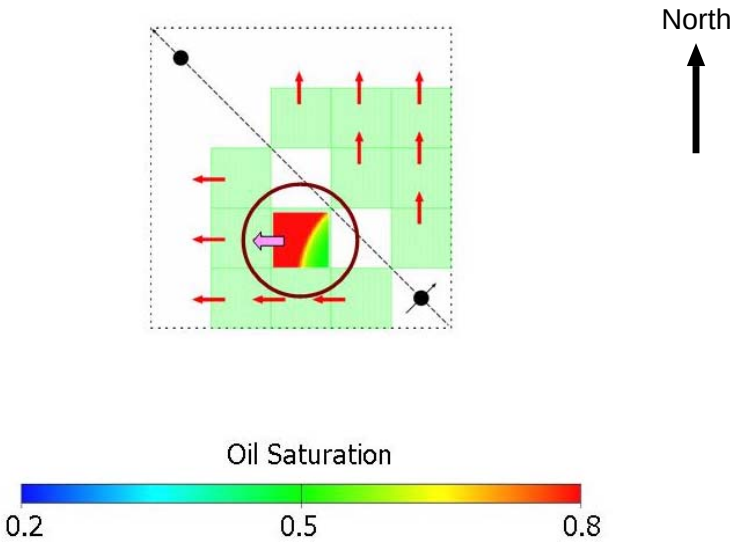

Figure 8.25: Cell and flow direction for the analysis. The target cell is circled in the diagram.

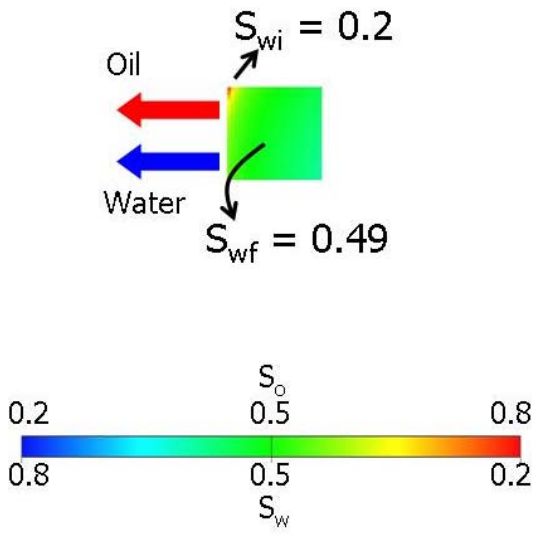

Figure 8.26: Saturation distribution at breakthrough in the cell. The permeability field is very homogeneous.

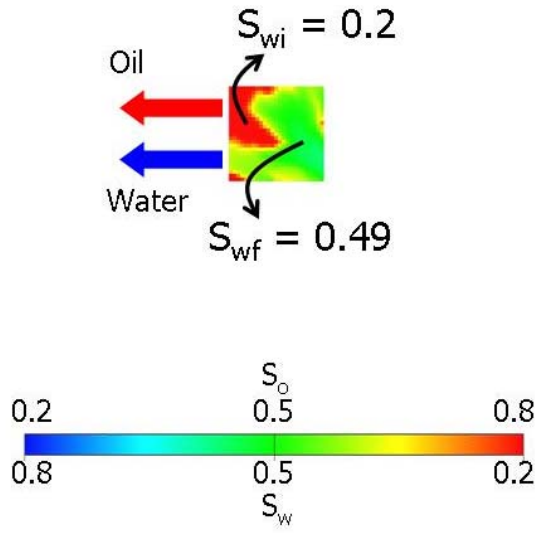

Figure 8.27: Saturation distribution at breakthrough in the cell. The permeability field is very heterogeneous. ($\sigma = 1.0, \lambda_1 = 100, \lambda_2 = 50$)

8.5.4 Range of Coarse-Scale Relative Permeabilities

As the final part of this section, the prior range of the coarse-scale relative permeabilities is estimated through numerical experiments on sub-grid heterogeneity. Imagine that the following information on the logarithmic permeability in the foregoing reservoir model was given:

- Correlation length in NW-SE direction (λ_1) is greater than 0 m and smaller than 200 m,
- Correlation length in NE-SW direction (λ_2) is greater than 0 m and smaller than 100 m,
- Standard deviation (σ) is 0.50.

Here the task is to set up the prior ranges for the calibration of relative permeabilities in advance of history-matching. In other words, it is to determine the limits of the curves from the static information.

According to the investigations so far in this chapter, the relative permeabilities in the coarse-scale models may be grouped into 4 types (apart from 2 well relative permeabilities). The minimum and maximum of the coarse-scale relative permeabilities for Groups 1 to 4 were calculated as follows. The focus was on the range of relative permeabilities resulting from a range of correlation lengths. As shown in Figure 8.28, 25 combinations of the correlation lengths were chosen from the λ_1-λ_2 parameter space. In total, 150 models were generated with 6 realisations per case. Figure 8.29 shows minimum / maximum limits of the upscaled relative permeabilities for all the models. Each figure corresponds to Groups 1 - 4 in the pattern. These limits represent the uncertainty in the coarse-scale relative permeabilities due to sub-grid heterogeneity and can be used as the prior range in the history-matching.

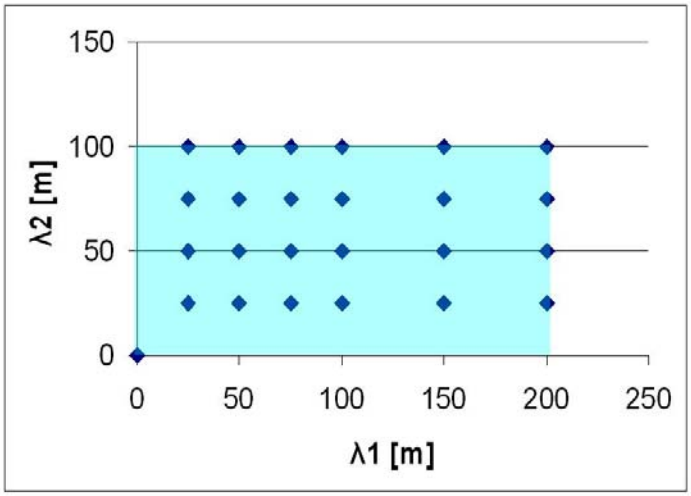

Figure 8.28: 25 cases chosen from the parameter space (λ_1, λ_2). The *x*-axis is correlation length in NW-SE direction and the *y*-axis is that in NE-SW direction.

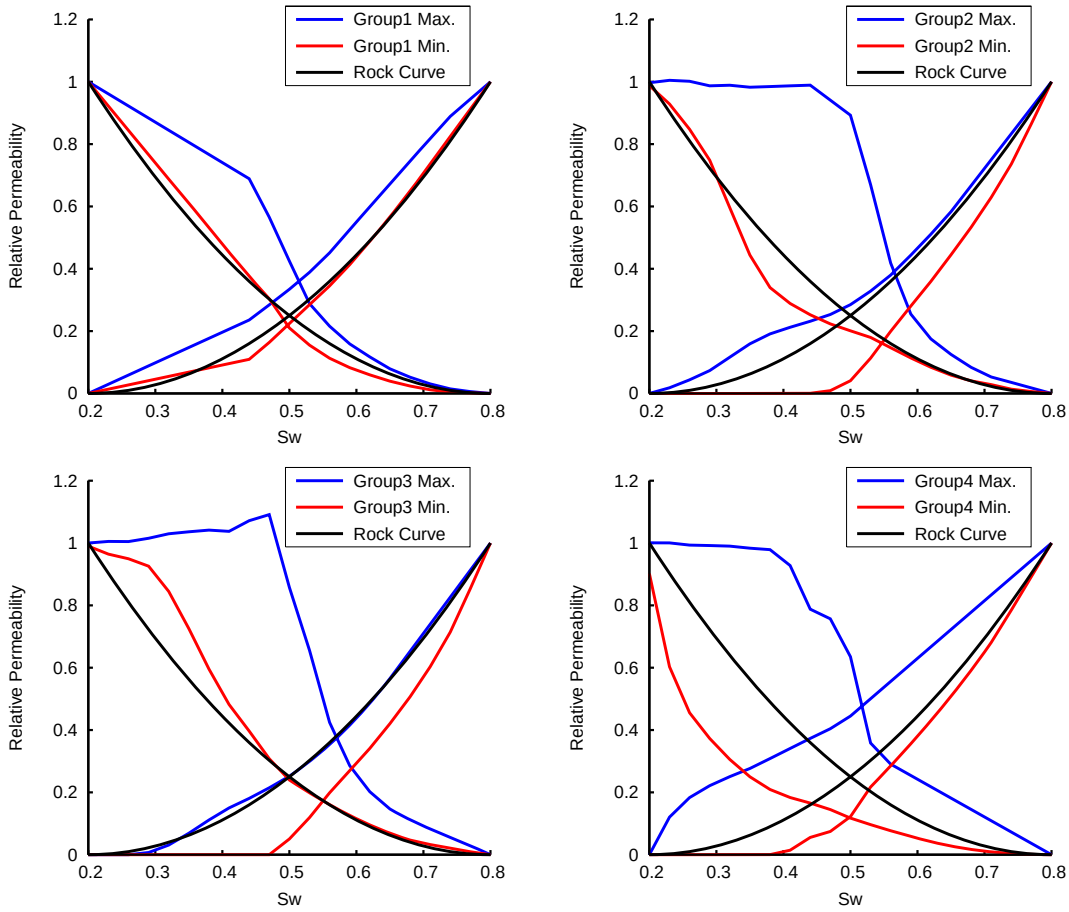

Figure 8.29: Min. and Max. of upscaled relative permeabilities. Top left is Group 1, top right is Group 2, bottom left is Group 3 and bottom right is Group 4.

8.6 Discussion and Conclusions

As a result of the investigation in this chapter, the following conclusions were drawn:

- The shape of coarse-scale relative permeabilities depends on the fingers induced by sub-grid heterogeneity.
- The larger the standard deviation and the correlation length are, the more clearly the fingers stand out from the front.
- The shape of coarse-scale curves also depends on the flow directions and the fluid viscosities.
- Minimum and Maximum limits for the coarse-scale curves can be determined using typical combinations of the geostatistical parameters.

The first three bullet points confirm previous works in the literature (e.g., Muggeridge, 1991; Christie, 1996; Hewett et al., 1998). However, in this thesis I have studied the curves using 2D quarter five-spot pattern models, whereas previous works have used linear models. The forth bullet point is new work.

In this chapter, the dynamic upscaling method was adopted to estimate the prior limits of the coarse-scale relative permeabilities. Obviously it requires the two-phase flow simulations at the fine scale. Hence, in practice, it may not be possible to use the field scale dynamic upscaling. It is necessary to utilise a computationally "cheap" method instead of relying on field-scale two-phase simulation. One of the computationally "cheap" methods is the local upscaling which uses certain boundary condition to the local model. Although the accuracy is controversial, the rough estimation may be enough for the purpose of determining the prior limits. The key is to predict the effect of sub-grid heterogeneity separately from the discretisation effect. This is one of the future works in the research area.

The use of four groups of coarse-scale relative permeability curves is prohibitive because of the considerable computational cost for history-matching. The same thing can be said for the

number of parameters to represent one curve. Actually the combination of these two numbers must be limited for history-matching. Chapter 9 describes the history-matching problem in the foregoing 2D model, and reduces the current number of groups by amalgamating them.

Chapter 9

Uncertainty in Relative Permeabilities for 2D Models

9.1 General Remarks

This chapter extends the problem of Chapter 6 to a two dimensional coarse-scale model. As in Chapter 6, the inverse problem arises from insufficient information on small-scale heterogeneity and the limited data in production history, which leads to uncertain coarse-scale relative permeabilities. The aim is to clarify its influence on the reservoir performance forecast.

A 2D synthetic reservoir model was set up for the numerical experiments, which mimics a five spot pattern waterflooding. As in the previous work of Chapter 6, the flow functions were parameterised using flexible B-splines, because they could encapsulate the effect of the detailed features. Also, because the number of calibration parameters for a 2D problem is larger than that of a 1D problem, a new methodology to restrict the calibration in history-matching is proposed by using physically based prior information. The prior information was derived from the numerical experiments in Chapter 8. The methodology aims to produce a sound basis for forecasting uncertainty in reservoir production.

9.2 Model and Problem Description

9.2.1 Fine-Scale and Coarse-Scale Models and Observed Data

As in Section 6.2, this chapter considers the simulations of a water flooding scenario in an oil reservoir. A 2D truth model was generated as shown in Figures 9.1 (permeability distribution) and 9.2 (permeability histogram). This is also referred to as the fine-scale model, in contrast to the coarse-scale model used for history matching. The size of the model is 1km square. There are 125×125×1 cells in this fine-scale model, each of size 8m×8m×20m. The parameters assigned in the fine-scale model are as follows. Porosity is 0.2 and is uniform throughout the model. The permeability was generated by Sequential Gaussian Simulation (SGS), (Deutsch and Journel, 1998), and was conditioned to data for 2 vertical wells (200mD). The correlation length is 100 m in the NW-SE direction (λ_1) and 50 m in the NE-SW direction (λ_2). The Gaussian random numbers were transformed to logarithmic permeabilities, ln(k), by multiplying them by the standard deviation and adding the mean. In this case, the mean and standard deviation of ln(k) were assumed to be 5.3 and 0.5 respectively. As in Section 6.2, relative permeability for the truth model was assigned by adopting Corey-type rock curves Corey (1954) with an exponent of 2. Oil viscosity is 1.0 [cp] and water viscosity is 0.3 [cp]. The other parameters for the fluid properties are the same as those in the second data set of the 10th SPE Comparative Solution Project (Christie and Blunt, 2001).

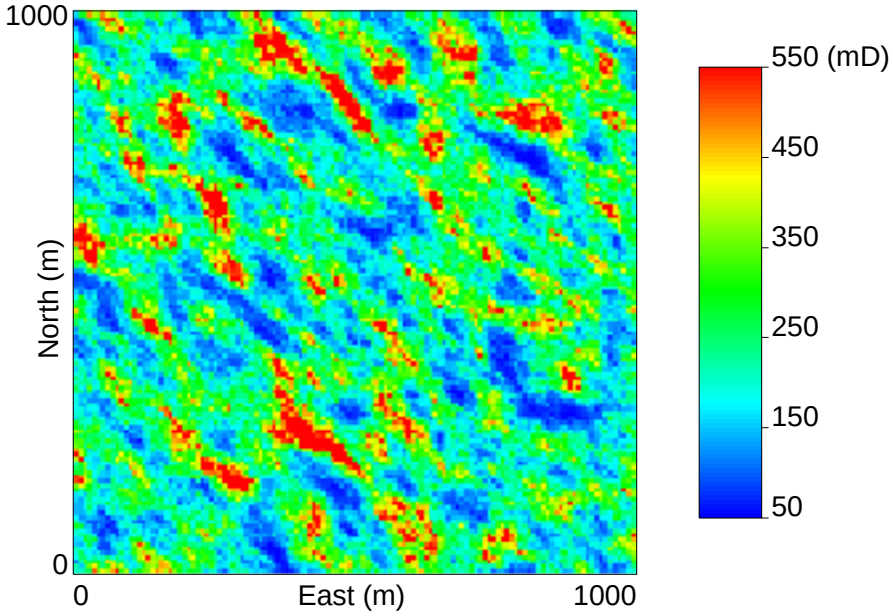

Figure 9.1: Permeability distribution of the "truth" fine-scale model. The "truth" permeability field was generated by Sequential Gaussian Simulation. Note that history-matching was conducted using the 2D coarse-scale models (Figure 9.3).

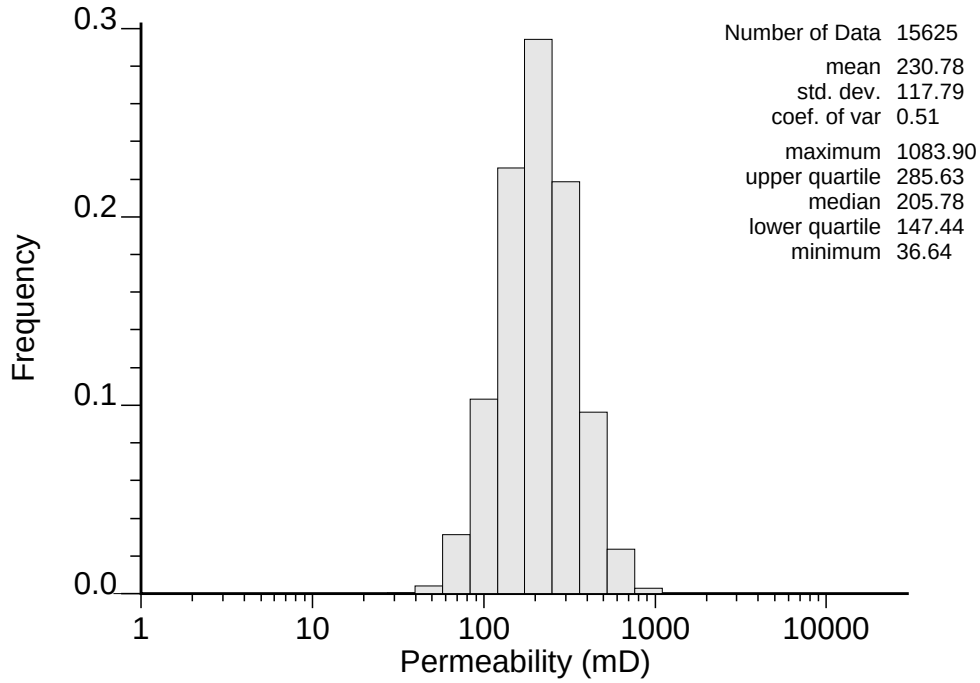

Figure 9.2: Permeability histogram of the "truth" fine-scale model (Figure 9.1). Note that the *x*-axis is logarithmic.

The coarse-scale model (Figure 9.3) was employed for multiple flow simulations for history-matching. The size of each coarse cell is 200m×200m×20m and the number of cells is 5×5×1. The producer and water injector wells were placed at the centres of the corner coarse cells, and the well positions in the coarse-scale model are exactly the same as those in the fine-scale model. The distance between the injector well and producer well is 1131 m. The boundary conditions were assumed to be the same in both scale models: the producer well was controlled by a bottom hole pressure (BHP) of 400 [bar], the injector well was controlled by a rate of 330.0 [m^3/day] (reservoir conditions) and BHP limit of 689.48 [bar], and the sides of the model were sealed.

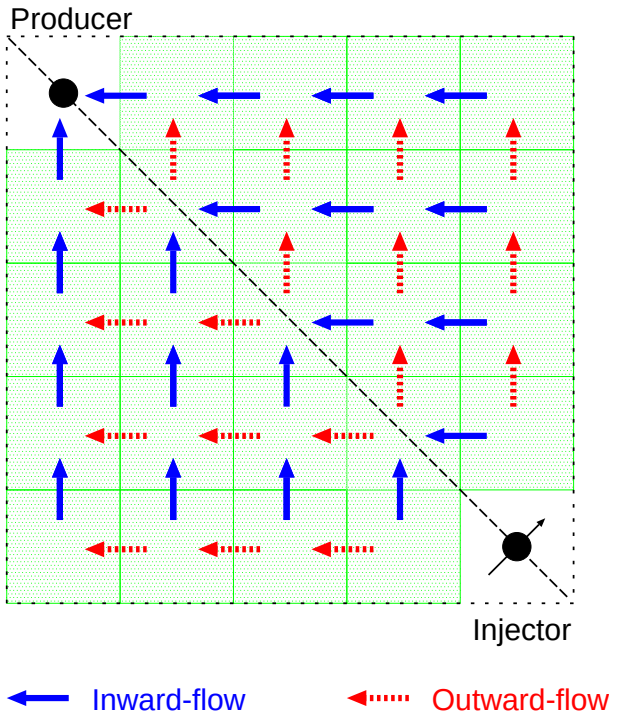

Figure 9.3: Coarse-scale model for history-matching. The 38 arrows in total represent flow for which the relative permeabilities are adjusted during the history-matching. The blue and red arrows denote “Inward flow” and “Outward flow”, respectively. The two types of the curves are assigned in each direction over the model apart from the well cells.

Apart from the permeability field, the description of the fine-scale and coarse-scale models in this chapter is the same as the description in Section 8.3. One of the fine-scale permeability fields generated in the previous chapter is used as the "truth" case in this chapter.

Here, the task is to estimate relative permeabilities at the coarse scale through history-matching rather than varying parameters at the fine scale. The correlation length of the truth model is less than half of a coarse-scale cell (200m). In other words, each coarse-scale cell contains sub-grid heterogeneity for which the range is smaller than a cell. In most models, a range of coarse-scale relative permeability curves is required to take account of fine-scale effects. The model was history-matched by adjusting two sets of relative permeability curves for the 38 inter-cell flows in the coarse-scale model, as shown in Figure 9.3. These are the flows between all the cells, apart from the flows from the injector to the adjacent cells, and are represented by the coloured region in Figure 9.3. The details for assigning the two sets of relative permeabilities are described later in this chapter. For simplification, although the truth model is unknown in real situations, it was used to fix all parameters other than relative permeabilities which determine the 38 flows. Details of the coarse-scale model are provided in the next paragraph.

As mentioned above, history-matching was conducted to estimate the coarse-scale relative permeabilities in the inter-well region, as shown in Figure 9.3. For setting up the problem, the injector near-well region, the injector well and the producer well were treated as special cases, as in Section 6.2. Their transmissibilities and relative permeabilities were upscaled separately from history-matching. The method adopted here is the same as that in Section 6.2 and is described in Ding (1995), Durlofsky et al. (2000) and Muggeridge et al. (2002). It calculated the coarse-scale well connection factor in the injector well and the producer well, and the transmissibilities from the injector cell and the adjacent cells. Then this method was extended to two-phase flow, to calculate the upscaled relative permeabilities for the well connections and the interfaces between the injector well and each adjacent cell (Appendix). In addition, the transmissibilities in the inter-well regions were calculated using global boundary conditions (Zhang, 2005).

For display purposes, the harmonic average of the adjacent coarse-scale permeabilities in the X (East-West) and Y (North-South) directions were calculated from the corresponding directional transmissibilities stated above: transmissibility multiplied by the distance between the cell centres, divided by the interface area between the cells and divided by Darcy's constant (0.008527 in metric units), (Schlumberger, 2004b). Note that these permeabilities were not used to run the coarse-scale simulations for history-matching, because the transmissibilities were assigned in the model. The spatial distribution and histogram of the directional permeabilities are shown in Figures 9.4 and 9.5, respectively. It can be confirmed that the permeability field at the coarse-scale is very homogeneous compared to that at the fine-scale (Figures 9.1 and 9.2).

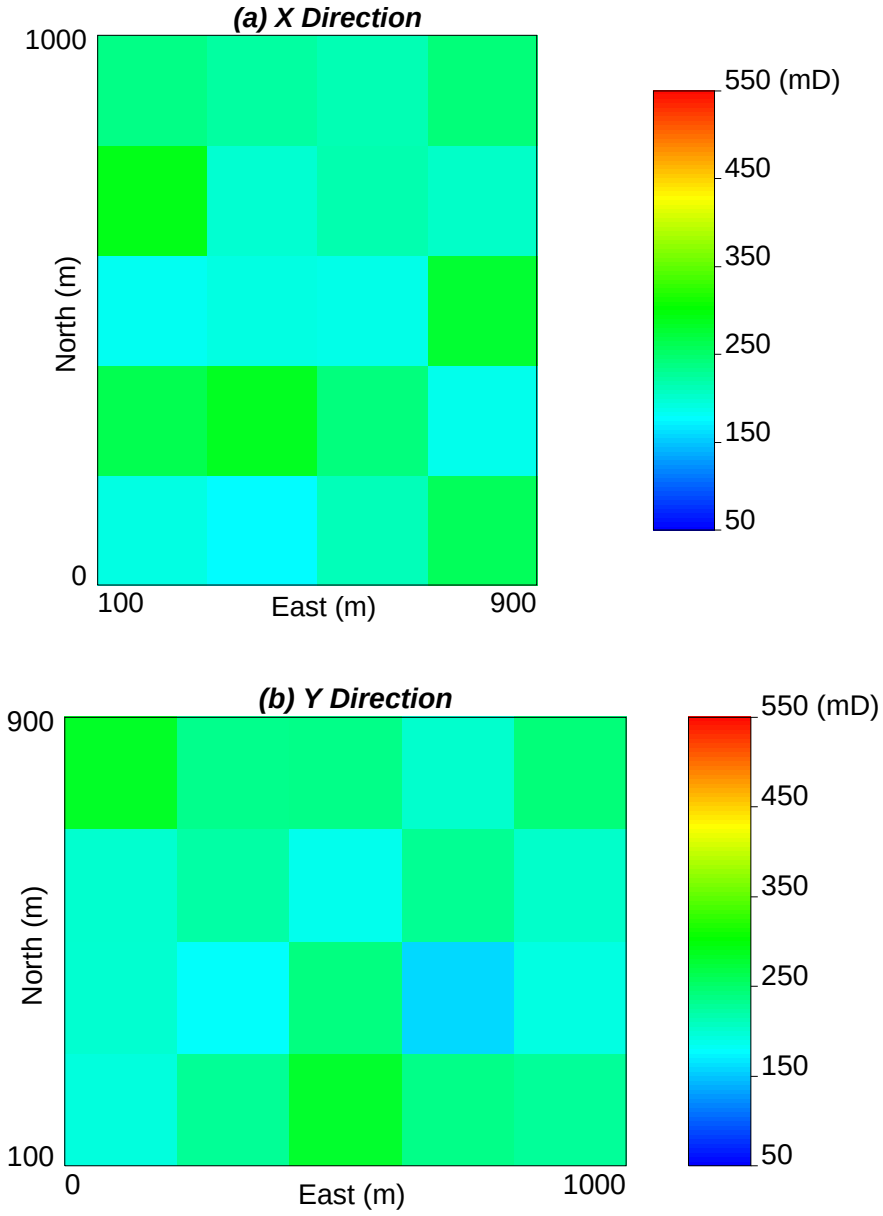

Figure 9.4: Permeability distribution at the coarse-scale: (a) X Direction (East-West), (b) Y Direction (North-South). The colour represents the harmonic average of the adjacent coarse-scale permeabilities which were calculated from the transmissibilities.

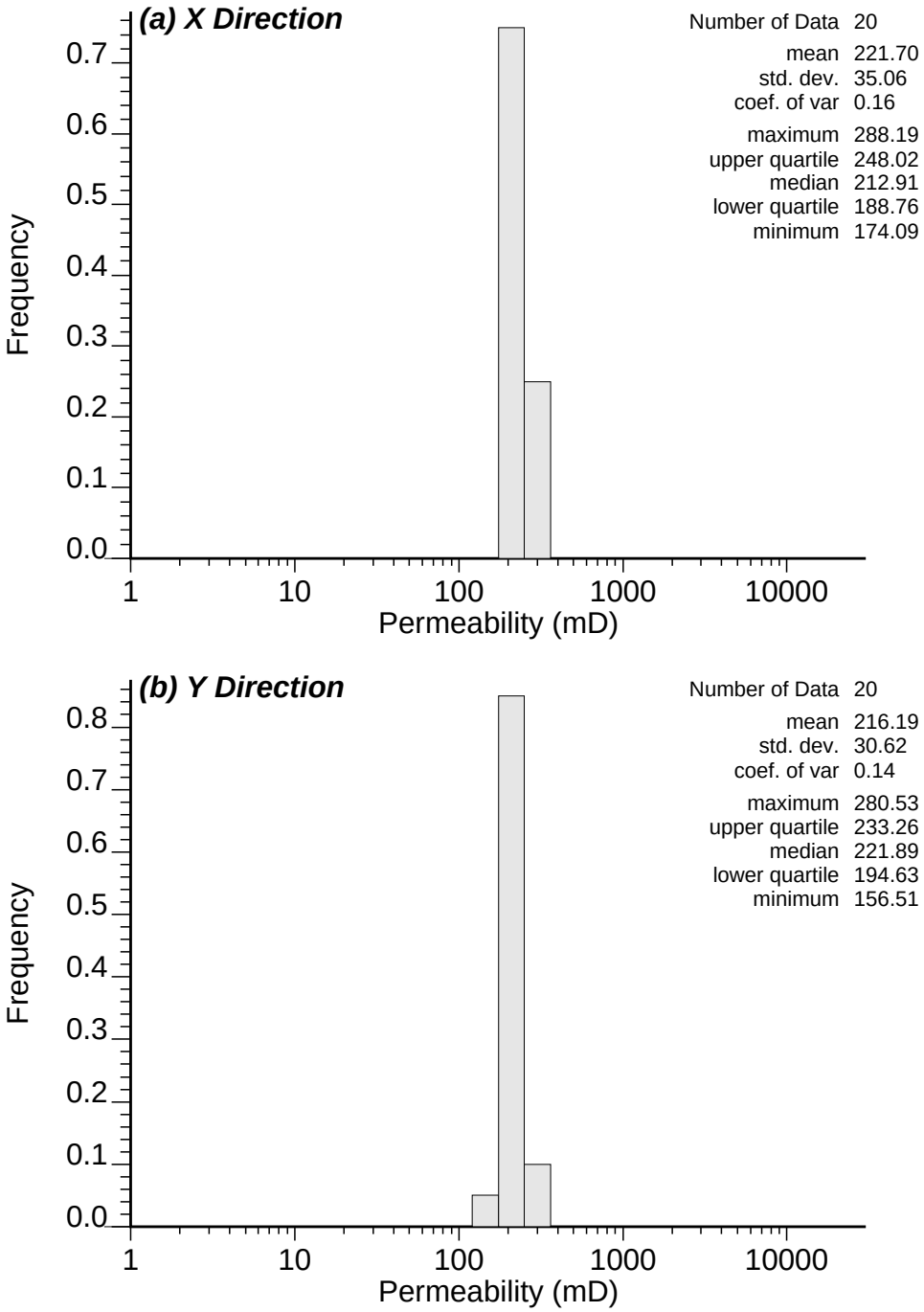

Figure 9.5: Permeability histogram at the coarse-scale: (a) X Direction (East-West), (b) Y Direction (North-South). Note that the x-axis is logarithmic.

It is necessary for this study to assess the estimated coarse-scale relative permeabilities after history-matching. For comparison, the sets of upscaled relative permeabilities for the 38 flows were calculated using two-phase dynamic upscaling. The two-phase upscaling scheme adopted here is the PVW method using an in-house software package of Heriot-Watt University as in Section 8.2. It uses transmissibilities which were calculated under global boundary conditions (i.e. the well controls and sealed boundaries, (Zhang, 2005)). During history-matching the 38 sets of upscaled relative permeabilities are replaced with the two sets of optimised relative permeability curves, and the results were compared. Figure 9.6 shows the production performance of the fine-scale model, the coarse-scale model with rock curves and the coarse-scale model with the upscaled relative permeabilities. The oil rate and injector bottom hole pressure (BHP) of the coarse-scale model with the upscaled relative permeabilities coincide with those of the fine-scale model, whereas the coarse-scale model with rock curves fails to reproduce the fine-scale profiles in some intervals.

The oil rate and injector BHP were used as production history and are referred to as history data. Uncorrelated random noise was added to the fine-scale simulation results using Equations (6.2.4) and (6.2.5). A set of random deviates was drawn from a normal distribution. The standard deviations of the data errors for the oil rate and injector BHP were $\sigma_q = 15.0\,[\mathrm{m}^3/\mathrm{day}]$ and $\sigma_p = 1.0\,[\mathrm{bar}]$, respectively. The fine-scale data is denoted as the truth in the sections below. Then using the data for 3300 days as history data, the task is to history-match the coarse-scale model to the observed data, by adjusting the relative permeability curves. The final step is to forecast the production performance to 12000 days and quantify the uncertainty in the forecast.

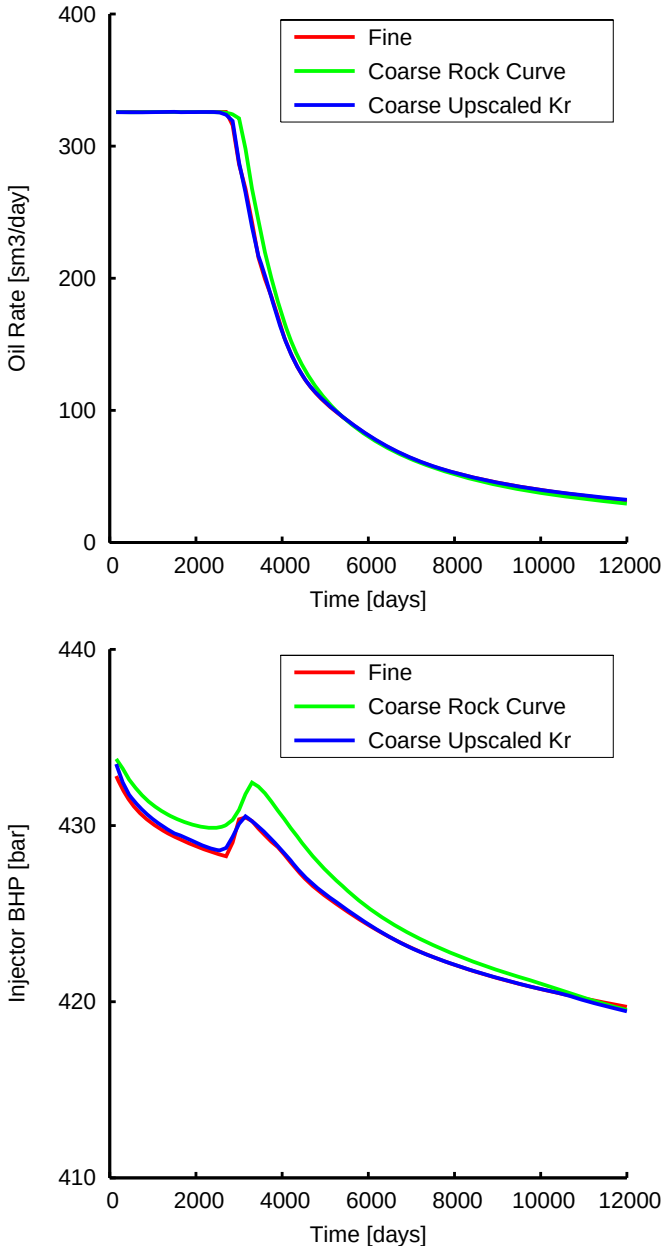

Figure 9.6: Simulated production profiles for the fine-scale model (the “truth” model) and the coarse-scale models with the rock curves and the upscaled curves. The top figure is oil production rate and the bottom figure is injector bottom hole pressure.

The likelihood function was defined by making the same assumptions as in Section 6.2. The misfit was calculated by Equation (6.2.7).

9.2.2 Description of Problem

Suppose that the following information on the sub-grid heterogeneity and viscosities in a reservoir was given.

- The distribution of the logarithmic permeability at the fine scale may be described as a correlated Gaussian field, and the mean is 5.3 corresponding to 200 [mD].
- Correlation length in NW-SE direction is greater than 0.0 [m] and smaller than 200.0 [m].
- Correlation length in NE-SW direction is greater than 0.0 [m] and smaller than 100.0 [m].
- Standard deviation is 0.50.
- Oil viscosity is 1.0 [cp] and water viscosity is 0.3 [cp].

Here, the task is to history-match the uncertain coarse-scale relative permeabilities. According to the investigation in Chapter 8, the shapes of relative permeabilities in the coarse-scale model are different in different locations and directions. There are 40 sets of curves corresponding to the inter-cell flows: 2 directions times 20 pairs of the adjacent cells. Note that the flows between a cell and a well were assumed to be known and the upscaled properties were assigned in advance of history-matching. In addition, the two sets of relative permeabilities for flows from the injector cell to the adjacent cells were also assumed to be known and the curves calculated using the “truth” model were assigned to the cell for the simplification. The flows correspond to Group 1 in the classification of Chapter 8. Hence, as shown in Figure 9.3, the remaining 38 flow functions are the properties to be calibrated in the history-matching. These correspond to Groups 2, 3 and 4 in the classification of Chapter 8.

In this chapter, Groups 2 and 3 were amalgamated, because they are similar and both can be categorised as “outward flow” altogether. However, Group 4 is distinguished from Groups 2 and 3 and can be categorised as “inward flow” in contrast to “outward flow”. Here, there are two groups of the curves to be history-matched. In other words, the “outward flow” which proceeds away from the NW-SE diagonal and the “inward flow” which proceeds toward the NW-SE diagonal were grouped separately. The reasons have been explained thoroughly in Section 8.4 and are summarised as follows. The advancing front of the “inward flow” enters from one side of the coarse cell and exits immediately to the adjacent perpendicular side. In this case, the average water saturation is so small that it may leave a large amount of oil in the coarse cell at breakthrough. By contrast, the advancing front of the “outward flow” may be nearly linear or an arc of a circle. The “outward flow” can have a larger average water saturation at the breakthrough than the “inward flow”. Therefore, in this chapter, the calibration parameters are these two sets of curves for the “inward” and “outward” flows, which are assigned to the inter-cell flows apart from the injector near-well flows.

In order to constrain the range of the calibration, the information on the upscaled relative permeabilities for a variety of models was utilised. Note that the models may have a range of correlation lengths. As described in Section 8.5, the minimum and maximum limits of relative permeabilities for each group were estimated using the upscaled relative permeabilities corresponding to the possible correlation lengths stated above. 25 combinations of the correlation lengths were chosen from the λ_1-λ_2 parameter space. In total, 150 models were generated with the 6 realisations per case. Here it was assumed that the ensemble of 6 realisations per case should be enough to extract the prior information. Figure 9.7 shows the limits for the two types of the upscaled relative permeabilities. These limits represent the uncertainty in the coarse-scale relative permeabilities due to sub-grid heterogeneity and can be used as the prior range in the history-matching.

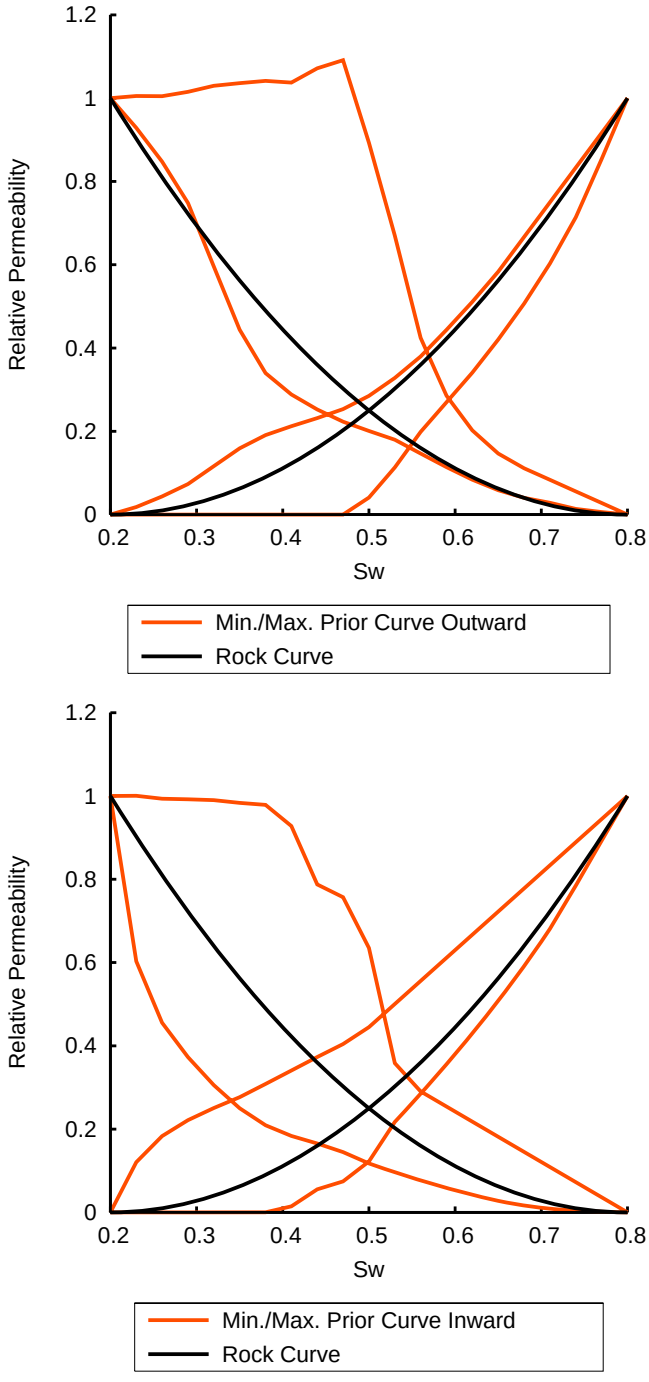

Figure 9.7: Min. and Max. of the upscaled relative permeabilities. The top figure is outward flow and the bottom figure is inward flow.

9.3 Parameterisation of Relative Permeabilities

9.3.1 B-spline Function for the Parameterisation

This chapter utilised the B-spline functions as in Section 6.3. The relative permeability was parameterised with the fourth order (cubic) B-spline function using Equation (6.3.1), and the B-spline basis functions are shown in Figure 6.6. There are 6 B-spline Basis functions (6-dimension), with non-uniformly spaced knots at water saturations of 0.20, 0.35, 0.50 and 0.80. This knot spacing is also the same as that used in Section 6.3.

9.3.2 Prior Probability

In this study, the prior information was based on both the rock curves and the scale-change effect, and then it was utilised in order to narrow down the parameter space of B-spline coefficients. This tends to not only reduce the computational cost for history-matching but also avoid unrealistic results. The prior information which had been obtained beforehand is the minimum and maximum curves of the coarse-scale relative permeabilities for two types (Figure 9.7). The approach used here has two steps to define the prior probability of the model.

First, the minimum and maximum values for each B-spline coefficient were determined as shown in Table 9.1. The two coefficients for Basis 1 (the left end) and Basis 6 (the right end) are set to be either 0 or 1 so that both ends of the relative permeability curve are fixed. The end point corresponds to either the connate water saturation or the irreducible oil saturation. Because it can be assumed that the upscaled relative permeability would have the same end-point values as those of the rock relative permeabilities, these end-point relative permeabilities were set to be either 0 or 1. It has been reported that the upscaled oil relative permeabilities can be greater than one, (Hewett et al., 1998). For example, the maximum curve in Figure 9.7 implies that the curves can rise up to 1.1. Based on this observation, the coefficients for bases 2 to 5 were set to range from 0 to 1.1, as shown in Table 9.1. Note that this merely ensures that the relative permeabilities are within the range of 0 to 1.1 apart from the vicinity of the fixed end points.

Then, the relative permeabilities were calibrated using 4 parameters for each phase and each type within these ranges in Table 9.1. That is to say, for the two types of relative permeability curves, there are 16 model parameters to be adjusted.

Table 9.1: Min. and Max. values for the B-spline coefficients

Basis No., j	c_j^o min.	c_j^o max.	c_j^w min.	c_j^w max.
1	1.0	1.0	0.0	0.0
2	0.0	1.1	0.0	1.1
3	0.0	1.1	0.0	1.1
4	0.0	1.1	0.0	1.1
5	0.0	1.1	0.0	1.1
6	0.0	0.0	1.0	1.0

Secondly, during the stochastic sampling for history-matching, if the model parameters result in the relative permeability straying outside the limits in Figure 9.7, nearly zero prior probability, namely huge misfit, is assigned to the model, instead of calculating misfit using Equation (6.2.7). This approach was implemented, because it had been confirmed that the constraints of Table 9.1 were not sufficient to obtain meaningful curves through history-matching (Subsection 9.4.1). Presumably, the interrelation of a large number of parameters led to unrealistic combinations, even if they had low misfits. Here, for the implementation of this step, when at least one point of curves was away from the band of Figure 9.7, a huge misfit value which is larger than 10^{10} was assigned. Also in order to improve the efficiency of the sampling, the sum of the deviations between the off-range curve and the band was incorporated into the huge misfit: $(1 + \mathit{Deviation}) \times 10^{10}$. The preliminary test for this problem revealed that the stochastic sampling could not converge to the curves inside the limits without the information on the deviations. To summarise, only if all parts of the curves are within the bands of Figure 9.7, a flow simulation is conducted to calculate the likelihood term of the model. Note that for the additional sampling of the modified NA-Bayes algorithm which was employed in this study, the huge misfit was used as a flag, in addition to the condition of the Gibbs sampler, so that it cannot sample the unlikely models for uncertainty quantification. This is because the models were assumed to have zero posterior probability based on the prior ranges of the curves.

This second step for history-matching is required rather than setting a 1D marginal prior probability distribution along each axis of 16 parameters. Since the order of the spline is 4 in this case, each curve at a certain point consists of 4 components, namely the product of a non-zero coefficient and a basis function at a certain point. Hence, a unique set of B-spline coefficients per curve cannot be determined from one particular point on the curve. Therefore, in order to determine the prior probability based on the values of relative permeability, it should be expressed as the joint probability of the interrelated model parameters instead of 1D marginal prior probability distributions.

In this representation, parameters 1 to 4 denote c_2^o to c_5^o for the oil phase of the outward flow. Parameters 5 to 8 denote c_2^w to c_5^w for the water phase of the outward flow. In the same manner,

parameters 9 to 12 denote c_2^o to c_5^o for the oil phase of the inward flow. Parameters 13 to 16 denote c_2^w to c_5^w for the water phase of the inward flow.

9.4 Results of Estimating Relative Permeabilities and Production Performance

History-matching multiple models and quantifying uncertainty require a huge number of realisations, especially when the number of unknown parameters is large. The NA-algorithm was used to generate 288096 models, 96 (models) $\times$ 3001 (iterations), by sampling a 16-dimensional parameter space. This large number of iterations was sufficient to reach the convergence in this case. As mentioned previously, the likelihood term was calculated through flow simulation, only if a model resulted in acceptable relative permeabilities which fell inside the limits shown in Figure 9.7. The number of the acceptable models in terms of the prior relative permeability limits was 128404 which was less than half of the total number. The characteristics of NA-sampling, in terms of exploration and exploitation, are largely controlled by the two tuning parameters n_s and n_r, (Sambridge, 1999a). The values of n_s and n_r used in this paper were 96 and 48 respectively, because it aimed at exploratory sampling within the limitation of computational cost. The sample size of the initial iteration was the same as n_s in this case. The performance of the NA algorithm for convergence was confirmed by increasing the number of iterations and the other tuning parameters. For example, even if both n_s and n_r were doubled, the resultant relative permeabilities were similar to the original case.

The observed data was used up to 3300 days, corresponding to 25.7% of water cut, for history-matching, and the forecast uncertainty was quantified up to 12000 days. The convergence to a good fit was confirmed in the history-matching. Figure 9.8 indicates that the misfit was reduced from the huge values (for the curves outside the prior ranges) to the lower values, the lowest misfit being 21.11. The lowest misfit divided by the number of the observed data and multiplied by 2 gives 0.96, since the number of the history data is 44 which means 22 for each of

the oil production rate and injector BHP. It reached the convergence criteria 1.0 as in Section 6.4.

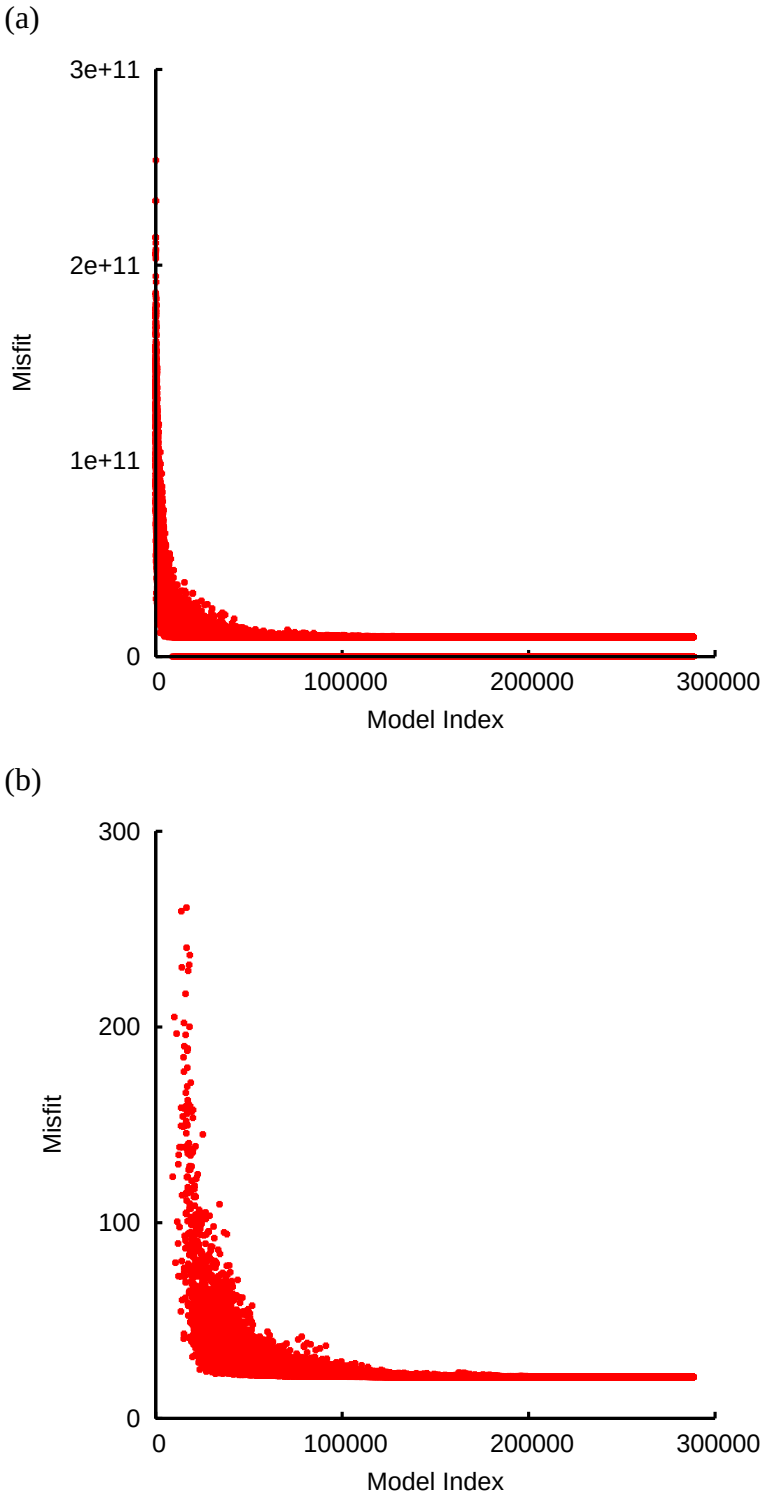

Figure 9.8: Misfit values during history-matching. (a) The *y*-axis covers the huge misfit values, where the coarse-scale curves fall outside the prior ranges. (b) The *y*-axis covers only the range of the misfit calculated by Equation (6.2.7), where the coarse-scale curves fall inside the prior ranges.

Figure 9.9 represents the optimised relative permeabilities for the outward and the inward flows. It indicates that the optimised relative permeability curves are close to the upscaled relative permeabilities. In this case, the parameterisation scheme of the B-spline and the two flow categories of the outward and inward flows worked appropriately so that the bunch of upscaled relative permeabilities could be grouped into two set of curves. Figure 9.11 illustrates the history-matching results for the oil rate and the injector BHP. The simulated oil rate and injector BHP seem to fit the observed data and surround the truth profile, although the pressure is slightly deviated from the truth profile in the magnified scale in Figure 9.12 because of the noise in the observed data. Note that these observations should be confirmed by other cases with the different realisations of random noise added to the observed data.

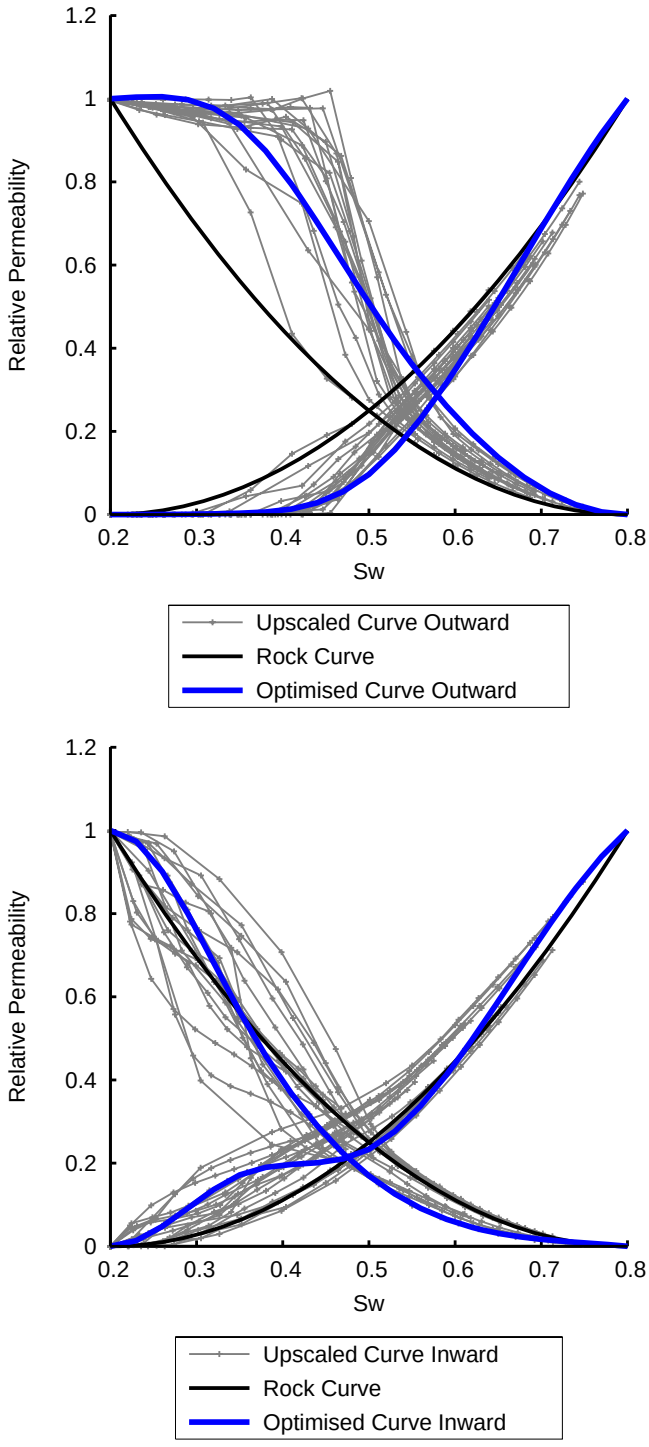

Figure 9.9: Optimised relative permeabilities. The top figure is outward flow and the bottom figure is inward flow.

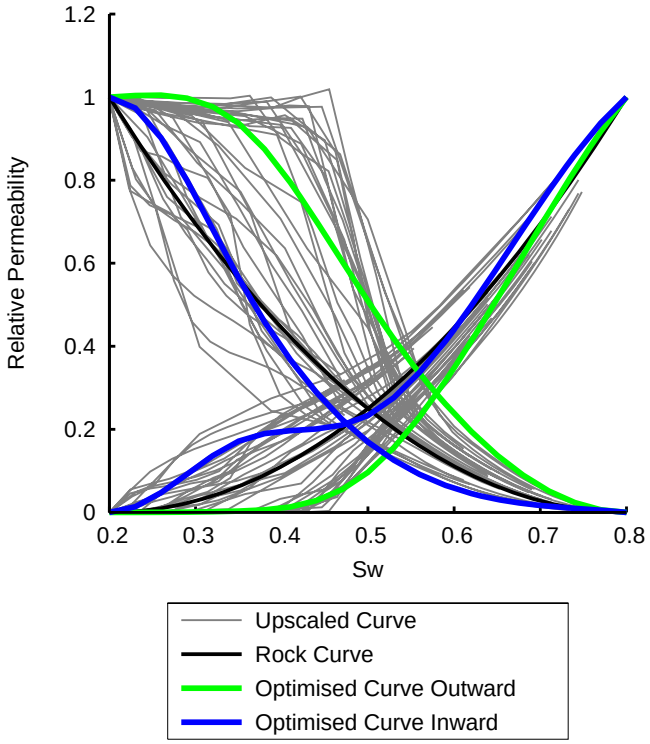

Figure 9.10: Optimised relative permeabilities. The two set of the curves (Outward flow and Inward flow) were plotted together for comparison.

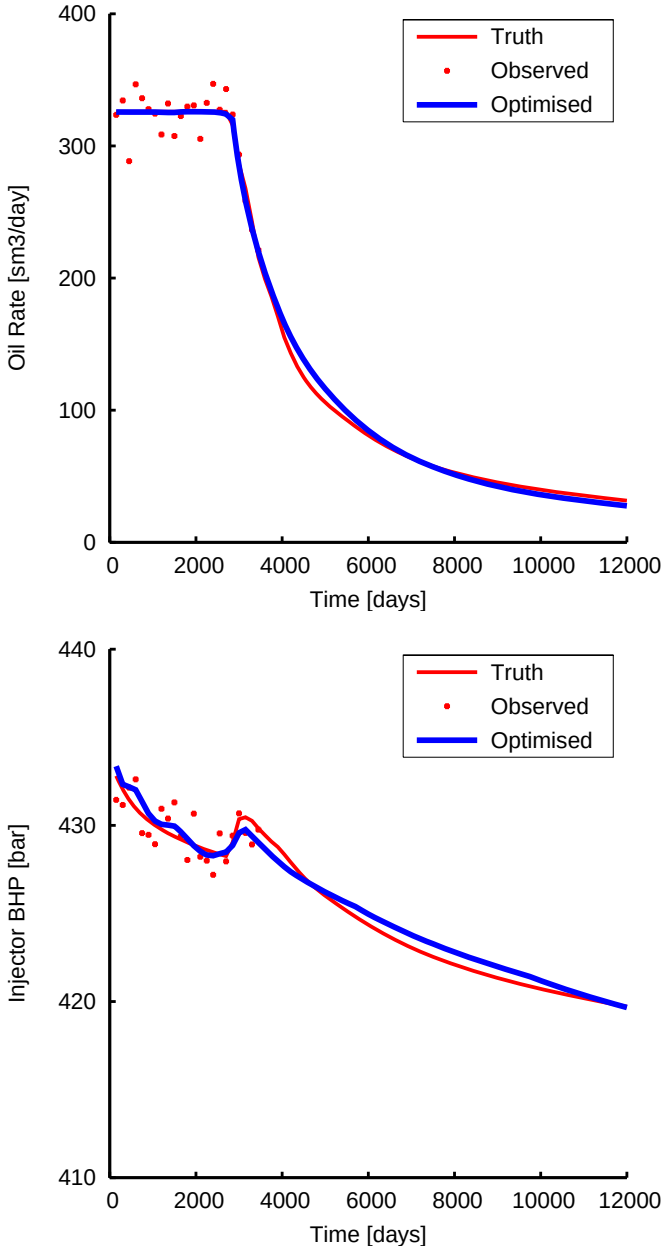

Figure 9.11: Production profiles calculated using the optimised relative permeabilities. The top figure is oil production rate and the bottom figure is injector bottom hole pressure.

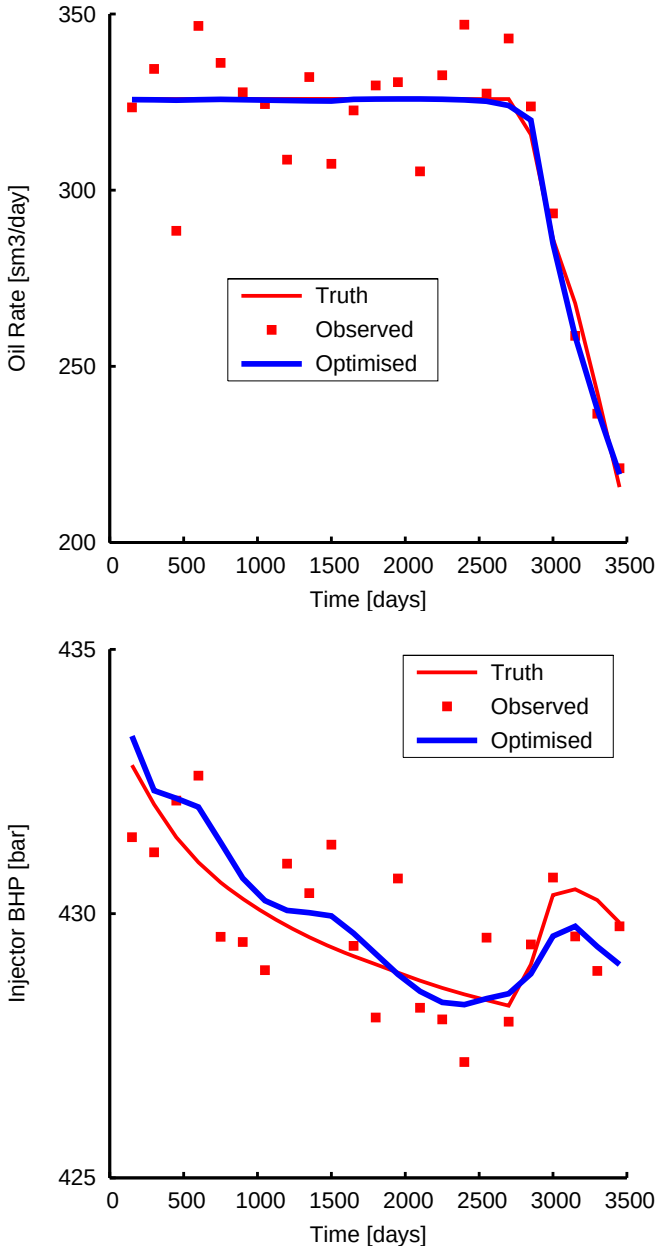

Figure 9.12: Production profiles calculated using the optimised relative permeabilities. Only the history period is shown. The top figure is oil production rate and the bottom figure is injector bottom hole pressure.

As demonstrated in Section 6.4, the next task is to sample the resulting ensemble using MCMC with the Neighbourhood Approximation. This step of MCMC is referred to as sampling from posterior probability distribution (PPD). Here, because of the Neighbourhood Approximation, the products of likelihood and prior distribution, prob(**o**|**m**) $\times$ prob(**m**), of the second ensemble have already been evaluated in the first step. To quantify the uncertainty in the predictions, a long chain of the MCMC was ran on the misfit surface, and 100000 models in total were collected. It was confirmed that this number reached convergence by increasing the number further. Then, the frequency of visits to each Voronoi cell was monitored during the random walk. Thus it calculated the relative probability of each model in the ensemble. Since the MCMC algorithm samples from the PPD through the product of the likelihood and the prior distribution, the calculated probability is representative of the posterior probability of each model. The probability of each model determined not only the expectation, but also P10 and P90 cut-offs for each of the estimated relative permeabilities and production profiles.

Figure 9.13 plots the 1-dimensional marginal distribution for each of the parameters. As shown in Figure 9.13, the marginal distributions of some parameters, e.g. Parameters 1, 3, 7, 8, 9, 10, 11, 15 and 16, have wide shapes rather than the narrow skewed shapes seen in the other parameters. The wide PPD means that the parameters may not be fixed through history-matching because of the insufficient information or noisy observed data. Also, the features of the wide PPD caused a wide uncertainty envelope in the relative permeability curves (Figure 9.14) and in the production profiles during the prediction period (Figure 9.15). The spread in oil rate, between the P10 and P90 values, is relatively small. However, in a real reservoir, this could represent a significant difference in cumulative oil production, and shows the importance of taking uncertainty into account when planning the development of a field.

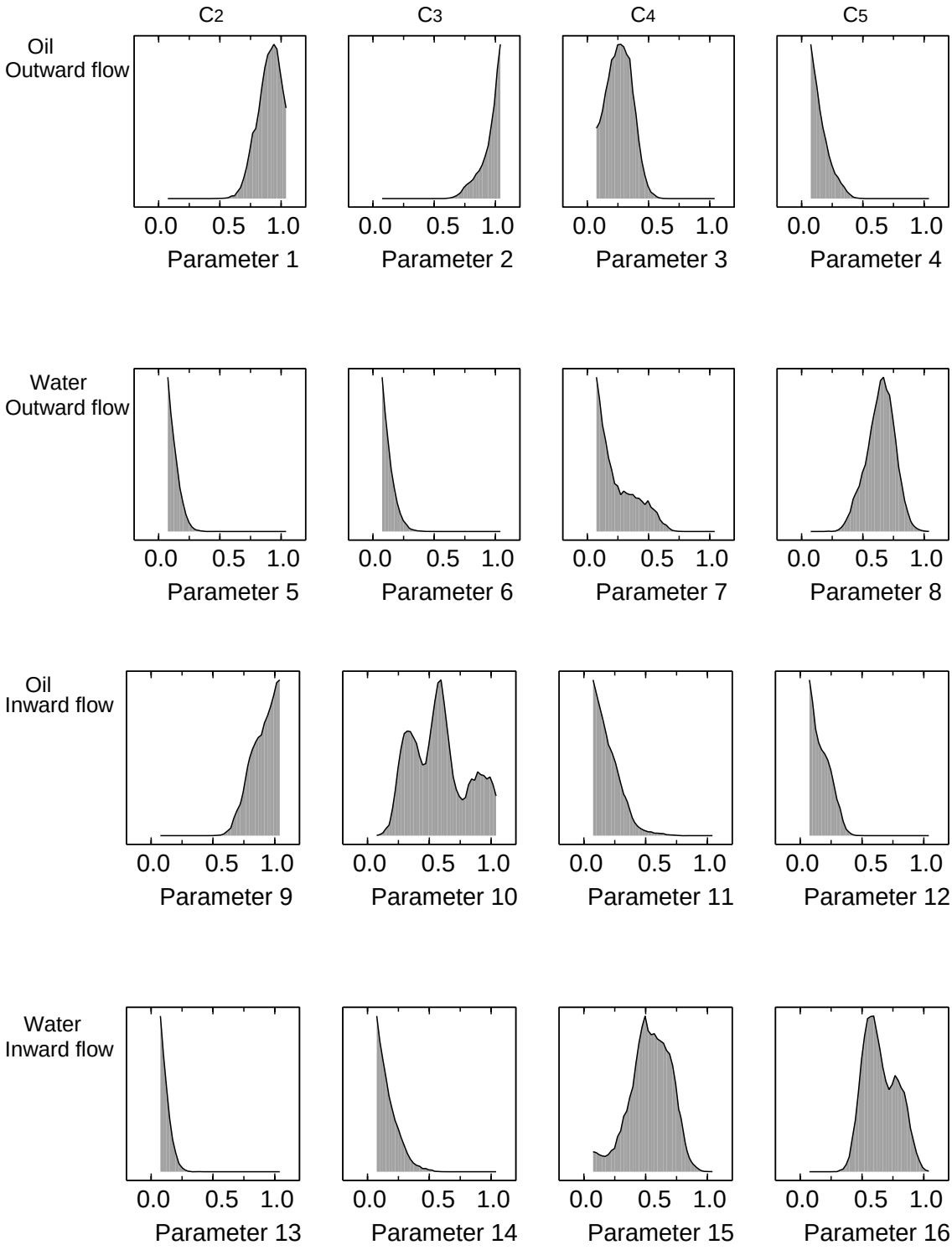

Figure 9.13: 1D marginal distribution for 100000 samples in the Markov chains. Note that each curve is scaled to its maximum height not the same area. The vertical axis ranges from 0 to each maximum with a linear scale. Each maximum height is provided in Table 9.2.

Table 9.2: Max. of each curve in Figure 9.13

	c_2	c_3	c_4	c_5
Oil, Outward flow	0.10	0.22	0.08	0.20
Water, Outward flow	0.29	0.29	0.13	0.09
Oil, Inward flow	0.11	0.06	0.13	0.17
Water, Inward flow	0.33	0.18	0.06	0.08

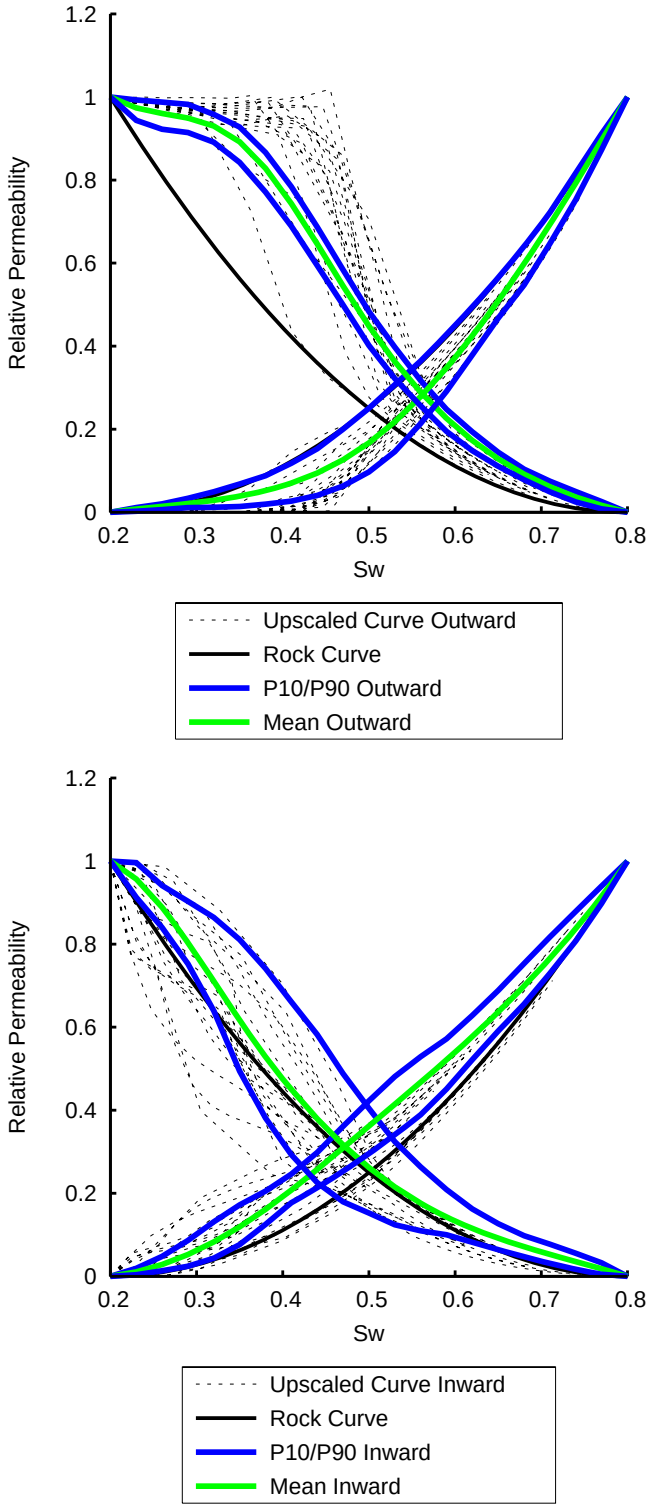

Figure 9.14: Relative permeabilities with uncertainty envelopes. The top figure is outward flow and the bottom figure is inward flow.

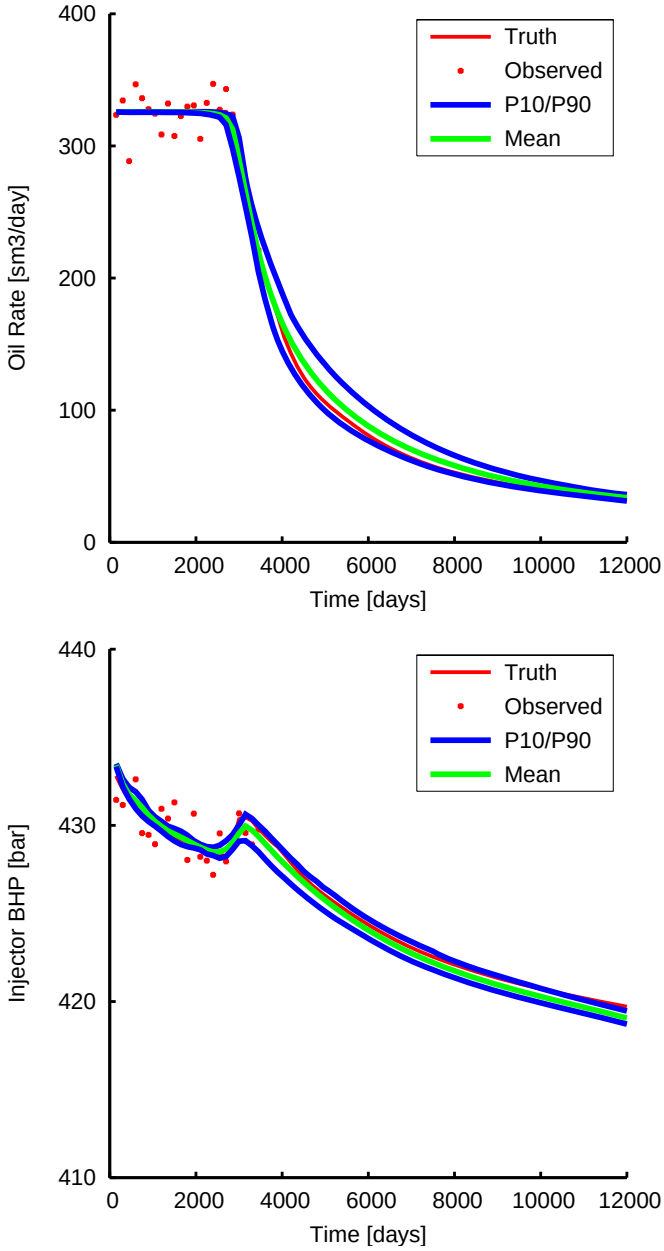

Figure 9.15: Production profiles with uncertainty envelopes. The top figure is oil production rate and the bottom figure is injector bottom hole pressure.

9.4.1 Results Without Prior Curves

As mentioned in Section 9.3, the constraints of Table 9.1 were not sufficient and the prior ranges of the curves in Figure 9.7 were required for history-matching. This subsection describes the corresponding results when the prior ranges of the curves were not included in the history-matching. The other settings are the same as above. Figure 9.16 shows the misfit values during history-matching, and the convergence was confirmed qualitatively by increasing the number of iterations of the NA-sampler. Figures 9.17 and 9.18 show the history-matched relative permeabilities. The resultant curves are not close to the reference upscaled curves. The estimated curves do not appear to be physically meaningful, because the oil production forecast was largely deviated from the truth profile as shown in Figure 9.19. Those results support the idea that the incorporation of the prior ranges is essential in this case. In addition, for the uncertainty appraisal, Figures 9.20 to 9.22 correspond to the results of Figures 9.13 to 9.15 and indicate that the width of uncertainty in each figure is much larger than the above case. This is because the prior limits used in the above case reduced the parameter space.

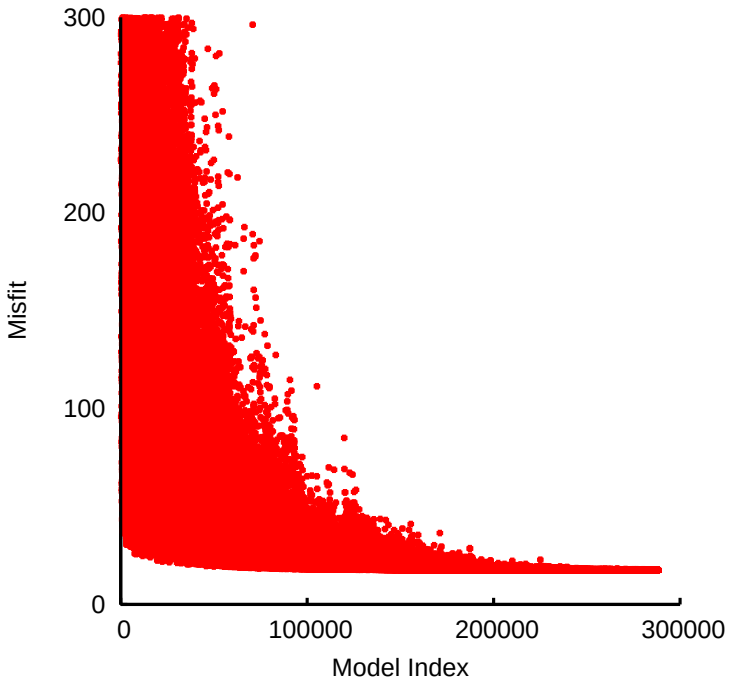

Figure 9.16: Misfit values during history-matching. The prior limits of the curves were not used.

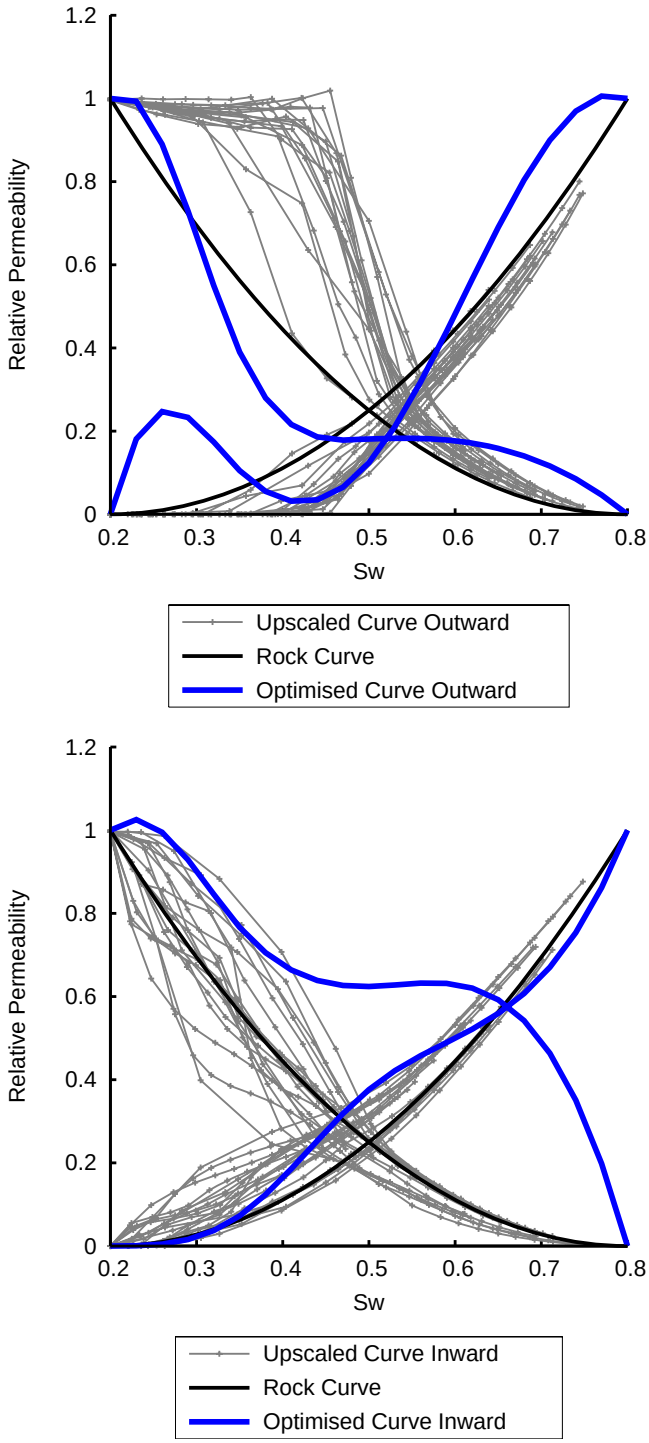

Figure 9.17: Optimised relative permeabilities (without the prior limits of the curves). The top figure is outward flow and the bottom figure is inward flow.

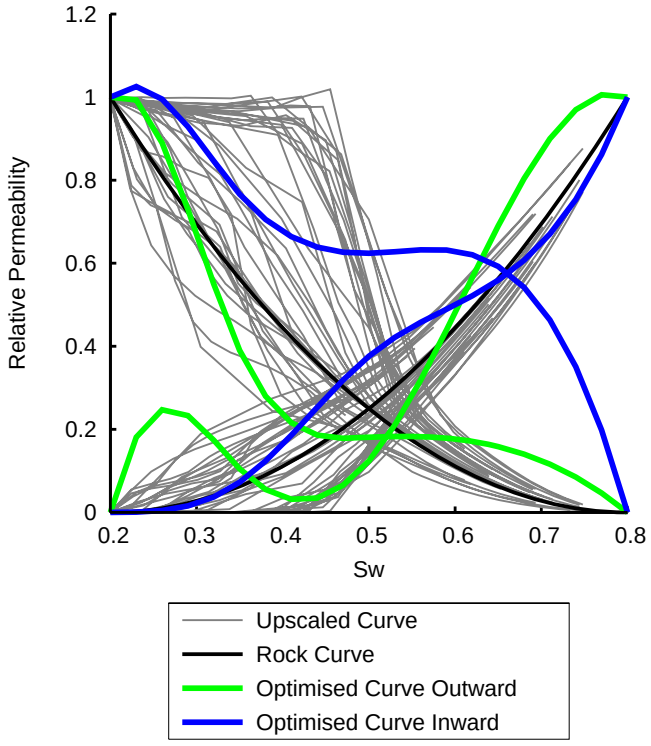

Figure 9.18: Optimised relative permeabilities (without the prior limits of the curves). The two set of the curves (Outward flow and Inward flow) were plotted together for comparison.

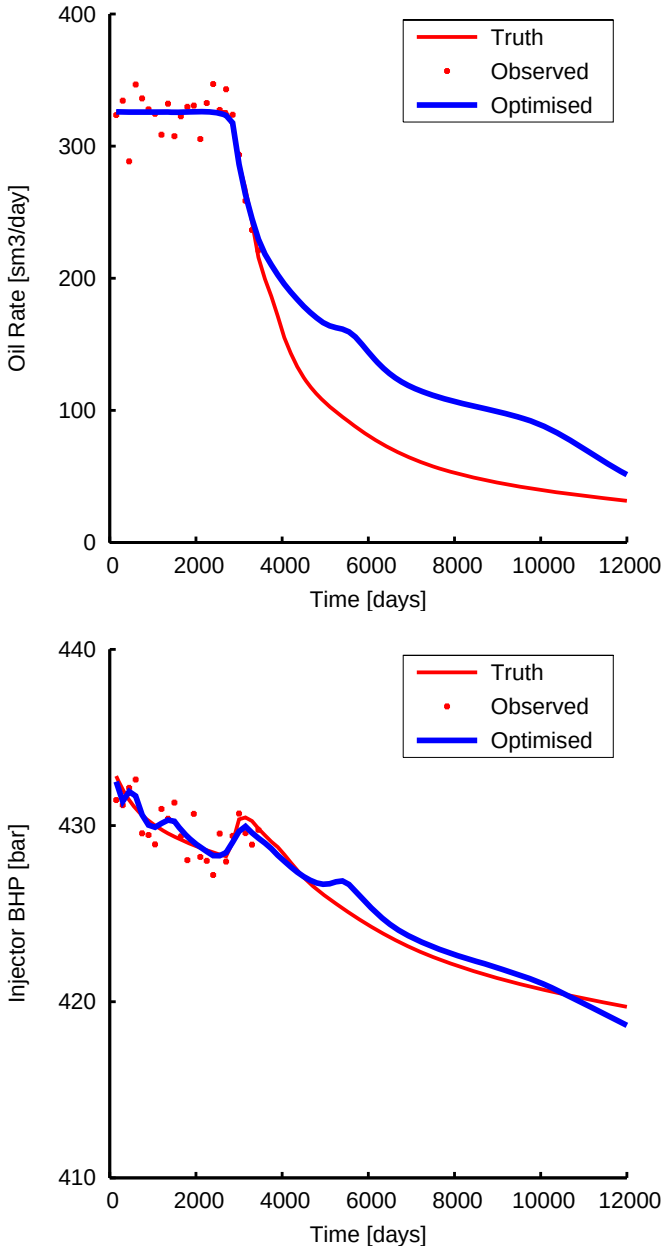

Figure 9.19: Production profiles calculated using the optimised relative permeabilities (without the prior limits of the curves). The top figure is oil production rate and the bottom figure is injector bottom hole pressure.

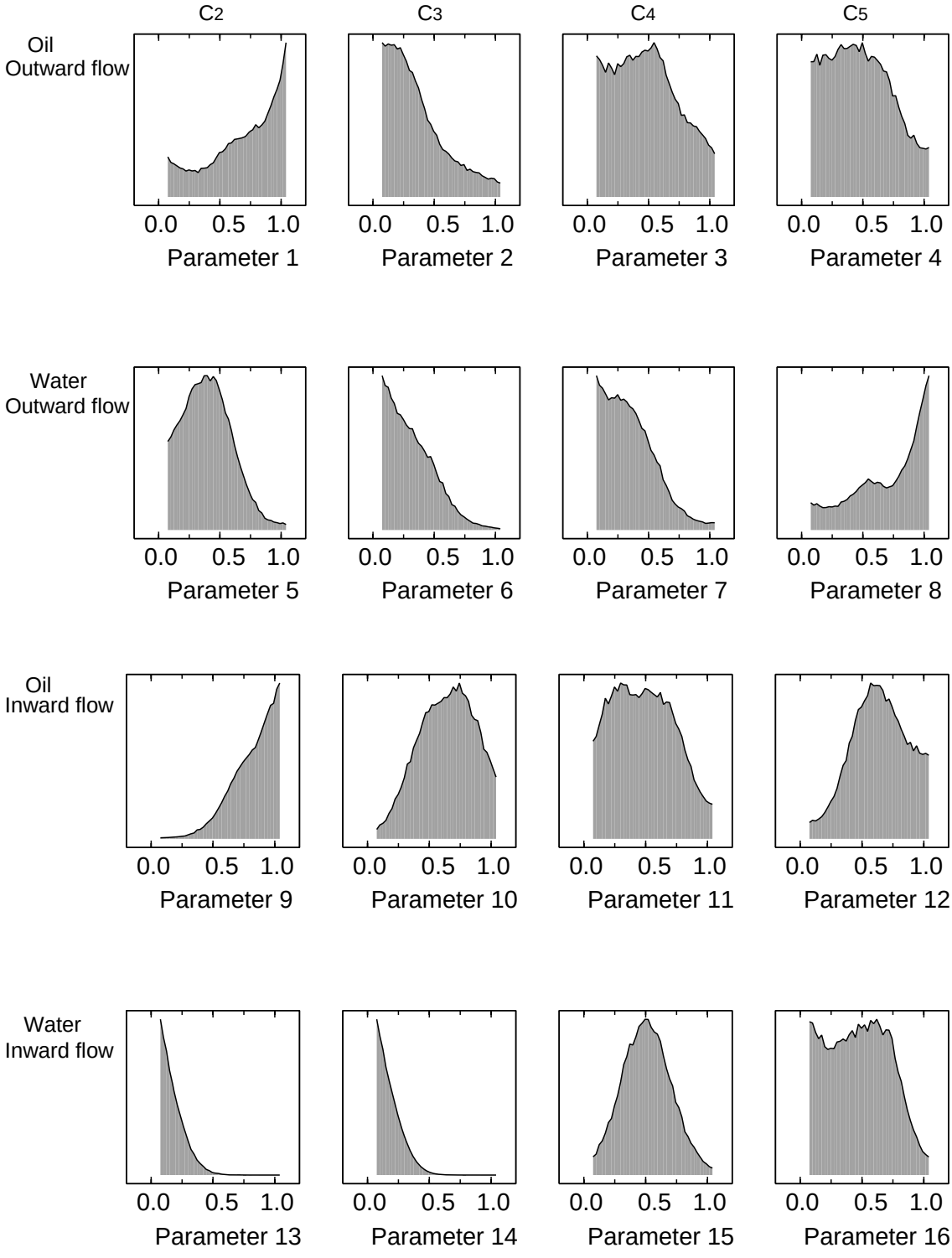

Figure 9.20: 1D marginal distribution for 100000 samples in the Markov chains (without the prior limits of the curves). Note that each curve is scaled to its maximum height not the same area. The vertical axis ranges from 0 to each maximum with a linear scale. Each maximum height is provided in Table 9.3.

Table 9.3: Max. of each curve in Figure 9.20

	c_2	c_3	c_4	c_5
Oil, Outward flow	0.07	0.05	0.03	0.03
Water, Outward flow	0.05	0.07	0.05	0.07
Oil, Inward flow	0.08	0.04	0.03	0.04
Water, Inward flow	0.16	0.15	0.05	0.03

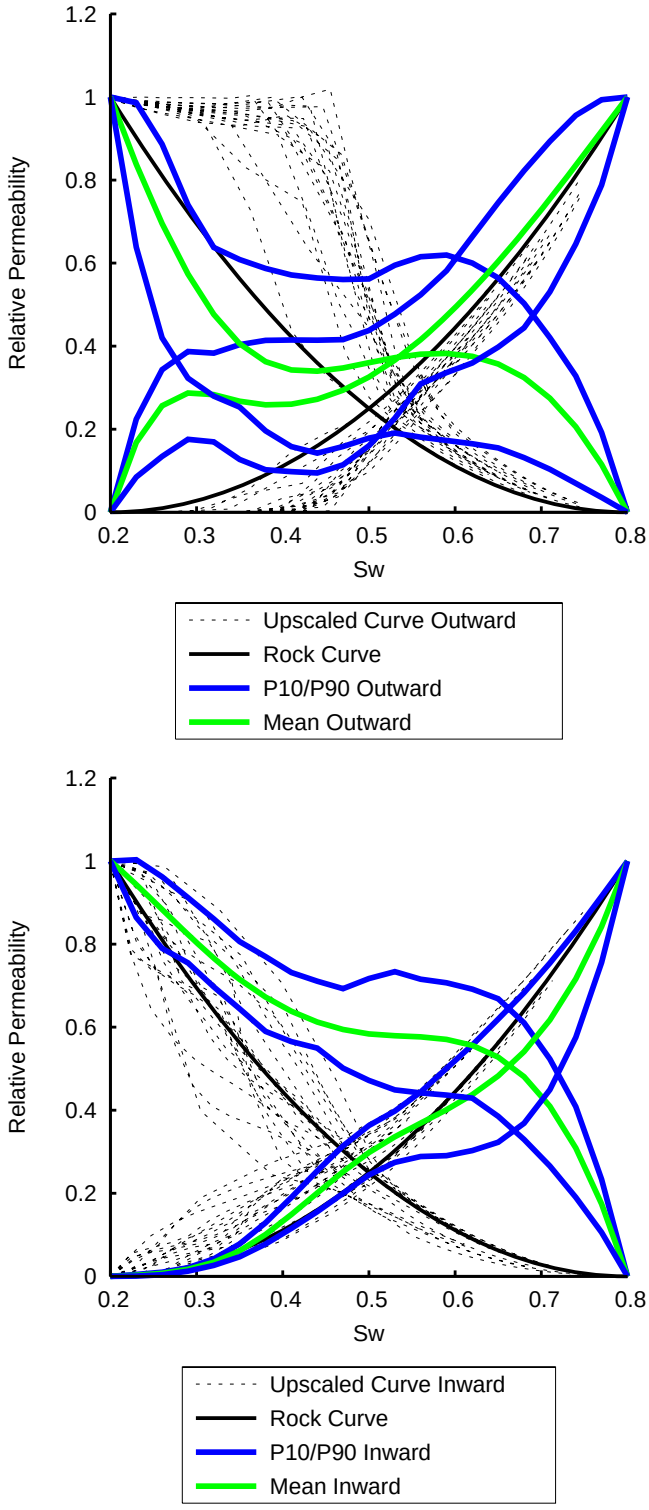

Figure 9.21: Relative permeabilities with uncertainty envelopes (without the prior limits of the curves). The top figure is outward flow and the bottom figure is inward flow.

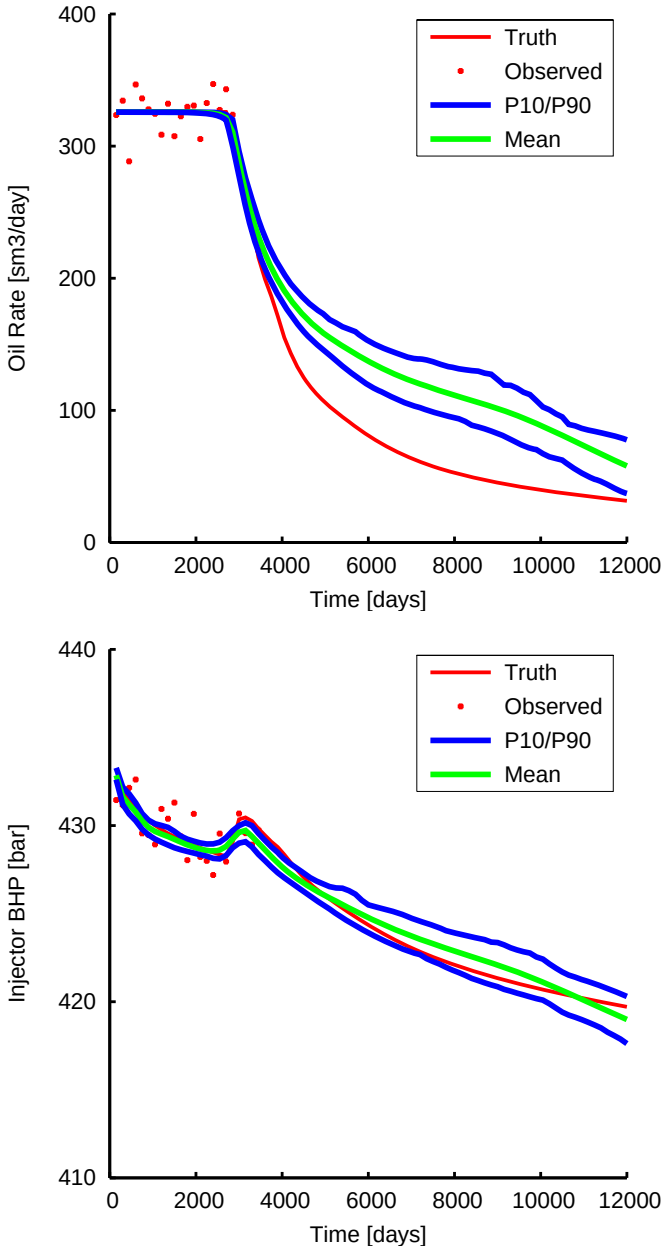

Figure 9.22: Production profiles with uncertainty envelopes (without the prior limits of the curves). The top figure is oil production rate and the bottom figure is injector bottom hole pressure.

In terms of the computational cost, when the constraints of the prior curves were incorporated, it took 83 minutes to conduct the history-matching using 48 CPU (24 nodes $\times$ 2 CPU) of a cluster machine owned by Heriot-Watt University. On the other hand, when the constraints of the prior curves were not incorporated, it took 110 minutes using the same number of CPU of the same machine. The computational time using single CPU is estimated by multiplying the time spent by the number of CPU used as follows. The cases with and without the prior ranges may take about 4000 minutes and 5300 minutes, respectively. The difference between the two cases is 1300 minutes. When the prior curves were estimated, a number of fine-scale flow simulations were conducted as explained in Section 9.2. It takes about 2 minutes to run a fine-scale flow simulation on the same machine, and the estimated computational cost for 150 models generated in this study is 300 minutes. Subtracting the computational time for estimating the priors, an estimate of the computational cost saved is 1000 minutes. Hence saving the computational cost as well as avoiding the unlikely curves is the benefit of the incorporation of the prior curves. Note that the coarse-scale model used in this study is small and it took only about 1 second to run a model. As the number of cells in the coarse-scale model increases, the difference between history-matching computational cost with the prior ranges and that without the prior ranges becomes larger. Also the use of local upscaling methods with appropriate boundary conditions can decrease the time spent estimating the priors of coarse-scale relative permeabilities. These aspects may highlight the reduction of the computational cost in a real situation. In addition, for higher dimensional problems, it will take a prohibitive amount of time to sample the physically meaningful curves, when one conducts history-matching and uncertainty appraisal without the constraints of the prior curves.

9.4.2 Production Profiles with Min. and Max. of Prior Curves

This subsection describes the oil production rate and injector BHP (Figure 9.23), when the minimum and maximum curves of the prior relative permeabilities in Figure 9.7 were used in the flow simulations. All the combinations of the minimum and maximum curves were tested and the cases were described in Table 9.4. According to Figure 9.23, the large variability in both

oil rate and pressure profiles indicates that the history-matching procedure is necessary for conditioning the model to the production history. Also it highlights the noble performance of the history-matching results shown in Figure 9.11.

Table 9.4: Combinations of the prior Min. and Max. curves used in Figure 9.19. Each of the curves (K_{ro}max, K_{ro}min, K_{rw}max and K_{rw}min) is shown in Figure 9.7.

	Oil	Water
Case 1	K_{ro}max	K_{rw}max
Case 2	K_{ro}min	K_{rw}min
Case 3	K_{ro}max	K_{rw}min
Case 4	K_{ro}min	K_{rw}max

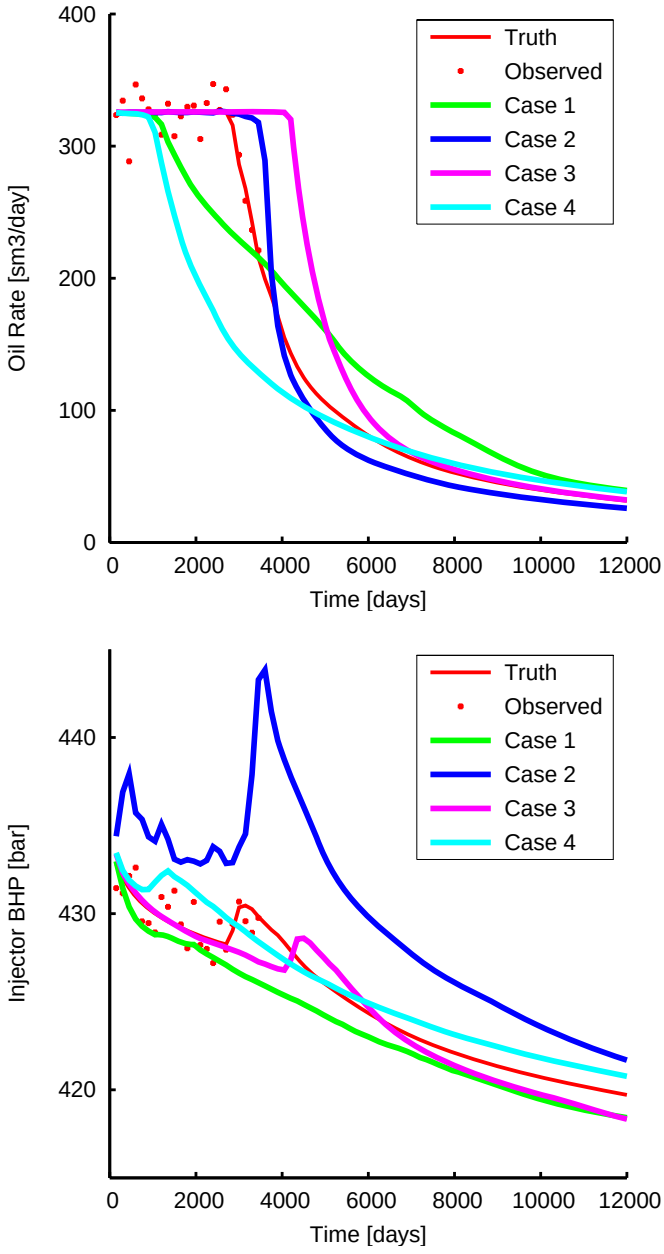

Figure 9.23: Production profiles calculated using the prior Min. and Max. curves. The Min. and Max. of the upscaled relative permeability curves are shown in Figure 9.7. The combination of the Min. and Max. curves for each of Cases 1-4 are provided in Table 9.4.

9.5 Adjustment of Absolute Permeability and Relative Permeability

This section presents additional results concerning the adjustment of absolute permeability. Note that only the average absolute permeability was adjusted at the coarse-scale instead of the permeability distribution at the fine scale. The aim is to investigate the result of Section 9.4 from the different point of view in conjunction with absolute permeability. Firstly, only the absolute permeability was adjusted during history-matching. Secondly, both the absolute permeability and the relative permeability were adjusted.

9.5.1 Absolute Permeability

For the adjustment of absolute permeability, logarithmic permeability was sampled using the NA algorithm and was transformed into the permeability value to be the input data of flow simulation. The prior range of logarithmic permeability was set to be 4.3 - 6.3. It was the width of "±2 Standard Deviation" around the mean value of 5.3. The mean and standard deviation had been assumed for the fine-scale permeability field in Section 9.2. For relative permeabilities, the curves of the 38 flows described above were replaced with the rock curve. For the other flows apart from the 38 flows, the single and two-phase flow properties remained the same as those in Section 9.2. In summary, only one parameter of logarithmic permeability was adjustable between 4.3 and 6.3 to calibrate the model. Therefore only the mean is changed.

After the history-matching, the optimised value was 5.5009 which corresponds to 244.92 mD. The history-matched results of the oil production rate and the injector BHP are shown in Figure 9.24. The posterior probability distribution of the logarithmic permeability is shown in Figure 9.25, and the results of the forecast uncertainty are shown in Figure 9.26. The oil production rate corresponding to the water breakthrough was not matched, and the simulated BHP also deviated from the observed data around the breakthrough timing (Figure 9.24). The uncertainly envelope of the oil production rate is invisible, and that of the BHP is fairly narrow

(Figure 9.26).

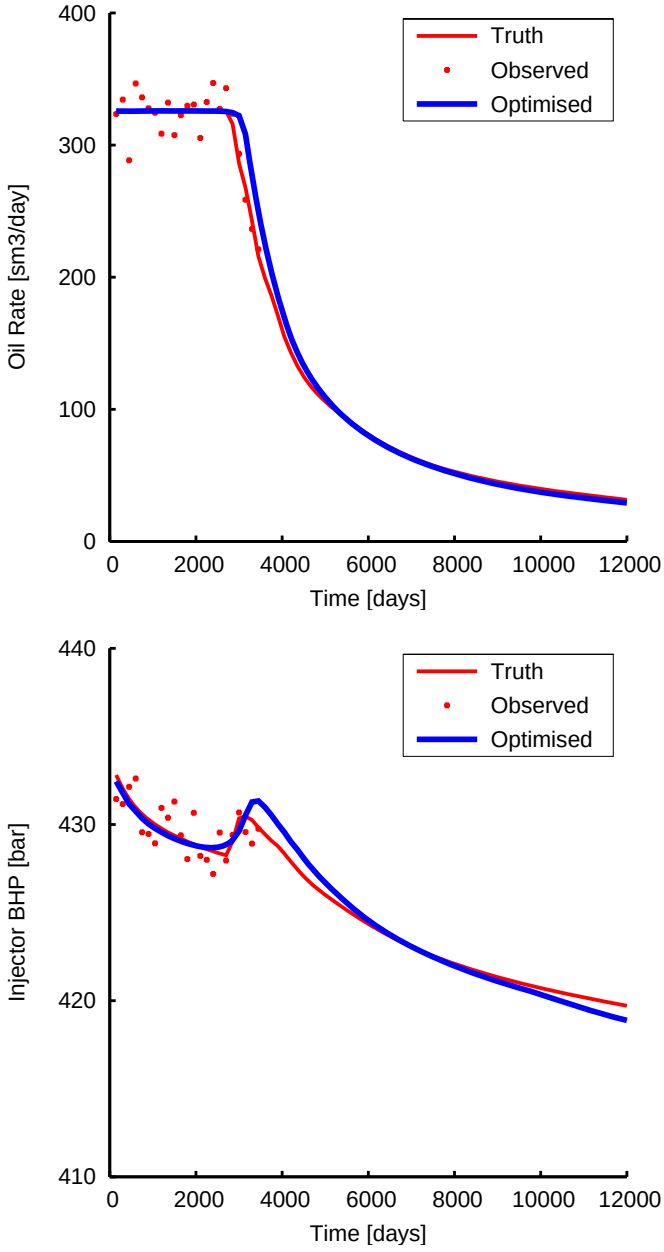

Figure 9.24: Production profiles calculated using optimised relative permeabilities. Absolute permeability was adjusted in history-matching. The top figure is oil production rate and the bottom figure is injector bottom hole pressure.

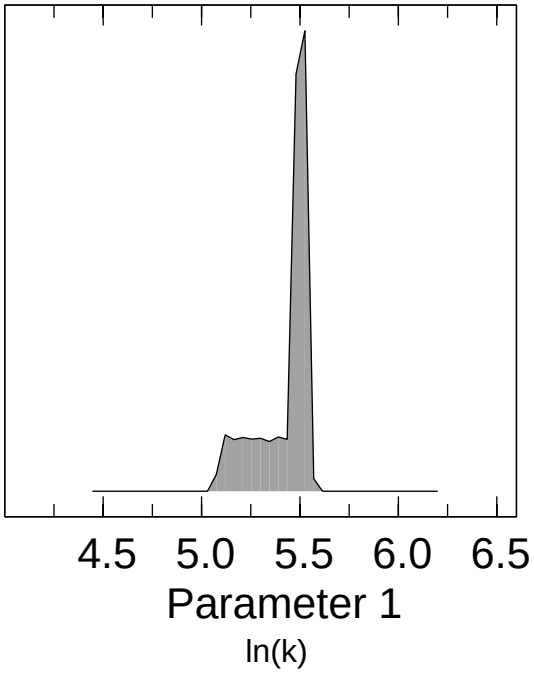

Figure 9.25: Posterior probability distribution for 100000 samples in the Markov chains. Absolute permeability was adjusted in history-matching. Note that the curve is scaled to its maximum height not the same area. The vertical axis ranges from 0 to 0.35 with linear scale.

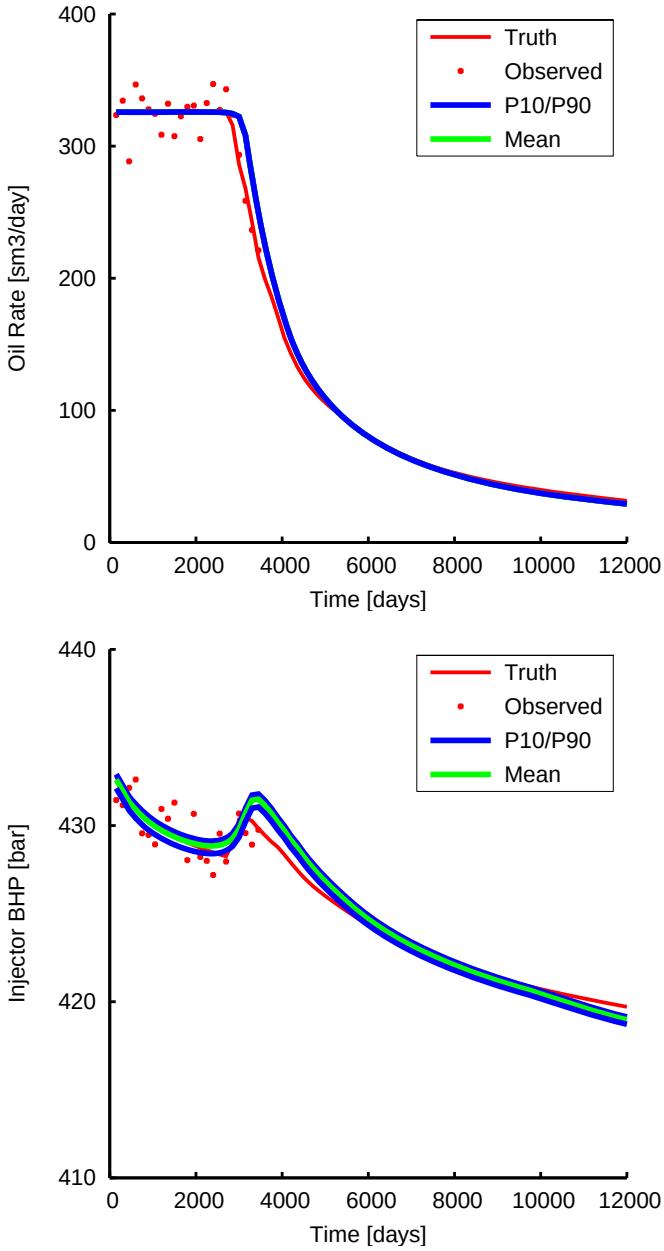

Figure 9.26: Production profiles with uncertainty envelopes. Absolute permeability was adjusted in history-matching. The top figure is oil production rate and the bottom figure is injector bottom hole pressure.

According to Figure 9.25, the permeability must become larger artificially to reduce the misfit but it could not match the breakthrough timing. The value of 5.5009 gives the highest probability with a very narrow peak, and the larger values than that point seems to have zero probability. For comparison, the arithmetic mean of permeability in the truth fine-scale model is 230.78 mD (Figure 9.2) and the geometric mean is 205.01 mD, whilst the arithmetic mean of logarithmic permeability is 5.323. In addition, the average permeability for the 38 flows can be calculated from the corresponding transmissibilities which were used in Section 9.4. The directional permeabilities for the 38 flows can be calculated from the transmissibilities and the size of each cell. The arithmetic mean is 217.82 mD and the geometric mean is 215.35 mD resulting from the arithmetic mean of logarithmic permeability 5.37. Hence, the most likely permeability value in Figure 9.25 was overestimated. Still it cannot match both the oil production rate and the pressure at the same time. The conclusion is that it requires additional parameters or corrections. One of the additional corrections is the error model (e.g., O'Sullivan, 2004), which is an area of current research. Of course another approach is the adjustment of the coarse-scale relative permeabilities which is the topic of this thesis.

9.5.2 Absolute Permeability and Relative Permeability

Both the absolute permeability and the relative permeability were adjusted during history-matching. The number of parameters was 17 in total. The relative permeabilities of the 38 flows were parameterised using 16 parameters as in Section 9.3. These are denoted as Parameters 1-16. The logarithmic permeability was also adjusted simultaneously within the prior range described above. This is denoted as Parameter 17. Again, the transformed value represented the absolute permeability for the 38 flows in the model. The other properties remained the same as those in Section 9.2.

The optimised relative permeabilities are shown in Figure 9.27 and the optimised logarithmic permeability was 5.5243 which corresponds to 250.71 mD. The history-matched results of the oil production rate and the injector BHP are shown in Figure 9.29. The 1D marginal

distributions of all the 17 parameters are shown in Figures 9.30 and 9.31, and the results of the forecast uncertainty are shown in Figure 9.34. The simulated production profiles matched to the observed data, apart from a little fluctuation in the simulated BHP. The uncertainly envelopes of the oil production rate and BHP are significant compared to the corresponding results in Figure 9.26. Also the bias around the breakthrough timing in Figure 9.26 was removed in the current results of Figure 9.34.

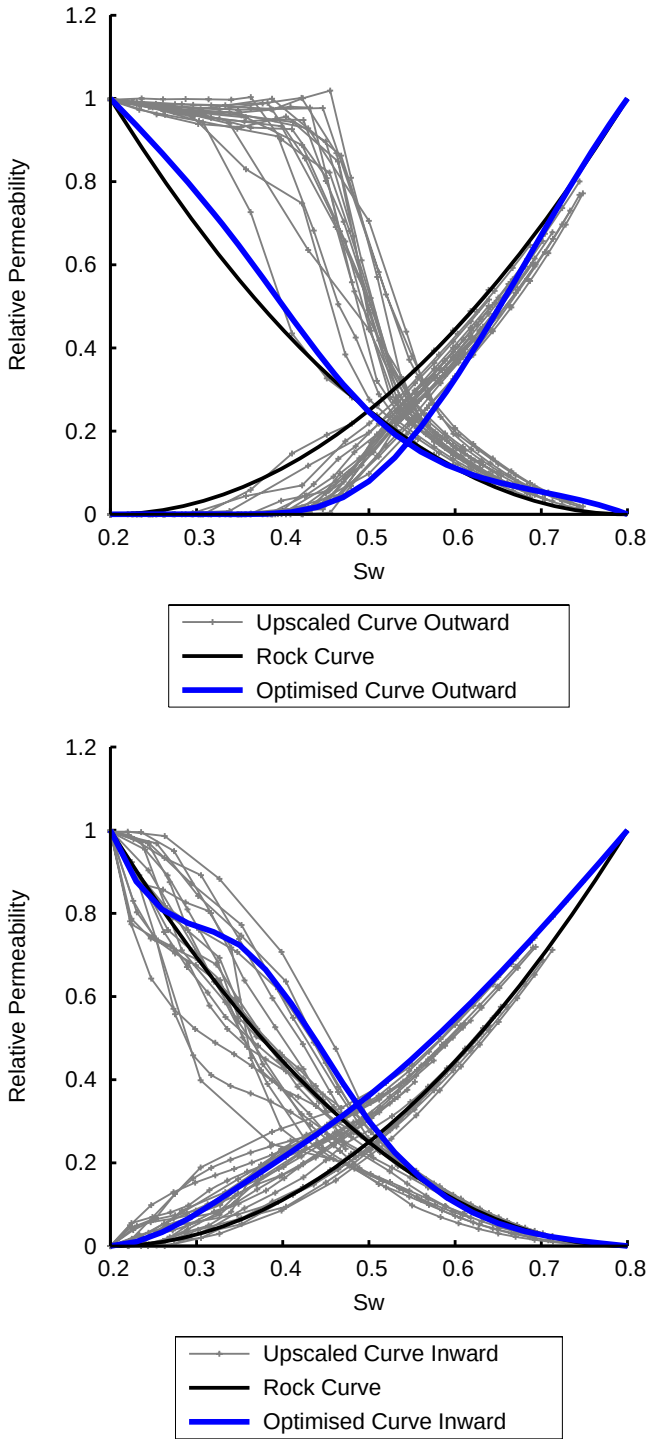

Figure 9.27: Optimised relative permeabilities. Absolute permeability and relative permeabilities were adjusted in history-matching. The top figure is outward flow and the bottom figure is inward flow.

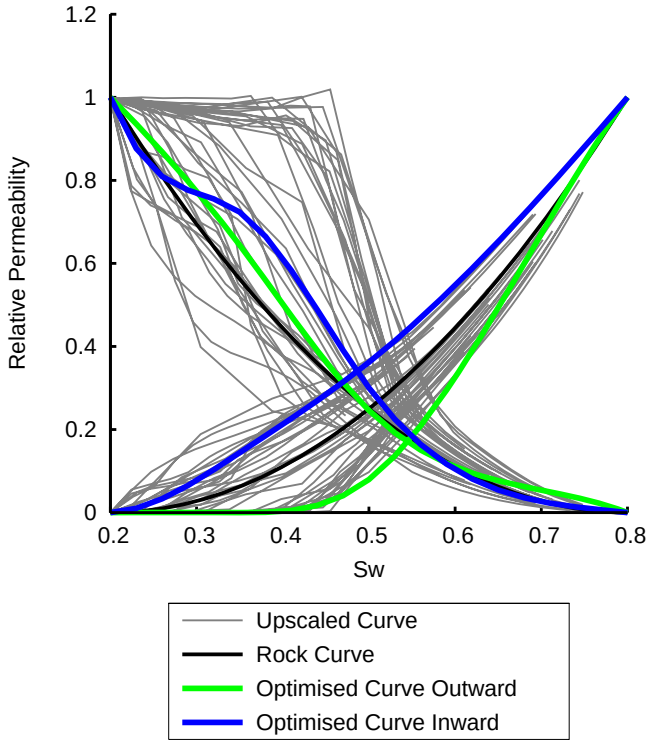

Figure 9.28: Optimised relative permeabilities. Absolute permeability and relative permeabilities were adjusted in history-matching. The two set of the curves (Outward flow and Inward flow) were plotted together for comparison.

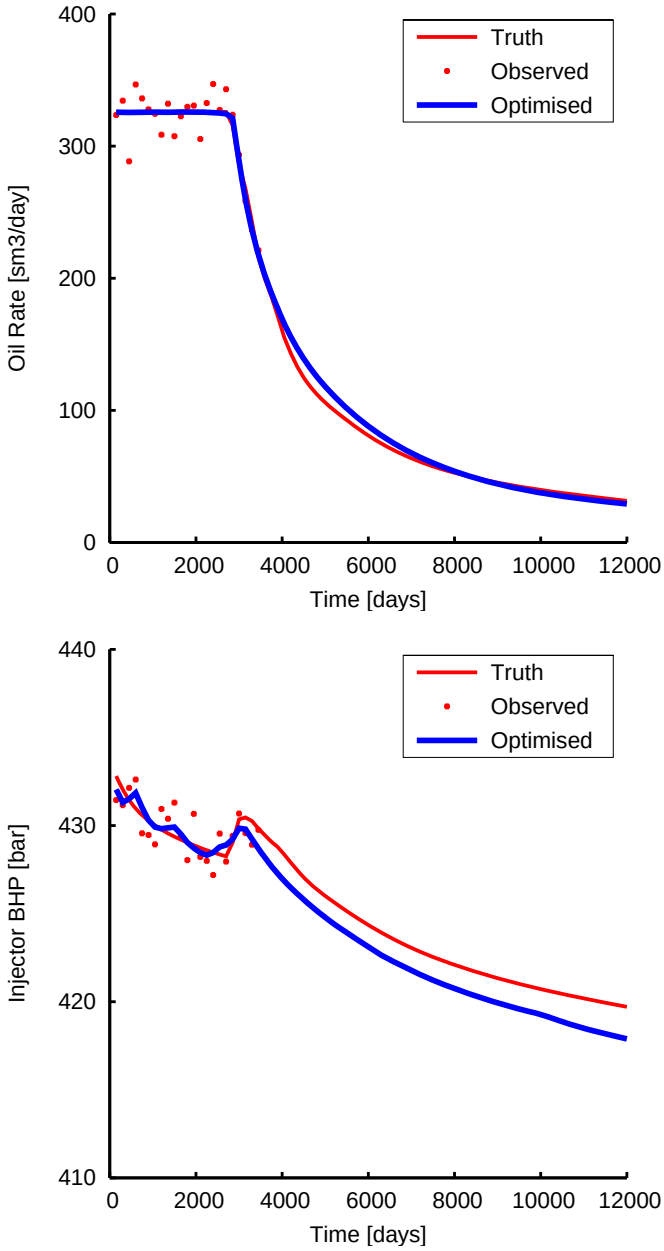

Figure 9.29: Production profiles calculated using optimised relative permeabilities. Absolute permeability and relative permeabilities were adjusted in history-matching. The top figure is oil production rate and the bottom figure is injector bottom hole pressure.

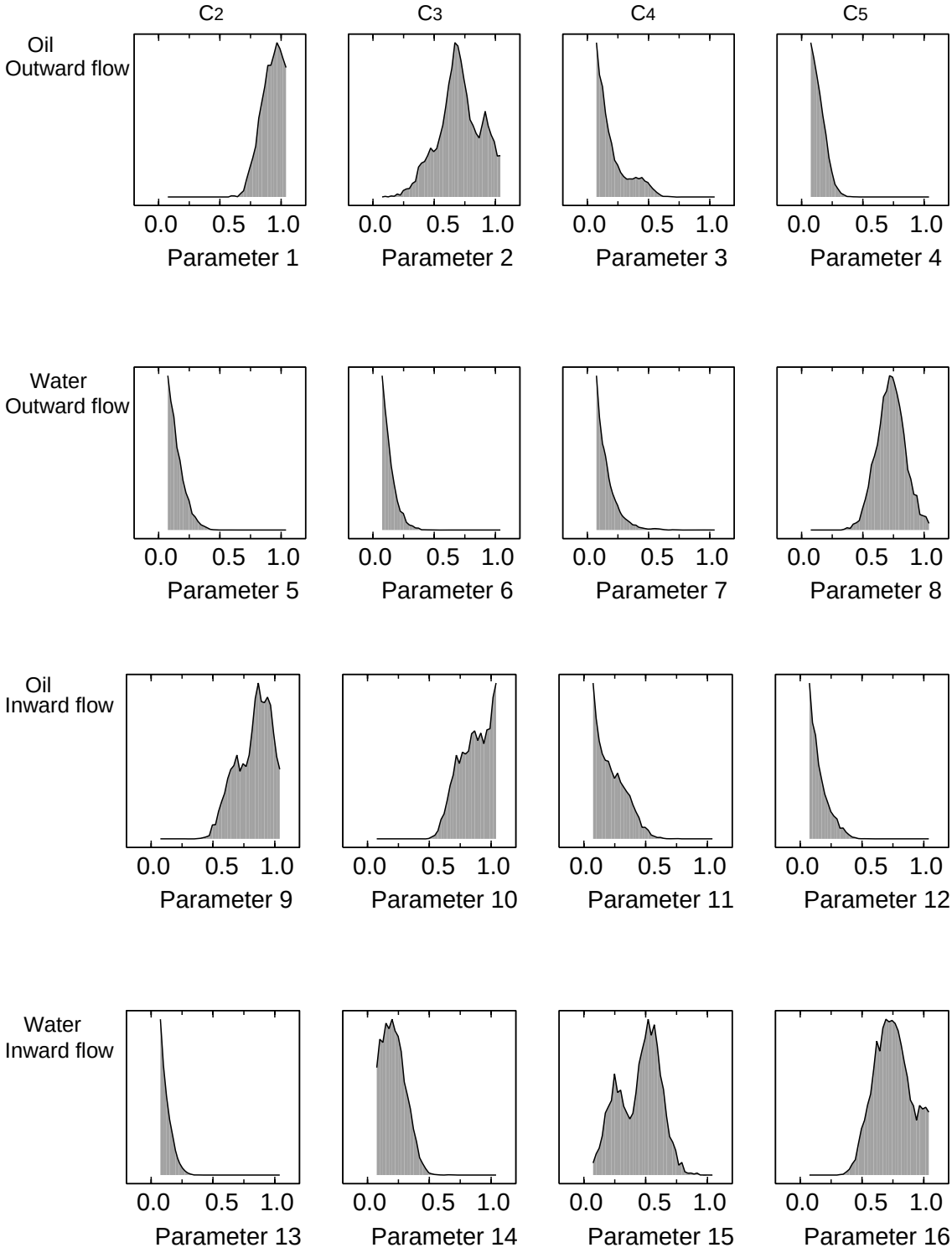

Figure 9.30: 1D marginal distribution for 100000 samples in the Markov chains (Parameters 1-16). Absolute permeability and relative permeabilities were adjusted in history-matching. Note that each curve is scaled to its maximum height not the same area. The vertical axis ranges from 0 to each maximum with a linear scale. Each maximum height is provided in Table 9.5.

Table 9.5: Max. of each curve in Figure 9.30

	c_2	c_3	c_4	c_5
Oil, Outward flow	0.11	0.07	0.18	0.20
Water, Outward flow	0.22	0.27	0.24	0.09
Oil, Inward flow	0.08	0.09	0.14	0.22
Water, Inward flow	0.32	0.10	0.07	0.07

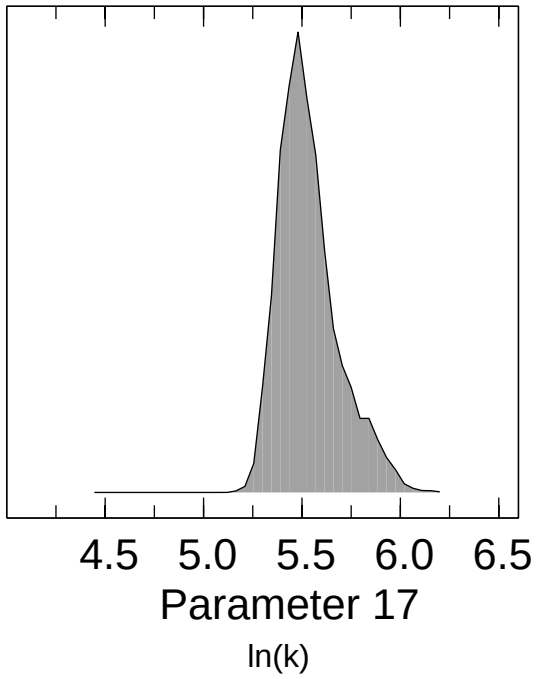

Figure 9.31: 1D marginal distribution for 100000 samples in the Markov chains (Parameter 17). Absolute permeability and relative permeabilities were adjusted in history-matching. Note that the curve is scaled to its maximum height not the same area. The vertical axis ranges from 0 to 0.14 with linear scale.

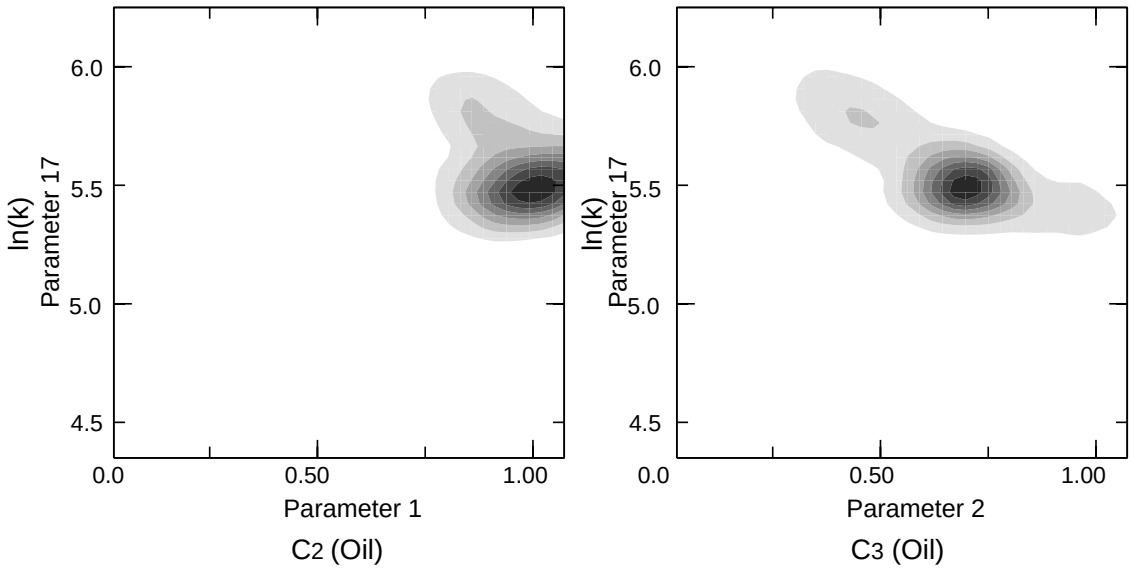

Figure 9.32: 2D marginal distribution for 100000 samples in the Markov chains. Note that the grey scale contour ranges linearly from 0 (white) to 0.06 (black).

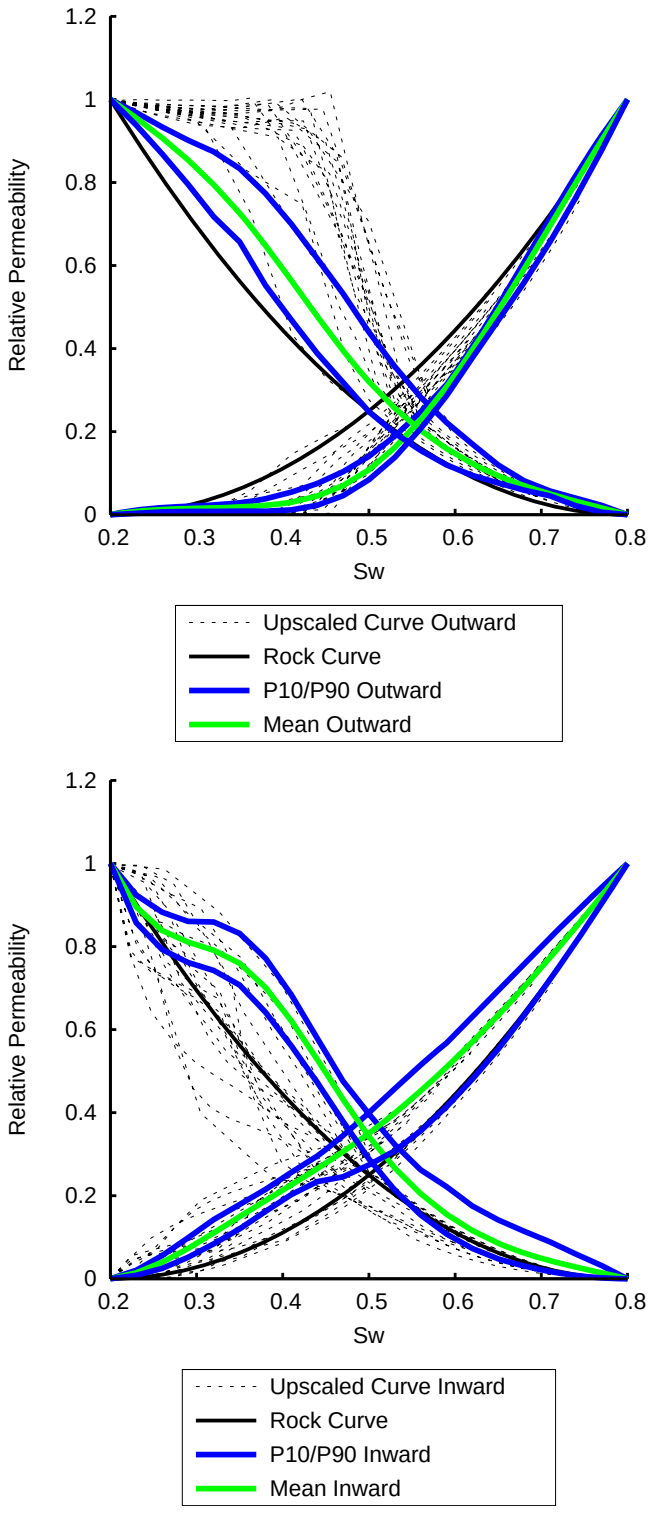

Figure 9.33: Relative permeabilities with uncertainty envelopes. Absolute permeability and relative permeabilities were adjusted in history-matching. The top figure is outward flow and the bottom figure is inward flow.

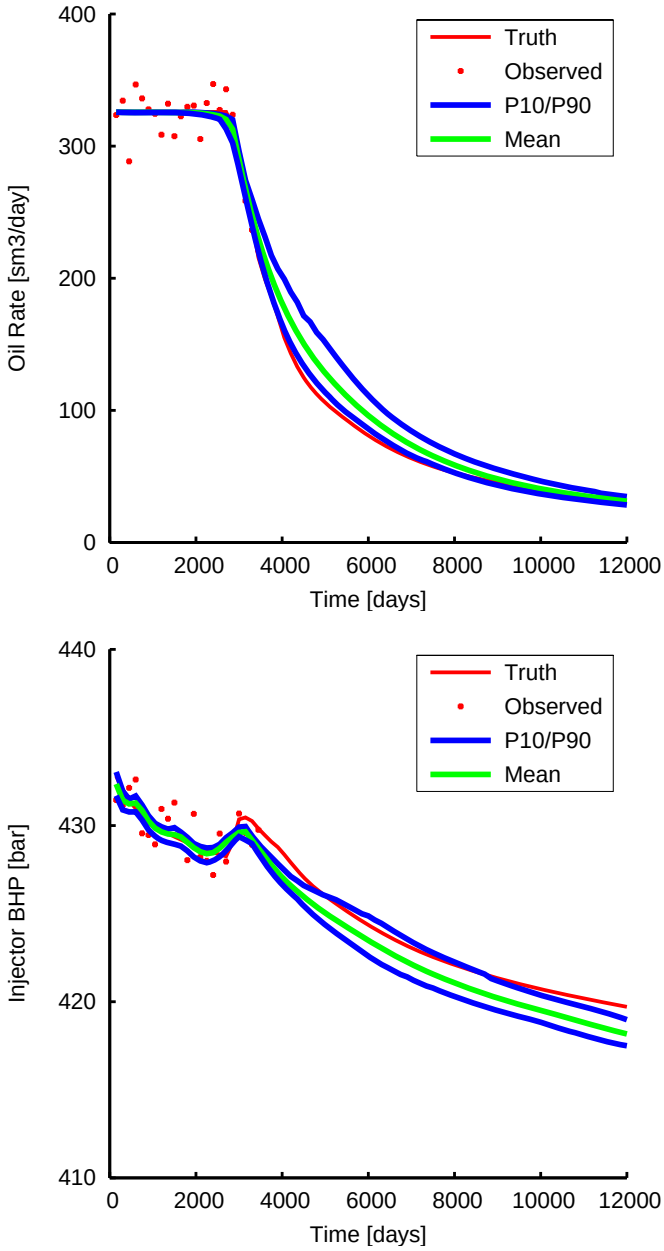

Figure 9.34: Production profiles with uncertainty envelopes. Absolute permeability and relative permeabilities were adjusted in history-matching. The top figure is oil production rate and the bottom figure is injector bottom hole pressure.

As mentioned above, the most likely permeability value was 250.71 mD, 5.5243 for the logarithmic permeability. Also Figure 9.31 indicates that the estimated permeability is higher than the reference value mentioned above: e.g., 215.35 mD corresponding to 5.37 in the logarithmic permeability, which can be calculated from the upscaled transmissibilities of the 38 flows. The width of the marginal distribution of the logarithmic permeability is larger than that of Figure 9.25. The wing of the high side reaches 6.0 in Figure 9.31, whereas it is truncated around 5.5 in Figure 9.25. This can be explained by considering the adjustment of both permeability and relative permeability as follows. If the absolute permeability becomes artificially large to reduce the misfit, the relative permeabilities tend to compensate for the excess total mobility. Compared to the results in Section 9.4 where permeability was fixed, the oil relative permeabilities of the outward flow in Figures 9.27 and 9.33 tend to have lower values than those in Figures 9.9 and 9.14. According to Figure 9.30, the distribution of Parameter 2 which represents a part of the oil relative permeabilities of the outward flow has wider shape and the x-axis value at the peak is smaller compared to the corresponding distribution in Figure 9.13. Figure 9.32 plots the 2-dimensional marginal posterior probability distribution for Parameters 1 and 17 and that for Parameters 2 and 17, where Parameter 17 represents the logarithmic permeability and Parameters 1 and 2 are the B-spline coefficients which represent oil relative permeability. Both the 2-dimensional marginal distributions represent the correlation between the permeability and the oil relative permeability in the small water saturation regions. They show a negative correlation between the parameters especially when the logarithmic permeability ranges from about 5.5 to 6.0, which is larger than the reference value of 5.37, (Figure 9.32). Hence the interrelation between permeability and relative permeabilities affects the results of history-matching and forecast uncertainty. This is why the uncertainty envelope of the production profiles in Figure 9.34 tends to show different trends from the result in Figure 9.15 where only relative permeabilities were adjusted.

9.6 Effect of Grouping

This section presents the results when only one group of relative permeability curves was adjusted during history-matching. That is to say, one set of the curve represents the multi-phase flow functions of the 38 flows, instead of the two sets of the curves in Section 9.3. The calibration parameters were 8 B-spline coefficients as explained in Section 9.3. The aim is to assess the grouping scheme and compare the results with those in Section 9.4. The prior information was provided as described in Section 9.2 and was incorporated into the stochastic sampling as in Section 9.3. Figure 9.35 shows the limits for the upscaled relative permeabilities where the limits of the two types in Figure 9.7 were amalgamated into one set of the curves.

Figure 9.36 represents the optimised relative permeabilities for one set of the curves. The history-matched results of the oil production rate and the injector BHP are shown in Figure 9.37. The simulated profiles were matched to the observed data, and the optimised relative permeabilities are surrounded by the reference curves. However, the reference curves labelled as “Upscaled Curve” in Figure 9.36 spread over a very large area of the graph, and it is difficult to assess the meaning of one set of the estimated curves. The 1D marginal distributions of 8 parameters are shown in Figures 9.38. Some distributions are similar to one of the corresponding parameters in Figure 9.13. The uncertainty envelopes of the relative permeabilities are shown in Figure 9.39, and those of the production profiles are shown in Figure 9.40. In this case, compared to the corresponding results in Section 9.4, the width of each envelope shows the different trend and tends to be smaller in some parts of the oil rate. Note that not only the parameterisations discussed in this thesis but also the choice and usage of history-matching algorithms affect the width of uncertainty. The latter topic is related to the sampling method and the approximation of parameter space, and those are discussed in some other publication (e.g., Christie et al., 2006; Erbas and Christie, 2006).

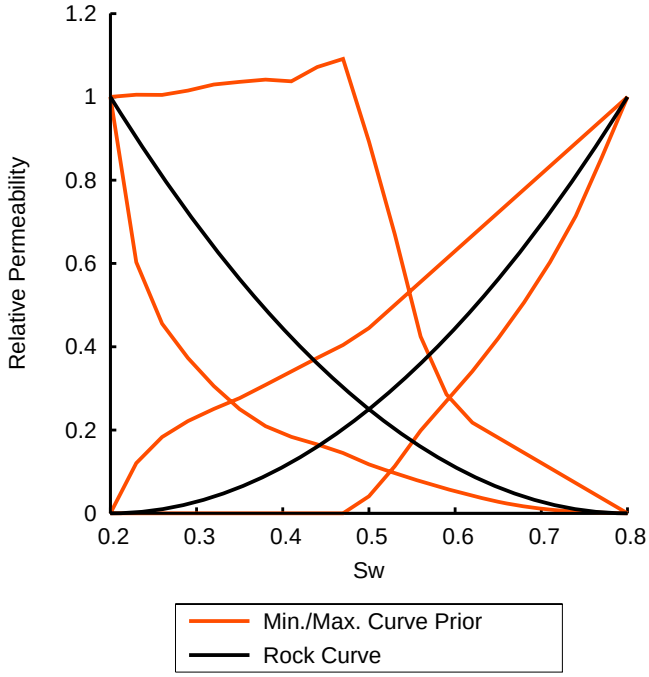

Figure 9.35: Min. and Max. of the upscaled relative permeabilities. One group of the curves is to be adjusted in history-matching.

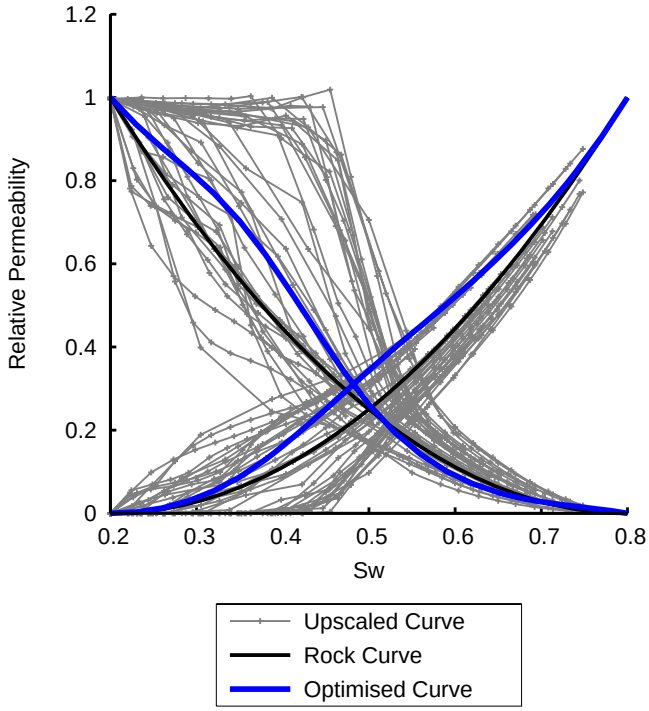

Figure 9.36: Optimised relative permeabilities. One group of the curves was adjusted in history-matching.

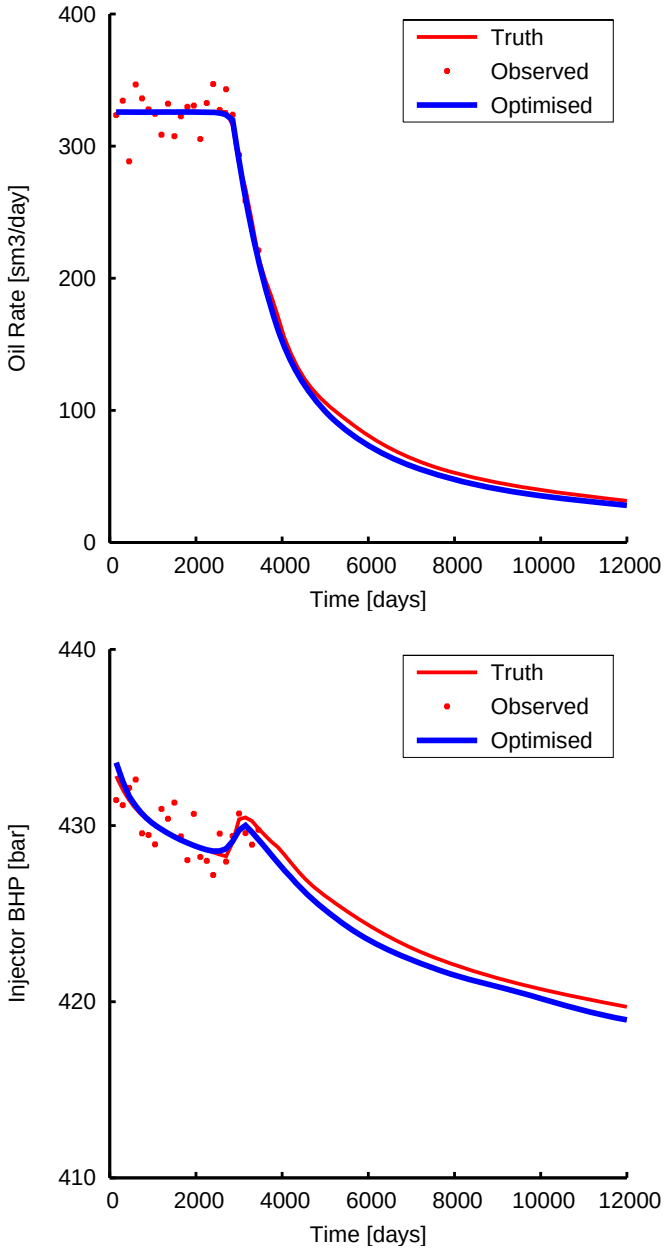

Figure 9.37: Production profiles calculated using optimised relative permeabilities. One group of the curves was adjusted in history-matching. The top figure is oil production rate and the bottom figure is injector bottom hole pressure.

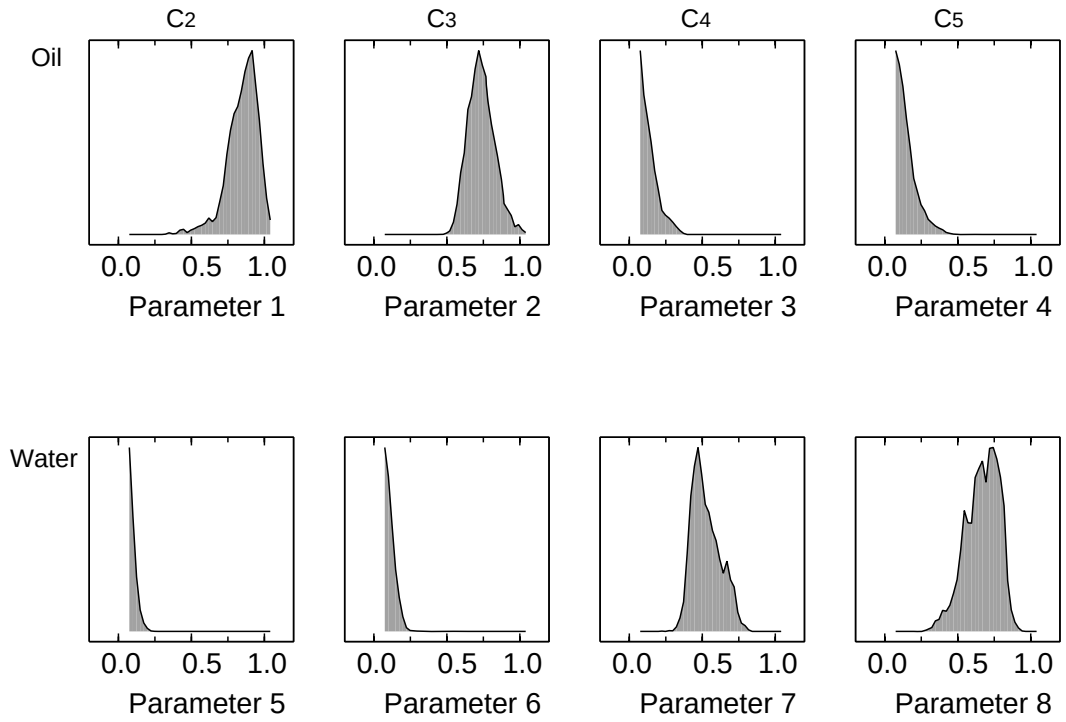

Figure 9.38: 1D marginal distribution for 100000 samples in the Markov chains. One group of the curves was adjusted in history-matching. Note that each curve is scaled to its maximum height not the same area. The vertical axis ranges from 0 to each maximum with a linear scale. Each maximum height is provided in Table 9.6.

Table 9.6: Max. of each curve in Figure 9.38

	c_2	c_3	c_4	c_5
Oil	0.11	0.12	0.25	0.20
Water	0.48	0.33	0.12	0.09

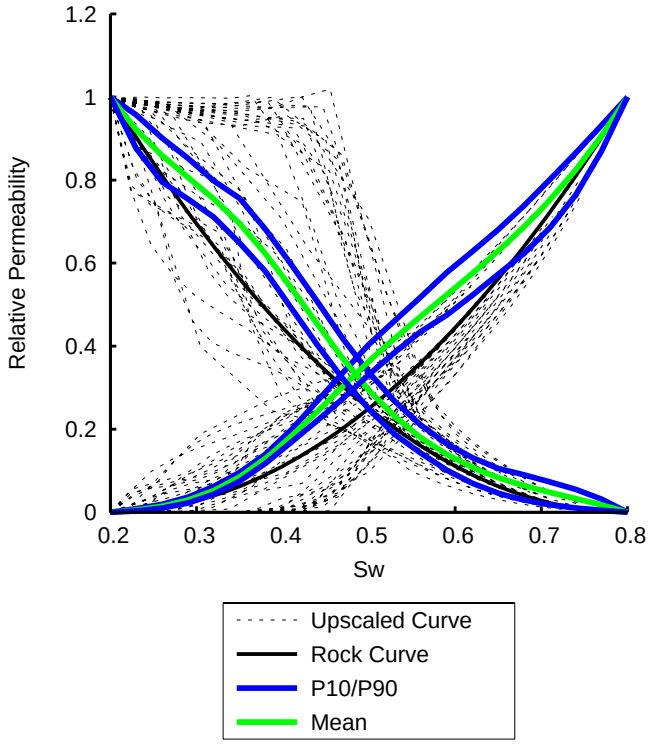

Figure 9.39: Relative permeabilities with uncertainty envelopes. One group of the curves was adjusted in history-matching.

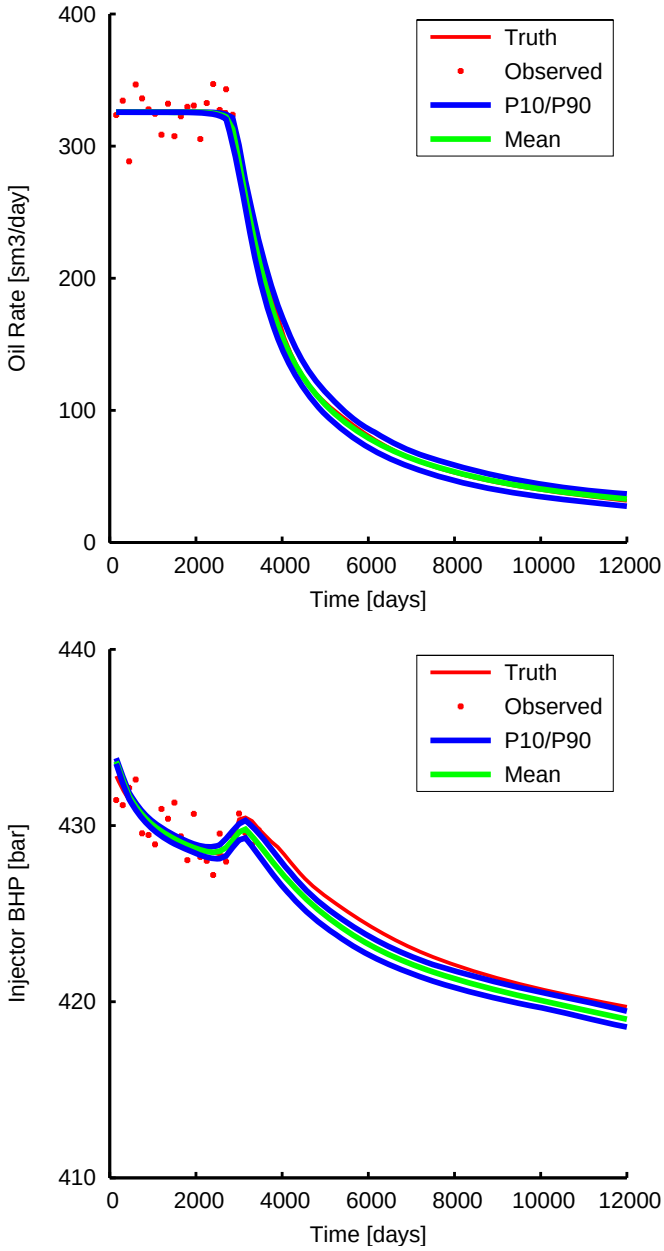

Figure 9.40: Production profiles with uncertainty envelopes. One group of the curves was adjusted in history-matching. The top figure is oil production rate and the bottom figure is injector bottom hole pressure.

9.7 Discussion and conclusions

The conclusions drawn in this chapter are:

- The prior information was successfully incorporated into the stochastic sampling for history-matching and uncertainty appraisal.
- The calibration range of the interrelated parameters can be restricted by the proposed prior model.
- The constraints of physically-based prior information are necessary in order to reduce the computational time and to avoid the unrealistic relative permeability curves.
- The two groups of the curves with B-splines have been history-matched in the synthetic quarter five-spot pattern model, and the resultant curves were examined in comparison with the reference upscaled curves.
- When relative permeabilities are adjusted simultaneously with absolute permeability, the interrelation between the two properties affects the history-matching result and the forecast uncertainty.

Although the 2D coarse-scale model could be history-matched by only one group of the curves, the meaning of the resultant curves was difficult to assess. This is because the total width of the reference upscaled curves was so wide. Specifically, the one group of the curves ignores the physical difference between the outward and inward flows to average the effect of both directions of the flows. Nevertheless, the reduction of the number of parameters is important in some situations. So this might require the further discussion.

9.8 Thoughts on the Extension to Three-Dimensional Problems

The proposed framework of the history-matching and uncertainty appraisal can be applied to three-dimensional problems, because a three-dimensional coarse-scale model can match the ob-

served data by adjusting the relative permeabilities. However, for the parameterisation methods and physical constraints of the coarse-scale relative permeabilities, it is necessary to consider the differences between the two-dimensional and three-dimensional problems. The differences are 1) the number of the curves, 2) the effect of vertical heterogeneity, 3) the connectivity and 4) the effect of gravity.

In a three-dimensional problem, the number of the coarse-scale curves is increased, because the directional relative permeabilities along the vertical axis must be added to those for the horizontal directions. The number of the groups which are to be adjusted is limited due to the computational time of the history-matching as well as due to the memory capacity. So the number of the curves categorised in each group tends to be larger than in a two-dimensional problem. Hence, a large number of the curves must be grouped together, but at the same time it should not ignore the physical categories of the curves, as discussed Sections 9.6 and 9.7. Also this issue is related to the choice of the functions which represent the coarse-scale relative permeabilities. If a three-dimensional problem needs to adjust a large number of the curves, it might be necessary to reduce the number of the parameters which represent each set of the coarse-scale curves. Again it should retain the minimum flexibility to represent the physical characteristic of the curves, as discussed in Chapter 7.

The vertical heterogeneity as well as the horizontal heterogeneity should be considered in terms of the sedimentary structure as shown in the literature (Pickup et al., 1994; Pickup and Hern, 2002; Stephen et al., 2002), since the variation of the petrophysical parameters is controlled by the sedimentary system. Well data such as core and well logging can assist the estimation of the vertical heterogeneity along a well, and so there is more information in the vertical direction than in the horizontal direction. Hence, the static information on the vertical heterogeneity can be obtained from the substantial amount of data. Note that of course there is no guarantee that the measured vertical heterogeneity extends to the area far from the well locations. However, the vertical information along the wells may help to estimate the relationship between the coarse-scale relative permeabilities and the sedimentary structure in the reservoir, when the horizontal measurements are very sparse.

Smith (1991) pointed out that, in a geometrical sense, a two-dimensional model tends to have poorer connectivity than a three-dimensional system. The vertical cross-flow at the small scale can contribute to the coarse-scale horizontal connectivity as well as the vertical connectivity. On top of that, the gravitational force affects the force balance which governs the fluid flow in a reservoir (e.g., Darman et al., 1999; Coll et al., 2001; Stephen et al., 2001). Hence, the priors of the coarse-scale relative permeabilities should be estimated from the three dimensional upscaling rather than the two-dimensional upscaling. As discussed in Section 8.6, a computationally "cheap" method with reasonable accuracy should be used for the upscaling, since a dynamic approach requires more time in three dimensions than in two dimensions.

Chapter 10

Discussion

As described in Chapter 1, the issues to be discussed in this thesis are:

- How should a reservoir engineer adjust coarse-scale relative permeabilities in history-matching?
- How should a reservoir engineer predict uncertain oil production based on the coarse-scale history-matching?

For these issues, Chapter 1 raised a number of questions. This chapter gives an answer to each of the questions. The following questions and answers form the discussion about the issues on coarse-scale relative permeabilities.

Question 1 Which parameterisation is suitable for coarse-scale relative permeabilities?

Answer Flexibility is required to reproduce the reference upscaled relative permeabilities, since the coarse-scale curves tend to have different shapes from rock curves to compensate for discretisation errors and to represent sub-grid physical dispersion. B-splines or end-point shifts enabled a better match to the reference curves (Figures 6.11, 7.18 and 7.27), whereas a

simple function with the fixed end-points failed to reproduce the reference curves (Figures 7.2 and 7.10). However a large number of parameters for the flexible formulations tends to raise another problem of the "curse of dimensionality". Hence, the minimum flexibility should be chosen from prior information.

Question 2 How many sets of the coarse-scale curves should be adjusted in history-matching?

Answer In the two-dimensional coarse-scale models of a quarter five-spot pattern, the adjustment of two sets of the curves for the inter-well region successfully captured the reference upscaled curves (Figure 9.9). Also when the number of curves was reduced to one, the history-matched curve fell within a large group of the reference curves (Figure 9.36). However, one set of the curves may be inadequate to represent all of the reference curves. Whichever the resultant one set of the curves is physically correct or not, it is likely that the one set of curves is surrounded by a wide group of the reference curves. Whereas the two sets of the curves represented outward and inward flow separately, the one set of the curves was difficult to justify the physical meaning in terms of flows in the model instead of merely averaging all the curves. This point made the assessment about the number of the curves difficult, and the answer could not be given clearly. Another point is that, although it was not seen in that particular case, two sets of the curves may compensate for some artificial features, and this might cause deviations from the reference curves. In this sense, the minimum number of the curves is preferred. When more than two sets of the curves are chosen, the constraints for the adjustment of the curves may be required to reduce the parameter space.

Question 3 Do the parameterisation scheme and the number of the curves affect the results of uncertainty quantification?

Answer Yes, the uncertainty envelopes depended both on the parameterisation schemes and on the number of the curves. For the parameterisation schemes, some flexible representations matched the observed data. Although the optimised curves resembled the reference curves to

some extent, the ways observed data constrained the relative permeabilities were different in the different parameterisation schemes. Since the difference affected the production forecast, the resulting uncertainty envelopes depended on the parameterisation of the relative permeabilities (Figures 6.16, 6.17, 7.24, 7.25, 7.32 and 7.33). For the number of the curves in the two dimensional model, the reduction in the number of the curves led to a reduction of the total number of the parameters in the model, namely the flexibility of the model. How the observed data constrained the model depended on the flexibility in the model as in the parameterisation scheme. Hence, the forecast uncertainty was affected by the number of the curves as well as each representation of the curves (Figures 9.15 and 9.40).

Question 4 How far is the rock curve allowed to change?

Answer The limits of the adjustment were estimated from the possible ranges of the geostatistical parameters (Figure 9.7). In the two-dimensional model, each of the correlation lengths in the principal direction and the perpendicular direction was assumed to vary within a certain range. Also based on the assumption of a Gaussian field for the fine-scale absolute permeability, the upscaled relative permeabilities were calculated to indicate the spread of the coarse-scale curves. Apart from the correlation lengths, the standard deviation was another key parameter which affected the limits of the curves. Each group of the curves had a different width between the limits, because each group represented different flow paths in the model. Since in this case the limits were set up to cover all the upscaled curves in each group, the width depended on the number of the groups which were chosen to be adjusted. That is to say, as the number of the groups decreased, the number of the upscaled curves in each group increased, and so the width of the limits became larger. Probably the averaging of all the curves in each group could have narrowed down the limits, although the way the averaging was carried out might need the justification or provoke another discussion.

Question 5 How can the limits of the adjustment be expressed?

Answer The limits of the coarse-scale curves were expressed as prior probability distributions so that any model outside the limits was given zero probability. This prior model was easily formulated by detecting models outside the limits, assigning zero probability to those outside models and assigning uniform probability to the other models. The uniform probability means that the models within the limits had a constant probability in terms of the prior belief. Actually, the constant in the prior probability distribution did not need to be calculated, neither in the normalisation constant of Bayes' theorem nor in the other constants of the likelihood function. This is because the MCMC method requires merely the ratio of posterior probability of a pair of models. Here any constant in the posterior probability can be omitted, since the constant is common to each model. Hence the simple prior model was easily fitted into a Bayesian framework using the MCMC method. If the variations of the upscaled curves within each group had been analysed and the degree of the variations within each group had been expressed more precisely rather than with a simple uniform distribution, the prior probability model would have more complex formulation. This may require the justification to variation of the prior probability in each model and the whole formulation apart from constants should be evaluated together with the likelihood functions for sampling from PPD through the MCMC method.

Question 6 How can the limits of the adjustment be incorporated into history-matching?

Answer As mentioned in the answer to Question 5, the simple prior model adopted here did not require the calculation of the constant in the prior probability. When the models fell inside the limits, the likelihood term was calculated in the NA-algorithm. On the other hand, when the models fell outside the limits, a huge misfit corresponding to zero probability was assigned and the likelihood function did not need to be calculated. In this way, once the models were evaluated in terms of the limits of the relative permeability curves, they were easily incorporated into the history-matching. This simple approach was applied to the B-spline representations of the curves. Also it can be applied to the end-point shift and Corey or Chierici function.

Chapter 11

Summary and Conclusions

11.1 Summary

This thesis has contributed towards developing a methodology for calculating reservoir production forecast uncertainty with coarse-scale reservoir simulations. The focus of the study was on coarse-scale relative permeabilities which are often adjusted in history-matching. The problems raised in Chapter 1 were:

Problem 1

Coarse-scale simulations are inaccurate due to numerical dispersion and the neglect of sub-grid physical dispersion.

Problem 2

Small-scale heterogeneity cannot be completely known due to the lack of detailed static information in a reservoir. Unless the fine-scale features are fixed, upscaling alone cannot solve the problems.

Problem 3

Insufficient dynamic data as well as the lack of static data results in non-uniqueness of

history-matching solutions. Therefore, history-matching solely cannot provide the well-founded production forecast.

Problem 4

It is impossible to evaluate all the models, in terms of mismatch between simulated and observed data, throughout the parameter space, and this may cause the difficulty of finding a truth solution in history-matching. Hence the resulting ensemble may consist of well-matched models, but may not include a truth solution.

In order to address all the above problems, the theme of this study was set up and the keys to solving the problems were investigated. The theme to solve the problems is the incorporation of sub-grid heterogeneity in multi-phase flow functions, and the keys are 'flexibility and constraints in history-matching' and 'quantification of uncertainty in reservoir production forecast'. Flexibility in the adjustment of coarse-scale relative permeabilities was implemented with B-splines or a shifting of the end points. This enables accurate flow simulations at the coarse scale by compensating for numerical dispersion and by taking account of sub-grid physical dispersion. On the other hand, constraints on coarse-scale relative permeabilities were estimated from rock curve and geological information. The assumption was that geological information was given only by a range of geostatistical parameters. Then the range in the geological parameters was transformed into the limits of coarse-scale relative permeabilities. Those limits were useful to restrict the ranges of the adjustments. Here the constraints reduce the parameter space and provide a feasible methodology for history-matching. Following the history-matching, uncertainty in coarse-scale relative permeabilities was quantified using a Bayesian framework. This can express each model or the corresponding production forecast with a probability, rather than sticking to a single solution in history-matching. Specifically, the NA-Bayes algorithm supplemented the output from history-matching by sampling from the posterior probability distribution. So the framework of uncertainty appraisal as well as history-matching can produce a reasonable forecast of reservoir performance. In summary, the keys stated above can solve the problems and leads to a 'feasible and reasonable' methodology for reservoir production forecast.

This thesis proposed a method along with the theme and these keys. The method was implemented by the following framework:

1. To use coarse-scale curves for the purposes of capturing the finer-scale flow phenomena ignored in the model and of compensating for numerical dispersion.

2. To estimate the physical limits of the coarse-scale curves from both rock curves and the static information such as the range of geostatistical parameters.

3. To express the physical constraints as prior probability distribution so that any model outside the limits has zero probability.

4. To parameterise the coarse-scale curves with a flexible function like B-splines to capture the possible shapes of the curves.

5. To history-match the coarse-scale curves using stochastic sampling like the NA algorithm to pursue the exploration and exploitation in the parameter space. Note that the misfit definition in the program includes the prior probability distribution as well as the mismatch between simulated and observed data.

6. To perform MCMC walks in the parameter space using NA-Bayes algorithm.

7. To plot 1D marginal distribution for each parameter.

8. To calculate and plot the uncertainty statistic, such as mean, P10 and P90, in coarse-scale relative permeabilities using the collected sample from the PPD.

9. To calculate and plot the uncertainty statistic in production profiles of interest such as oil rate, pressure and recovery in the same way as above.

10. To check the relation among these statistical plots on the PPD and present the forecast uncertainty.

This work fits into the context of top-down reservoir modelling (Williams et al., 2004), the concept of which was introduced recently as a strategy of reservoir modelling. The modelling

strategy starts with a simple coarse model, because it is much quicker to adjust large-scale heterogeneity such as channel and fault in a coarse-scale model than in a detailed fine-scale model. Then, the second task is to tune the coarse-scale model to account for more details. For example, the small-scale heterogeneity inside a channel is not resolved in a coarse-scale model. As a consequence, the physical dispersion due to the sub-grid structure is ignored in the flow simulation. In this context the contribution of this thesis is to represent sub-grid flow phenomena using coarse-scale relative permeabilities and to predict uncertainty without refining the model.

In order to demonstrate the proposed framework, a number of numerical experiments were conducted in this thesis. The main features of the numerical experiments are:

- The Bayesian framework along with a stochastic sampling was applied to the history-matching of coarse-scale relative permeabilities.
- The framework was demonstrated using a 1D coarse-scale model. The history-matched relative permeabilities and their uncertainty envelopes were examined and compared with the reference upscaled relative permeabilities.
- The uncertainty in the estimation was explained by analysing the relation between the observed production data, model parameters, relative permeabilities and the calculated production profiles.
- Physical limits of the coarse-scale curves were determined from the possible combinations of the geostatistical parameters.
- The physical constraints were expressed as prior probability distribution and were incorporated into the stochastic sampling for history-matching and uncertainty appraisal.
- Two groups of the curves have been history-matched using a 2D coarse-scale model of quarter five-spot pattern, and the resultant curves were examined in comparison with the reference upscaled curves.

11.2 Conclusions

In summary, the conclusion drawn in this thesis are:

- The parameterisation scheme defines the way in which the observed production data restricts the coarse-scale model in history-matching. Therefore it definitely influences the resulting uncertainty forecast.
- The stochastic sampling methods used for history-matching and uncertainty quantification can be improved by the incorporation of the prior belief on the coarse-scale relative permeabilities. The prior belief is inferred from the static geological information and the knowledge on fine-scale flow phenomena.
- The proposed method uses computational experiments to determine the reasonable prior ranges for coarse-scale relative permeabilities.
- Even if the rock curve is known, uncertainty in small-scale heterogeneity leads to the variability in the coarse-scale relative permeabilities.
- Insufficient and noisy observed data result in a substantial amount of uncertainty in relative permeabilities which are inferred from history-matching.

11.3 Future Work

The issues to be investigated further are:

- Coarse-scale curves should be estimated not only by assessing the effect of heterogeneity but also by including the uncertainty both in the rock curves and in their spatial distribution. In real problems, it is almost impossible to obtain complete and appropriate knowledge of the two-phase flow functions throughout a field. Therefore for coarse-scale relative permeabilities, not only the process of upscaling but also the rock curve itself is subject to errors due to the lack of information. The awkwardness both in the upscaling process and in the evaluation of the rock curve is the main motivation for adjusting the coarse-scale curves in real history-matching problems. Accordingly, the total ambiguity

raised in the both aspects needs to be assessed in advance of the history-matching in order to provide the physical constraints for the adjustment.

- The choice of the functions and the grouping schemes for the coarse-scale curves should be discussed using real field models by considering the trade-off between the physical meaning and the minimisation of the model parameters. Both the function and the grouping control the flexibility in a coarse-scale model. Moreover, the number of the groups definitely determines the classifications of the inter-cell flows in a model. Although large-scale heterogeneity has not been examined in this thesis, there might be some large-scale structures in a field. This also affects the classifications of the flows, since streamlines drawn by a pressure solver depend on the large-scale heterogeneity as well as small-scale features. Ideally the precise classification for the various curves and the abundant flexibility for each curve may lead to a robust representation of two-phase flow. Hence as large-scale heterogeneity is distinguished in a model, a number of parameters should be adjusted in history-matching. The trade-off between the physical consistency and the limitation of parameter dimensions needs to be examined in a real field model which has large-scale structures.

- For the estimation of the prior curves, it is necessary to utilise a computationally "cheap" method: e.g. local upscaling which uses certain boundary conditions in the local model. Although the rock curve was assumed to represent a fine-scale property in this thesis, there is a gap between the scale of a fine cell and the scale at which rock curve is evaluated in practice. Theoretically, rock curve measured by the JBN method represents a point value in one dimension rather than a total volume of a core sample. If the point value is assumed to satisfy the concept of the REV, the gap between rock curve and a coarse-scale property is huge. When the task is to estimate the coarse-scale curves based on rock curves, it is necessary to consider heterogeneity at the very small scale which corresponds to the scale of the rock curve. Since the relative permeabilities are adjusted in history-matching directly at the coarse scale in the context of top-down reservoir modelling, fine-scale models which were used to estimate coarse-scale curves in this thesis must be replaced with 'very small'-scale models in which rock curve can be assigned

without any scale-change. In other words, the estimation of the coarse-scale curves requires the calculations of upscaling with a huge upscaling factor. Accordingly, the computationally "cheap" upscaling method is preferable for the purpose of the estimation of coarse-scale curves. When local upscaling is utilised, the key is to predict the effect of sub-grid heterogeneity separately from the discretisation effect.

- The synthetic truth fine-scale model in this thesis was generated by assuming stationarity throughout the model and using the geostatistical method. A real reservoir may be more heterogeneous where different facies are present. In general, rock relative permeabilities are different in the different facies. If the focus on an important facies is appropriate, the process to estimate the prior curves is similar to the proposed method. However, if the region for one set of coarse-scale curves covers some facies which have different rock curves, it may lead to the variability of the prior curves compared to a single facies model. The method to estimate the prior curves and to model the prior probability needs to be developed for multi-facies models.

- Although the prior probability was determined by the limits of the coarse-scale curves based on the upscaling effects in this thesis, there might be other constraints to be considered. For example, the physical correlation between oil and water relative permeabilities can be modelled. Also in each curve the physical correlation between relative permeability value at one saturation and that at another saturation can be considered: e.g., slope of a curve. If one can extract some likely trends of the correlation between the curves as well as the correlation between the parts of a curve, it is possible to model the relations as prior probability of a set of the parameters. The way to extract the trend and to express it as prior probability might be one of the topic of the future work.

- Since the coarse-scale curves are closely related to the feature of solution errors, the investigation of the shape of the coarse-scale curves can contribute to the prediction of the solution errors, and vice versa. In addition, whether the rock curve should be altered without any error models or be completely fixed using an error model is a topic to be discussed. One might prefer the solution error models to the alternation of rock curve at the coarse scale. As long as the rock curve is fixed at the coarse-scale in real problems, a

major issue might be that the error in the evaluation of the rock curve itself must be taken into account in the error modelling, because all the errors due to the fixed properties need to be encapsulated in the error model. When a coarse-scale model is history-matched with the fixed relative permeabilities and the error model, the discretisation effect, sub-grid physical dispersion and the error in rock curve itself are subject to the investigation for the purpose of developing the error model. On the other hand, if relative permeabilities are adjusted in history-matching together with the other parameters, all the errors stated above need to be corrected by adjusting relative permeabilities. Presumably this topic is linked to the amount of error and the limitation of parameter dimensions. Also it depends on what sort of errors can be modelled properly.

APPENDIX

Near-Well Upscaling for Two-Phase Flow

The program used for two-phase near-well upscaling is an in-house software developed at Heriot-Watt University. It uses the results of the single-phase near-well upscaling which consists of well connection factor and transmissibility and also requires the results of two-phase flow simulation of the wells and surrounding cells. Then it calculates upscaled relative permeabilities for the wells and surrounding blocks. The method adopted for single-phase near-well upscaling is described in Ding (1995), Durlofsky et al. (2000) and Muggeridge et al. (2002). Also the method to calculate upscaled relative permeabilities between a well block and the surrounding blocks is the PVW method described in Section 8.2. The next paragraph explains the procedure to calculate upscaled relative permeabilities for the well connections.

The method developed by Ding (1995) was extended to two-phase flow by calculating upscaled relative permeabilities for the well block and the surrounding blocks so that the flow of each fluid into the well is the same for the coarse-scale and fine-scale simulations. The upscaled relative permeabilities for the well connections can be calculated using the following equation.

$$\overline{K_{rf}} = \frac{\overline{q_f}\mu_f}{\overline{I_w}\left(\overline{P_f} - \overline{P_w} - \overline{H_w}\right)}, \tag{A.1}$$

$$\tag{A.2}$$

where $\overline{K_{rf}}$ is the upscaled relative permeability for the f-th phase, μ_f is the viscosity of the f-th phase fluid, $\overline{q_f}$ is the total flow of the fluid, $\overline{I_w}$ is the upscaled well connection transmissibility factor, $\overline{P_f}$ is the average pressure in the coarse cell containing the well, $\overline{P_w}$ is the pressure in the well at the depth of the centre of the coarse cell and $\overline{H_w}$ is the pressure head between the centre of the coarse cell and the well bottom hole pressure datum. Note that the above equation considers all the flows at reservoir conditions.

As mentioned above, the upscaled well connection factor $\overline{I_w}$ was calculated using the single phase near-well upscaling (Ding, 1995). The average pressure $\overline{P_f}$ was calculated from the pressures in the fine-scale cells using pore-volume weighting. The total flow $\overline{q_f}$ was calculated from the fine-scale flows into the fine-scale cell containing the well. For both producer and injector wells, average saturation in the coarse cell containing the well was calculated at each time step. Note that even in the case of injection wells, the upscaled water relative permeability as a function of the average saturation at the cell was required to control the total mobility, (Schlumberger, 2004a).

Bibliography

Artus, V., Noetinger, B., and Ricard, L.: 2004, Dynamics of the water-oil front for two-phase, immiscible flows in heterogeneous porous media. 1 - stratified media, *Transp. Porous Media* **56**(3), 283–303.

Ayub, M. and Bentsen, R.G.: 1999, Interfacial viscous coupling: a myth or reality?, *Journal of Petroleum Science and Engineering* **23**, 13–26.

Aziz, K. and Settari, A.: 1979, *Petroleum Reservoir Simulation*, Applied Science Publishers Ltd, London.

Bancroft, T. and Han, C.: 1981, *Statistical Theory and Inference in Research*, Marcel Dekker, Inc., New York.

Barker, J.W., Cuypers, M., and Holden, L.: 2001, Quantifying uncertainty in production forecasts: Another look at the PUNQ-S3 problem, *Soc. Petrol. Engr. Jour.* 433–441.

Barker, J.W. and Dupouy, P.: 1999, An analysis of dynamic pseudo-relative permeability methods for oil-water flows, *Petroleum Geoscience* **5**, 385–394.

Barker, J.W. and Thibeau, S.: 1997, A critical review of the use of pseudorelative permeabilities for upscaling, *Soc. Petrol. Engr. Reservoir Engr.* **12**, 138–143.

Bear, J.: 1972, *Dynamic of Fluids in Porous Media*, American Elsevier Publishing Company, Inc., New York.

Bear, J. and Bachmat, Y.: 1990, *Introduction to Modelling of Transport Phenomenon in Porous Media*, Kluwer Academic Publishers, Dordrecht.

Behrens, R.A., MacLeod, M.K., Tran, T.T., and Alimi, A.O.: 1998, Incorporating seismic attribute maps in 3D reservoir models, *Soc. Petrol. Engr. Reservoir Evaluation & Engr.* 122–126.

Bevington, P. and Robinson, D.: 2003, *Data Reduction and Error Analysis for the Physical Sciences*, The McGraw-Hill Companies, Inc., New York, third edition.

Buckley, S.E. and Leverett, M.C.: 1942, Mechanism of fluid displacement in sands, *Transactions American Institute of Mining, Metallurgical and Petrol. Engr.* **146**, 107–116.

Burdine, N.: 1953, Relative permeability calculations from pore size distribution data, *Journal of Petroleum Technology* **198**, 71–78.

Chierici, G.L.: 1981, Novel relations for drainage and imbibition relative permeability, *Soc. Petrol. Engr. Jour.* 275–276.

Christie, M., Demyanov, V., and Erbas, D.: 2006, Uncertainty quantification for porous media flows, *Jour. of Computational Physics* **Special Issue**, In press.

Christie, M., MacBeth, C., and Subbey, S.: 2002a, Multiple history-matched models for Teal South, *The Leading Edge* **21**(3), 286–289.

Christie, M., Subbey, S., and Sambridge, M.: 2002b, Prediction under uncertainty in reservoir modeling, presented at the 2002 European Conference on the Mathematics of Oil Recovery, Freiberg, September 3-6.

Christie, M., Subbey, S., Sambridge, M., and Thiele, M.: 2002c, Quantifying prediction uncertainty in reservoir modelling using streamline simulation, presented at the 2002 Am. Soc. Civil Engr. Engineering Mechanics Conference, June.

Christie, M.A.: 1996, Upscaling for reservoir simulation, *Jour. Petrol. Technology* **48**, 1004–1008.

Christie, M.A. and Blunt, M.: 2001, Tenth SPE comparative solution project: A comparison of upscaling techniques, *Soc. Petrol. Engr. Reservoir Evaluation & Engr.* **4**(4), 308–317.

Christie, M.A. and Clifford, P.J.: 1998, Fast procedure for upscaling compositional simulation, *Soc. Petrol. Engr. Jour.* 272–278.

Christie, M.A., Mansfield, M., King, P.R., Barker, J.W., and Culverwell, I.D.: 1995, A renormalisation-based upscaling technique for WAG floods in heterogeneous reservoirs, Soc. Petrol. Engr. Paper 29127 presented at the 1995 SPE Symposium on Reservoir Simulation, San Antonio, February 12-15.

Christie, M. and Bond, D.: 1985, Multidimensional flux-corrected transport for reservoir simulation, Soc. Petrol. Engr. Paper 13505 presented at the 1985 SPE Middle East Oil Technical Conference and Exhibition, Bahrain, March, 11-14.

Christie, M. and Bond, D.: 1986, Detailed simulation of unstable process in miscible flooding, Soc. Petrol. Engr. Paper 14896 presented at the 1986 SPE/DOE Symposium on Enhanced Oil Recovery, Dallas, April, 20-23.

Coll, C., Muggeridge, A., and Jing, X.: 2001, Regional upscaling: A new method to upscale waterflooding in heterogeneous reservoirs for a range of capillary and gravity effects, *Soc. Petrol. Engr. Jour.* **66**(3), 299–310.

Corey, A.T.: 1954, The interrelation between gas and oil relative permeabilities, *Producers Monthly* 38–41.

Cowan, G.: 1998, *Statistical Data Analysis*, Oxford University Press, Inc., New York.

Crotti, M.A. and Cobenas, R.H.: 2001, Scaling up of laboratory relative permeability curves. an advantageous approach based on realistic average water saturations, Soc. Petrol. Engr. Paper 69394 presented at the 2001 SPE Latin American and Caribbean Petroleum Engineering Conference, Buenos Aires, March 25-28.

Dake, L.: 1978, *Fundamentals of Reservoir Engineering*, Elsevier, Amsterdam.

Darman, N., Pickup, G., and Sorbie, K.: 2002, A comparison of two-phase dynamic upscaling methods based on fluid potentials, *Computational Geoscience* **6**, 5–27.

Darman, N., Sorbie, K., and Pickup, G.: 1999, The development of pseudo functions for gravity-dominated immiscible gas displacements, Soc. Petrol. Engr. Paper 51941 presented at the 1999 SPE Reservoir Simulation Symposium, Houston, February 14-17.

de Boor, C.: 2001, *A Practical Guide to Splines*, Splinger, New York, revised edition.

Demyanov, V., Subbey, S., and Christie, M.: 2004, Uncertainty assessment in PUNQ-S3: Neighbourhood algorithm framework for geostatistical modelling, Paper presented at the 9th European Conference on the Mathematics of Oil Recovery, Cannes, August 30 - September 2.

Deutsch, C.V. and Journel, A.G.: 1998, *GSLIB: Geostatistical Software Library and User's Guide*, Oxford University Press, Inc., New York, 2nd edition.

Dierckx, P.: 1993, *Curvature and Surface Fitting with Splines*, Oxford University Press, Oxford.

Ding, Y.: 1995, Scaling-up in the vicinity of wells in heterogeneous field, Soc. Petrol. Engr. Paper 29137 presented at the 1995 SPE Symposium on Reservoir Simulation, San Antonio, February 12-15.

Dullien, F.A.L.: 1992, *Porous Media: Fluid Transport and Pore Structure*, Academic Press, Inc., San Diego, second edition.

Dupouy, P., Barker, J.W., and Valois, J.: 1998, Grouping pseudo relative permeability curves, *IN SITU* **22**(1), 1–33.

Durlofsky, L.J., Milliken, W.J., and Bernath, A.: 2000, Scaleup in the near-well region, *Soc. Petrol. Engr. Jour.* **5**(1), 110–117.

Engl, H., Hanke, M., and Neubauer, A.: 1996, *Regularization of Inverse Problems*, Kluwer Academic Publishers, Dordrecht.

Erbas, D. and Christie, M.: 2006, How does sampling strategy affect uncertainty estimations?, *Oil & Gas Science and Technology -Revue de l'IFP* (Under review).

Ewing, R.: 1983, Problems arising in the modeling of process for hydrocarbon recovery, In Ewing, R., editor, *The Mathematics of Reservoir Simulation*, 3–34. Society for Industrial and Applied Mathematics, Philadelphia.

Eydinov, D., Chen, S., Gao, G., and Reynolds, A.: 2005, Incorporating uncertainty in relative permeability curves in history matching, *TUREP Research Report* (22), 134–183, The University of Tulsa.

Firoozabadi, A. and Aziz, K.: 1986, Relative permeability from centrifuge data, Soc. Petrol. Engr. Paper 15059 presented at the 1986 SPE California Regional Meeting, Oakland, April 2-4.

Floris, F., Bush, M., Cuypers, M., Roggero, F., and Syversveen, A.R.: 2001, Methods for quantifying the uncertainty of production forecasts: a comparative study, *Petroleum Geoscience* **7(SUPP)**, 87–96.

Gamerman, D.: 1997, *Markov Chain Monte Carlo: Stochastic Simulation For Bayesian Inference*, Chapman & Hall, London.

Gilks, W.R., Richardson, S., and Spiegelhalter, D.J.: 1996, *Markov Chain Monte Carlo in Practice*, Chapman & Hall, London.

Glimm, J., Hou, S., Lee, Y., Sharp, D., and Ye, K.: 2001, Prediction of oil production with confidence intervals, **146**, Soc. Petrol. Engr. Paper 66350 presented at the 2001 SPE Reservoir Simulation Symposium, Houston, February 11-14.

Haberman, C.: 1998, *Mathematical Models: Mechanical Vibrations, Population Dynamics, and Traffic Flow*, SIAM, Philadelphia.

Haberman, R.: 1987, *Elementary Applied Partial Differential Equations: with Fourier Series and Boundary Value Problems*, Prentice-Hall, Inc., New Jersey, second edition.

Hagoort, J.: 1974, Displacement stability of water drives in water-wet connate-water-bearing reservoirs, *Soc. Petrol. Engr. Jour.* 63–74.

Harten, A.: 1977, The artificial compression method for computation of shocks and contact discontinuities, *Communications on Pure and Applied Mathematics* **30**, 611–638.

Hastings, J.J., Muggeridge, A.H., and Blunt, M.J.: 2003, A new streamline method for evaluating uncertainty in small-scale, two-phase flow properties, *Soc. Petrol. Engr. Jour.* **8**(1), 32–40.

Hewett, T.A., Suzuki, K., and Christie, M.A.: 1998, Analytical calculation of coarse-grid corrections for use in pseudofunctions, *Soc. Petrol. Engr. Jour.* **3**(3), 293–305.

Hewett, T. and Behrens, R.: 1991, Scaling laws in reservoir simulation and their use in a hybrid finite difference / streamtube approach to simulating the effects of permeability heterogeneity, In Lake, L., Carroll, H., and Wesson, T., editors, *Reservoir Characterization II*, 402–441. Academic Press, Inc., San Dirgo.

Honapour, M., Koederitz, L., and Harvey, A.H.: 1986, *Relative Permeability of Petroleum Reservoirs*, CRC Press, Inc., Boca Raton.

Huang, Y., Ringrose, P., and Sorbie, K.: 1996, The effects of heterogeneity and wettability on oil recovery from laminated sedimentary structures, *Soc. Petrol. Engr. Jour.* 451–462.

Jaynes, E. and Bretthorst, G.: 2003, *Probability Theory: The Logic of Science*, Cambridge University Press, Cambridge.

Jensen, J., Lake, L., Corbett, P., and Goggin, D.: 2000, *Statistics for petroleum engineers and geoscientists*, Elservier, New York, second edition.

Johnson, E.F., Bossler, D.P., and Naumann, V.O.: 1959, Calculation of relative permeability from displacement experiments, *Transactions American Institute of Mining, Metallurgical and Petrol. Engr.* **216**, 370–372.

Johnson, J., Nanney, M.M. Killough, J., and Lin, Y.: 1982, The Kuparuk river field: A regression approach to pseudo-relative permeabilities, presented at the 1982 SPE Symposium on Reservoir Simulation, New Orleans, January 31 - February 3.

JPT: 1996, SPE / WPC draft reserves definitions, *Jour. Petrol. Technology* **48**(8), 694–696.

Kerig, P.D. and Watson, A.T.: 1986, Relative-permeability estimation from displacement experiment:an error analysis, *Soc. Petrol. Engr. Reservoir Engr.* **1**, 175–182.

Kerig, P.D. and Watson, A.T.: 1987, A new algorithm for estimating relative permeabilities from displacement experiments, *Soc. Petrol. Engr. Reservoir Engr.* **2**, 103–112.

King, M.J. and Dunayevsky, V.A.: 1989, Why waterflood works: A linearized stability analysis, Soc. Petrol. Engr. Paper 19648 presented at the 1989 SPE Annual Technical Conference and Exhibition, San Antonio, October 8-11.

King, P.: 1989, The use of renormalization for calculating effective permeability, *Transp. Porous Media* **4**, 37–58.

Kulkarni, K.N. and Datta-Gupta, A.: 1999, Estimating relative permeability from production data: A streamline approach, Soc. Petrol. Engr. Paper 56751 presented at the 1999 SPE Annual Technical Conference and Exhibition, Houston, October 3-6.

Kyte, J.R. and Berry, D.W.: 1975, New pseudo functions to control numerical dispersion, *Soc. Petrol. Engr. Jour.* **5**(2), 269–275.

Lake, L.: 1989, *Enhanced Oil Recovery*, Prentice-Hall, Inc., Englewood Cliffs.

Lake, L. and Srinivasan, S.: 2004, Statistical scale-up of reservoir properties: concepts and applications, *Journal of Petroleum Science and Engineering* **44**, 27–39.

Lantz, R.B.: 1971, Quantitative evaluation of numerical diffusion (truncation error), *Soc. Petrol. Engr. Jour.* 315–320.

Lee, S.H., Malallah, A., Datta-Gupta, A., and Higdon, D.: 2002, Multiscale data integration using Markov random fields, *Soc. Petrol. Engr. Reservoir Evaluation & Engr.* 68–78.

Lenormand, R.: 1996, Determining flow equations from stochastic properties of a permeability field: the mhd model, *Soc. Petrol. Engr. Jour.* 179–190.

Lepine, O., Bissell, R., Aanonsen, S., Pallister, I., and Barker, J.: 1999, Uncertainty analysis in predictive reservoir simulation using gradient information, *Soc. Petrol. Engr. Jour.* 251–259.

Li, D., Beckner, B., and Kumar, A.: 1999, A new efficient averaging technique for scaleup of multimillion-cell geologic models, Soc. Petrol. Engr. Paper 56554 presented at the 1999 SPE Annual Technical Conference and Exhibition, Houston, October, 3-6.

Li, D. and Lake, L.: 1995, Scaling fluid flow through heterogeneous permeable media, *Soc. Petrol. Engr. Advanced Technology Series* **3**(1), 188–197.

Liu, N. and Oliver, D.S.: 2003, Evaluation of Monte Carlo methods for assessing uncertainty, *Soc. Petrol. Engr. Jour.* **146**, 188–195.

Lucia, F.: 1999, *Carbonate Reservoir Characterization*, Splinger-Verlag, Berlin.

Muggeridge, A.: 1991, Generation of effective relative permeabilities from detailed simulation of flow in heterogeneous porous media, In Lake, L., Carroll, H., and Wesson, T., editors, *Reservoir Characterization II*, 197–225. Academic Press, Inc., San Dirgo.

Muggeridge, A., Cuypers, M., Bacquet, C., and Barker, J.: 2002, Scale-up of well performance for reservoir flow simulation, *Petroleum Geoscience* **8**(2), 133–139.

Muskat, M.: 1981, *Physical Principals of Oil Production*, International Human Resources Development Corporation, Boston, second edition.

Muskat, M. and Meres, M.W.: 1936, The flow of heterogeneous fluids through porous media, *Physics* **7**, 346–363.

Muskat, M., Wyckoff, R.D., Botset, H.G., and Meres, M.W.: 1937, Flow of gas-liquid mixtures through sands, *Transactions American Institute of Mining, Metallurgical and Petrol. Engr.* **123**, 69–96.

Namba, T. and Hiraoka, T.: 1995, Capillary force barriers in a carbonate reservoir under waterflooding, Soc. Petrol. Engr. Paper 29773 presented at the 1995 SPE Middle East Oil Show, Bahrain, March, 11-14.

Namba, T. and Horne, R.: 1989, Estimation of water and oil relative permeabilities from pressure transient analysis of water injection well data, Soc. Petrol. Engr. Paper 19829 presented at the 1989 SPE Annual Technical Conference and Exhibition, San Antonio, October, 8-11.

Noetinger, B., Artus, V., and Ricard, L.: 2004, Dynamics of the water-oil front for two-phase, immiscible flows in heterogeneous porous media. 2 - isotropic media, *Transp. Porous Media* **56**(3), 305–328.

Nomura, N.: 2002, Fast and robust computation for effective permeabilities, Soc. Petrol. Engr. Paper 78514 presented at the 2002 Abu Dhabi International Oil Conference, Abu Dhabi, October, 13-16.

Oliver, D.S., Cunha, L.B., and Reynolds, A.C.: 1997, Markov chain Monte Carlo methods for conditioning a permeability field to pressure data, *Math. Geology* **29**(1), 61–91.

Oliver, D.S., Nanqun, H., and Reynolds, A.C.: 1996, Conditioning permeability fields to pressure data, Paper presented at the 5th European Conference on the Mathematics of Oil Recovery, Leoben, Austria, September 3-6.

Omre, H., Tjelmeland, H., and Wist, H.: 1999, Uncertainty in history matching - model specification and sampling algorithms, *Technical Report Statistics, Norwegian U. of Science & Technology* (No. 6/1999).

O'Sullivan, A.E.: 2004, *Modelling Simulation Error for Improved Reservoir Prediction*, PhD thesis, Institute of Petroleum Engineering, Heriot-Watt University.

O'Sullivan, A.E. and Christie, M.A.: 2005, Solution error models: A new approach for coarse grid history matching, Soc. Petrol. Engr. Paper 93268 presented at the 2005 SPE Reservoir Simulation Symposium, Houston, January 31-February 2.

Ouenes, A., Bhagavan, S., Bunge, P., and Travis, B.: 1994, Application of simulated annealing and other global optimization methods to reservoir description: myths and realities, Soc. Petrol. Engr. Paper 28415 presented at the 1994 SPE Annual Technical Conference and Exhibition, New Orleans, September, 25-28.

Panda, M.N., Mosher, C., and Chopra, A.K.: 2001, Reservoir modelling using scale-dependent data, *Soc. Petrol. Engr. Jour.* **6**(2), 157–170.

Peaceman, D.W.: 1977, *Fundamentals of numerical reservoir simulation*, Elsevier Scientific Publishing Company, Amsterdam.

Pickup, G.E., Ringrose, P.S., and Sharif, A.: 2000, Steady-state upscaling: From lamina-scale to full field model, *Soc. Petrol. Engr. Jour.* **5**(2), 208–217.

Pickup, G. and Hern, C.: 2002, The development of appropriate upscaling procedures, *Transp. Porous Media* **46**, 119–136.

Pickup, G., Jensen, J., Ringrose, P., and Sorbie, K.: 1992, A method for calculating permeability tensors using perturbed boundary conditions, Paper presented at the 3rd European Conference on the Mathematics of Oil Recovery, Delft, June, 17 - 19.

Pickup, G., Monfared, H., Zhang, P., and Christie, M.: 2004, A new way of looking at upscaling, Paper presented at the 9th European Conference on the Mathematics of Oil Recovery, Cannes, August 30 - September 2.

Pickup, G., Ringrose, P., Forrester, M., Jensen, J., and Sorbie, K.: 1994, The Geopseudo Atlas: Geologically based upscaling of multiphase flow, Soc. Petrol. Engr. Paper 27565 presented at the 1994 European Petroleum Computer Conference, Aberdeen, March 15-17.

Pickup, G., Stephen, K., Ma, J., Zhang, P., and Clark, J.: 2005, Multi-stage upscaling: Selection of suitable methods, In Das, D. and Hassanizadeh, S., editors, *Upscaling Multiphase Flow in Porous Media: From Pore to Core and Beyond*, 191–216. Springer, Dordrecht.

Portella, R. and Prais, F.: 1999, Use of automatic history matching and geostatistical simulation to improve production forecast, Soc. Petrol. Engr. Paper 53976 presented at the 1999 SPE Latin American and Caribbean Petroleum Engineering Conference, Caracas, April, 21-23.

Press, W.H., Teukolsky, S.A., Vetterling, W.T., and Flannery, B.P.: 1992, *Numerical Recipes in C*, Cambridge University Press, Cambridge, 2nd edition.

Purcell, W.: 1949, Capillary pressure - their measurement using mercury and the calculation of permeability therefrom, *Transactions American Institute of Mining, Metallurgical and Petrol. Engr.* **186**, 39–48.

Renard, P. and de Marsily, G.: 1997, Calculating equivalent permeability: a review, *Advances in Water Resources* **20**, 253–278.

Reynolds, A., Li, R., and Oliver, D.: 2004, Simultaneous estimation of absolute and relative permeability by automatic history matching of three-phase flow production data, *Jour. Canadian Petrol. Technology* **43**(3), 37–46.

Richards, L.A.: 1931, Capillary conduction of liquids through porous media, *Physics* **1**, 318–333.

Richmond, P.C. and Watson, A.T.: 1990, Estimation of multiphase flow functions from displacement experiments, *Soc. Petrol. Engr. Reservoir Engr.* 121–127.

Ringrose, P., Sorbie, K., Corbett, P., and Jensen, J.: 1993, Immiscible flow behaviour in laminated and cross-bedded sandstones, *Journal of Petroleum Science and Engineering* **9**, 103–124.

Roggero, F.: 1997, Direct selection of stochastic model realizations constrained to historical data, Soc. Petrol. Engr. Paper 38731 presented at the 1997 SPE Annual Technical Conference and Exhibition, San Antonio, October, 5-8.

Romero, C., Carter, J., Zimmerman, R., and Gringarten, A.: 2000, Improved reservoir characterisation through evolutionary computation, Soc. Petrol. Engr. Paper 62942 presented at the 2000 SPE Annual Technical Conference and Exhibition, Dallas, October, 1-4.

Rose, W.: 1999, Relative permeability ideas - then and now (Richards to Leverett to Yester, and beyond), Soc. Petrol. Engr. Paper 57442 presented at the 1999 SPE Eastern Regional Meeting, Charleston, October 20-22.

Sambridge, M.: 1999a, Geophysical inversion with a neighbourhood algorithm -I.: Searching a parameter space, *Geophysical Journal International* **138**, 479–494.

Sambridge, M.: 1999b, Geophysical inversion with a neighbourhood algorithm -II.: Appraising the ensemble, *Geophysical Journal International* **138**, 727–746.

Schlumberger: 2004a, *ECLIPSE Reference Manual 2004A*.

Schlumberger: 2004b, *PSEUDO Reference Manual 2004A*.

Schulze-Rlegert, R., Axmann, J., Haase, O., Rian, D., and You, Y.L.: 2002, Evolutionary algorithms applied to history matching of complex reservoirs, *Soc. Petrol. Engr. Jour.* 163–173.

Schulze-Rlegert, R. and Haase, O.: 2003, Combined global and local optimisation techniques applied to history matching, Soc. Petrol. Engr. Paper 79668 presented at the 2003 SPE Reservoir Simulation Symposium, Houston, February, 3-5.

Schumaker, L.L.: 1981, *Spline Functions: Basic Theory*, J. Wiley & Sons, Inc., New York.

Siddiqui, S., Hicks, P.J., and Ertekin, T.: 1999, Two-phase relative permeability models in reservoir engineering calculations, *Energy Sources* **21**, 145–152.

Sigmund, P. and McCaffery, F.: 1979, An improved unsteady-state procedure for determining the relative-permeability characteristics of heterogeneous porous media, *Soc. Petrol. Engr. Jour.* 15–28.

Sivia, D.S.: 1996, *Data Analysis: A Bayesian Tutorial*, Oxford University Press, Inc., New York.

Smith, C., Tracy, G., and Farrar, R.: 1992, *Applied Reservoir Engineering*, volume 1, OGCI Publications, Tulsa.

Smith, E.: 1991, The influence of small-scale heterogeneity on average relative permeability, In Lake, L., Carroll, H., and Wesson, T., editors, *Reservoir Characterization II*, 52–76. Academic Press, Inc., San Dirgo.

Sorbie, K., Feghi, F., Pickup, G., Ringrose, P., and Jensen, J.: 1994, Flow regimes in miscible displacements in heterogeneous correlated random fields, *Soc. Petrol. Engr. Advanced Technology Series*, **2**(2), 78–87.

Sorbie, K., Zhang, H., and Tsibuklis, N.: 1995, Linear viscous fingering: New experimental results, direct simulation and the evaluation of averaged models, *Chemical Engineering Science* **50**(4), 601–616.

Stephen, K.D., Pickup, G.E., and Sorbie, K.: 2001, The local analysis of changing force balance in immiscible incompressible two-phase flow, *Transp. Porous Media* **45**, 63–88.

Stephen, K., Clark, J., and Pickup, G.: 2002, Modelling and flow simulations of a North Sea turbidite reservoir: Sensitivities and upscaling, Soc. Petrol. Engr. Paper 78292 presented at the 2002 SPE European Petroleum Conference, Aberdeen, October 29-31.

Stephen, K., Soldo, J., MacBeth, C., and Christie, M.: 2005, Multiple model seismic and production history matching: A case study, Soc. Petrol. Engr. Paper 94173 presented at the 2005 SPE Europec / EAGE Annual Conference, Madrid, June, 13-16.

Stone, H.L.: 1991, Rigorous black oil pseudo functions, Soc. Petrol. Engr. Paper 21207 presented at the 1991 SPE Symposium on Reservoir Simulation, Anaheim, February 17-20.

Subbey, S., Christie, M., and Sambridge, M.: 2002, Uncertainty reduction in reservoir modelling, In Chen, Z. and Ewing, R., editors, *Fluid Flow and Transport in Porous Media: Mathematical and Numerical Treatment, Proceedings of an AMS-IMS-SIAM joint seminar research conference*, 457–467. American Mathematical Society, Providence.

Subbey, S., Christie, M., and Sambridge, M.: 2003, A strategy for rapid quantification of uncertainty in reservoir performance prediction, Soc. Petrol. Engr. Paper 79678 presented at the 2003 SPE Reservoir Simulation Symposium, Houston, February 3-5.

Subbey, S., Monfared, H., Christie, M., and Sambridge, M.: 2006, Quantifying uncertainty in flow functions derived from SCAL data: USS relative permeability and capillary pressure, *Transp. Porous Media* in press.

Sun, X. and Mohanty, K.: 2003, Estimation of flow functions during drainage using genetic algorithm, Soc. Petrol. Engr. Paper 84548 presented at the 2003 SPE Annual Technical Conference and Exhibition, Denver, October 5-8.

Suzuki, K., Asada, J., and Yoshida, K.: 2004, Accelerated history matching through process independent scale-up techniques in a giant carbonate reservoir, Soc. Petrol. Engr. Paper 87012 presented at the 2004 SPE Asia Pacific Conference on Integrated Modelling for Asset Management, Kuala Lumpur, March, 29-30.

Suzuki, K. and Hewett, T.: 2000, Sequential scale-up of relative permeabilities, Soc. Petrol. Engr. Paper 59450 presented at the 2000 SPE Asia Pacific Conference on integrated Modelling for Asset Management, Yokohama, April 25-26.

Tan, T.: 1995, Estimating two and three dimensional pseudo-relative permeabilities with nonlinear regression, Soc. Petrol. Engr. Paper 29129 presented at the 1995 SPE Symposium on Reservoir Simulation, San Antonio, February, 12-16.

Taylor, J.: 1997, *An Introduction to Error Analysis: The Study of Uncertainties in Physical Measurements*, University Science Books, Sausalito, second edition.

Thomas, G.: 1983, An extension of pseudofunction concepts, Soc. Petrol. Engr. Paper 12274 presented at the 1983 Reservoir Simulation Symposium, San Francisco, November 15-18.

Thomas, J.: 1995, *Numerical Partial Differential Equations: Finite Difference Methods*, Springer-Verlag.

Tiab, D. and Donaldson, E.: 2002, *Petrophysics*, Gulf Professional Publishing, Burlington, second edition.

Tokuda, N., Takahashi, S., Watanabe, M., and Kurose, T.: 2004, Application of genetic algorithm to history-matching for core flooding, Soc. Petrol. Engr. Paper 88621 presented at the 2004 SPE Asia Pacific Oil and Gas Conference and Exhibition, Perth, October, 18-20.

Tran, T.T., Wen, X.H., and Behrens, R.A.: 2001, Efficient conditioning of 3D fine-scale reservoir model to multiphase production data using streamline-based coarse-scale inversion and geostatistical downscaling, *Soc. Petrol. Engr. Jour.* **6**(4), 364–374.

Valestrand, R., Grimstad, A., Kolltveit, K., and Nævdal, G.: 2002, Simultaneous determination of absolute and relative permeabilities, *International Journal of Thermal Science* **41**, 546–556.

Waggoner, J., Castillo, J., and Lake, L.: 1992, Simulation of eor process in stochastically generated permeable media, *Soc. Petrol. Engr. Formation Evaluation.* 173–180.

Watson, A.T., Richmond, P.C., Kerig, P.D., and Tao, T.M.: 1988, A regression-based method for estimating relative permeabilities from displacement experiments, *Soc. Petrol. Engr. Reservoir Engr.* **3**, 953–958.

Welge, H.J.: 1952, A simplified method for computing oil recovery by gas or water drive, *Transactions American Institute of Mining, Metallurgical and Petrol. Engr.* **195**, 91–98.

Wen, X.H., Durlofsky, L., and Chen, Y.: 2005, Efficient three-dimensional implementation of local-global upscaling for reservoir simulation, Soc. Petrol. Engr. Paper 92655 presented at the 2005 SPE Reservoir Simulation Symposium, Houston, 31 January - 2 February.

White, C., Willis, B., Narayanan, K., and Dutton, S.: 2001, Identifying and estimating significant geologic parameters with experimental design, *Soc. Petrol. Engr. Jour.* 311–324.

Willhite, G.P.: 1986, *Waterflooding*, Society of Petroleum Engineers, Richardson.

Williams, G.J.J., Mansfield, M., MacDonald, D.G., and Bush, M.D.: 2004, Top-down reservoir modelling, Soc. Petrol. Engr. Paper 89974 presented at the 2004 SPE Annual Technical Conference and Exhibition, Houston, September 26-29.

Williams, M., Keating, J., and Barghouty, M.: 1998, The stratigraphic method: A structured approach to history-matching complex simulation models, *Soc. Petrol. Engr. Reservoir Evaluation & Engr.* **1**(2), 169–176.

Wyckoff, R.D. and Botset, H.G.: 1936, The flow of gas-liquid mixtures through unconsolidated sands, *Physics* **7**, 325–345.

Yang, P.H. and Watson, A.T.: 1991, A Bayesian methodology for estimating relative permeability curves, *Soc. Petrol. Engr. Reservoir Engr.* **1**, 259–265.

Yoon, S., Malallah, A.H., Data-Gupta, A., Vasco, D.W., and Behrens, R.A.: 2001, A multiscale approach to production-data integration using streamline models, *Soc. Petrol. Engr. Jour.* 182–192.

Zhang, D., Li, L., and Tchelepi, H.: 2000, Stochastic formulation for uncertainty analysis of two-phase flow in heterogeneous reservoirs, *Soc. Petrol. Engr. Jour.* **5**(1), 60–70.

Zhang, D. and Tchelepi, H.: 1999, Stochastic analysis of immiscible two-phase flow in heterogeneous media, *Soc. Petrol. Engr. Jour.* **4**(4), 380–388.

Zhang, P.: 2005, *Upscaling in Highly Heterogeneous Reservoir Models*, PhD thesis, Institute of Petroleum Engineering, Heriot-Watt University.